

TECHNISCHE UNIVERSITÄT MÜNCHEN

Lehrstuhl für Nukleartechnik

**Development and Validation of Bubble Breakup and
Coalescence Constitutive Models for the One-Group
Interfacial Area Transport Equation**

Filippo Pellacani

Vollständiger Abdruck der von der Fakultät für Maschinenwesen
der Technischen Universität München zur Erlangung des akademischen Grades eines

Doktor-Ingenieurs (Dr.-Ing.)

genehmigten Dissertation.

Vorsitzender: Univ.-Prof. Wolfgang H. Polifke, Ph.D. (CCNY)

Prüfer der Dissertation:

1. Univ.-Prof. Rafael Macián-Juan, Ph.D.

2. Prof. Sergio Chiva Vicent, Ph.D.

Univ. Jaume I, Castellón / Spanien

Die Dissertation wurde am 18.09.2012 bei der Technischen Universität München
eingereicht und durch die Fakultät für Maschinenwesen am 04.12.2012 angenommen.

Dedication

Ai miei genitori.

Acknowledgement

I would like to express my greatest gratitude to my supervisor Prof. Rafael Macián Juan. During the interview I had with him in the October 2007 he greeted me with an unforgettable “Welcome aboard”. He gave me the unique chance to work freely in a field that is also a personal passion; this thesis would not have been possible without his generous support. It has been definitely a pleasure working with him during these years and helping him in establishing the department.

During the late spring 2008 Prof. Sergio Chiva Vicent was contacted by Prof. Macián to become a supervisor of my work. Since I met him for the first time, Sergio became immediately a reference to me and has been a constant source of inspiration, confidence and help. He always had time for me and for fruitful discussions. It has been an honor working with him.

Furthermore, I would like to say thank you to Dr. Martin Ohlerich for taking time to listen and answer all my questions in the best and most professional way possible. I would like to thank also the colleagues and the students at the chair for the pleasant atmosphere and especially Miriam Däubler, Matthias Frankl, Genís Riba Sanmartí and Abdullah Alali with whom I had beneficial conversations during the last months of work. Special thanks are also due to Mr. Jamel Rhouma for the efficient IT support that he always provided.

I would like to give thanks to my family in Italy, they are my source of encouragement and helped me to look always forward. Last but not least, I am deeply grateful to my lovely Diana to support me in any circumstances, to stay at my side and to share with me good and bad moments.

Abstract

A local mechanistic model for bubble coalescence and breakup for the one-group interfacial area transport equation has been developed, in agreement and within the limits of the current understanding, based on an exhaustive survey of the theory and of the state of the art models for bubble dynamics simulation.

The new model has been tested using the commercial 3D CFD code ANSYS CFX. Upward adiabatic turbulent air-water bubbly flow has been simulated and the results have been compared with the data obtained in the experimental facility PUMA. The range of the experimental data available spans between 0.5 to 2 m/s liquid velocity and 5 to 15 % volume fraction.

For the implementation of the models, both the monodispersed and the interfacial area transport equation approaches have been used. The first one to perform a detailed analysis of the forces and models to reproduce the dynamic of the dispersed phase adequately and to be used in the next phases of the work. Also two different bubble induced turbulence models have been tested to consider the effect of the presence of the gas phase on the turbulence of the liquid phase.

The interfacial area transport equation has been successfully implemented into the CFD code and the state of the art breakup and coalescence models have been used for simulation. The limitations of the actual theory have been shown and a new bubble interactions model has been developed.

The simulations showed that a considerable improvement is achieved if compared to the state of the art closure models. Limits in the implementation derive from the actual understanding and formulation of the bubbly dynamics. A strong dependency on the interfacial non-drag force models and coefficients have been shown. More experimental and theory work needs to be done in this field to increase the prediction capability of the simulation tools regarding the distribution of the phases along the pipe radius.

Contents

Dedication.....	iii
Acknowledgement	v
Abstract	vii
Contents	ix
Nomenclature	xv
Latin letters.....	xv
Greek letters.....	xvi
Subscripts	xvii
Superscripts	xix
Symbols	xix
Acronyms	xix
1 Introduction	1
1.1 Outline of the Thesis	7
2 Fluid-Dynamics of Two-Phase Flow.....	9
2.1 Notation	9
2.1.1 Averaging Operators.....	9
2.1.2 Cross Sectional Phase Averages	10
2.1.3 Definition of Main Variables	10
2.2 Main Two-Phase Flow Regimes.....	13
2.2.1 Stratified Flow.....	13
2.2.2 Slug Flow.....	14
2.2.3 Annular Flow.....	14
2.2.4 Bubbly Flow.....	14
2.3 Two-Phase Flow Classification Based on Interfacial Structure	16
2.4 Two-Phase Flow Regimes Maps and Transition Criteria.....	17
2.4.1 Flow Regime Maps	17
2.4.2 Transition Criteria for Vertical Flows	19
3 Introduction to Turbulent Flows	23
3.1 Types of Turbulent Flows.....	24
3.2 Main Characteristics of Turbulent Flows.....	24
3.3 Reynolds Decomposition Principle	26

3.4	Turbulence Intensity and Turbulence Kinetic Energy.....	27
3.5	Length Scales in Turbulent Flows	27
3.6	Conservation Equations for Turbulent Flows.....	28
3.6.1	Mass and Momentum Conservation Equations.....	29
3.6.2	Turbulent Kinetic Energy Conservation Equation	30
3.6.3	Closure Models of the Turbulence Problem	31
3.7	Homogeneous Isotropic Turbulence	32
3.8	Difference of Fluctuation Velocities at Two Neighboring Points under Isotropic and Homogeneous Turbulent Conditions	32
4	Two-Phase Flow Models.....	35
4.1	The Two-Fluid Model	38
4.2	Two-Phase Flow Turbulence Modeling	42
4.2.1	Brief Introduction on Single-Phase Turbulence Modeling	42
4.2.2	Turbulence Enhancement Generated by the Presence of a Dispersed Phase	44
4.3	Bubbly Flow Modeling.....	46
4.3.1	Bubble Interaction Mechanisms.....	49
4.3.2	Interfacial Forces Acting on the Bubbles.....	52
5	Interfacial Area Transport	63
5.1	Particle number density transport equation.....	64
5.2	Interfacial area density transport equation	65
6	Review of Theoretical Models for Bubble Coalescence and Breakup Processes of Interest for the One-Group Interfacial Area Density Transport Equation.....	69
6.1	Turbulence Fluctuation and Collision Particle Breakup Frequency Models ...	72
6.1.1	Coulaloglou and Tavlarides Model	74
6.1.2	Konno et al. Model.....	74
6.1.3	Prince and Blanch model	75
6.1.4	Tsouris and Tavlarides Model	77
6.1.5	Luo and Svendsen Model	79
6.1.6	Martinez Bazán Model	80
6.2	Physical Models for the Determination of the Coalescence Frequency.....	83
6.2.1	Collision frequency.....	84
6.2.2	Coalescence Efficiency	86

7	Review of Most Important Constitutive Models for the One-Group Interfacial Area Transport Equation	89
7.1	Wu, Ishii and Kim – 1998	89
7.1.1	Modeling of Bubble Coalescence Due to Random Collision	89
7.1.2	Modeling of Bubble Coalescence Due to Wake Entrainment	91
7.1.3	Modeling of Bubble Breakup Due to Turbulence Impact	92
7.2	Hibiki and Ishii – 2000	93
7.2.1	Modeling of Bubble Coalescence Due to Random Collision	93
7.2.2	Modeling of Bubble Breakup Due to Turbulence Impact	94
7.3	Ishii and Kim – 2001	95
7.4	Yao and Morel – 2004	96
7.4.1	Modeling of Bubble Coalescence Due to Random Collision	96
7.4.2	Modeling of Bubble Breakup Due to Turbulence Impact	98
7.5	Wang – 2010	100
7.6	Comparison of the Bubble Coalescence and Breakup Frequency and Efficiency Terms	102
7.6.1	Bubble Coalescence Due to Random Collision	102
7.6.2	Bubble Breakup Due to Turbulence Impact	104
8	Implementation of the One-Group Interfacial Area Transport Equation in ANSYS CFX107	
8.1	The Computational Fluid Dynamics Code ANSYS CFX	107
8.2	Two-phase Flow Solution Methods	108
8.3	Additional Variable for the Interfacial Area Density Under the Form of a Transport Equation in ANSYS CFX	112
8.3.1	The Elimination of the Diffusion Term	112
8.3.2	Calculation of the Derivatives in the Source and Sink Terms	114
8.3.3	The Transformation of the Source and Sink Terms	114
9	Simulation of Upward Adiabatic Bubbly Flow with the State of the Art Available Models with ANSYS CFX 12.1	117
9.1	Upward Turbulent Adiabatic Bubbly Flow Experimental Data from Santos Mendez 2008	117
9.1.1	Description of the Experimental Facility	118
9.1.2	The Experimental Matrix	119
9.2	The ANSYS CFX Model	120

9.2.1	Definition of the Boundary Conditions and Fluid Domain Models	120
9.3	Mesh Sensitivity Analysis	122
9.4	Analysis of the Effects on the Simulation Results of the Interfacial Forces Models.....	125
9.4.1	Drag Force	126
9.4.2	Lift force.....	127
9.4.3	Wall Lubrication Force	129
9.4.4	Turbulent Dispersion Force	130
9.5	Analysis of the Effects on the Simulation Results of the Bubble Induced Turbulence (BIT) Modeling.....	131
9.6	Analysis of the Combined Effect on the Results of the Lift Force Coefficient and the Bubble Induced Turbulence Model	134
9.7	Analysis of the Simulation Results Using the Interfacial Area Density Transport Equation and the State of the Art Coalescence and Breakup Models.....	136
9.8	Conclusions of the Analysis	151
9.8.1	Main Conclusions for the Monodispersed Simulations.....	151
9.8.2	Main Conclusions for the Monodispersed Simulations Together with the Interfacial Area Transport Equation and the State of the Art Bubble Interaction Models	152
10	Development of New Bubble Interaction Terms for the One-Group Interfacial Area Transport Equation.....	155
10.1	Constitutive Models	157
10.1.1	Bubble Breakup	157
10.1.2	Bubble Coalescence	159
10.2	Main Conclusions of this Chapter	166
10.2.1	Bubble Breakup	166
10.2.2	Bubble Coalescence	168
11	Simulation of Upward Adiabatic Bubbly Flow Using the Newly Implemented One-Group Interfacial Area Constitutive Models in ANSYS CFX 12.1	171
11.1	Analysis of the Effects of Several Parameters on the Results.....	171
11.2	Results of the Simulations for Several Experimental Conditions	193
11.3	Main Conclusions of this Chapter	204
11.3.1	Main Conclusions of the Analysis of the Effects of Several Parameters on the Results	204
11.3.2	Main Conclusions of the Analysis for Several Experimental Conditions	205
12	Conclusions and Further Work.....	209

12.1	Conclusions	209
12.2	Further Work.....	209
	References.....	219
	Appendix A	229
	iacexpdivergence.F	229
	cfxgradientx.F	232

Nomenclature

Latin letters

Variable	Description	Units
A	Area	m^2
C	Constant	–
D	Particle/bubble diameter	m
	Turbulent energy spectrum,	
E	Aspect ratio, Energy	–
Eo	Eötvös number	–
	Interfacial force,	
F	Collision frequency per unit volume	
I	Turbulence intensity	–
K	Constant	–
L	Distance	m
Mo	Morton number	–
N	Particles/bubbles number	–
	Maxwell distribution function ,	
P	Pressure, R-squared value,	Pa
R	Source or sink term, Particle/bubble radius	m
Re	Reynolds number	–
	Source or sink term,	
S	Cross sectional collision area	m^2
Sc	Schmidt number	–
V	Volume	m^3
We	Weber number	–
a	Area density	$1/m$
a	Acceleration	m/s^2

	Distribution function,	
f	Factor,	
	Frequency	1/s
g	Gravitational acceleration	m/s ²
h	Mean distance between particles/bubbles	m
j	Mixture volumetric flux	m/s
k	Turbulence kinetic energy	m ² /s ²
l	Mean path length	m
n	Particle/bubble number density	1/m ³
	Pressure,	Pa
p	Probability	–
q	Heat flux	W/m ²
	Distance between two points,	m
r	Particle/bubble radius	m
t	Time	s
u	Velocity	m/s
v	Velocity	m/s
x	Position	–

Greek letters

Variable	Description	Units
Γ	Rate of mass production	kg/s
Π	Collision factor due to mean particle distance	–
	Kolmogorov constant	–
α	Gas volume fraction	–
	Asimmetry factor	–
β	Constant	–
	Distorsion factor	–
γ	Excluded volume factor	–
	Constant	–
ε	Turbulent energy dissipation	m ² /s ⁻³
	Rate of volume source per unit mixture volume	
η	Efficiency	–

μ	Dynamic viscosity	$Pa \cdot s$
ρ	Density	kg/m^3
σ	Surface tension	
	Stress	N/m^2
τ	Time constant	
	Time	
φ	Source and sink term	
ψ	Shape factor	–
	Specific turbulence dissipation	
ω	Mean frequency of turbulence	$1/s$
ϕ	Source and sink term	

Subscripts

Letter	Description
Bi	Birth
D	Drag
De	Death
De	Bubble - Eddy
F	Friction
L	Lift
RC	Random collision
S	Sauter
S	Surrounding
TD	Turbulence dispersion
TI	Turbulent Impact
W	Wake
WE	Wake entrainment
WL	Wall lubrication
b	Bubble, Breakup
	Critical,
c	Coalescence, Continuous

<i>cd</i>	Interface drag force
<i>coll</i>	Collision
<i>cr</i>	Critical
<i>d</i>	Distorted, Dispersed
<i>e</i>	Eddy
<i>f</i>	Frontal, Free
<i>g</i>	Gas
<i>h</i>	Horizontal
<i>i</i>	i-th component, interfacial
<i>i</i>	Impact, Interaction
<i>j</i>	j-th component
<i>k</i>	k-th phase
<i>l</i>	Liquid
<i>m</i>	Mean, Mixture
<i>p</i>	Particle average
<i>ph</i>	Phase change
<i>r</i>	Terminal, Relative
<i>ref</i>	Reference
<i>rel</i>	Relative
<i>rms</i>	Root mean square
<i>t</i>	Turbulent
<i>w</i>	Wall
<i>x</i>	Coordinate x
<i>y</i>	Coordinate y
<i>z</i>	Coordinate x
12	Bubbles 1 and 2 involved in the collision

Superscripts

Letter	Description
T	Turbulent
μ	Viscous

Symbols

Symbol	Description
'	Fluctuating component
	Parallel component
⊥	Normal component

Acronyms

BIT	Bubble Induced Turbulence	
BWR	Boiling Water Reactor	
CFD	Computational Fluid Dynamics	m
CHF	Critical Heat Flux	
DNS	Direct Numerical Simulation	
IATE	Interfacial Area Transport Equation	Units
LOCA	Loss Of Coolant Accident	
MUSIG	MUltiple Size Group	
PWR	Pressurized Water Reactor	
SST	Shear Stress Transport	
TH	Thermal Hydraulics	m^2
VOF	Volume Of Fluid	

Chapter 1

Introduction

In 2011, the total gross electric energy production in Germany has been about 614,5 TWh [DAtf 2012]. A 17.6% of the electricity has been produced by means of nuclear energy in the 17 nuclear power plants (NPPs) operating in the country until March 2011, and then by the 9 remaining on-line [DAtf 2012]. Since then, the base load electricity part related to nuclear energy reached the level of 39% of the total produced [DAtf 2012]. The average availability factor of the German NPPs has been historically higher than 90% [IAEA 2011], which means that nuclear plants have been providing energy to the grid almost continuously except for the planned outages prescribed by periodic maintenance. Given these conditions, a prerequisite for the safety analysis is to have on hand exact and reliable calculation tools.

In order to license a nuclear power plant (NPP) a broad range of analyses can be carried out by using 1D thermal-hydraulic Best Estimate (BE) codes (such as, for example, RELAP5, TRAC, TRACE, CATHARE and ATHLET) able to simulate the entire plant in transient and accident conditions. By using them, it is possible to simulate a wide variety of scenarios not only involving accident conditions, such as, for instance, Loss of Coolant Accidents (LOCAs), but also transients of interest for normal operation, like the insertion or extraction of control rods. These transients can be analyzed with the available coupled thermal-hydraulic-neutronic code systems which are capable of simulating the thermalhydraulic and neutronic behavior of a nuclear reactor with a high grade of reliability.

Nevertheless, the detailed study of asymmetries in the power and mass flow distributions inside the fuel assemblies, even using the coarse 3D flow capabilities available in some of the BE codes, is somehow beyond the scope of these coupled code systems.

A high degree of intra-fuel assembly flow spatial resolution can be achieved with Computational Fluid Dynamic (CFD) codes, They are able to reproduce detailed 3D flow phenomena at the level of single fuel rods, and can also consider turbulence and

its effect on the dynamics of the flow that determine local heat transfer phenomena of importance in the evaluation of fuel integrity. CFD codes yield very detailed velocity and temperature fields in the moderator, which can then be coupled to refined neutronic and fuel material descriptions in order to obtain an unprecedented degree of fidelity in the analysis of nuclear fuel behavior.

Nevertheless, simulating normal operation of Boiling Water Reactors (BWRs) or accidental conditions of Pressurized Water Reactors (PWRs) means to deal with the modelling of two-phase flows. CFD codes nowadays still do not allow to simulate in a reliable and accurate way their steady state or transient behavior. Experiments, theory and simulation of two-phase flow are still basic research themes and there remains a number of open issues yet to be investigated.

A two-phase flow is a fluid flow where two well defined phases consisting of the same or of two different substances, are flowing together along the same system. The range of application of two-phase flows is not only nuclear technology but many other's industrial processes. It can be found from refrigerators to internal combustion engines, distillation towers, phase separators, chemical reactors, boilers, crude oil transportation etc.

Among others subcategories, that of gas-liquid flows is one of the most complicated to be physically described and modeled. It is due mainly to the fact that these flows combine a deformable interface together with a compressible phase. It is possible to explain briefly such a concept if we consider the case of a vertical homogeneously heated tube as shown in Figure 1. It is possible to note how the flow develops by adopting a number of different configurations along the tube.

From the lower end up to the upper end of the pipe the flow transitions from single phase to two-phase conditions. In the lower pipe region the gas phase is dispersed and covers only a small percent of the total flow area. On the contrary, in the upper pipe region, the liquid phase is dispersed while the gas can be considered as continuous. As all the liquid phase is converted into vapour again a single phase gas flow moves along the pipe.

Current 1D thermal-hydraulic Best Estimate codes are reasonably able to deal with the dynamics of two-phase flow for most configurations as a whole; CFD codes can only approach the problem by simulating each flow condition separately. This is due to the fact that it is difficult to define locally the concept of two-phase flow regime and to

quantify it mathematically, since it is defined at a scale more similar to that of the whole system [Ishii and Hibiki 2006].

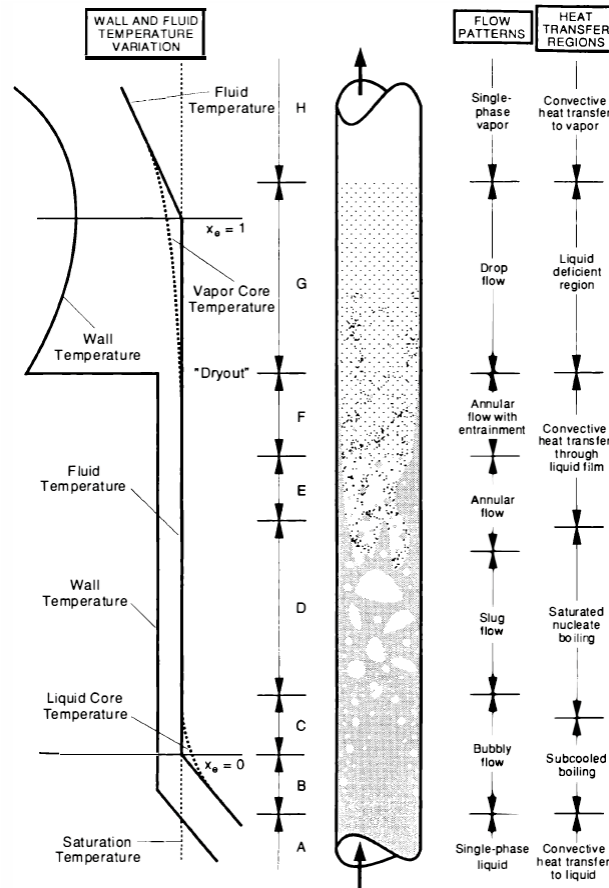


Figure 1: Regions of heat transfer in convective boiling [Todreas and Kazimi 1990]

Even for the cases in which CFD codes are capable of reproducing the Two-phase flow transient behavior, they are able to consider only very restricted computational domains (i.e. the case of Volume Of Fluid (VOF) technique) This is due to the high computational effort needed for simulation.

Ishii proposed a two-fluid model suitable for the analysis of transient phenomena, wave propagations and for flow regime changes [Ishii 1975]. In Ishii's approach each phase is considered separately and six conservation equations are written: 3 for each phase, for mass, momentum and energy. These equations are coupled through the so called jump conditions, which take into account the magnitude of the interchanges of mass, momentum and energy between the phases and are proportional to the interfacial area.

In the first two-fluid model formulation, no constitutive models for the interfacial area concentration were proposed and its determination relied on simple geometric

considerations. Later in 1995, Kocamustafaogullari and Ishii [Kocamustafaogullari and Ishii 1995] proposed to model the interfacial area concentration ($[m^2/m^3]$) by means of a transport equation and derived it based on the Boltzmann transport equation. The value of interfacial area concentration is modified along the flow path due to several effects. They are namely: particle volume change, change in pressure, interaction mechanisms between the phases and phase change phenomena.

The work reported in this Thesis represents the effort of implementing the interfacial area transport equation in CFD codes, in particular in the general purpose CFD code ANSYS CFX. If compared to the polydispersed calculation methods currently in use, since only one group of bubbles is considered in the interfacial area transport equation approach, there is no need to implement complicated and resources intensive integrals for the statistical determination of the size of the daughter bubbles produced after a coalescence or a breakup event. This aspect simplifies enormously the problem to be solved.

In the first part of the Thesis, the actual database of constitutive models, introduced and analyzed in detail in sections 7.1 to 7.5, for the determination of the bubble interaction mechanisms for the determination of the interfacial area change rate has been tested. In this analysis the monodispersed approach together with the self-implemented additional interfacial area transport equation and several constitutive models for bubble breakup and coalescence from the literature have been compared to the experimental data of Santos Mendez [Santos Mendez 2008]. These experimental data for upward adiabatic turbulent bubbly flow regime have been obtained thanks to the joint effort of the University of Valencia and the University Jaume I in Spain and have been made available to the NTech Department of Nuclear engineering of the Technische Universität München for the purposes above cited.

The main goals of this analysis are: testing the correct implementation of the additional transport equation and analyzing the influence of the results and the limits of the state of the art models present in the literature for its constitutive models. Formulations from [Hibiki and Ishii 2001], [Yao and Morel 2004], [Wu at al. 1998], [Ishii and Kim 2001] and [Wang 2010] have been implemented and tested.

Nevertheless, these models contain a number of empirical coefficients. For [Wu at al. 1998], [Ishii and Kim 2001] and [Hibiki and Ishii 2001] the empirical coefficients have been tuned to fit the 1D vertical evolution of the main flow parameters. In case of [Wang 2010], the new set of coefficients for the [Wu at al. 1998] model has been

obtained through a very time-and-resources-intensive calibration procedure for three-dimensional flow configurations. It means that they are not universal and modifying the flow conditions or the geometry of the system under exam would require the calibration of the model coefficients again.

As result of the analysis described above, the limits of the actual formulation have been understood and a new local, mechanistic formulation of bubble interaction models for coalescence and breakup for the one-group interfacial area transport equation has been developed, in agreement and within the limits of the actual theory.

The new formulation, non-geometry or configuration dependent, has been developed and implemented successfully in ANSYS CFX. The **breakup model** developed in the current work is based on the work of Martinez Bazán [Martinez Bazan 1998] where no closure parameters that can significantly alter the model behavior need to be set and no bubble breakup efficiency has to be defined. These two aspects linked together bring to a greater simplification the breakup problem. The current work represents the first attempt to model bubble breakup for the interfacial area transport equation by using the approach proposed in 1998 by Martinez Bazán. The bubble breakup model is based only on kinematic considerations and, if compared with previous formulations, is practically independent from tuning parameters. The bubble surface is deformed by the energy provided by the turbulent stresses generated by the surrounding fluid. Once these turbulent stresses overcome the surface tension stresses, breakup happens. Using this approach means that no bubble breakup frequency model is involved in the calculation. There is also no need to define an “a priori” size and energy content of turbulent eddies in the fluid flow. Another advantage of this model is that all the energy spectrum of turbulence is considered while other authors selected a specific range to obtain a better agreement with the experimental data.

For the coalescence process, the events due to the random collision of bubbles have been taken into account. In particular the flow-driven collisions. The result is the setup of a mechanistic and geometry independent set of expressions describing the coalescence probability and particle collision: both in frequency and duration. Uncertainties in this model are related to the determination of a correct collision cross sectional area. This area is derived from the kinetic theory of ideal gases and has been defined for rigid spheres, while in most industrial processes bubbles have a form far from spherical and the interfaces between the phases are constantly moving.

In order to define the **bubble coalescence** frequency, physical models for the bubble collision, liquid drainage and film rupture, for the collision efficiency, are needed.

The collision model, derived from the gas kinetic theory, has been based on the widely used collision of spheres behaving as ideal particles (see section 6.2.1). Coefficients are applied to take into consideration that bubbles in reality do not interact like ideal particles. This manner in which to define the bubble collision frequency is not new and other authors previously derived general expressions similar to the one presented here. However, in the current work attention has been concentrated on consistent sub-models based only on geometric consideration and neglecting, as much as possible, simplifications based on the order of magnitude of the phenomena described. The only consideration based on the order of magnitude that has been used, largely accepted in the literature, is that the eddies interacting with the bubbles possess a characteristic dimension of the same order of magnitude of the bubbles present in the system.

In order to calculate the collision efficiency, the widely used film drainage model (see section 6.2.2.3) has been used. The expressions used for the definition of the interaction and drainage time to calculate the coalescence efficiency are those proposed by Chesters and Hoffman in 1982. These models have yet not been used in the literature for the definition of constitutive terms for the interfacial area density transport equation. In the expression of the drainage time, the relative velocity of the centers of colliding particles has been defined consistently with the case of bubble collision explained above.

The new constitutive models introduced above have been implemented in ANSYS CFX and have been tested against data from the PUMA facility in Chapter 11, where a sensitivity analysis of the influence on the results for several parameters have been performed. It is clear that actual bubble dynamics models are based on sphericity or nearly sphericity assumptions and have a major influence on the results in chapter 9. In order to increase the accuracy of the results more experimental and theory work is needed to clarify the dependence of important flow parameters and to develop expressions for the determination of the bubble form or distortion based on local conditions. More work is expected in the next years in the field of bubble dynamics, because of the great influence of these parameters on the simulation results.

1.1 Outline of the Thesis

This thesis consists of four main parts.

The first part, Chapters 2 to 4, is an introduction regarding the theory of two-phase flow, turbulence and the most important models to simulate the dynamic behavior of two phase flows.

- In Chapter 2, the basics of two-phase flows, the flow regimes and their transition criteria for horizontal and vertical flows are presented.
- In Chapter 3, the basic concepts regarding turbulence, its main parameters and definitions are explained. Attention is paid to fluctuating velocities at two neighboring points under isotropic and homogeneous turbulent conditions.
- In Chapter 4, the modeling approaches for the simulation of two-phase flows are introduced. The two-fluid model and the limits of the actual calculation methods are presented. Furthermore, two-phase flow turbulence modeling and specific bubbly flow models are explained in detail.

In the second part, Chapters 5 to 7, the interfacial area transport equation is introduced and a literature review of the most important bubbles interaction models is presented.

- In Chapter 5, the interfacial area transport equation is derived from the more general Maxwell Boltzmann transport equation. Its physical meaning and the relation with the population balance equation are explained.
- In Chapter 6, the general form of source and sink terms for the one-group equation is derived from the multi-group population balance equation. Following this, a literature review regarding the coalescence and breakup models for the definition of bubble interaction terms for the one-group interfacial area transport equation is presented.
- Chapter 7 deals with the review of the most important constitutive models for the one-group interfacial area transport equation. The models are critically analyzed and the collision and breakup rates and the coalescence and breakup efficiencies to be obtained using the models are compared among them.

In the third part, Chapters 8 and 9, the state of the art bubbly flow simulation methods and models are used for the simulation of upward vertical bubbly flow conditions.

- In Chapter 8, the two-phase simulation methods available in the general CFD commercial code ANSYS CFX are presented. The differences in the theoretical

form of the interfacial area transport equation and that of the additional transport equation to be implemented in the code are shown. A solution to reduce the numerical diffusion and to implement the source and sink terms in the correct form in the code has been proposed.

- In Chapter 9, the PUMA experimental facility and the data used for validation are described. The computational domain, the boundary conditions and mesh sensitivity analysis are presented. Furthermore, simulation results using the state of the art simulation methods and models for upward adiabatic turbulent bubbly flow are reported.

In the fourth and last part, Chapters 10 and 11, new local and mechanistic constitutive models for one-group interfacial area transport equation are presented and tested.

- In Chapter 10, the inconsistencies in the use of the 1D definition of the bubble interaction terms for 3D simulations are explained. A new local mechanistic formulation of bubble interaction models for coalescence and breakup is presented.
- In Chapter 11, the effect on the simulation results of various model parameters and coefficient is shown in detail. Radial profiles of the main variables are shown in order to explain the behavior of the newly developed models. Several set of experimental data have been simulated in order to test the model for a wide range of flow conditions.

Chapter 2

Fluid-Dynamics of Two-Phase Flow

In this chapter the basics of two-phase flow, the regimes and the transition criteria for horizontal and vertical conditions are presented.

The joint flow of gas and liquid in pipes may result in many types of phase interaction patterns (flow regimes) depending on the values of flow variables. The two-phase flow hydrodynamics is strongly affected by these flow patterns; for instance, many of the pressure drop and hold-up correlations are flow pattern dependent. In general, a flow regime developed in a pipe flow is a strong function of the following variables [Saleh 2002]:

1. Angle of inclination,
2. Pipe diameter,
3. Gas and liquid flow rate,
4. Gas and liquid physical properties including densities, surface tension and viscosity.

2.1 Notation

The introduction to two-phase flow given here applies to one-dimensional two-phase flows in channels. It is derived from Yadigaroglu [Yadigaroglu 2008].

2.1.1 Averaging Operators

The parameters adopted in two-phase flow analysis are often averaged in time, area and space, and the following definitions are commonly used.

$$\langle f \rangle = \frac{1}{A} \int_A f \, dA \quad \text{Cross-sectional-average of a flow variable } f$$

$$\langle f_k \rangle_k = \frac{1}{A_k} \int_{A_k} f_k \, dA \quad \text{Phase cross-sectional-average of a phase flow variable } f_k$$

$$\bar{f} = \frac{1}{T} \int_T f dt \quad \text{Time or statistical average of a flow variable } f$$

$$\bar{f}_k^k = \frac{1}{T_k} \int_{T_k} f_k dt \quad \text{Phase time or statistical average of a phase flow variable } f_k$$

In the expressions above k represents the phase that, in case of a gas-liquid system can assume the values G (gas) or L (liquid). A is the cross-sectional area of the channel. A_k the area of the channel occupied by the phase k at a given instant. T is the total averaging time and T_k the sum of the presence time of the phase k at a given point.

2.1.2 Cross Sectional Phase Averages

The product of a phase related quantity f_k by the local phase fraction ε_k is equal to the product of the cross-sectional-average phase fraction $\langle \varepsilon_k \rangle$ by the average of the quantity calculated only over the area of the channel occupied by the particular phase $\langle f_k \rangle_k$:

$$\langle \varepsilon_k f_k \rangle = \langle \varepsilon_k \rangle \langle f_k \rangle_k .$$

However, in general

$$\langle fg \rangle \neq \langle f \rangle \langle g \rangle .$$

2.1.3 Definition of Main Variables

The **flow quality**, or simply **quality**, x is defined as the ratio of the gas flow rate to the total flow rate of the phases

$$x \equiv \frac{\dot{M}_G}{\dot{M}} .$$

It is also valid

$$1 - x \equiv \frac{\dot{M}_L}{\dot{M}} .$$

The flow quality is different from the thermodynamic static quality, which is, in fact, the ratio of the mass of steam on the total mass of mixture.

The **enthalpy of the mixture** h is given as:

$$h = x \langle h_L \rangle_L + (1 - x) \langle h_G \rangle_G ,$$

where $\langle h_L \rangle_L$ and $\langle h_G \rangle_G$ are the cross-sectional averages of the phase enthalpies.

The **local statistical or time average void fraction** is defined as the presence time of the gas phase at a given point:

$$\bar{\varepsilon}_G = \frac{T_G}{T}.$$

It is also valid

$$1 - \bar{\varepsilon}_G \equiv \bar{\varepsilon}_L = \frac{T_L}{T}.$$

T_k is the summation of all the times during which phase k is present at the measuring point and T is the total period of observation.

The **cross-sectional-averaged instantaneous void fraction** is the fraction of the cross-section occupied at a given instant by the gas:

$$R_G \equiv \frac{A_G}{A}.$$

For the liquid phase it is valid:

$$1 - R_G \equiv R_L \equiv \frac{A_L}{A},$$

A_G is the area occupied at a given instant by the gas and A to total cross-sectional area. Because of the commutativity of the space ($\langle \rangle$) and time ($\bar{}$) averaging operations, we have:

$$\langle \bar{\varepsilon}_k \rangle = \bar{R}_k.$$

To simplify the notation in the following parts of this work the bar, meaning time average, is neglected and the time and cross-sectional averages of gas and liquid fraction will be expressed as $\langle \varepsilon_G \rangle$ and $\langle \varepsilon_L \rangle$ respectively. The local time average values will be ε_G and ε_L . A very common notation, when the context is clear is, for simplicity $\langle \alpha \rangle$ and α for the cross sectional-averaged void fraction and $\langle 1 - \alpha \rangle$ and $1 - \alpha$ for the liquid fraction.

The **mixture density** $\langle \rho \rangle$ is a void fraction (or volume) weighted quantity (total mass over total volume):

$$\langle \rho \rangle \equiv \frac{M}{V} = \frac{M_G + M_L}{V_G + V_L} = \frac{\rho_G V_G + \rho_L V_L}{V_G + V_L} = \rho_G \langle \alpha \rangle + \rho_L \langle 1 - \alpha \rangle.$$

The (true) **cross-sectional-averaged phase velocities** are given by

$$\langle u_k \rangle_k = \frac{\dot{M}_k}{\rho_k A_k} = \frac{\dot{M}_k}{\rho_k \langle \varepsilon_k \rangle A} = \frac{\dot{m} x_k}{\rho_k \langle \varepsilon_k \rangle},$$

where the **mass fluxes** are defined as the mass flow rates per unit total flow area

$$\dot{m} = \frac{\dot{M}}{A},$$

$$\dot{m}_k \equiv \frac{\dot{M}_k}{A} = \frac{\dot{M}x_k}{A} = \dot{m}x_k.$$

The **total mass flux of the mixture** is related to the phase velocity and the void fraction by:

$$\begin{aligned}\dot{m} &= \frac{\dot{M}}{A} = \dot{m}_G + \dot{m}_L = \frac{\dot{M}x}{A} + \frac{\dot{M}(1-x)}{A} = \frac{\rho_G \langle u_G \rangle_G A_G + \rho_L \langle u_L \rangle_L A_L}{A} \\ &= \rho_G \langle u_G \rangle_G \langle \alpha \rangle + \rho_L \langle u_L \rangle_L \langle 1 - \alpha \rangle.\end{aligned}$$

The **volumetric flow rates** Q_k are defined as

$$Q_L = \frac{\dot{M}_L}{\rho_L}, Q_G = \frac{\dot{M}_G}{\rho_G} \text{ and } Q = Q_L + Q_G.$$

The **cross-sectional averaged volumetric fluxes**, the volume flow rates per unit total flow area are defined as follows:

$$\langle j_G \rangle = \frac{Q_G}{A} = U_{sG}, \langle j_L \rangle = \frac{Q_L}{A} = U_{sL},$$

and the **total or mixture volumetric flux** is

$$\langle j \rangle = \langle j_G \rangle + \langle j_L \rangle.$$

These volumetric fluxes are cross-sectional-average quantities. Their units are m/s and, for this reason, the channel-average volumetric fluxes are also called **superficial phase velocities** U_{sG} and U_{sL} . They are the velocities that the phase would have if they were flowing alone in the pipe:

$$\langle j_k \rangle = \frac{Q_k}{A} = \frac{\dot{M}_k}{\rho_k A} = \langle u_k \rangle_k \langle \varepsilon_k \rangle.$$

The **local volumetric fluxes** are defines as:

$$j_k = u_k \varepsilon_k,$$

that are the values that the $\langle j_k \rangle$ would assume if the channel dimensions shrink to a point.

The true and the superficial velocities of volumetric fluxes are related as follows:

$$\langle u_G \rangle_G = \frac{1}{A_G} \int_{A_G} u_G dA = \frac{\langle j_G \rangle}{\langle \alpha \rangle} = \frac{U_{sG}}{\langle \alpha \rangle},$$

and

$$\langle u_L \rangle_L = \frac{1}{A_L} \int_{A_L} u_L dA = \frac{\langle j_L \rangle}{\langle 1 - \alpha \rangle} = \frac{U_{sL}}{\langle 1 - \alpha \rangle}.$$

The local variables are related as expressed as follows:

$$j_L = (1 - \alpha)u_L,$$

$$j_G = \alpha u_G,$$

$$j = j_G + j_L.$$

The ratio of the average gas and liquid velocities is called **velocity ratio**. Customary, it is also possible to refer to it as **slip ratio** S .

$$S = \frac{\langle u_G \rangle_G}{\langle u_L \rangle_L}.$$

It is possible to express S in function of the void fraction and the quality:

$$S = \frac{\frac{\dot{m}x}{\rho_G \langle \varepsilon_G \rangle}}{\frac{\dot{m}(1-x)}{\rho_L \langle \varepsilon_L \rangle}} = \frac{\frac{x}{\rho_G \langle \varepsilon_G \rangle}}{\frac{(1-x)}{\rho_L \langle \varepsilon_L \rangle}} = \frac{x}{1-x} \frac{\rho_L \langle \varepsilon_L \rangle}{\rho_G \langle \varepsilon_G \rangle} = \frac{x}{1-x} \frac{\rho_L \langle 1-\alpha \rangle}{\rho_G \langle \alpha \rangle},$$

which is a triangular relationship between S , $\langle \alpha \rangle$ and x . If only two of these quantities are known, the third can be obtained.

2.2 Main Two-Phase Flow Regimes

Many descriptions of the several two-phase flow regimes can be found in the literature. Here, a brief description of the most important two-phase flow regimes in both vertical and horizontal conditions based on Saleh [Saleh 2002] is given. Figure 2 and Figure 3 show a schematic representation of the main two-phase flow regimes.

2.2.1 Stratified Flow

In stratified flow, a distinct horizontal surface boundary separates the liquid and the gas phases. Liquid flows in the lower section of the pipe while gas flows above it. This flow pattern is characterized by low gas and liquid flow rates, which results in the gravity force acting on the liquid being much higher than the drag forces acted on the liquid by the gas-phase. Depending on the smoothness of the gas-liquid surface, many other terms may be used such as: 1) stratified smooth, 2) stratified wavy. The wavy behavior appears at higher gas flow rates. Stratified flow does not occur in pipes with an upward inclination of more than one degree, it is the most common flow pattern in pipes with downward inclination [Saleh 2002]. The stratified wavy flow regime is referred to as wavy flow by many investigators. Stratified flow is also known as segregated flow.

2.2.2 Slug Flow

As the liquid flow rate increases in a stratified wavy flow, the liquid waves grow higher until they fill the entire pipe section at irregular intervals forming a slug flow. The slug flow is characterized by alternating slugs of liquid and large gas bubbles. The term plug flow may be used to characterize a slug flow with a smaller gas volume fraction. Slug flow is a common flow regime in horizontal or near horizontal and upward vertical or near vertical flow. In upward vertical flow, slugs are characterized by a smaller size than that in the horizontal flow. Slug flow may cause serious problems due to vibrations and corrosion. For this reason, slug catchers are normally inserted to eliminate slug formation in many installations. Other terms used by many investigators to describe this flow include: plug flow, intermittent flow, churn flow, etc. Slug flow may be classified into terrain slug or hydrodynamic slug based on the initiation mechanism. In terrain slug, the gravity forces due to the topography of the hilly terrain causes the liquid to accumulate in the lower pipe sections as the gas pressure increases, liquid will be pushed and slug flow will form. A hydrodynamic slug is initiated by the instability of waves on the gas-liquid interface in stratified flow under certain conditions.

2.2.3 Annular Flow

In annular flow, the liquid flows as a film around the inner circumference of the pipe, while gas flows in the center. Liquid mist or droplets may be carried in the pipe center due to the high speed of the gas. As the gas velocity increases, the film thickness decreases and more liquid is carried by the gas phase as a mist. For a given flow rate, the liquid film thickness in a vertical flow is uniform, however, in horizontal flow, due to gravity, the liquid film thickness is larger at the bottom of the pipe. Annular flow is very common in most high-pressure gas transfer lines and may exist for any angle of inclination. Depending on the ratio of mist entrained and film thickness, this flow may be referred to as annular-mist (low ratio) or mist flow (high ratio).

2.2.4 Bubbly Flow

Dispersed bubbly flow is the opposite of annular flow. The liquid-phase is the continuous flow while gas flows as dispersed entrained bubbles. As the gas flow rate increases, bubbles start to grow in size and plug or slug flow starts to form. Bubbly flow is very common in upward vertical flow lines and also in horizontal ones with high liquid flow rates.

The boundaries of flow regimes are not easily defined. Rather the gradual change between them may contain a combination of many flow patterns fluctuating until a stabilized distinct pattern characterizes the new flow regime once again.

In paragraph 4.3, modeling of bubbly flow is explained in detail.

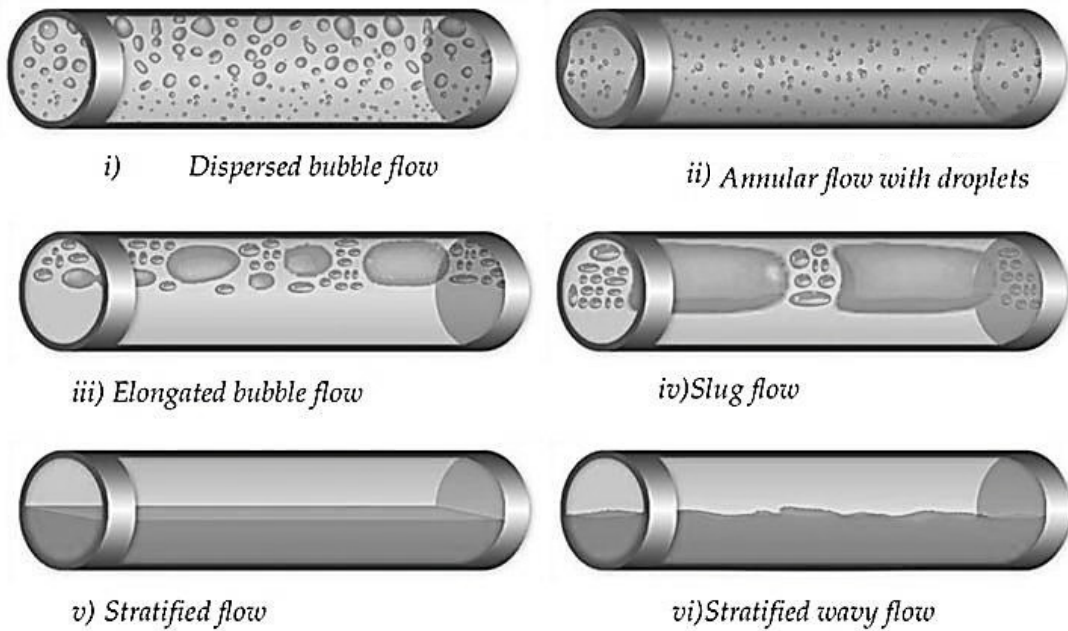


Figure 2: Gas-liquid flow regimes in horizontal pipes [Bratland 2009]

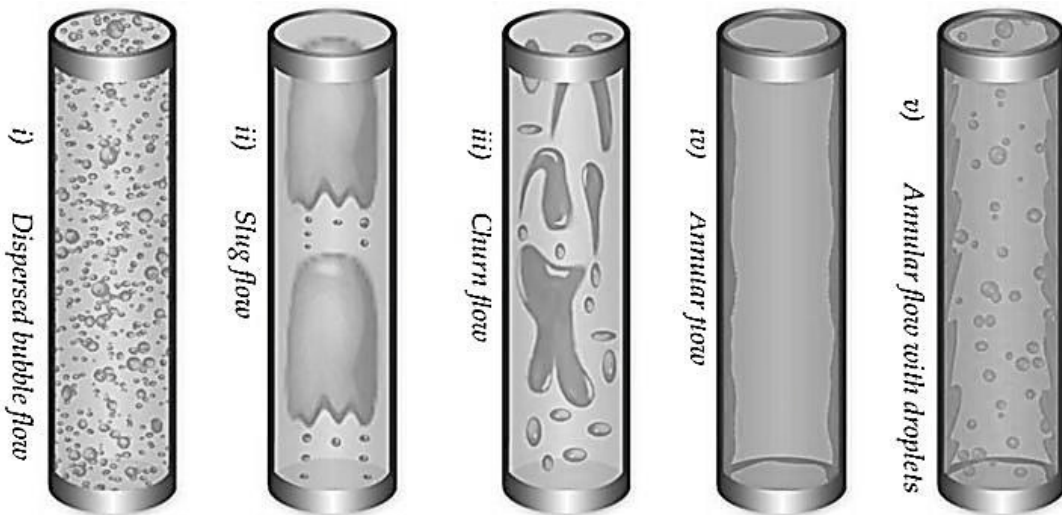


Figure 3: Gas-liquid flow regimes in vertical pipes [Bratland 2009]

2.3 Two-Phase Flow Classification Based on Interfacial Structure

Following Ishii and Hibiki [Ishii and Hibiki 2006], two-phase flow can be classified according to the geometry of the interfaces into three main classes, namely, separated flow, transitional or mixed flow and dispersed flow as shown in Figure 4. This second classification based on the interface structures and the topographical distribution of each phase is far more difficult to make, since these interface structure changes occur continuously [Ishii and Hibiki 2006].


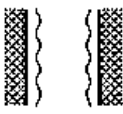



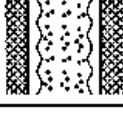
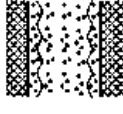
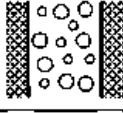
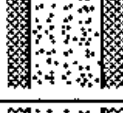
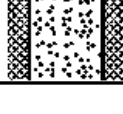
Class	Typical regimes	Geometry	Configuration	Examples
Separated flows	Film flow		Liquid film in gas Gas film in liquid	Film condensation Film boiling
	Annular flow		Liquid core and gas film Gas core and liquid film	Film boiling Boilers
	Jet flow		Liquid jet in gas Gas jet in liquid	Atomization Jet condenser
Mixed or Transitional flows	Cap, Slug or Churn-turbulent flow		Gas pocket in liquid	Sodium boiling in forced convection
	Bubbly annular flow		Gas bubbles in liquid film with gas core	Evaporators with wall nucleation
	Droplet annular flow		Gas core with droplets and liquid film	Steam generator
	Bubbly droplet annular flow		Gas core with droplets and liquid film with gas bubbles	Boiling nuclear reactor channel
Dispersed flows	Bubbly flow		Gas bubbles in liquid	Chemical reactors
	Droplet flow		Liquid droplets in gas	Spray cooling
	Particulate flow		Solid particles in gas or liquid	Transportation of powder

Figure 4: Classification of two-phase flow (Ishii, 1975) [Ishii and Hibiki 2006]

2.4 Two-Phase Flow Regimes Maps and Transition Criteria

2.4.1 Flow Regime Maps

It is necessary to determine flow regimes as a basis for carrying out calculations on two-phase flow [Hewitt 2012]. The usual procedure is to plot the available information in terms of a flow regime map (i.e. Figure 5) which is shown in terms of primary flow variables such as, for instance, superficial velocity of the phases or mass flux and quality. The maps presented below are those obtained by Taitel and coworkers. Of course, they are not the only ones to be found in the literature, as different authors have developed their own maps tailored to specific conditions. They are intended to be representative of an intensive work conducted in the past decades on gas-liquid mixtures flows.

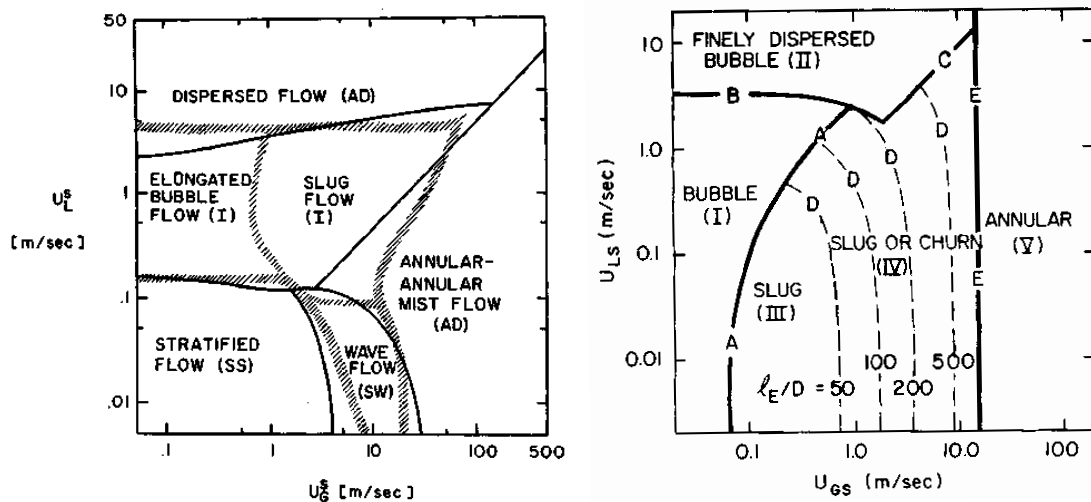


Figure 5: Effect of gas and liquid superficial velocity on flow regimes in horizontal (left) [Taitel et al. 1976] and in vertical upward flow (right) [Taitel et al. 1980]

A flow regime map is a simplified method to give some prediction of the particular flow pattern likely to occur for a given set of local variables [Collier and Thome 1994]. The experimental approach has been to collect data for many different flow rates and fluid properties and to visually observe the flow pattern through a transparent test section window [Taitel et al. 1976]. Then a search is undertaken for a way to map the data in a two-dimensional plot by locating transition boundaries between the regimes (the lines reported in the diagrams of Figure 5). The respective sets of data collected in this way are represented as areas on a graph, the coordinates of which are the actual superficial phase velocities or some generalized variables containing these velocities

[Collier and Thome 1994]. A real 3D flow pattern is influenced by a number of secondary variables and it is impossible to show their influence by means only of a two-dimensional plot. The limitation of using the actual superficial phase velocities for the axes of the map restricts its applicability to only a particular situation, while the choice of a more generalized variable may be adequate to represent a particular transition process; it is unlikely that the same variable will also be suitable to describe a different transition governed by a different balance of forces [Collier and Thome 1994].

There has been a great deal of work aimed at generalizing the plots, so that they can be applied to a wider range of channel geometries and physical properties of the fluids [Hewitt 2012]. In fact, the main objective of the experimental work carried out in the past decades work has been to suggest physically based mechanisms which underlie each transition and to model them based on these mechanisms [Taitel 1980]. In this way, the results may be applicable to a wider range of properties and pipe sizes than would be expected from empirically determined transitions [Taitel 1980].

Taitel et al. compared several flow regime maps from the literature. The maps they analyzed proposed transition boundaries in a two-dimensional coordinate system as determined from their own experiments and, in other cases, coming from observations of third part work. They pointed out that limits in the analysis occurs both if dimensional or dimensionless coordinates systems are used for the definition of the maps coordinate system.

For instance, in case of **dimensional coordinates** such as superficial velocities or superficial momentum flux, given any single pipe size and set of fluid properties, these coordinates will map the transitions. There is no reason to expect that the location of these transition curves will be unchanged for changes in superficial velocities or superficial momentum flux. Taitel et al. also reported that attempts had been performed to modify these dimensional coordinates for systems other than air-water by considering property ratios between the fluids of interest and that of the air-water system. However, their conclusion had been that there is no basis in theory to suggest this generalizes the results in any way.

In case of **dimensionless coordinates**, the nondimensionalization process had been performed in the hope that the results would apply to pipe sizes and fluid properties other than those of the data used to locate the transition curves. The conclusions of the Taitel at al. analysis had been that, in the absence of a theoretical basis, the use of

dimensionless coordinates is no more general than the use of dimensional ones and that one pair of dimensionless groups does not characterize the variety of transition boundaries that may exist.

In the next paragraph an overview of some flow patterns transition criteria from the literature is presented for vertical flow, as an example.

2.4.2 Transition Criteria for Vertical Flows

In order to predict the conditions under which transition between flow patterns will take place, it is essential to understand the physical mechanisms by which such transitions occur. Fluid properties and pipe size play an important role, as already mentioned. Unfortunately, there is considerable disagreement among authors as to the mechanism for these transitions [Taitel et al. 1980].

2.4.2.1 The Bubbly to Slug Transition

Transition from the condition of dispersed bubbles to slug flow observed at low gas rates requires a process of agglomeration or coalescence [Taitel et al. 1980]. In this way discrete bubbles combine into larger vapour space having a diameter near to that of the pipe. The length of such formations is 1 to 2 pipe diameters, which can be observed at the transition to slug flow. As the gas rate is increased the amount of gas in the pipe is increased. The bubbles are now much closer and this results in an increase of the coalescence rate. This is compensated by the fact that, as the liquid rate increases, the turbulence fluctuations associated with the flow can cause the breakup of larger bubbles resulting from the coalescence process. The dispersed bubbly flow can be maintained if the breakup rate is sufficiently high to prevent re-coalescence [Taitel et al. 1980]. If the gas is introduced at very low gas flow rates into a column of liquid flowing at low velocity the gas phase is distributed into discrete bubbles. If they are very small behave as rigid spheres rising vertically and rectilinearly. Above a critical size (about 15 mm for air water at low pressure), the bubbles are deformed and move following a zigzag path randomly. They collide and coalesce forming occasionally larger individual spherical cap bubbles very similar to Taylor bubbles but with diameter smaller than the pipe. Increasing the gas flow rate, while keeping low the liquid flow rate, the bubble packing increases and a point is reached at which the dispersed bubbles become so closely packed that many collisions occur and the coalescence rate to larger bubble increases sharply. This process described by Taitel et al. is the transition to slug flow and the value of the void

fraction at which this happen is around 0.25 to 0.3. Taitel et al. considering the transition happening at $\alpha = 0.25$ wrote the following equation characterizing this transition for conditions where the dispersion forces are not dominant:

$$U_{sL} = 3.0U_{sG} - 1.15 \left[\frac{g(\rho_L - \rho_G)\sigma}{\rho_L^2} \right]^{1/4} .$$

2.4.2.2 The Slug to Churn Transition

The slug flow pattern develops from a bubbly flow pattern if enough small bubbles coalesce to form Taylor bubbles. If the liquid slug between two consecutive Taylor bubbles is so small to be stable, then the churn regime develops. Taitel et al. [Taitel et al. 1980] presented the theory that the churn flow is essentially a developing length region for slug flow and proposed a maximum entry length or length for churn flow l_e at which it is likely to appear:

$$\frac{l_e}{D} = 40.6 \left(\frac{\langle j \rangle}{\sqrt{gD}} + 0.22 \right) .$$

If a position along the tube length is shorter than the developing length, churn or slug flow may be observed. If the developing length is short relative to the position of interest along the tube only slug flow exists. In Figure 5 right, this situation is represented by the D-lines for different value of the ratio l_e/D . Such a flow regime map is valid for air-water at 25°C and 0.1 MPa in 50 mm diameter tubes.

2.4.2.3 The Slug/Churn to Annular Flow Transition

For high gas flow rates the flow becomes annular. The liquid film flows upwards adjacent to the wall and gas flows in the center carrying entrained liquid droplets. The upward flow of the liquid film against gravity results from the forces exerted by the fast moving gas core. This film has a wavy interface and the waves tend to shatter and enter the gas core as entrained droplets. For this transition, Taitel et al. argued that the gas velocity should be sufficient to prevent liquid droplets from falling and bridging between the liquid films. In fact, when the gas flow rate is insufficient, the droplets fall back, accumulate, form a bridge, and churn or slug flow takes place [Taitel et al. 1980].

The minimum gas velocity to suspend a drop is determined from the balance between gravity and drag forces acting on it so that [Taitel et al. 1980]:

$$U_{sG} = \frac{2}{\sqrt{3}} \left[\frac{g(\rho_L - \rho_G)d}{\rho_G C_D} \right]^{1/2} ,$$

where d is the drop diameter and C_D is the drag coefficient that will be introduced later.

Chapter 3

Introduction to Turbulent Flows

In this chapter basic concepts regarding turbulence, its main parameters and definitions are explained. Particular attention is paid to fluctuation velocities at two neighboring points under isotropic and homogeneous turbulent conditions.

The instability that typically occurs in a laminar flow, with the increase of its kinetic energy in relation to viscous forces, gives rise to a turbulent flow. Turbulence is mainly characterized by fluctuations of the speed which are self-sustaining and lead to a considerable complexity of the flow. The fluid motions that are observed frequently in nature and industry are characterized by sufficiently high values of the Reynolds number to be considered turbulent.

With reference to the case of a single-phase fluid moving in a duct, it is known that at sufficiently large distance from the inlet section occurs that the flow becomes fully developed and it behaves independently from the entrance conditions. In this new state, the turbulence assumes the typical characteristics explained in the next paragraphs.

Turbulence will greatly influence the exchange of mass, momentum and energy. Its detailed simulation is still a problem of tremendous scope and object of extensive research work. It is possible to approach the problem from a macroscopic point of view, for instance, and to obtain the shear stress at the wall or to calculate the profile of average speed in the vicinity of a wall or even the mass transfer rate in exchange processes involving multiple phases or components in a turbulent flow. For this purpose, it is customary to characterize the turbulence statistically with reference to the effect that the turbulent structures have on the variables that characterize the motion of the fluid [Panton 1996].

In the following sections some basic concepts about turbulence are presented [Panton 1996, Wilcox 1993] with the aim of explaining topics used in this Thesis.

3.1 Types of Turbulent Flows

Turbulent flows have different characteristics depending on the boundary conditions imposed on the motion. For example, a turbulent jet has different characteristics from a turbulent flow of a fluid in a duct.

It is possible to classify roughly turbulent flows into three groups [Panton 1996]:

- Turbulence due to the presence of grids ("grid-like")
- Wall turbulence (in the boundary layer or in ducts)
- Mixing layers ("free shear layers" - i.e. wake and jets)

The "**grid-like**" turbulence is not self-sustaining. It is obtained artificially by placing perpendicular to the flow direction a grid of cylinders with a circular section. The vortices generated by the passage of fluid through the grid interact with each other and, at a certain distance from it, a field of turbulence relatively homogeneous and isotropic is achieved. This means that the turbulence has equal intensity in all directions and decays slowly so that its variations in the different directions are not important.

In the case of **wall turbulence**, the fluid interaction with a solid surface has a dominant effect on the processes that generate turbulence. In particular, the characteristics of the turbulence in these cases exhibit non-uniformity and anisotropy. The presence of a wall has a dominant effect on the processes that generate turbulence. The turbulent characteristics of flow in a pipe are determined by the wall and the presence of a fluid core region and the presence of the wall on the other side play only a minor role [Panton 1996]. In this category one can also include boundary layers and all internal flows.

Free shear layer flows include not only the typical mixing layer between two fluids moving at different velocities, but also all sorts of jets and wakes. A transition region near the origin of these flows precedes the turbulent region.

3.2 Main Characteristics of Turbulent Flows

There is no rigorous definition of turbulent flows, but what is called turbulent does have certain common properties. Turbulent flows have irregular fluctuations of velocity in all three directions. The intensity of the fluctuations is variable and is around 10% to 30% of the mean velocity [Panton 1996]. A time history of the velocity at a point looks like a

random signal. Nevertheless, there's a structure to the fluctuations, so it's not absolutely accurate to say that the fluctuations are random.

The irregularities in the velocity field have certain spatial structures known as eddies. This term may be applied to any spatial flow pattern that persists for a short time. An eddy may be like a vortex, an imbedded jet, a mushroom shape, or any other recognizable form. These structures are not isolated in the flow, small eddies exist inside larger eddies, and even smaller eddies exist inside the small eddies. One of the main characteristic of turbulence is a continuous distribution of eddy sizes.

The rigorous way to decide whether a fluid is turbulent or non-turbulent is based on vorticity. By definition turbulent fluid has vorticity, non-turbulent fluid does not. Turbulent flows are also diffusive: a turbulent eddy can transport fluid from a region of low momentum and deposit it in a region of high momentum. Although the actual process is more complicated than this, it is clear that turbulence tends to mix fluids and thereby has a diffusive effect. The term eddy diffusion is frequently used to distinguish this effect from molecular diffusion. Eddy diffusion can be 10 or 100 times stronger than molecular diffusion [Panton 1996].

All turbulent flows involve processes that change the length scale of the eddies but not much is actually known about these processes that can act in two directions: a modest-size irregularity or eddy grows and becomes a large eddy, or the inverse process also occurs and reduces the eddy size. Turbulent eddies are continually formed with smaller and smaller length scales. There are, however, limits to these processes. The dimensions of the system are the upper bound; the lower bound, instead, is fixed by the viscosity: when the dimension of an eddy becomes very small, viscous forces, because of the steep velocity gradient, become very important and no smaller eddies are then possible.

The last important characteristic of turbulent flows is that they are dissipative. Any flow with viscosity has viscous dissipation, but turbulent flows have much more of it because the small-scale eddies have sharp velocity gradients. The energy dissipated in the small eddies dominates that dissipated in the large eddies. Since the small eddies dissipate energy and tend to destroy themselves, the scale-changing process that produces smaller eddies is a necessary element of self-sustaining turbulence [Panton 1996].

3.3 Reynolds Decomposition Principle

The direct solution of the Navier-Stokes equations in problems of technical interest is an interesting field of research (DNS: Direct Numerical Simulation). It is currently used as a source of data for the validation of macroscopic models of turbulence. However, it requires computational resources that are still too large if compared to the potential of modern computers when problems of practical importance are considered. This is due to the fact that wide time and length scale ranges are involved in the calculations.

Often, a less time and resources intensive approach, the so-called statistical methods for the analysis of turbulence are preferred. These allow to express in terms of average variables and amplitude of fluctuations the balance equations needs for the turbulent flow description.

The basic approach is still the same to that Reynolds used when he proposed to decompose the instantaneous velocity into a mean and a fluctuating component. Figure 6 shows the behaviour of a fluctuating variable along the time coordinate. It is possible to notice the decomposition into two, mean and fluctuating, components.

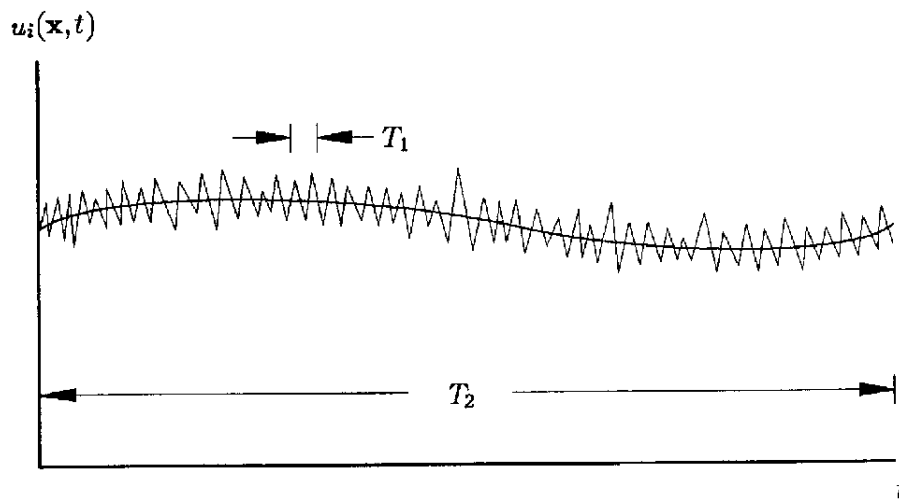


Figure 6: Velocity as a function of the time in a turbulent flow [Wilcox 1993].

Given a point in the flow, the time evolution of any one of its variables, can then be decomposed as follows

$$u_i = \bar{u}_i + u'_i, \quad (\text{Eq.1})$$

where \bar{u}_i represents the time averaged quantity of the i -th component of the velocity vector and u'_i the fluctuating one. By definition the time-average of a purely fluctuating quantity is zero. In the next paragraphs and chapters only time averaged quantities will be taken into consideration unless explicitly stated.

3.4 Turbulence Intensity and Turbulence Kinetic Energy

Based on the fluctuating component of the velocity, it is possible to define several parameters of interest for the study of turbulence.

In particular, the relative turbulence intensity is defined as the ration of the root mean square value of the fluctuation velocity referred to the mean velocity of the flow [Turns 2000]:

$$I = \frac{u'_{rms}}{\bar{u}} = \frac{\sqrt{\frac{1}{3}(u_x'^2 + u_y'^2 + u_z'^2)}}{\bar{u}}, \quad (\text{Eq.2})$$

where u'_{rms} is called the absolute turbulence intensity.

In case of isotropic turbulence, $u'_x = u'_y = u'_z$, so for the turbulence intensity is valid the following relationship $I_x = I_y = I_z$.

The turbulence kinetic energy is defined as [Wilcox 1993]

$$k = \frac{1}{2}(\overline{u_x'^2} + \overline{u_y'^2} + \overline{u_z'^2}) = \frac{3}{2}u_{rms}'^2. \quad (\text{Eq.3})$$

3.5 Length Scales in Turbulent Flows

In the turbulence literature, the following four scales are of general relevance and are also frequently cited [Tennekes and Lumley 1972].

- L characteristic flow width or macroscale
- l_0 integral scale or turbulence macroscale
- l_λ Taylor microscale
- l_K Kolmogorov microscale

The **characteristic flow width** or **macroscale** is the largest length scale of the system and represents also the upper bound for the largest possible eddies. For example, in a pipe flow the largest eddy would be equal to the pipe diameter. In general, this length scale is used to define a Reynolds number based on a mean velocity of the flow, but not to define a turbulent Reynolds number, as for the other three scales.

The **integral scale** or **turbulence macroscale** physically represents the mean size of the large eddies in a turbulent flow. These eddies have low frequency and large wavelength. However, it's always smaller than the characteristic L , but of the same order of magnitude. It can be evaluate by integrating the correlation coefficient of the fluctuating component of the velocity $R_i(r)$, obtained as a function of the distance

between two points in the flow. Along the generic i -th coordinate the integral scale or turbulence macroscale l_0 is [Turns 2000]

$$l_0 = \int_0^{\infty} R_i(r) dr, \quad (\text{Eq.4})$$

where

$$R_i(r) = \frac{\overline{u'_i(0)u'_i(r)}}{u'_{i,rms}(0)u'_{i,rms}(r)}. \quad (\text{Eq.5})$$

Qualitatively, it represents the mean distance between two points in the flow where the velocity correlation between the fluctuating velocities is other than null.

The **Taylor scale** is between the largest and the smallest scales which make **the inertial subrange**. Taylor micro-scales are not dissipative scales but pass down the energy from the largest to the smallest without any dissipative effects. **Taylor micro-scales play a dominant role in energy and momentum transfer**. It can be mathematically formulated as follows [Turns 2000]:

$$l_\lambda = \frac{u'_{i,rms}}{\left[\left(\frac{\partial u_i}{\partial x_i} \right)^2 \right]^{\frac{1}{2}}}. \quad (\text{Eq.6})$$

The **Kolmogorov length scale** is the smallest scale associated with a turbulent flow and represents the dimension at which the dissipation of turbulent kinetic energy to fluid internal energy occurs. It's the scale at which the molecular effects, like for example, the kinematic viscosity, are significant. It is linked with the energy dissipation rate ε and it is formulated as follows [Turns 2000]:

$$l_K \approx \left(\frac{\nu^3}{\varepsilon} \right)^{\frac{1}{4}}, \quad (\text{Eq.7})$$

where ν is the kinematic viscosity and

$$\varepsilon \approx \frac{3 u'_{i,rms}{}^3}{2 l_0}. \quad (\text{Eq.8})$$

3.6 Conservation Equations for Turbulent Flows

The equation governing laminar flows may also be applied to turbulent ones. Given the non stationarity of a turbulent flow, it is necessary to consider the transient terms also in the cases where the boundary conditions are constant with the time [Panton 1996, Wilcox 1993].

In continuum mechanics, models are formulated in terms of differential conservation equations for the mass momentum and energy that are written together with closure relationships. These can be the equation of state or the equations defining the components of the stress tensor, the thermal fluxes or the chemical reactions involved in the problem [Ishii and Hibiki 2006].

In practice, most two-phase flow systems have extremely complicated interfacial geometries and motions. For this reason it is not possible to solve the equations for local instant motions of the fluid particles. Such a level of detail is rarely needed for an engineering problem, but rather macroscopic aspects of the flow are much more important [Ishii and Hibiki 2006]. It is possible to obtain the mean values of fluid motions and properties that effectively eliminate local instant fluctuations if a proper averaging procedure is applied. It is possible to see the averaging as low-pass filtering, excluding unwanted frequency signals coming from local instant fluctuations [Ishii and Hibiki 2006].

3.6.1 Mass and Momentum Conservation Equations

In case of an incompressible Newtonian fluid, using the Einstein notation, it is possible to write the following general conservation equations for mass and momentum [Turns 2000]:

$$\frac{\partial u_i}{\partial x_i} = 0, \quad (\text{Eq.9})$$

$$\rho \left(\frac{\partial u_i}{\partial t} + u_j \frac{\partial u_i}{\partial x_j} \right) = - \frac{\partial p}{\partial x_i} + \mu \frac{\partial^2 u_i}{\partial x_j^2}, \quad (\text{Eq.10})$$

where $\mu = \rho\nu$.

If the Reynolds decomposition principle previously introduced is applied and the eulerian averaging procedure is applied, it is then possible to obtain from (Eq.9)

$$\overline{\frac{\partial u_i}{\partial x_i}} = \overline{\frac{\partial(\bar{u}_i + u'_i)}{\partial x_i}} = 0, \quad (\text{Eq.11})$$

as already explained, by definition, the averaging of a fluctuation quantity is zero, then

$$\frac{\partial \bar{u}'_i}{\partial x_i} = 0, \quad (\text{Eq.12})$$

which is the **mass conservation equation for turbulent flows**.

Applying the same method to (Eq.10) one obtains

$$\begin{aligned}
\frac{\partial \bar{u}_i}{\partial t} + \frac{\partial \bar{u}'_i}{\partial t} + \bar{u}_j \frac{\partial \bar{u}_i}{\partial x_j} + \bar{u}'_j \frac{\partial \bar{u}_i}{\partial x_j} + \bar{u}_j \frac{\partial \bar{u}'_i}{\partial x_j} + \bar{u}'_j \frac{\partial \bar{u}'_i}{\partial x_j} \\
= -\frac{1}{\rho} \frac{\partial \bar{p}}{\partial x_i} - \frac{1}{\rho} \frac{\partial \bar{p}'}{\partial x_j} + \nu \frac{\partial^2 \bar{u}_i}{\partial x_j^2} + \nu \frac{\partial^2 \bar{u}'_i}{\partial x_j^2},
\end{aligned} \tag{Eq.13}$$

with the help of mass conservation equation and considering that the average value of a fluctuating velocity is equal to zero, it is possible to write

$$\frac{\partial \bar{u}_i}{\partial t} + \bar{u}_j \frac{\partial \bar{u}_i}{\partial x_j} = \frac{1}{\rho} \frac{\partial}{\partial x_j} \left[-\rho \overline{u'_i u'_j} - \bar{p} \delta_{ij} + \mu \left(\frac{\partial \bar{u}_i}{\partial x_j} + \frac{\partial \bar{u}_j}{\partial x_i} \right) \right], \tag{Eq.14}$$

which is the **momentum conservation equation for turbulent flows**. δ_{ij} is the Kronecker delta in the pressure term, $\mu \left(\frac{\partial \bar{u}_i}{\partial x_j} + \frac{\partial \bar{u}_j}{\partial x_i} \right)$ is the Navier tensor and $-\rho \overline{u'_i u'_j}$ is the Reynolds tensor. It represents the contribution to the momentum transfer due to velocity fluctuations.

In order to compute all mean-flow properties of the turbulent flow under consideration, we need to compute the tensor $\overline{u'_i u'_j}$ [Wilcox 1993]. The tensor has been introduced by the Reynolds averaging procedure introduced above. This tensor has 6 independent components. Furthermore, for a general three-dimensional flow, there are other 4 unknown variables (pressure and 3 velocity components). Up to now only 4 equations are on hand and the system is not yet closed. Finding a way to evaluate these stresses and solving for any additional unknowns that may be introduced represents the **closure problem** of turbulence [Turns 2000].

3.6.2 Turbulent Kinetic Energy Conservation Equation

It is possible to derive the turbulent kinetic energy conservation equation from the Navier-Stokes equation:

$$\left(\frac{\partial (\bar{u}_i + u'_i)}{\partial t} + (\bar{u}_j + u'_j) \frac{\partial (\bar{u}_i + u'_i)}{\partial x_j} \right) = -\frac{1}{\rho} \frac{\partial (\bar{p} + p')}{\partial x_i} + \nu \frac{\partial^2 (\bar{u}_i + u'_i)}{\partial x_j^2}. \tag{Eq.15}$$

Applying a statistical averaging, it becomes

$$\frac{\partial \bar{u}_i}{\partial t} + \bar{u}_j \frac{\partial \bar{u}_i}{\partial x_j} + \frac{\partial \overline{u'_i u'_j}}{\partial x_j} = -\frac{1}{\rho} \frac{\partial \bar{p}}{\partial x_i} + \nu \frac{\partial^2 \bar{u}_i}{\partial x_j^2}. \tag{Eq.16}$$

Subtracting (Eq.16) from (Eq.15) gives

$$\frac{\partial \bar{u}_i}{\partial t} + \bar{u}_j \frac{\partial \bar{u}'_i}{\partial x_j} + \bar{u}'_j \frac{\partial \bar{u}_i}{\partial x_j} + \frac{\partial}{\partial x_j} (\overline{u'_i u'_j} - \bar{u}_i \bar{u}_j) = -\frac{1}{\rho} \frac{\partial \bar{p}'}{\partial x_i} + \nu \frac{\partial^2 \bar{u}'_i}{\partial x_j^2}. \tag{Eq.17}$$

Multiplying for u'_i the **turbulent kinetic energy** k is introduced. Summing on all the component and then applying a statistical averaging procedure

$$\frac{\partial \overline{k^2}}{\partial t} + \bar{u}_j \frac{\partial \overline{k^2}}{\partial x_j} = -\bar{u}_i \bar{u}_j \frac{\partial \bar{u}_i}{\partial x_j} - \frac{\partial}{\partial x_j} (\overline{k^2 u'_j}) - \frac{1}{\rho} \frac{\partial \overline{p' u'_i}}{\partial x_i} + \nu u'_i \frac{\partial^2 u'_i}{\partial x_j^2}, \quad (\text{Eq.18})$$

where the first term on the RHS represents the amount of turbulent kinetic energy due to the interaction with the mean flow. The second term represents the transfer of turbulent kinetic energy caused by velocity fluctuations. The third term is representative of kinetic energy transfer due to the interactions between the pressure and velocity fields. The fourth takes into account the joint turbulent kinetic energy transfer due to velocity and thermal dissipation.

3.6.3 Closure Models of the Turbulence Problem

Once the equation for the turbulent kinetic energy is known, there are still other two variables that need to be calculated. Namely, the mixing length l_m and the energy dissipation rate ε . Assuming that they are not dependent on the physical properties of the fluid and that they are only functions of the turbulence as modeled above, thanks to dimensional analysis, similarly to combine (Eq.3) with (Eq.8), it is possible to write

$$\varepsilon = \frac{k^{\frac{3}{2}}}{l_m}. \quad (\text{Eq.19})$$

A way to close the system is to use the so called **one-equation models**. These models use the turbulent kinetic energy written as a function of the mixing length. The mixing length is considered as an unknown and several models use different expressions depending on the flow characteristics and conditions. For this reason the one equation models are considered **incomplete**.

Another way to close the turbulence problem is to express the turbulent viscosity or equivalent variables similarly to what has been done with the turbulent kinetic energy. These models are called **complete** or **two-equation models**. In these models, the overwhelming choice for the first variable is k , while the second variable, linked to the turbulent viscosity is less generally agreed [Turns 2000]. Furthermore, several empirical closure coefficients are needed.

The first complete model was introduced by Kolmogorov in 1942 based on dimensional analysis considerations. His basic idea was to model the turbulent kinetic energy k and the rate of energy dissipation ω and then to relate the missing information of length and time scales to these quantities. This is a so called $k - \omega$

model. Other later two-equation models are based on a $k - \varepsilon$ formulation. A relationship between ω and ε exists and is, in general, $\varepsilon = k^n \omega^m$.

The $k - \varepsilon$ and $k - \omega$ models will be discussed more in detail in Chapter 4.

3.7 Homogeneous Isotropic Turbulence

In order to obtain valid relationship defining the turbulent problem, several assumptions need to be done in order to simplify the problem. The approximation used in many fluid-dynamical models corresponds to an idealized state where the turbulent flow has two properties:

- Homogeneity
- Isotropy

Homogeneity is the equivalent concept related to the space variable as the stationarity is to the time variable. It means that the quantity is considered to assume the same constant value in the system under study.

Isotropy means uniformity in all direction. Related to turbulence, it means that the averaged value of the velocity components is the same independently from the orientation of the reference system.

Applying the conditions expressed above, the relationship describing the turbulent phenomena are written in a simple form. This allows the mathematic treatment and an easier discussion of the results as also the comparison of the theory with the results of the experiments [Rotta 1972].

3.8 Difference of Fluctuation Velocities at Two Neighboring Points under Isotropic and Homogeneous Turbulent Conditions

In the next chapters the attention will be concentrated on the fluctuation velocity of two points in the fluid in order to calculate the characteristic velocity of bubbles moving towards each other in the flow (coalescence case) or to calculate the turbulent energy applied on the bubbles by the fluid surrounding them (breakup case).

In this section, two different cases will be considered. The first case, taken from Rotta [Rotta 1972], is valid for the determination of the **longitudinal fluctuation velocity difference** between two points (in particular this concept will be useful for the determination of the relative bubble approaching velocity in case of bubble collision).

The second case, from Batchelor [Batchelor 1956], is valid for the determination of the **absolute value of the fluctuation velocity difference** between two points (in particular this concept will be useful for the determination of the turbulent stresses applied on the bubbles by the surrounding fluid).

In order to simplify the notation we will refer to u'_{rms} as u . In the classic turbulence theory, the vectors of the velocity fluctuation of two points in the flow at given distance r are correlated and can be represented as in Figure 7.

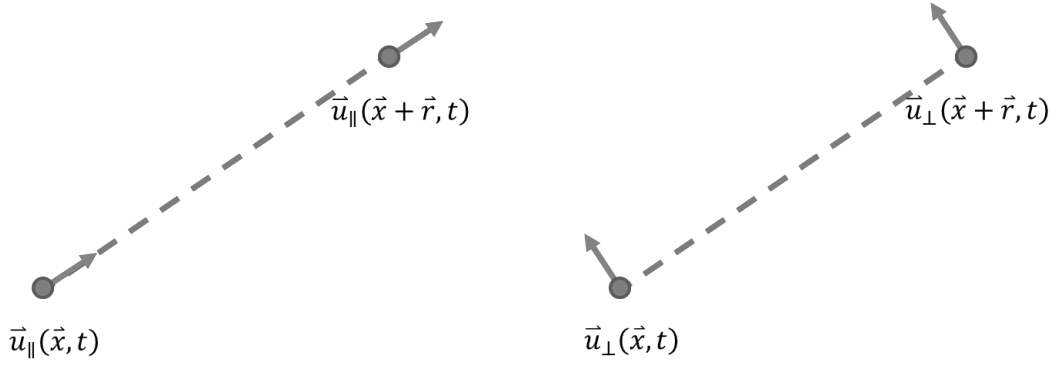


Figure 7: Longitudinal and lateral velocity correlations

Considering no correlation between the lateral and the longitudinal components of the velocity fluctuation, it is possible to write the mean value of the square of the difference of velocities at two neighboring points under isotropic and homogeneous turbulent conditions as:

$$\overline{|\vec{u}(\vec{x} + \vec{r}, t) - \vec{u}(\vec{x}, t)|^2} = \overline{|\vec{u}_{\parallel}(\vec{x} + \vec{r}, t) - \vec{u}_{\parallel}(\vec{x}, t)|^2} + \overline{|\vec{u}_{\perp}(\vec{x} + \vec{r}, t) - \vec{u}_{\perp}(\vec{x}, t)|^2}. \quad (\text{Eq.20})$$

If the longitudinal and the lateral components are correlated, (Eq.20) becomes more complicated.

Rotta [Rotta 1972] obtained the longitudinal fluctuation velocity difference between two points, the first term on the RHS in (Eq.20), as

$$\overline{|\vec{u}_{\parallel}(\vec{x} + \vec{r}, t) - \vec{u}_{\parallel}(\vec{x}, t)|^2} = 4 \int_0^{\infty} E(k) \left[\frac{1}{3} - \frac{1}{k^2 r^2} \left(\frac{\sin(kr)}{kr} - \cos(kr) \right) \right] dk, \quad (\text{Eq.21})$$

while Batchelor [Batchelor 1956] obtained the absolute value of the mean value of the square of the difference of velocities at two neighboring points, the term on the RHS in (Eq.20), as

$$\overline{|\vec{u}(\vec{x} + \vec{r}, t) - \vec{u}(\vec{x}, t)|^2} = 4 \int_0^{\infty} E(k) \left[1 - \left(\frac{\sin(kr)}{kr} \right) \right] dk. \quad (\text{Eq.22})$$

Both Rotta and Batchelor, integrate the energy from 0 to ∞ . In this way, they consider the contribution of the whole turbulence spectrum energy scales; from the large, integral scale, L , to the small, Kolmogorov scale, l_K .

In both cases, it is possible to simplify the formulation applying the Kolmogorov theory and considering the dimension of the turbulent eddies lying in the inertial subrange only. As proposed by both authors, in this subrange, at the lower end of the equilibrium range, at enough large Reynolds number, the transfer of energy by inertia forces is the dominant process and negligible dissipation occurs [Batchelor 1956]. In this case it is possible to define the energy spectrum by means of the Kolmogorov theory

$$E = \alpha \varepsilon^{2/3} k^{-5/3}, \quad (\text{Eq.23})$$

where α is a dimensionless constant (also called the Kolmogorov constant) deduced experimentally and characteristic of the actual turbulence conditions. It is of order 1. The variable ε is the so called turbulent energy dissipation and k is the turbulent kinetic energy.

If the expression for the turbulent energy spectrum in (Eq.23) is substituted in (Eq.21) and (Eq.22) respectively, it is possible to approximate the integrals by means of gamma functions leading to the following expressions [Rotta 1972, Batchelor 1956]:

$$\overline{|\vec{u}_{\parallel}(\vec{x} + \vec{r}, t) - \vec{u}_{\parallel}(\vec{x}, t)|^2} = \frac{27}{55} \Gamma\left(\frac{1}{3}\right) \alpha (\varepsilon r)^{2/3} = 1.315 \alpha (\varepsilon r)^{2/3} \quad (\text{Eq.24})$$

and

$$\overline{|\vec{u}(\vec{x} + \vec{r}, t) - \vec{u}(\vec{x}, t)|^2} = \frac{9}{5} \Gamma\left(\frac{1}{3}\right) \alpha (\varepsilon r)^{2/3} = 4.82 \alpha (\varepsilon r)^{2/3}. \quad (\text{Eq.25})$$

where, as already expressed, r is a generic distance between two points in the flow.

As reported by Gibson [Gibson 1962], in case of a high turbulent Reynolds number flow in pipes, the value of the Kolmogorov constant α is defined to be 1.96.

Applying to the Kolmogorov constant the value reported by Gibson for high turbulent Reynolds number flow in pipes would lead to the following results

$$\overline{|\vec{u}_{\parallel}(\vec{x} + \vec{r}, t) - \vec{u}_{\parallel}(\vec{x}, t)|^2} \approx 2.58 (\varepsilon r)^{2/3} \quad (\text{Eq.26})$$

and

$$\overline{|\vec{u}(\vec{x} + \vec{r}, t) - \vec{u}(\vec{x}, t)|^2} \approx 9.45 (\varepsilon r)^{2/3}. \quad (\text{Eq.27})$$

Chapter 4

Two-Phase Flow Models

In this chapter the modeling approaches for the simulation of two-phase flows are introduced. The two-fluid model is explained in detail and the limits of the actual calculation methods are presented. Furthermore, the two-phase flow turbulence modeling and the specific bubbly flow models are explained in detail.

Two-phase flow as any other flow in nature obeys the laws of fluid mechanics and the Navier-Stokes equations are valid to describe the flow in each condition. Its description is much more complicated than single phase flow since the presence of a deformable gas-liquid interface leads to an infinite number of possible configurations.

The equations describing two-phase flow can be presented in two different formulations:

- Eulerian - Lagrangian
- Eulerian

In the **Eulerian - Lagrangian** formulation, the disperse phase is treated under the lagrangian point of view. In this case the dispersed particles are tracked and the continuous phase is treated from the eulerian point of view. This model is practical only if applied to the simulation of a very dilute disperse phase.

In the **Eulerian** formulation there are three main approaches to the modeling of two-phase flow:

1. the homogeneous model,
2. the drift flux model,
3. the separated or two-fluid model.

The simplest mixture model is the **homogeneous equilibrium model** - HEM. This model considers the two phases having the same velocity and in thermodynamic equilibrium. Using this model, the flow is described by solving the mass, momentum

and energy equations for the mixture only. The basic mass, momentum and energy equations are respectively:

$$\frac{\partial \rho_m}{\partial t} + \nabla \cdot \rho_m \vec{v}_m = 0, \quad (\text{Eq.28})$$

$$\frac{\partial \rho_m \vec{v}_m}{\partial t} + \nabla \cdot \rho_m \vec{v}_m^2 = -\nabla \rho_m K \vec{v}_m |\vec{v}_m| - g \rho_m \cos \theta, \quad (\text{Eq.29})$$

$$\frac{\partial \rho_m e_m}{\partial t} + \nabla \cdot \rho_m e_m \vec{v}_m + P \nabla \cdot \vec{v}_m = q, \quad (\text{Eq.30})$$

where the properties and variables are written for the mixture as follows

$$\rho_m = \alpha \rho_G + (1 - \alpha) \rho_L, \quad (\text{Eq.31})$$

$$\rho_m e_m = \alpha \rho_G e_G + (1 - \alpha) \rho_L e_L, \quad (\text{Eq.32})$$

and for the following relations are valid:

$$v_m = v_G = v_L, \quad (\text{Eq.33})$$

$$v_m = v_G = v_L T_m = T_G = T_L, \quad (\text{Eq.34})$$

$$P = P_G = P_L. \quad (\text{Eq.35})$$

In (Eq.29), the term K represents the mixture wall friction loss term.

A more complex model in comparison to the HEM is the thermal equilibrium **drift flux model**. If compared to the HEM, this model allows for the presence of a relative velocity (slip) between the phases. The slip is obtained using an algebraic relationship, or by solving a transport equation. This model contains 2 mass equations (mixture and gas), two energy equations, and one momentum equation. The drift flux mass conservation equations in one dimension are:

$$\frac{\partial \rho_m}{\partial t} + \frac{\partial \rho_m \vec{v}_m}{\partial x} = 0, \quad (\text{Eq.36})$$

$$\frac{\partial \alpha \rho_G}{\partial t} + \frac{\partial \alpha \rho_G \vec{v}_m}{\partial x} + \frac{\partial}{\partial x} \left[\frac{\alpha \rho_G (1 - \alpha) \rho_L \vec{v}_r}{\rho_m} \right] = \Gamma, \quad (\text{Eq.37})$$

where \vec{v}_r is the drift velocity that takes into account the effects of relative motions between two phases. Γ is the boiling (+) or condensation (-) term.

The drift flux mixture momentum equation in one dimension is:

$$\frac{\partial \vec{v}_m}{\partial t} + \vec{v}_m \frac{\partial \rho_m \vec{v}_m}{\partial x} + \frac{1}{\rho_m} \frac{\partial}{\partial x} \left[\frac{\alpha \rho_G (1 - \alpha) \rho_L \vec{v}_r^2}{\rho_m} \right] = -\frac{1}{\rho_m} \frac{\partial P}{\partial x} - K \vec{v}_m |\vec{v}_m| + g. \quad (\text{Eq.38})$$

The drift flux gas energy conservation equation in one dimension is:

$$\begin{aligned} \frac{\partial \alpha \rho_G e_G}{\partial t} + \frac{\partial \alpha \rho_G \vec{v}_m e_G}{\partial x} + \frac{\partial}{\partial x} \left[\frac{\alpha \rho_G (1 - \alpha) \rho_L \vec{v}_r e_G}{\rho_m} \right] + P \frac{\partial \vec{v}_m}{\partial x} + P \frac{\partial}{\partial x} \left[\frac{\alpha (1 - \alpha) \rho_L \vec{v}_r}{\rho_m} \right] \\ = q_{wG} + q_{iG} - P \frac{\partial \alpha}{\partial t} + \Gamma h_{sG}, \end{aligned} \quad (\text{Eq.39})$$

where Γh_{sG} is the energy transferred across the interface and acts as an energy source term for the gas phase.

For the mixture the energy equation is:

$$\begin{aligned} \frac{\partial \rho_m e_m}{\partial t} + \frac{\partial \rho_m \vec{v}_m e_m}{\partial x} + \frac{\partial}{\partial x} \left[\frac{\alpha \rho_G (1 - \alpha) \rho_L \vec{v}_r (e_G - e_L)}{\rho_m} \right] + P \frac{\partial \vec{v}_m}{\partial x} \\ + P \frac{\partial}{\partial x} \left[\frac{\alpha (1 - \alpha) (\rho_G - \rho_L) \vec{v}_r}{\rho_m} \right] = q_{wG} + q_{wL}. \end{aligned} \quad (\text{Eq.40})$$

The following relationships are valid:

$$\rho_m = \alpha \rho_G + (1 - \alpha) \rho_L, \quad (\text{Eq.41})$$

$$\vec{v}_m = \frac{\alpha \rho_G \vec{v}_G + (1 - \alpha) \rho_L \vec{v}_L}{\rho_m}, \quad (\text{Eq.42})$$

$$\vec{v}_r = \vec{v}_G + \vec{v}_L, \quad (\text{Eq.43})$$

$$\Gamma = \frac{-q_{iG} - q_{iL}}{h_{sG} + h_{sL}}, \quad (\text{Eq.44})$$

$$q_{iG} = h_{iG} A_i \frac{(T_s - T_G)}{Vol}, \quad (\text{Eq.45})$$

$$q_{iL} = h_{iL} A_i \frac{(T_s - T_L)}{Vol}, \quad (\text{Eq.46})$$

$$q_{wG} = h_{wG} A_i \frac{(T_w - T_G)}{Vol}, \quad (\text{Eq.47})$$

$$q_{wL} = h_{wL} A_i \frac{(T_w - T_L)}{Vol}. \quad (\text{Eq.48})$$

The complexity increases if the **two-fluid model** is used. In this case, the mass, momentum and energy equations are solved for both phases. This model is also known as six-equation model. Since each phase is separately simulated, the need for modeling, in an explicit way, the presence of an interface arises. Furthermore, since an interface is present, balances (jump conditions) to describe the mass, momentum, and energy transfer between the phases must also be included. For this reason the two-fluid model needs constitutive equations for the mass, momentum and energy transfer between the phases at the interface liquid-vapour or liquid-gas. In order to develop these constitutive relations, several specific models can be considered. In all cases, from the simplest to the most complicated model, further constitutive equations are also needed to describe the phenomena taking place at the wall or at the interface for each phase.

The two fluid model will be explained more in detail in the next section since it forms the basis of the work carried out in this Thesis.

4.1 The Two-Fluid Model

The two fluid model was formulated by Ishii in 1975 and later modified by Ishii and Mishima in 1984 [Ishii 1975, Ishii and Mishima 1984]. It is suitable for the analysis of transient phenomena, wave propagation and for flow regime changes. In this model each phase is considered separately by means of a set of six conservation equations to describe the balance of mass, momentum and energy; three for each phase. This set of equation is not independent and there are coupling terms between the different equations. These terms are usually expressed as Γ_k , M_k and E_k , the mass, momentum and energy transfer to the k^{th} -phase from the **interfaces** respectively. It should be noted that without these interfacial exchanges, the two sets of equations, for each phase, are essentially independent.

The interfacial transfer conditions are derived from the so-called local jump conditions; three interfacial transfer conditions govern the macroscopic behavior of the two-phase flow system.

Of course the two-fluid model can predict more detailed changes than the drift-flux model, but this means that it is much more complicated to solve and needs the formulation of **accurate** constitutive equations [Ishii and Hibiki 2006]. The grade of coupling of the two sets of equations is established by the choice of the constitutive models.

As reported by Ishii and Hibiki [Ishii and Hibiki 2006], the real importance of the two-fluid model is that it can take into account the dynamics and non-equilibrium conditions between the phases thanks to two independent momentum equations, two velocity fields and two energy equations.

Ishii and Hibiki also point firmly the attention to the fact that mathematical models of two-phase flow systems are not yet firmly established and that further research is needed to complete the three-dimensional models for a general two-phase flow.

The differential form of the local time-averaged formulation of the **continuity** (mass) equation per unit volume for the k^{th} -phase is:

$$\frac{\partial(\alpha_k \rho_k)}{\partial t} + \nabla \cdot (\alpha_k \rho_k \vec{v}_k) = \Gamma_k, \quad (\text{Eq.49})$$

where Γ_k represents the rate of production of the k^{th} -phase mass from the other phase present at the interface per unit volume.

The local time-averaged formulation of the **momentum** equation for the k^{th} -phase is:

$$\begin{aligned}
& \frac{\partial(\alpha_k \rho_k \vec{v}_k)}{\partial t} + \nabla \cdot (\alpha_k \rho_k \vec{v}_k \vec{v}_k) \\
& = -\nabla(\alpha_k p_k) + \nabla \cdot [\alpha_k (\bar{\tau}_k^\mu + \bar{\tau}_k^T)] + \alpha_k \rho_k \vec{g} + \Gamma_k \vec{v}_{i,k} + p_{i,k} \nabla \alpha_k \\
& - \nabla \alpha_k \cdot \bar{\tau}_{i,k} + \vec{F}_{i,k}.
\end{aligned} \tag{Eq.50}$$

The local time-averaged formulation of the **enthalpy** equation for the k^{th} -phase is:

$$\begin{aligned}
& \frac{\partial(\alpha_k \rho_k H_k)}{\partial t} + \nabla \cdot (\alpha_k \rho_k \vec{v}_k H_k) \\
& = -\nabla \cdot [\alpha_k (\bar{q}_k + \bar{q}_k^T)] + \frac{D_k(\alpha_k p_k)}{Dt} + \Gamma_k H_{i,k} + a_i q''_{i,k} - p_{i,k} \frac{D_k \alpha_k}{Dt} \\
& + \phi_k.
\end{aligned} \tag{Eq.51}$$

In the momentum and energy equations the subscript i stands for the interface between the phases and the term D/Dt are the material derivative: $\partial/\partial t + \vec{v} \partial/\partial \vec{r}$.

The variables α , ρ , \vec{v} and H are the local time-averaged void fraction, density, velocity and enthalpy, respectively and $\bar{\tau}_k^\mu$, $\bar{\tau}_k^T$, \bar{q}_k and \bar{q}_k^T represent, the average viscous stress tensor, the average turbulent stress tensor, conduction heat flux tensor and turbulent heat flux tensor.

The unknown terms in (Eq.49), (Eq.50) and (Eq.51) represent the coupled effects of one phase with the other as described previously. They are called transfer terms and are:

- Γ_k mass generation,
- $\vec{F}_{i,k}$ generalized interfacial force,
- $\bar{\tau}_{i,k}$ interfacial shear stress,
- $q''_{i,k}$ interfacial heat flux.

The interfacial transfer terms follow the balance laws at the interface and the resulting local jump conditions are:

$$\sum_{k=1}^2 \Gamma_k = 0, \tag{Eq. 52}$$

$$\sum_{k=1}^2 \vec{F}_{i,k} = 0, \tag{Eq. 53}$$

$$\sum_{k=1}^2 (\Gamma_k H_{i,k} + a_i q''_{i,k}) = 0. \tag{Eq. 54}$$

These terms should be separately modeled and are proportional to a geometric parameter called **interfacial area density** a_i . This is the total interfacial area between the phases per unit volume.

As discussed in Ishii and Hibiki [Ishii and Hibiki 2006], the importance of this parameter remains in the fact that, since it represents the available area of contact between the phases, the interfacial mass momentum and energy transfer are widely influenced by its determination. Constitutive relations for a_i are extremely complicated as this parameter represents the local geometric configuration of the phases.

In current system codes like RELAP5, TRAC, TRACE, CATHARE and ATHLET, the interfacial area density prediction is based on empirical correlations. These correlations are flow regime dependent and, at a given flow condition, the code selects automatically which correlation needs to be used based on flow regime maps. Traditionally flow regime maps have been constructed using superficial velocities which do not univocally define the flow regime. Ishii and Mishima [Ishii and Mishima 1980] reported that while flow regime maps based on superficial velocities may be suitable for steady, developed flow, the same is not true in case of transient or developing conditions. They recommended a direct geometric parameter, such as void fraction, for flow regime determination for unsteady and entrance flows.

As an example, in Figure 8, it is possible to understand how a code such as RELAP5/MOD3.3 is able to determine flow-regime transitions as functions of void fraction, average mixture velocity, and boiling regime (pre-critical heat flux (CHF), transition, and post-dryout). The vertical volume flow regime map is for upflow, downflow, and countercurrent flow in volumes whose elevation angle is between 45 and 90 degrees [Relap 2001].

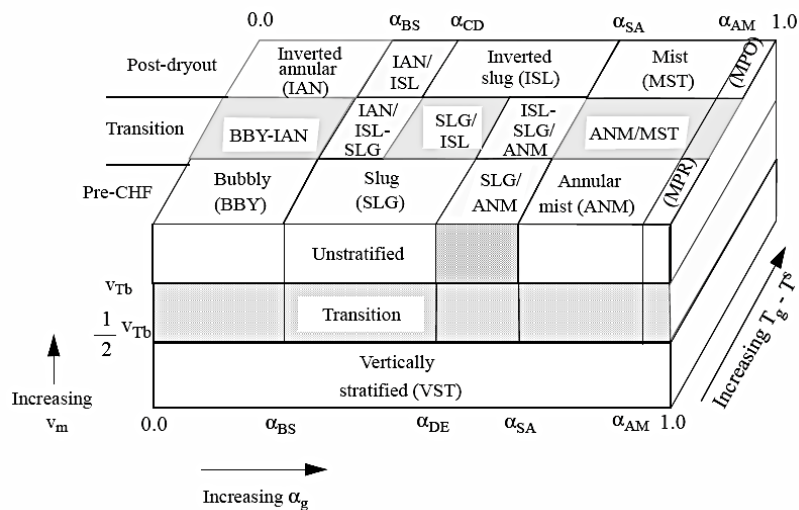


Figure 8: Schematic of vertical flow-regime map with hatching indicating transitions [Relap 2001]

Hibiki and Ishii [Hibiki and Ishii 2000a] pointed out that the correlations and the flow regime transition criteria used today do not dynamically represent the changes in the interfacial structure and reported three main limitations:

1. Flow regime transition criteria are algebraic relations for steady-state, fully developed flows.
2. The method based on flow regime transition is a two-step method that requires the determination of transition criteria and correlations for the interfacial area for different flow configurations. The resulting compound error can be significant.
3. The transition criteria and the correlations have a limited validity range regarding operational conditions and geometries. They have been obtained experimentally for simplified scaled geometries and under conditions far away from the operational ones. This can cause significant discrepancies and numerical errors or instabilities.

In modern 3D CFD codes, the interfacial area density prediction is based on a simplification of the structure of the interface between the phases. Furthermore, the flow morphology is a required user input that needs to be defined “a priori” by the user. For example, this is the case of eulerian multiphase flow modeling where, at the moment, no predictive model for flow morphology exists.

In case of monodispersed flow calculations a unique constant bubble diameter is set by the user and the void fraction is calculated by the solution of the mass conservation equation. Considering bubbles as rigid spheres it is possible to determine the interfacial area concentration by means of the following equation:

$$a_i = \frac{6\alpha}{D_s}, \quad (\text{Eq. 55})$$

where D_s is the Sauter mean diameter. It is defined as the diameter of a sphere that has the same volume/surface area ratio as a particle of interest.

In case of polydispersed flow, the prediction of the interfacial area concentration is similarly determined taking into account the contributions of the several bubble groups that have been defined by the user. Each bubble group is contributing to the global value of the interfacial area concentration based on its size fraction. In this case the interactions between bubbles of the same and different groups are taken into account and the size fractions are dynamically modified.

Creating a new set of constitutive relations in the case of dispersed two-phase flow to improve the interfacial area concentration prediction capability of three dimensional simulation CFD based tools is the main goal of this work.

4.2 Two-Phase Flow Turbulence Modeling

Turbulence is one of the important mechanisms that lead to bubble interactions. Since the development of the flow is influenced by the dynamics of the bubbles migrating from one flow region to another and by the bubble interactions, the effect of the presence of an additional phase on the flow turbulence should be modeled in order to obtain an accurate determination of interfacial area densities and interfacial transfer rates.

Bubbly two-phase flow turbulence modeling is based on a two-equation model formulated for single phase flow with and the turbulence of the gas phase calculated by means of a zero equation model: essentially an algebraic formula based on a geometric length scale and on the mean calculated velocity [Ansys 2009]. The dispersed bubbles are transported by the turbulent fluctuations of the continuous phase. In order to consider the observed turbulence enhancement generated by the presence of the gas phase on the turbulence of the liquid phase, two approaches are considered in the literature:

- an additional viscosity term,
- or an additional source terms for the turbulence equations

Given the considerations above, in order to explain the treatment of turbulence in two-phase flow systems an introduction on single phase turbulence modeling is needed.

4.2.1 Brief Introduction on Single-Phase Turbulence Modeling

The most widely used in case of CFD calculations are the so called $k - \varepsilon$ or $k - \omega$ models. Rodi and Scheuerer, [Rodi and Scheuerer 1986] showed that models based on the ε -equation lead to an over-prediction of the turbulent length scale in flows with adverse pressure gradients (static pressure increase in the direction of the flow so that $\partial P / \partial x > 0$), resulting in higher wall shear stress and higher heat transfer rates. In addition, these models require a very fine near-wall resolution, which is typically one order of magnitude higher than for other one- and two-equation turbulence models [Vieser et al. 2008]. In order to alleviate this limitation the concept of a two-layer formulation [Patel et al. 1985] has been derived. In such a case the ε -equation is

solved in the outer part of the boundary layer and the inner part is treated by a mixing length formulation. As this location is usually determined by user input, the uniqueness of the solution is not guaranteed [Vieser et al. 2008] and alternative formulations, both of the scale-equation and of the near-wall treatment are required.

Alternative to the ε -equation is the ω -equation. In this case instead of an equation for the turbulence eddy dissipation ε , an equation for the turbulence eddy frequency of the large turbulent scales ω is solved. Two main advantages of the $k - \omega$ formulation, if compared to the $k - \varepsilon$ formulation, have been listed by Vieser et al. [Vieser et al. 2008]. The ω -equation has significant advantages if compared to the ε -equation near the solid surface and can accurately predict the turbulent length scale in adverse pressure gradient flows, leading to improved wall shear stress and heat transfer predictions. The model has a very simple low-Reynolds number formulation, which does not require additional non-linear wall damping terms. Menter [Menter 1992] pointed out that the main deficiency of the standard $k - \omega$ model is the strong sensitivity of the solution to free-stream turbulence quantities (like turbulence intensity, turbulent length scale or eddy viscosity) for ω outside the wall boundary layer.

Based on these considerations Menter [Menter 1992], in order to avoid the sensitivity problem, proposed a combination of the $k - \omega$ near the wall the $k - \varepsilon$ model away from it. Such a model led to the formulation of the Shear Stress Transport (SST) model.

In the SST model a blending function F_1 is defined and it is equal to 1 at the wall node and 0 away from it, so that at the wall the $k - \omega$ is used and it changes to the $k - \varepsilon$ for the rest of the flow geometry.

The SST turbulence model is expressed as a function of k and ω only. The $k - \varepsilon$ part is written based on ω by means of the following relationship [Ansys 2009]:

$$\varepsilon = \beta' \omega k, \quad (\text{Eq. 56})$$

with $\beta' = 0.09$.

The set of equations for $k - \omega$ is multiplied by the blending function F_1 and that for the $k - \varepsilon$ written as a function of ω and then multiplied by $1 - F_1$. The two sets of equations are then summed up. The final form of the SST turbulence model for the liquid phase is:

$$\frac{\partial \rho_l k}{\partial t} + \nabla \cdot (\rho_l \vec{v}_l k) = \nabla \cdot \left[\left(\mu_l + \frac{\mu_t}{\sigma_{k_3}} \right) \nabla k \right] + P_k - \beta' \rho_l k \omega. \quad (\text{Eq. 57})$$

$$\begin{aligned}
& \frac{\partial \rho_l \omega}{\partial t} + \nabla \cdot (\rho_l \vec{v}_l \omega) \\
& = \nabla \cdot \left[\left(\mu_l + \frac{\mu_t}{\sigma_{\omega_3}} \right) \nabla \omega \right] + (1 - F_1) 2 \rho_l \frac{1}{\sigma_{\omega_2} \omega} \nabla k \nabla \omega + a_3 \frac{\omega}{k} P_k \\
& \quad - \beta_3 \rho_l \omega^2,
\end{aligned} \tag{Eq. 58}$$

where μ_l is the dynamic viscosity of the liquid phase, μ_t is the shear-induced turbulence viscosity term also called eddy viscosity. The terms σ_{k_3} , σ_{ω_3} , σ_{ω_2} , a_3 and β_3 are coefficients. The value of these coefficients is not relevant for our purposes. In fact, in this work, the standard values of the empirical coefficients proposed by the CFD code ANSYS CFX have been used. Modifying these values would need to start a new validation procedure based on calibration against experimental data generated ad-hoc for this task. Furthermore, in the SST model, a limiter to the formulation of the eddy-viscosity is set:

$$\mu_t = \rho_l \frac{a_1 k}{\max(a_1 \omega \sqrt{2} S F_2)}, \tag{Eq. 59}$$

where a_1 is a constant whose default value is per default 0.31. $S = \sqrt{S_{ij} S_{ji}}$ is the absolute value of the strain rate used in the definition of the eddy viscosity instead of the vorticity in order to increase the generality of the method beyond aerodynamic applications [Vieser et al. 2008]. F_2 is another blending function similar to F_1 , which restricts the limiter to the wall boundary layer, as the underlying assumptions are not correct for free shear flows.

4.2.2 Turbulence Enhancement Generated by the Presence of a Dispersed Phase

4.2.2.1 Additional Viscosity Term

The dynamic viscosity of the liquid phase is modified by adding an additional Bubble Induced Turbulence (BIT) viscosity term μ_b similarly to the case of the eddy viscosity μ_t . The effective viscosity of the liquid phase is modified to be

$$\mu_{eff} = \mu_l + \mu_t + \mu_b. \tag{Eq. 60}$$

In case of the Sato model [Ansys 2009], the BIT term is written as follows:

$$\mu_b = C_{\mu_b} \rho_l \alpha D |\vec{u}_l - \vec{u}_g|, \tag{Eq. 61}$$

where C_{μ_b} is a constant whose value is 0.6.

In this case the turbulence eddy dissipation ε , the turbulence eddy frequency ω and the turbulence kinetic energy k , are not directly modified by the model formulation. The results will be influenced by the fact that the effective viscosity is modified not only by the shear-induced turbulence viscosity term but also by the bubble induced turbulent viscosity term. The modified μ_{eff} is then used in the conservation equation for the momentum.

4.2.2.2 Additional Source Terms in the Turbulence Equations

Different from the additional viscosity term model explained above is the model explained in this paragraph where the general single-phase two-equation turbulence model shown in (Eq. 57) and in (Eq. 58) is modified by means of the additional source terms φ_k and φ_ω as follows:

$$\frac{\partial \rho_l k}{\partial t} + \nabla \cdot (\rho_l \vec{v}_l k) = \nabla \cdot \left[\left(\mu_l + \frac{\mu_t}{\sigma_{k_3}} \right) \nabla k \right] + P_k - \beta' \rho_l k \omega + \varphi_k, \quad (\text{Eq. 62})$$

$$\begin{aligned} & \frac{\partial \rho_l \omega}{\partial t} + \nabla \cdot (\rho_l \vec{v}_l \omega) \\ &= \nabla \cdot \left[\left(\mu_l + \frac{\mu_t}{\sigma_{\omega_3}} \right) \nabla \omega \right] + (1 - F_1) 2 \rho_l \frac{1}{\sigma_{\omega_2} \omega} \nabla k \nabla \omega + a_3 \frac{\omega}{k} P_k \\ & - \beta_3 \rho_l \omega^2 + \varphi_\omega. \end{aligned} \quad (\text{Eq. 63})$$

Most of BIT correlations for φ_k and φ_ω in the literature consider the influence of the interfacial drag forces; in some correlations a contribution of non-drag forces is considered [Al Issa and Lucas 2009]. A benchmark for a number of correlations was done by Wörner et al. [Wörner et al. 2004] using a DNS calculation of eight bubbles rising in a rectangular duct (see Figure 9). The results of the DNS simulation is compared with those obtained using several other formulations for the bubble induced turbulence. The correlation of Morel [Yao and Morel 2004], indicated by (M), is the closest one to the exact DNS based profile. The coordinate x_3 represents the distance from the wall. Computational details are found in Wörner et al. [Wörner et al. 2004].

In case of the Yao and Morel model [Yao and Morel 2004], the BIT terms are written as follows:

$$\varphi_k = 0.75 \frac{C_D}{D_s} \alpha \rho_l |\vec{u}_l - \vec{u}_g|^3, \quad (\text{Eq. 64})$$

$$\varphi_\varepsilon = \frac{\varphi_k}{\tau} = \frac{\varphi_k}{\left(\frac{D_s^2}{\varepsilon} \right)^{1/3}}. \quad (\text{Eq. 65})$$

The turbulence eddy frequency term is given by

$$\varphi_\omega = \frac{1}{\beta'k} \varphi_\varepsilon - \frac{\omega}{k} \varphi_k. \quad (\text{Eq. 66})$$

The term C_D in (Eq. 64) is the interfacial drag coefficient.

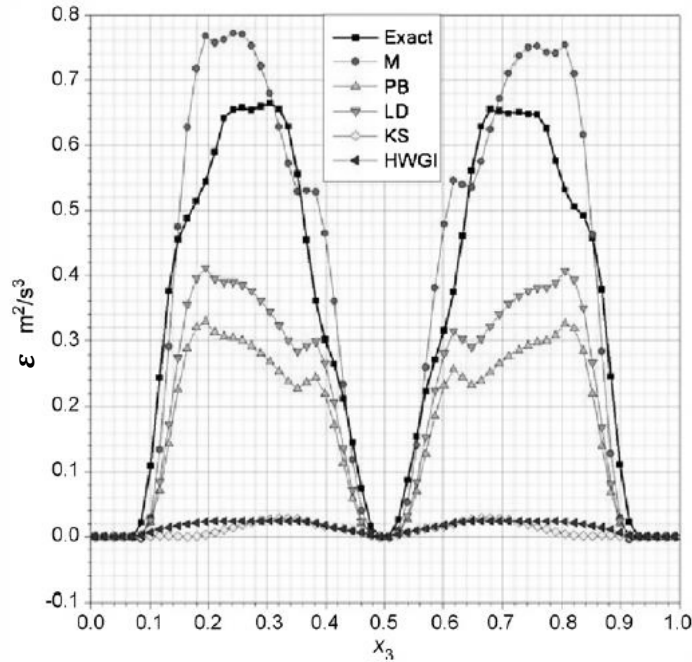


Figure 9: DNS calculations of different closure laws for the bubble-induced turbulence [Wörner 2004]

4.3 Bubbly Flow Modeling

If dispersed bubbly flow is considered, a set of constitutive relationships has to be written based on mechanistic considerations in order to describe adequately the physical phenomena happening in such a flow regime. This set of equations will then be implemented in the two-fluid model to numerically describe it.

The development of the flow along a path is influenced by the dynamic of the bubbles migrating from one region to the other and by the bubble interactions. These phenomena are summarized in Figure 10. In Figure 10 left, it is possible to see a stable bubbly flow far away from the transition region to slug flow. In such a case bubbles are nearly spherical and they are concentrated in the near wall region. Coalescence and breakup are present and happen between bubbles having more or less the same diameter. In Figure 10 right, it is possible to see the bubbly flow in transition to slug flow. In this case, not only small nearly spherical bubbles are present, also bigger bubbles in the form of ellipses or cap bubbles concentrate in the pipe central region. It is not possible to simulate these bubbles with the spherical approximation without losing detail and, more complex form factors needs to be used. Eventually two cap

bubbles can coalesce and form bigger bubbles with a diameter of the same order of magnitude as the pipe diameter. The resulting bubble is very similar to a slug and it is very difficult to differentiate from it. It means that the transition to slug flow is very near. If the bubble or drop is sufficiently large, it fills most of the pipe cross section and a slug flow regime results.

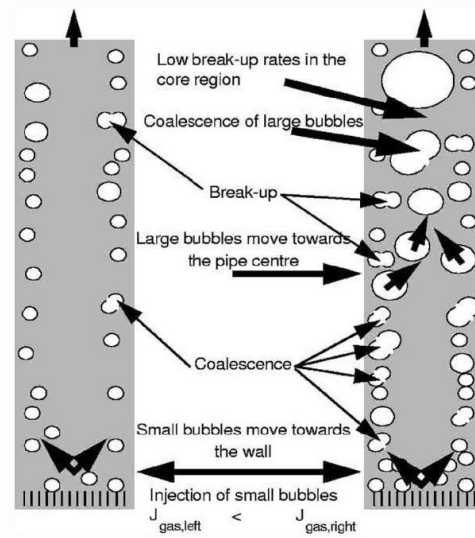


Figure 10: Stable bubbly flow (left) and transition to slug flow (right) [Krepper et al. 2005]

For complex bubble size distributions, in order to describe the different physical behavior of bigger bubbles if compared to smaller ones, a three-fluid approach is needed. In fact, even if the models describing the forces acting on the bubbles are dependent on the diameter, their validity is limited to restricted flow conditions or is flow regime dependent. Furthermore, bubbles belonging to different groups share different velocity fields.

It is possible to classify bubbles rising freely in infinite media with a generalized graphical correlation in terms of the Eötvös number Eo , the Morton number Mo and the bubble Reynolds number Re_b [Clift et al. 1978]:

$$Eo = \frac{gD^2\Delta\rho}{\sigma}, \quad (\text{Eq.67})$$

$$Mo = \frac{g\mu_l^4\Delta\rho}{\rho_l^2\sigma^3}, \quad (\text{Eq.68})$$

$$Re_b = \frac{\rho_l u_{rel} D}{\mu_l}. \quad (\text{Eq.69})$$

Figure 11 shows boundaries between the three principal shape regimes described above as given by Grace et al. [Grace et al. 1976]. While the boundaries between the

principal shape regimes are somewhat arbitrary, it is clear that bubbles and drops are ellipsoidal at relatively high Re_b and intermediate Eo while the spherical- or ellipsoidal-cap regime requires that both Eo and Re_b be large [Clift et al. 1978]. Various sub-regimes may also be mapped and some of these are included in Figure 11. Again the boundaries are somewhat arbitrary [Clift et al. 1978]. The dashed lines represented in Figure 11 and the colored area delimits ideally the region in which the bubbles of the experiments of Santos Mendez [Santos Mendez 2008], simulated in chapters 9 and 11, could be classified.

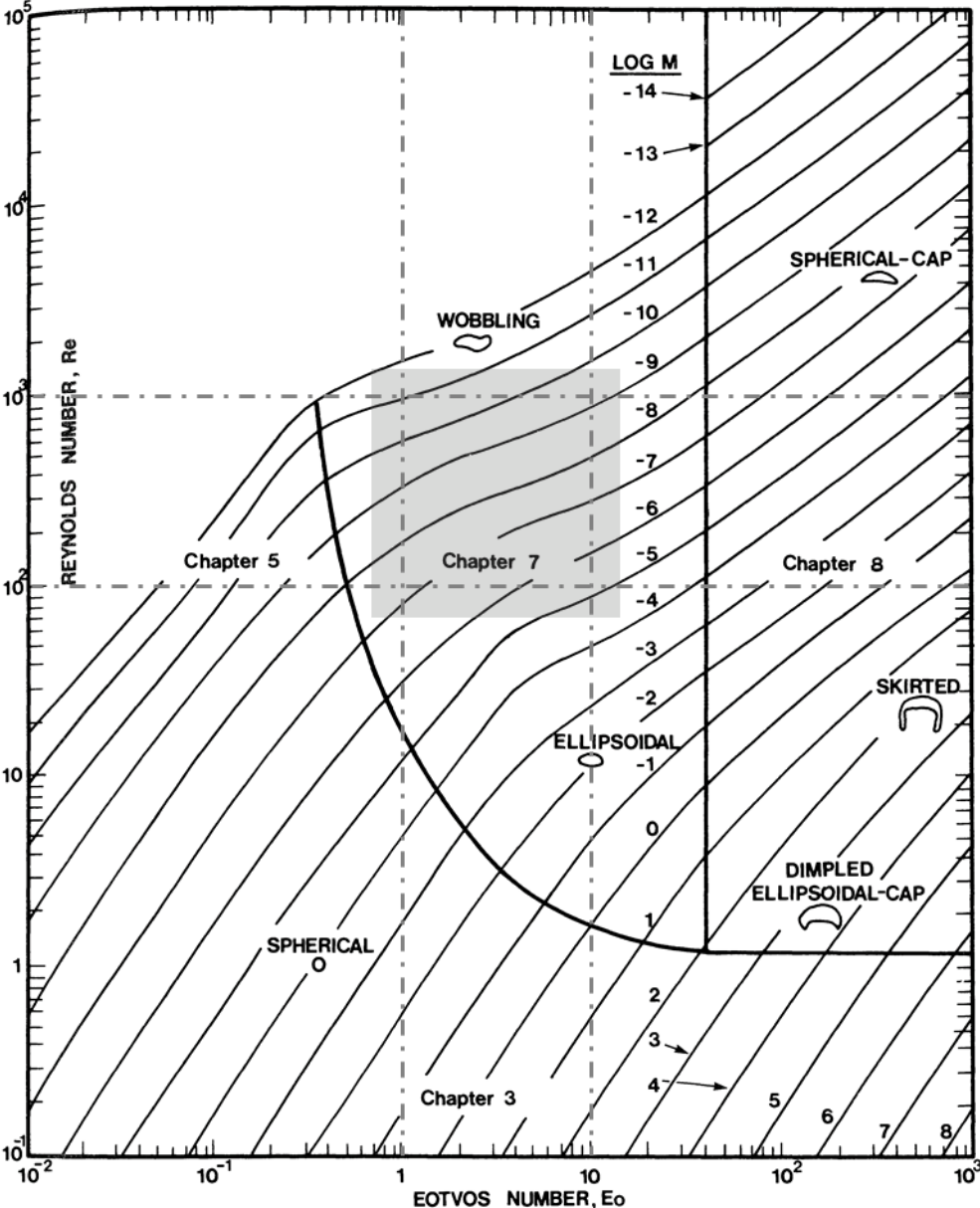


Figure 11: Shape regimes for bubbles and drops in unhindered gravitational motion through liquids [Clift et al. 1978].

4.3.1 Bubble Interaction Mechanisms

The bubbles interaction mechanisms that have been identified by Ishii and coworkers are explained in the following sections.

4.3.1.1 Bubble Type and Flow Geometry

Bubble interactions and also bubble transport mechanisms depend on the bubble type. Since a wide range of bubble shape and size exists depending on the flow regime, a set of transport equations describing the bubble transport in a wide range of two-phase flow regimes is needed [Ishii and Hibiki 2006]. This set of equations must account for the differences in the transport characteristics of different types of bubbles, since the variations in shape and size of bubbles cause substantial differences in their transport mechanisms due to the drag forces [Ishii et al. 2002].

Given the above considerations, a general approach to treat the bubbles in two main groups has been proposed in the past [Ishii et al. 1998, Uhle et al. 1998, and Wu et al. 1998a]. Hibiki and Ishii [Hibiki and Ishii 2000a] classified these two groups as:

- Spherical/distorted bubble group,
- Cap/slug bubble group,

and proposed that they result in two bubble number density transport equations involving the intra- and inter-group interactions. If only spherical (or nearly spherical) or distorted bubbles exist, only one transport equation can be used. If also cap bubbles or slugs exist, then a second transport equation needs to be written with adequate transfer terms between these two bubble groups. In fact, when the flow conditions are changing and bubbles of different diameter and shape are formed, the definition of an equation for the second group is justified because the interfacial structures in different flow regimes change dramatically [Ishii and Hibiki 2006]. Furthermore, the bubble interaction mechanisms in such flow conditions, driven by two bubble types, can be quite different compared with those in the one-bubble-group model.

It is also needed to establish criteria to define the critical diameter to separate bubbles belonging to the first group from those belonging to the second one [Kocamustafaogullari et al. 1994]. Fu and Ishii [Fu and Ishii 2002a], referencing Ishii and Zuber [Ishii and Zuber 1979], reported the boundary D_c between group one and two bubble types to be approximately equal to:

$$D_c = 4 \sqrt{\frac{\sigma}{g\Delta\rho}}, \quad (\text{Eq. 70})$$

where D_c is the volumetric equivalent diameter (the diameter of the sphere having the same volume of a particle with volume V_c), σ is the liquid phase surface tension and $\Delta\rho$ is the density difference between the phases. In case of air-water mixture at nearly atmospheric pressure and room temperature condition D_c is approximately 10.9 mm. Above this value the bubble becomes capped in shape and the drag effect starts to deviate from that of the smaller quasi-spherical bubbles due to a large bubble wake region [Ishii and Hibiki 2006].

The contribution of group-two capped bubbles may be very small or even negligible [Sun et al. 2002] if nearly spherical bubbles with diameters around or below the critical diameter D_c and with an almost uniform bubble size distribution are present and if the void fraction is relatively low (around or below 20%). Under these conditions a one-group transport equation is able to describe well the dynamic characteristics of the flow interfacial structure [Sun et al. 2002]. This approximation is valid in the bubbly flow regime. The derivation of and further details on the one-group interfacial area transport equation is provided in section 5.2.

The flow area affects the interaction mechanisms [Hibiki et al. 2001a]; thus the dominant mechanisms are not the same for moderate as for large diameter pipes. Bubble coalescence and breakup are schematically represented in Figure 12.

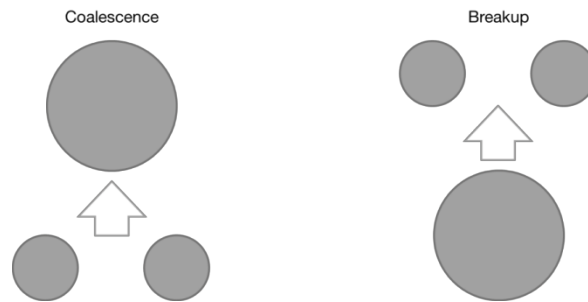


Figure 12: Schematic representation of bubble coalescence and breakup

4.3.1.2 Bubble Coalescence

In case of coalescence a new bubble is generated from the union of two existing bubbles. For air water two-phase flow two main coalescence mechanisms have been identified [Ishii and Hibiki 2006]: bubble coalescence due to random collision (due to turbulent impact of bubbles) and bubble coalescence due to wake entrainment (collision of bubble with different velocity; smaller bubbles that lay in the wake of

preceding bigger bubbles). For a schematic illustration of these processes see Figure 13.

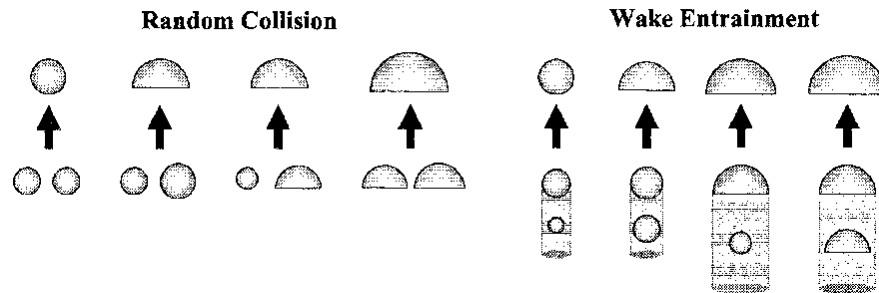


Figure 13: Schematic illustration of coalescence mechanisms [Ishii and Hibiki 2006]

A more detailed description and schematic representation of the models in the literature for the simulation of the coalescence process in case of random collision is given in section 6.2.

4.3.1.3 Bubble Breakup

In case of bubble breakup, two or more new bubbles are generated from the disintegration of an existing one. If breakup happens, the interfacial area increases and with it, and, as a consequence, the interfacial transfer rate between the phases. Several mechanisms have been identified [Ishii and Hibiki 2006]: for small spherical or nearly spherical bubbles, the relevant one is bubble breakup due to turbulent impact of the eddies against the bubble. In case of bigger bubbles (caps or slugs) other mechanisms have been identified. They are the shearing off of smaller bubbles from bigger bubbles and the formation of smaller bubbles due to disintegration caused by surface instability. For a schematic illustration of these processes see Figure 14.

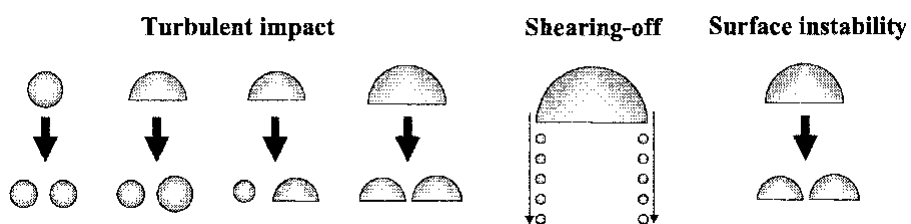


Figure 14: Schematic illustration of breakup mechanisms [Ishii and Hibiki 2006]

A more detailed description and schematic representation of the models in the literature for the simulation of the breakup process in case of turbulent impact is given in chapter 6.1.

4.3.2 Interfacial Forces Acting on the Bubbles

Several interfacial forces have been identified as having a main influence on the dynamics of bubbly flow. One is the drag force that is parallel to the flow direction; the others are non-drag forces and are perpendicular to the flow direction. The non-drag forces considered are: the lift force, the wall lubrication force, the turbulent dispersion force and the virtual mass force. The virtual mass force can be neglected since tests conducted by Frank et al. [Frank et al. 2008] showed that its influence is of minor importance in comparison with the amplitude of the other drag and non-drag forces.

In case of the presence of external fields, other forces could be also taken into consideration, but this aspect goes beyond the scope of this work.

In the next paragraphs, the forces are explained in detail and their formulation is shown. Since each force needs empirical closure relationships, the models used for the calculations in chapters 9 and 11 are introduced.

4.3.2.1 Drag Force

The drag force or friction force accounts for the drag of one phase on the other. In its generic form it can be expressed as:

$$\vec{F}_D = \frac{3}{4} C_D \frac{\alpha \rho_l}{D} |\vec{u}_g - \vec{u}_l| (\vec{u}_g - \vec{u}_l), \quad (\text{Eq. 71})$$

where C_D is the drag coefficient. In the simulations performed in chapters 9 and 11, the Grace [Grace et al. 1976] formulation is used for its determination. In fact, even if it is formulated for flow past a single bubble it is suitable also in case of low volume fractions. This model has been developed using air-water data and produces better results for air-water systems [Ansys 2009]. The Grace model for the drag coefficient considers the bubble having a distorted form similar to an ellipse. The expression for the drag coefficient is:

$$C_D = \frac{4}{3} \frac{gD}{u_r^2} \frac{\Delta\rho}{\rho_l}. \quad (\text{Eq.72})$$

Where the bubble terminal velocity is expressed as

$$u_r = \frac{\mu_l}{\rho_l} Mo^{-0.149} (J - 0.857). \quad (\text{Eq.73})$$

The parameter J is defined as it follows:

$$J = 0.94H^{0.751}, \text{ if } 2 < H < 59.3, \quad (\text{Eq.74})$$

$$J = 3.24H^{0.441}, \text{ if } H > 59.3, \quad (\text{Eq.75})$$

where H is equal to

$$H = \frac{4}{3} Eo Mo^{-0.149} \left(\frac{\mu_g}{\mu_{ref}} \right)^{-0.14}. \quad (\text{Eq.76})$$

In the equation above μ_{ref} is the water reference viscosity and it is taken to be 0.0009 kg/ms.

The Morton number and the Eötvös number are dimensionless numbers and are used to characterize the shape of bubbles or drops moving in a surrounding fluid or continuous phase. Their expressions are:

$$Mo = \frac{g\mu_l^4\Delta\rho}{\rho_l^2\sigma^3}, \quad (\text{Eq.77})$$

$$Eo = \frac{gD^2\Delta\rho}{\sigma}. \quad (\text{Eq.78})$$

4.3.2.2 Lift Force

If a bubble is rising in a liquid where velocity gradients are presents, the relative velocity will not be the same on its entire surface. This will create an asymmetric distribution of the pressure resulting in a net force applied perpendicular to the flow motion. This force is called lift force. In general it can be expressed for spherical rigid particles as [Drew and Lahey 1987]:

$$\vec{F}_L = -C_L\alpha\rho_l (\vec{u}_g - \vec{u}_l)\overrightarrow{rot}(\vec{u}_l), \quad (\text{Eq.79})$$

It has been experimentally proven that smaller bubbles migrate to the near wall region, while bigger bubbles do it towards the pipe center. The parameters that affect more the lift force are the relative velocity between the phases, the velocity gradient of the continuous phase in the curl vector and the induced particle rotation. C_L is the lift force coefficient and it takes into account the change in sign of the lift force depending on the bubble conditions. As explained previously in paragraph 4.3, there is the possibility for the bubble to move towards the pipe center or towards the wall. This is due to the change in sign of the lift force because of different effects such as:

- deformation of the bubble [Tomiya et al. 1995, Ervin and Tryggvason 1997]
- bubble rotation and asymmetries in the wake produced by the bubble itself [Moraga et al. 1999]

The debate on the causes of this force and its understanding is still open and more experimental and theoretical work is needed to deeply understand the nature of this force.

In the simulations performed in chapters 9 and 11, the Tomiyama [Tomiyama 1998] formulation is used for the evaluation of the lift coefficient as it reproduces quite well the bubble migration process introduced in paragraph 4.3. Its use is widely accepted in the scientific community for air water vertical upward bubbly flow.

In order to evaluate the lift coefficient the modified Eötvös number needs to be introduced:

$$Eo_d = \frac{g \cdot (\rho_l - \rho_g) \cdot D_h^2}{\sigma}, \quad (\text{Eq.80})$$

where D_h is the maximum horizontal bubble dimension (see Figure 15).

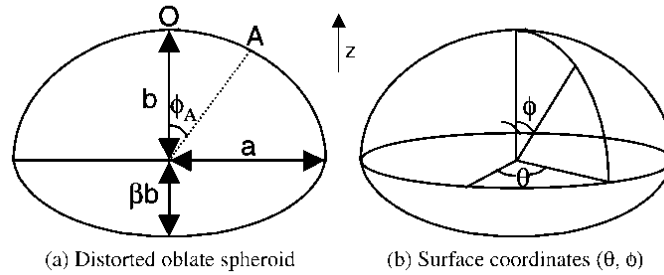


Figure 15: Dimensions and coordinates of a distorted bubble:
(a) distorted oblate spheroid (b) surface coordinates [Tomiyama et al. 2002].

It is defined by Tomiyama et al. [Tomiyama et al. 2002] to be equal to

$$D_h = 2a = D \left(\frac{\gamma}{E_f} \right)^{1/3}, \quad (\text{Eq.81})$$

where γ is a distortion factor defined by

$$\gamma = \frac{2}{1 + \beta}, \quad (\text{Eq.82})$$

and E_f is the aspect ratio for the frontal part of the bubble

$$E_f = \frac{b}{a} = \gamma E. \quad (\text{Eq.83})$$

The empirical correlation implemented in Ansys CFX for the calculation of the D_h is

$$D_h = D \sqrt[3]{1 + 0.163 \cdot Eo^{0.757}}, \quad (\text{Eq.84})$$

and is derived for **liquid drops moving in liquid media** by Wellek et al. [Wellek et al. 1966]. This correlation has been derived based on data of forty-five dispersed-continuous (**liquid-liquid**) phase systems and has been further proposed by Clift et al. [Clift et al. 1978] for the case of bubbles and drops in contaminated liquid media. In

this case the bubble distortion is much less than in gas-liquid systems. In Figure 16 it is possible to appreciate how drops and bubbles in purified systems (red dots/curve) are significantly more deformed than corresponding fluid particles in contaminated systems (green curve) [Clift et al. 1978]. In case of air-water systems (dispersed to continuous phase viscosity ratio $k=0.02$ – the data are reported from Aybers and Tapucu [Aybers and Tapucu 1969]) the aspect ratio can be at around $Eo > 0.5$ much lower, reaching measured value of up to 0.24. The greatest effect of system purity is in the ellipsoidal regime, small bubbles and drops being spherical with an aspect ratio $E = 1$; for large ones approaching $E = 0.24$ it does not matter how pure the system is [Clift et al. 1978].

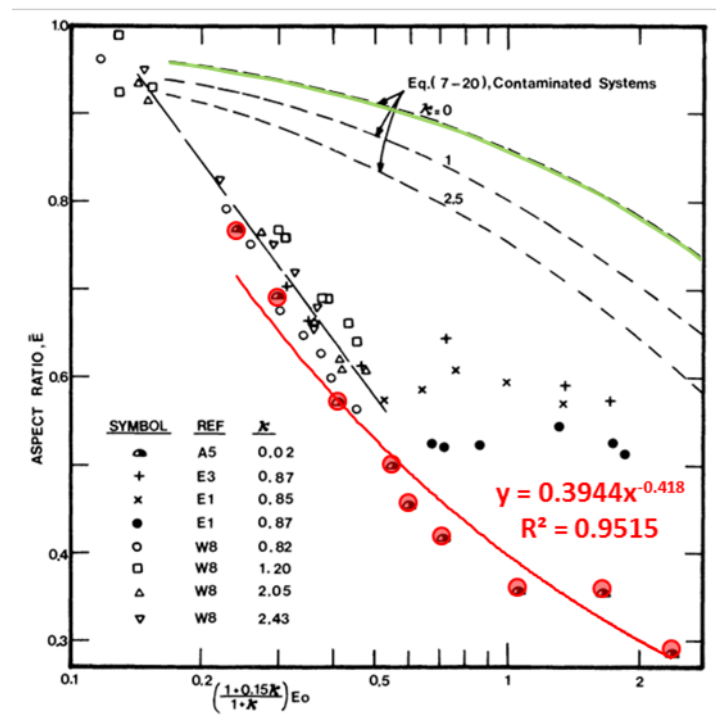


Figure 16: Deformation of drops and bubbles in pure water [Clift et al. 1978]

It is possible to find out a correlation for the data of Aybers and Tapucu (the red dots) reported in Figure 16 for the air-water case. The power law derived from this data series and shown in the figure corrected for the Eo is then

$$E = 0.3971Eo^{-0.418} . \tag{Eq.85}$$

The R-squared value of the correlation with the experimental data is

$$R^2 = 0.9515 . \tag{Eq.86}$$

Using the correlation derived from the data of Aybers and Tapucu in (Eq.85) and setting a value of $\beta = 0.5$ in order to obtain the characteristic oblate distorted spheroid it is possible to determine through (Eq.81) a characteristic maximum horizontal bubble dimension for the case of air-water mixture much larger than in case of Wellek et al.

More recently, Cai et al. [Cai et al. 2010] reported a correlation for the aspect ratio E as a function not only of the EO but also of the Re_b and of the Mo .

Cai et al. investigated the rising behaviour of single bubbles in six systems with different viscosity, and wide spectrums of the Morton number, bubbles maximum equivalent diameter and bubble Reynolds number and proposed the following correlation

$$E = 4.67Re_b^{0.625}EO^{-1}Mo^{0.291}. \quad (\text{Eq.87})$$

The lift coefficient proposed by Tomiyama [Tomiyama 1998] has this form

$$C_L = \begin{cases} \min[0.2888 \cdot \tanh(0.121 \cdot Re), f(Eo_d)] & Eo_d < 4 \\ f(Eo_d) & 4 < Eo_d < 10, \\ -0.27 & Eo_d > 10 \end{cases} \quad (\text{Eq.88})$$

where $f(Eo_d)$, the modified Eötvös number function, is defined as

$$f(Eo_d) = 0.00105Eo_d^3 - 0.0159Eo_d^2 - 0.0204Eo_d + 0.474. \quad (\text{Eq.89})$$

The behavior of the Tomiyama lift coefficient is a function of the bubble diameter D . In Figure 17 a diagram of the Tomiyama lift coefficient as a function of the bubble diameter is shown for the three distorted diameter equations presented above.

Series 2 is obtained for a value of the parameter $\beta = 0.5$ and Series 3 for a value of the $Re_b = 700$. These values are indicative and representative of the conditions of the experiments to be simulated in chapters 9 and 11.

A change in sign occurs, for air-water at atmospheric conditions, when the bubble reaches the critical diameter of ca. 5.8 mm using the correlation obtained by Wellek et al. (Wellek et al.) (see (Eq.84)). Smaller values of the critical diameter are observed if the correlations of (Eq.85) and (Eq.87) are used for the determination of the aspect ratio (Aybers and Tapucu and Cai et al.). Bubbles with a diameter smaller than the critical value will be pushed towards the wall. Bubble with a diameter bigger than that will be moved towards the pipe centerline. At higher pressures the critical diameter becomes even smaller.

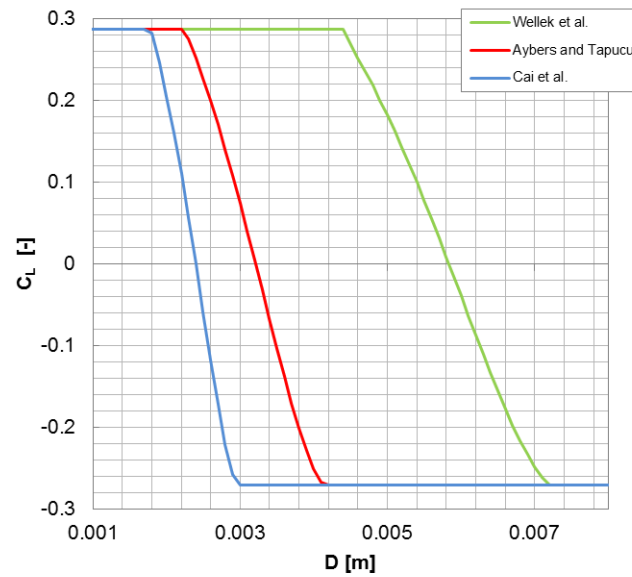


Figure 17: The behavior of the Tomiyama 1998 lift coefficient as a function of the spherical bubble diameter and different distorted diameter correlations

Doubts about the validity of using the Wellek et al. correlation in order to determine the distorted diameter for the calculation of the lift coefficient have been formulated also by Lopez de Bertodano and Prabhudharwadkar [Lopez de Bertodano and Prabhudharwadkar 2010].

They simulated the upward adiabatic bubbly two-phase flow experiment from Serizawa et al. [Serizawa et al. 1986] using the monodispersed approach. They indicated the need of adjust the lift coefficient because of the oblate distorted forms of the bubbles to the value of 0.1. In line with the value that is possible to obtain using the Aybers and Tapucu bubble distortion correlation in Figure 17.

Lopez de Bertodano and his coworker justify the choice of a constant smaller value for the lift coefficient as follows: “This is done so because the bubbles are oblate and the measurements correspond to the smaller diameter, whereas the distance from the wall is determined by the larger diameter.” [Lopez de Bertodano and Prabhudharwadkar 2010].

Furthermore, they set the average diameter of the bubbles for simulation to be 5 mm instead of using the experimental value of the Sauter diameter of 3 mm that had been measured by Serizawa et al.

In Figure 18, using the distorted diameter correlations derived from Aybers and Tapucu [Aybers and Tapucu 1969] (Eq.85) and Cai et al. [Cai et al. 2010] (Eq.87) the lift coefficient is calculated. Furthermore, each correlation is represented assuming

several values of the bubble Reynolds number or the bubble distortion to show its high sensitivity on these flow parameters. For the case of Aybers and Tapucu several bubble distortion level have been taken into considerations while for Cai et al. the bubble Reynolds number has been changed.

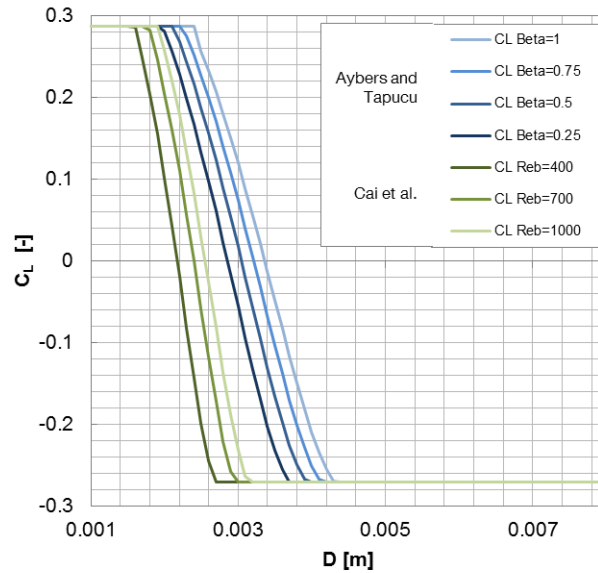


Figure 18: The behavior of the Tomiyama 1998 lift coefficient as a function of the spherical bubble diameter, different distorted diameter correlations and as a function of the bubble shape or bubble Reynolds number

Figure 17 and Figure 18 show large differences in the determination of the lift coefficient, and then of the intensity and sign of the lift force, by using different correlations for its determination. Furthermore, other important parameters depending of the flow conditions such as, for example, the bubble distortion or the bubble Reynolds number should be taken into consideration as their influence is not negligible. Concluding, the correlation defined by Wellek et al. included by default in the code Ansys CFX for the determination of the distorted diameter seems to underestimate the value of the bubble distortion, if compared to other authors, and consequently to overestimate the value of the lift coefficient. Moreover, the Wellek et al. correlation does not include the influence of the important flow parameters discussed above in his formulation.

4.3.2.3 Wall Lubrication Force

In the near wall region, the velocity of the flow on the bubble surface is modified. The created velocity gradient generates a force on the bubble to displace it away from the wall. This force is only applicable in the very near wall region. The strength of this force decays exponentially and its effect is already zero a few millimeters away from the

solid wall. Similarly to the case of the lift force, the debate on the truly causes of such a force is still open. More experimental and theoretical work is still needed to deeply understand the nature of this force.

Antal [Antal et al. 1991] derived a formula for the repulsive force that prevents bubbles attaching on the solid wall. The tests to develop his formulation have been developed for a value of the bubble Reynolds number smaller than 1500 and for a gas volume fraction less than 10%. These conditions are representative of those that are possible to be found in the near wall region and are of the same order of magnitude as the experiments simulated in chapters 9 and 11. The wall lubrication force has been modeled by Antal [Antal et al. 1991] as follows:

$$\vec{F}_{WL} = -C_{WL}\alpha\rho_l Du_{\parallel}^2 \vec{n}_w, \quad (\text{Eq.90})$$

where u_{\parallel} is the wall parallel component of the slip velocity.

The wall lubrication coefficient C_{WL} in the Antal formulation [Antal et al. 1991] has the following expression:

$$C_{WL} = \max\left(0, \frac{C_{WL1}}{D/2} + \frac{C_{WL2}}{y_w}\right). \quad (\text{Eq.91})$$

The values used for C_{WL1} and C_{WL2} that have been used for the simulations performed in chapters 9 and 11 are -0.0064 and 0.016 as proposed by Krepper et al. [Krepper et al. 2005] if the bubble induced turbulence model of Sato is used. The coefficients are -0.01 and 0.05 if the Morel model for the bubble induced turbulence is considered. Different sets of coefficient are needed if a different simulation approach is used in order to obtain these two effects: achieve a higher/lower absolute value of the wall lubrication force and extend its action not only at the near wall region.

The implementation of the wall lubrication force is necessary for the adiabatic two-phase flows, as it reproduces the void fraction peak near the wall [Lucas et al. 2004]. Krepper et al. [Krepper et al. 2007] report that its use at high-pressure wall boiling conditions may be questionable, but it is of primary importance when considering isothermal upward bubbly flow at atmospheric pressure and room temperature.

In Figure 19 a diagram of the wall lubrication force coefficient as a function of the wall distance is shown not only for the Antal [Antal et al 1991] but also for the Frank model [Frank et al. 2008].

The two models present the same decreasing exponential behavior suggested by the physical observations. Tuning the model parameters would allow to get the same

influence on the flow for both of them. Frank’s formulation is based on the Tomiyama model [Tomiyama 1998] for the wall lubrication force [Frank et al. 2008]. The problem with the formula of Tomiyama is its dependency on the pipe diameter. Following this consideration Frank proposed a generalized geometry independent formulation for the wall lubrication force [Frank et al. 2008]. Furthermore, Frank’s model has offers more tuning possibilities.

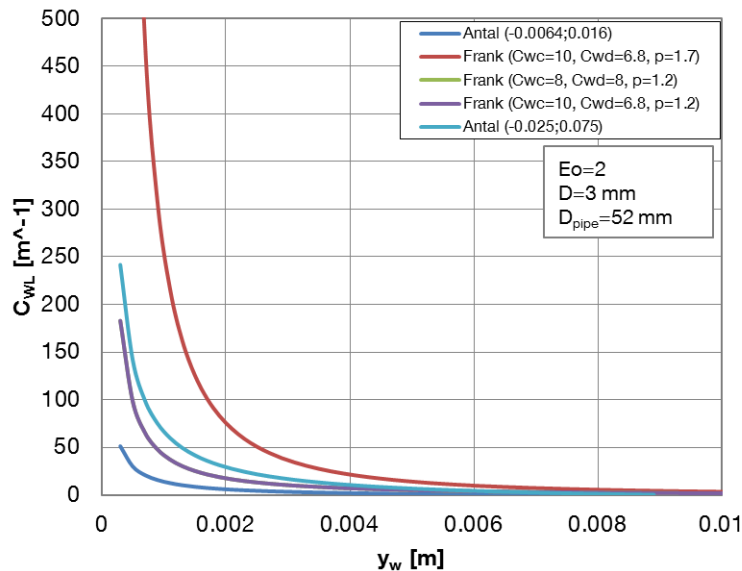


Figure 19: The behavior of the wall lubrication force coefficient as a function of the wall distance for various authors and sets of coefficients

4.3.2.4 Turbulent Dispersion Force

The turbulent dispersion force takes into account the phase dispersion from zones at higher concentration to those at a lower one due essentially to turbulent fluctuations. This force is due to a combination of the effects of the turbulent eddies and the drag force between the phases. This force has a high influence on the radial profiles of the void fraction and determines the form of the characteristic “wall peak”. In case of small bubbles (below the lift force critical diameter) concentrated in the near wall region, this force is the only one that causes a displacement of the gas phase from the wall towards the pipe centerline. On the contrary, in the bubbly to slug transition region, where the characteristic “center peak” radial distribution of the void fraction appears, this force is the only responsible for the displacement of the gas phase from the pipe centerline to the near wall region.

The turbulent dispersion force has been considered in the simulations performed in chapters 9 and 11. The Favre Averaged Drag force (FAD) [Burns et al. 2004] formulation is used for the evaluation of the turbulent dispersion force.

This force is modeled as:

$$F_{TD} = -C_{TD} \cdot C_{cd} \cdot \frac{\nu_{t,c}}{Sc_{t,c}} \left(\frac{\nabla \alpha}{\alpha} - \frac{\nabla(1-\alpha)}{(1-\alpha)} \right), \quad (\text{Eq.92})$$

where C_{cd} is the momentum transfer coefficient for the interphase drag force. The model depends on the details of the drag correlation used. $Sc_{t,c}$ is the turbulent Schmidt number for continuous phase, in general it is defined as

$$Sc = \frac{\nu}{D} = \frac{\text{viscous diffusion rate}}{\text{molecular diffusion rate}}. \quad (\text{Eq.93})$$

And it is taken to be 0.9. D is the mass diffusion coefficient due to turbulence. C_{TD} is a multiplier. Its default value is 1 in Ansys CFX, and it can be modified to increase or decrease the influence of the turbulent dispersion force.

Chapter 5

Interfacial Area Transport

In this chapter the interfacial area transport equation is derived from the more general Maxwell Boltzmann transport equation. Its physical meaning and the relation with the population balance equation are explained.

In chapter 4 the two-fluid model for the simulation of two-phase flow has been introduced and the concept of the coupling between the equation systems of the two fluids has been introduced. The interfacial transfer of mass, momentum and energy are proportionally related to the interfacial area density and to a driving force particular to each local transfer mechanism and needs to be modeled separately.

The interfacial transfer rate in a given volume can be expressed as the product of an interfacial flux by the available interfacial area:

$$\text{Interfacial transfer rate} = A_i \times \text{Interfacial flux} ,$$

where A_i represents the actual interfacial area and not the volumetric one, or interfacial area concentration.

It is therefore clear that an accurate determination of the interfacial area is important to achieve good local and global prediction of two-phase flow characteristics.

Nevertheless, it is difficult to define the concept of two-phase flow regime mathematically based on a local formulation, because it is defined at a geometric scale more similar to that of the entire system [Ishii and Hibiki 2006]. For this reason, a better manner to model the interfacial area concentration is to do it directly by means of a transport equation, especially for the three-dimensional formulation of two-phase flow.

Based on the Boltzmann transport equation Kocamustafaogullari and Ishii [Kocamustafaogullari and Ishii 1995] derived the interfacial area transport equation.

The Boltzmann equation is an integro-differential equation of the particle distribution function $f(V, \vec{x}, \vec{v}, t)$ and describes the particle transport across the system domain.

The distribution function is defined per unit of mixture and bubble volume. In neutron transport theory, because the energy of neutrons can vary within several orders of magnitude, the velocity of the particles \vec{v} cannot be neglected. In case of a two-phase flow system, however, if the space and time intervals considered are sufficiently small, the particle distribution function can then be simplified to be $f(V, \vec{x}, t)$, which means a uniform particle velocity for a given particle size.

The Boltzmann transport equations of particles having the distribution function $f(V, \vec{x}, t)$ is:

$$\frac{\partial f}{\partial t} + \nabla \cdot (f\vec{v}) + \frac{\partial}{\partial V} \left(f \frac{dV}{dt} \right) = \sum_j S_j + S_{ph}. \quad (\text{Eq.94})$$

In order to be used in practice, (Eq.94) furnishes a too high detailed level of information. Furthermore, as discussed by Ishii and Hibiki [Ishii and Hibiki 2006], a more macroscopic formulation is desirable. This more suitable version of the Boltzmann transport equation for practical applications is the so-called bubble number density transport equation. Since the interfacial area of fluid particles is closely related to the particle number and size [Ishii and Hibiki 2006], in the next section first the particle number density and then the interfacial area transport equation will be derived from (Eq.94).

5.1 Particle number density transport equation

The particle number density transport equation, also known as Population Balance Equation (PBE), can be derived from (Eq.94) by integrating it over the volume of all particle sizes (from V_{min} to V_{max}) and applying the Leibnitz integration rule [Ishii and Hibiki 2006].

The bubble particle density transport equation can be written as:

$$\frac{\partial n}{\partial t} + \nabla \cdot (n\vec{v}_{pm}) = \sum_j R_j + R_{ph}, \quad (\text{Eq.95})$$

where \vec{v}_{pm} is the average local particle velocity weighted by particle, n is the number of particles of all sizes per unit mixture volume and R_j are the source and sink rates. They are defined as:

$$\vec{v}_{pm}(\vec{x}, t) = \frac{\int_{V_{min}}^{V_{max}} f(V, \vec{x}, t) \vec{v}(V, \vec{x}, t) dV}{\int_{V_{min}}^{V_{max}} f(V, \vec{x}, t) dV}, \quad (\text{Eq.96})$$

$$n(\vec{x}, t) = \int_{V_{min}}^{V_{max}} f(V, \vec{x}, t) dV, \quad (\text{Eq.97})$$

and

$$R(\vec{x}, t) = \int_{V_{min}}^{V_{max}} S(V, \vec{x}, t) dV. \quad (\text{Eq.98})$$

5.2 Interfacial area density transport equation

In a similar way as shown for the particle number density transport equation, Ishii and Hibiki [Ishii and Hibiki 2006] obtained the interfacial area transport equation. The Boltzmann transport equations is multiplied by the surface area of the particles of volume V and integrated again over the volume of all particles:

$$\frac{\partial a_i}{\partial t} + \nabla \cdot (a_i \vec{v}_i) - \left(\frac{1}{V} \frac{dV}{dt} \right) \int_{V_{min}}^{V_{max}} f V dA_i = \int_{V_{min}}^{V_{max}} \sum_j (S_j + S_{ph}) A_i dV, \quad (\text{Eq.99})$$

where a_i , the average interfacial area density of all fluid particles of volume between V_{min} and V_{max} , and \vec{v}_i , the interfacial velocity are given by:

$$a_i(\vec{x}, t) = \int_{V_{min}}^{V_{max}} f(V, \vec{x}, t) A_i(V) dV \quad (\text{Eq.100})$$

and

$$\vec{v}_i(\vec{x}, t) = \frac{\int_{V_{min}}^{V_{max}} f(V, \vec{x}, t) A_i(V) \vec{v}(V, \vec{x}, t) dV}{\int_{V_{min}}^{V_{max}} f(V, \vec{x}, t) A_i(V) dV}. \quad (\text{Eq.101})$$

In order to define the third term on the LHS of (Eq.99), the concept of volume-equivalent diameter D_e and surface-equivalent diameter D_s need to be introduced. The volume-equivalent diameter D_e is the diameter of the sphere having the same volume of a particle with volume V so that $V \equiv \pi/6 D_e^3$. The surface-equivalent diameter D_s is the diameter of the sphere having the same surface area of a particle with surface area A_i so that $A_i \equiv \pi D_s^2$.

Furthermore, if the expression of volume source given by Ishii and Hibiki [Ishii and Hibiki 2006] is used one obtains:

$$\frac{\partial a_i}{\partial t} + \nabla \cdot (a_i \vec{v}_i) - \frac{2}{3} \left(\frac{a_i}{\alpha} \right) \left[\frac{\partial \alpha}{\partial t} + \nabla \cdot (\alpha \vec{v}_g) - \eta_{ph} \right] = \int_{V_{min}}^{V_{max}} \sum_j (S_j + S_{ph}) A_i dV, \quad (\text{Eq.102})$$

where the third term on the LHS is the change of the interfacial area density due to particle volume change.

The source and sink terms are:

$$\int_{V_{min}}^{V_{max}} \sum_j S_j dV = \sum_j R_j \text{ (in the bubble number density transport equation)} \quad (\text{Eq.103})$$

and

$$\int_{V_{min}}^{V_{max}} \sum_j S_j A_i dV = \sum_j \Phi_j \text{ (in the interfacial area density transport equation)} \quad (\text{Eq.104})$$

The relationship between them is:

$$\Phi_j = R_j \Delta A_i . \quad (\text{Eq.105})$$

R_j can be modeled mechanistically for each interaction mechanism and ΔA_i , the general change of surface area after one interaction, can be rewritten as a function of a_i and α by:

$$a_i = n A_i \quad (\text{Eq.106})$$

and

$$\alpha = n V , \quad (\text{Eq.107})$$

so that, according to Ishii and Hibiki [Ishii and Hibiki 2006],

$$n = \psi \frac{a_i^3}{\alpha^2} . \quad (\text{Eq.108})$$

In (Eq.108), ψ is the so called shape factor that in general is equal to

$$\psi = \frac{1}{36\pi} \left(\frac{D_{Sm}}{D_e} \right)^3 , \quad (\text{Eq.109})$$

where D_{Sm} is the Sauter mean diameter given by

$$D_{Sm} = \frac{6\alpha}{a_i} , \quad (\text{Eq.110})$$

Combining (Eq.109) and (Eq.110) with (Eq.105), Φ_j is given by

$$\Phi_j = \frac{1}{3\psi} \left(\frac{\alpha}{a_i} \right)^2 R_j . \quad (\text{Eq.111})$$

Similarly for the nucleation process:

$$\Phi_{ph} = \pi D_{bc}^2 R_{ph} , \quad (\text{Eq.112})$$

where D_{bc} is the bubble critical size.

Finally the interfacial area density transport equation can be rewritten like this:

$$\frac{\partial a_i}{\partial t} + \nabla \cdot (a_i \vec{v}_i) = \frac{2}{3} \left(\frac{a_i}{\alpha} \right) \left[\frac{\partial \alpha}{\partial t} + \nabla \cdot (\alpha \vec{v}_g) - \eta_{ph} \right] + \frac{1}{3\psi} \left(\frac{\alpha}{a_i} \right)^2 \sum_j R_j + \pi D_{bc}^2 R_{ph}. \quad (\text{Eq.113})$$

In (Eq.113), the LHS represent the time dependent and the convective rate of change of the interfacial area density. In the RHS, the first term represent the rate of change due to particle volume change due to change in pressure, the second term the rate of change due to particle interaction mechanisms and, the third, due to phase change.

In case of small spherical bubbles and without any phase change equation (Eq.113) becomes:

$$\frac{\partial a_i}{\partial t} + \nabla \cdot (a_i \vec{v}_i) = \frac{2}{3} \left(\frac{a_i}{\alpha} \right) \left[\frac{\partial \alpha}{\partial t} + \nabla \cdot (\alpha \vec{v}_g) \right] + 12\pi \left(\frac{\alpha}{a_i} \right)^2 \sum_j R_j \quad (\text{Eq.114})$$

since $\psi = 1/36\pi$ in case of small spherical bubbles.

In steady state condition equation (Eq.114) becomes

$$\nabla \cdot (a_i \vec{v}_i) = \frac{2}{3} \left(\frac{a_i}{\alpha} \right) \left[\frac{\partial \alpha}{\partial t} + \nabla \cdot (\alpha \vec{v}_g) \right] + 12\pi \left(\frac{\alpha}{a_i} \right)^2 \sum_j R_j. \quad (\text{Eq.115})$$

Chapter 6

Review of Theoretical Models for Bubble Coalescence and Breakup Processes of Interest for the One-Group Interfacial Area Density Transport Equation

In this chapter the general form of source and sink terms for the one-group is derived from the multi-group population balance equation. Following this, a literature review regarding the coalescence and breakup models for the definition of bubble interaction terms for the one-group interfacial area transport equation is presented.

The bubble interaction mechanisms source and sink terms of the population balance equation (Eq.95) can be expressed in an explicit way as follows:

$$\sum_j R_j = R_b - R_c = R_{b,Bi} - R_{b,De} + R_{c,Bi} - R_{c,De} \quad (\text{Eq.116})$$

where:

$R_{c,Bi}$ = number of particles of volume v generated from coalescence of smaller bubbles.

$R_{b,Bi}$ = number of particle of volume v generated from breakup of bigger bubbles.

$R_{c,De}$ = number of particles of volume v destroyed from coalescence into bigger bubbles.

$R_{b,De}$ = number of particle of volume v destroyed from breakup into smaller bubbles.

It is possible to group the bubble coalescence birth and death rates in the following form

$$Bi = R_{b,Bi} + R_{c,Bi} , \quad (\text{Eq.117})$$

$$De = -R_{b,De} - R_{c,De} , \quad (\text{Eq.118})$$

in order to express the global birth and the death rate of bubbles.

If the population balance equation is written for a polydispersed flow the above cited coalescence and breakup death and birth rate are written for each bubble group following the scheme in Figure 20. The arrows entering and exiting the i -th group represent the birth Bi and the death De rate of bubbles of the i -th group respectively.

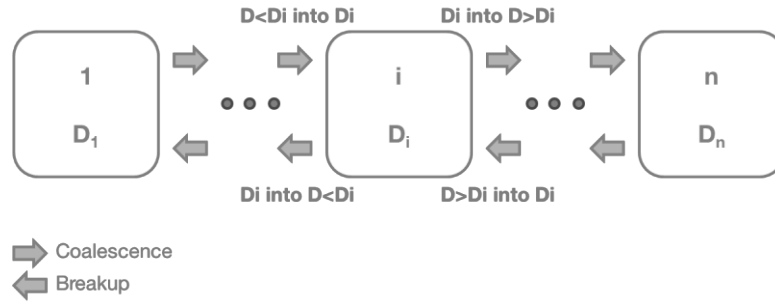


Figure 20: Schematic representation of coalescence and breakup birth and death rate for the i -th group of bubbles

In general, if no nucleation is assumed, it is possible to express Bi and De as follows [Martinez Bazan 1998]:

$$Bi = \underbrace{\int_v^\infty m(v') f_b(v') p(v, v') n(v') dv'}_{R_{b,Bi}} + \underbrace{\int_0^v f_{coll}(v - v', v') n(v - v') n(v') \eta_c(v - v', v') dv'}_{R_{c,Bi}} \quad (\text{Eq.119})$$

$$De = - \underbrace{f_b(v) n(v)}_{R_{b,De}} - \underbrace{n(v) \int_0^\infty f_{coll}(v, v') n(v') \eta_c(v, v') dv'}_{R_{c,De}} \quad (\text{Eq.120})$$

where $m(v')$ is the mean number of daughter bubbles formed upon the breakup of a mother bubble of volume v' , $f_b(v)$ and $f_b(v')$ are the breakup frequency of bubbles of volume v and v' , $p(v, v')$ is the size probability density function of daughter bubbles resulting from breakup of bubble of volume v' , $f_{coll}(v - v', v')$ and $f_{coll}(v, v')$ are the collision frequency of bubbles of volume v' with bubbles of volume $v - v'$ and v , $\eta_c(v - v', v')$ and $\eta_c(v, v')$ are the coalescence efficiency of a collision between bubbles of volume v' and bubbles of volume $v - v'$ and v .

On the contrary, if the monodispersed approach is considered, the information of the several bubble size groups is lost and only one bubble group with an average bubble size is present, calculated considering all the bubbles in the system. For this reason, only bubbles of this class can collide between them and breakup. The source and sink terms of (Eq.119) and (Eq.120) can be expressed as follows:

$$Bi = f_b n, \quad (\text{Eq.121})$$

$$De = -\frac{1}{2} f_{coll} n \eta_c, \quad (\text{Eq.122})$$

where the coefficient 1/2 has been introduced in order to consider only one collision event for each bubble pair.

A breakup efficiency is not explicitly expressed in (Eq.121) since it is contained, when considered by the different authors, in the breakup frequency term. In fact, similarly to the coalescence case the breakup frequency could be expressed as the collision frequency of the turbulent eddies against the bubble multiplied by a collision efficiency. Other authors consider a breakup event happens as soon as certain turbulence conditions are reached.

Bubble interaction mechanisms are very complex processes and their numerical reproduction should be based on a series of assumptions that simplify the problem to be solved. Jo and Revankar [Jo and Revankar 2010a] summarize them as follows.

For the **breakup** process:

- 1) Binary breakup: one bubble splits into two bubbles of equal or unequal size.
- 2) Local isotropic and nearly homogenous turbulence: the statistics of the small scale motion of eddies are universal.
- 3) The bubble size lies in the inertial subrange: characteristics of bubble and eddy motion in turbulent flow can be expressed as a function of the kinetic energy dissipation only.

For the **coalescence** process:

- 1) Collision and entrapment of a liquid film between the bubbles.
(this process determines the collision frequency)
- 2) The liquid film drains until it reaches a critical thickness.
- 3) Liquid film rupture: coalescence occurs.
(process 2 and 3 determine the collision efficiency)

In the next subsections, a literature review of the **physical models** developed for the prediction of the bubble breakup, collision frequency and for the coalescence efficiency is presented. Only the models related to the random collision and turbulent impact mechanisms have been considered because of interest for the definition of the birth and death rate of bubbles for the one-group interfacial area density (see paragraph 4.3.1).

The review is based on the work of Lasheras et al. [Lasheras et al. 2002] and on the works of Liao and Lucas [Liao and Lucas 2009, 2010] which, at the moment, represent the most actual, accurate and complete literature reviews in the field. For a more detailed overview, consider reading Lasheras et al. [Lasheras et al. 2002] and Liao and Lucas [Liao and Lucas 2009, 2010].

6.1 Turbulence Fluctuation and Collision Particle Breakup Frequency Models

The breakup of fluid particles is caused mainly by two effects, pressure fluctuations along their surface or by particle-eddy collisions. Liao and Lucas [Liao and Lucas 2009] describe briefly the initiation of the disintegration process caused by these two effects. The particle modifies its spherical form and when the oscillations reach a critical amplitude required to make the surface unstable, it starts to deform and stretch up to a point where it fragments in two or more daughter particles. Under the point of view of forces causing disintegration, the breakup process can be expressed as a balance between the dynamic pressure τ_i and the surface stress τ_s .

Liao and Lucas distinguished 5 breakup criteria in the literature (see Figure 21):

- a) Turbulent kinetic energy of the particle greater than a critical value
 - Coualoglou and Tavlarides 1977 [Coualoglou and Tavlarides 1977]
 - Chatzi et al. [Chatzi et al. 1983 1987 1989]
- b) Velocity fluctuation around the particle surface greater than a critical value
 - Narsimhan and Ghupta 1979 [Narsimhan and Ghupta 1979]
 - Alopaeus et al. 2002a, b [Alopaeus et al. 2002a, b]
- c) Turbulent kinetic energy of the hitting eddy greater than a critical value
 - Lee et al. 1987 [Lee et al. 1987 a, b]
 - Prince and Blanch 1990 [Prince and Blanch 1990]
 - Tsouris and Tavlarides 1994 [Tsouris and Tavlarides 1994]
 - Luo and Svendsen 1996 [Luo and Svendsen 1996]
 - Martinez Bazán et al. 1999 [Martinez Bazan et al. 1999]
- d) Inertial force of the hitting eddy greater than the interfacial force of the smallest daughter particle
 - Lehr and Mewes 1999 [Lehr and Mewes 1999]
 - Lehr et al. 2002 [Lehr et al. 2002]
- e) Combination of c and d

- Wang et al. 2003 [Wang et al. 2003]
- Zhao and Ge 2007 [Zhao and Ge 2007]

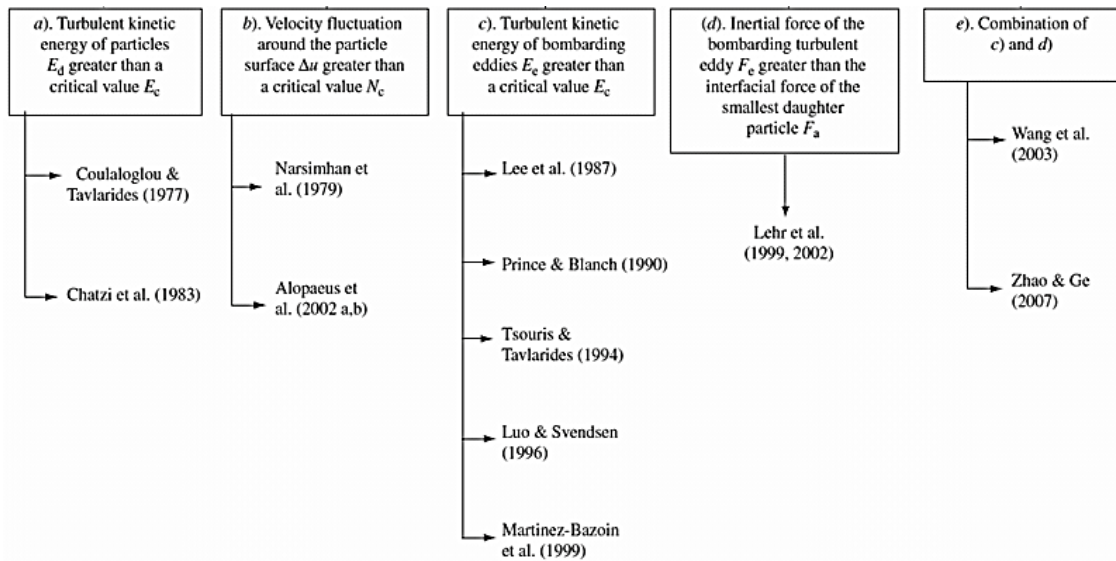


Figure 21: Classification of models for breakup frequency in case of turbulent fluctuation and collision [Liao and Lucas 2009]

Martinez Bazán [Martinez Bazan 1998] argued that most of the models in the literature are based on a theory essentially similar to the kinetic theory of gases. Furthermore, the models assume that turbulence is manifested as an array of eddies with well-defined sizes and densities. In order to obtain values from these models a collision cross section has to be defined and from this an eddy arrival frequency. Furthermore, closure parameters that can alter significantly their behavior, such as integration limits, have to be set.

Liao and Lucas [Liao and Lucas 2009] reported that it is impossible to validate the models based on the eddy concept. It is in fact difficult to obtain reliable data regarding the density or size of eddies that take part to interactions with bubbles. The only model avoiding the eddy concept is that proposed by Martinez Bazán.

The models presented in the literature are written for homogeneous isotropic turbulence and considering eddies with characteristic dimension lying in the inertial subrange.

In general, the models deliver results with a difference of several orders of magnitude between them. Furthermore the breakup frequency models are inconsistent and different models present completely different behavior (monotonic functions vs. functions presenting a peak) [Liao and Lucas 2009].

Lasheras et al. [Lasheras et al .2002] presented a review of models for the break-up of an immiscible fluid immerse into a fully developed turbulent flow for particle breakup frequency. The works of Coualoglou and Tavlarides [Coualoglou and Tavlarides 1977], Konno et al. [Konno et al. 1980], Prince and Blanch [Prince and Blanch 1990], Tsouris and Tavlarides [Tsouris and Tavlarides 1994] Luo and Svendsen [Luo and Svendsen 1996] and Martinez Bazán [Martinez Bazan 1999] have been critically analyzed in order to point out the limits of the actual theory. Even in case where the authors argued not to use empirically determined constants in their models, these shown a strong dependency on upper and lower integration limits for the calculation of the breakup frequency. In the next sections a short overview of the above cited models is given.

6.1.1 Coualoglou and Tavlarides Model

Coualoglou and Tavlarides [Coualoglou and Tavlarides 1977], defined the breakup frequency of a particle with diameter D as:

$$f_b = \left(\frac{\text{fraction of drops breaking}}{\text{breakup time}} \right) = \frac{1}{t_b} \frac{\Delta N(D)}{N(D)}, \quad (\text{Eq.123})$$

where $N(D)$ is the total number of particles with diameter D. the fraction of drops breaking have been modeled as follows:

$$\frac{\Delta N(D)}{N(D)} = \exp\left(-\frac{E_c}{\bar{E}}\right) = \exp\left(-\frac{c_1 \sigma D^2}{c_2 \rho D^3 \overline{\Delta u^2}(D)}\right), \quad (\text{Eq.124})$$

where E_c is the surface energy and \bar{E} the mean turbulent kinetic energy between two points separated by a distance D.

The breakup time has been assumed to be the turbulent turnover time as

$$t_b \propto D^{2/3} \varepsilon^{-1/3}. \quad (\text{Eq.125})$$

Substituting (Eq.124) and (Eq.125) in (Eq.123) leads to

$$f_b = C_{CT1} D^{-2/3} \varepsilon^{1/3} \exp\left(-\frac{C_{CT2} \sigma}{\rho D^3 \varepsilon^{2/3} D^{5/3}}\right), \quad (\text{Eq.126})$$

where C_{CT1} and C_{CT2} are two constants to be found experimentally.

6.1.2 Konno et al. Model

Departing from the Coualoglou and Tavlarides formulation Konno et al. [Konno et al. 1980] expressed the breakup frequency by considering a Maxwell distribution for the probability density function of relative fluctuating velocity between two points in the flow $\overline{\Delta u}(D)$.

$$f_b = C_K \frac{\sqrt{\Delta u^2(D)}}{D} \int_{u^*}^{\infty} 3 \sqrt{\frac{6}{\pi}} x^2 \exp\left(-\frac{3x^2}{2}\right) dx , \quad (\text{Eq.127})$$

where $u^* = u_c / \sqrt{\Delta u^2(D)}$ and u_c is a critical velocity.

6.1.3 Prince and Blanch model

Prince and Blanch [Prince and Blanch 1990] theorized that the breakup process is the results of the collisions between the particles and the turbulent eddies and defined the breakup frequency as the results of the eddy-particle collision frequency $f_{b,coll}$ multiplied by the breakup efficiency η_b as follows

$$f_b = f_{b,coll} \eta_b , \quad (\text{Eq.128})$$

where

$$f_{b,coll} = n_e S_{De} u_{rel,De} . \quad (\text{Eq.129})$$

In (Eq.129), n_e is the number density of eddies, S_{De} is the collision cross sectional area between eddies and particles and $u_{rel,De}$ is the relative collision velocity between the eddy and the particle.

They used an expression for the number of eddies as a function of wavenumber as developed by Azbel and Athanasios [Azbel and Athanasios 1983]:

$$\frac{dn_e(D)}{dk(D)} = 0.1k^2 . \quad (\text{Eq.130})$$

The wavenumber is a property of a wave and is proportional to the reciprocal of the wavelength. In order to avoid the problem that equation (Eq.130) goes to infinity with the wavenumber k , **Prince and Blanch set arbitrarily the lower integration limit to 20% of the bubble size.**

The cross-sectional collision area has been defined to be

$$S_{De} = \frac{\pi}{4} \left(\frac{D}{2} + \frac{D_e}{2} \right)^2 , \quad (\text{Eq.131})$$

while, following the classic kinetic theory of gases [Houston 2001], it should be

$$S_{De} = \frac{\pi}{4} (D + D_e)^2 = \pi \left(\frac{D}{2} + \frac{D_e}{2} \right)^2 . \quad (\text{Eq.132})$$

(Eq.131) delivers a value 4 times smaller than (Eq.132).

The relative collision velocity between the particles and the eddies has been defined as

$$u_{rel,De} = (\overline{\Delta u_D^2} + \overline{\Delta u_e^2})^{1/2}, \quad (\text{Eq.133})$$

where in general $\overline{\Delta u_{\parallel}^2}$ is following Rotta [Rotta 1972]

$$\overline{\Delta u_{\parallel}^2} \approx 2(\varepsilon D)^{2/3}.$$

The bubble breakup efficiency η_b similarly to Coulaloglou and Tavlarides has been defined as

$$\eta_b = \exp\left(-\frac{u_{cD}^2}{\Delta u_e^2}\right), \quad (\text{Eq.134})$$

where the critical value of the particle velocity u_{cD} is

$$u_{cD} = 1.52 \left(\frac{\sigma}{\rho D}\right)^{1/2}. \quad (\text{Eq.135})$$

Substituting the equations above from (Eq.129) to (Eq.135) in (Eq.128), in integral form the breakup frequency is

$$f_b(D) = \int_0^{10\pi/D} \frac{0.14\pi}{16} \left(D + \frac{2\pi}{k}\right)^2 \left(D^{2/3} + \left(\frac{2\pi}{k}\right)^{2/3}\right)^{1/2} \varepsilon^{1/3} \exp\left(-\frac{1.18}{(2\pi)^{2/3}} \frac{\sigma k^{2/3}}{\rho D \varepsilon^{2/3}}\right) k^2 dk. \quad (\text{Eq.136})$$

The lower limit of integration have not been set by Prince and Blanch and **the upper limit has been set arbitrarily** to $2\pi/0.2D$ claiming that eddies with characteristic dimension less than 20% of the bubble size do not have enough energy to break up the bubble. Lasheras et al. [Lasheras et al. 2002] argued that one can simply show that the model is very sensitive to the upper integration limit and, therefore, it cannot be chosen arbitrarily. In Figure 22 the breakup frequency as a function of the bubble diameter obtained using the Prince and Blanch model for different values of the upper limit of the integration is shown. The surface tension, the liquid density and the turbulence eddy dissipation values have been kept constant and are $\sigma = 0.072 \text{ N/m}^{-1}$, $\rho = 1000 \text{ kg/m}^3$ and $\varepsilon = 1 \text{ m}^2/\text{s}^3$ respectively.

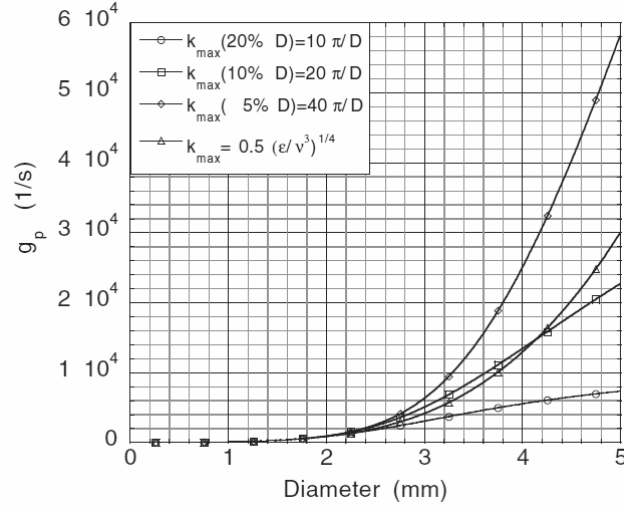


Figure 22: Breakup frequency calculated as Prince and Blanch 1990 model for different values of the upper integration limit as a function of the bubble diameter [Lasheras et al. 2002]

6.1.4 Tsouris and Tavlarides Model

Tsouris and Tavlarides [Tsouris and Tavlarides 1994] reviewed critically the Coualoglou and Tavlarides model. They argued that the model predicted a critical diameter at which the breakup frequency is maximized. Lasheras et al. [Lasheras et al 2002] reports that also the model of Konno et al. and that of Prince and Blanch present the same behavior. The new model proposed by Tsouris and Tavlarides predicted a monotonic increase of the breakup frequency with the particle diameter.

Similarly to Prince and Blanch, the bubble breakup frequency can be written as

$$f_b(D) = C_{T1} \int_{n_e} S_{D_e} (\overline{\Delta u_D^2} + \overline{\Delta u_e^2})^{1/2} \exp\left(-\frac{C_{T2} E_c}{e}\right) dn_e, \quad (\text{Eq.137})$$

where the cross sectional area is

$$S_{D_e} = \pi(D + D_e)^2 \quad (\text{Eq.138})$$

and the average turbulent velocities of a particle of diameter D and of a turbulent eddy of length $D_e = 2/k$ are

$$\overline{\Delta u_D^2} = 1.07(\varepsilon D)^{2/3}, \quad (\text{Eq.139})$$

$$\overline{\Delta u_e^2} = 8.2\varepsilon^{2/3} k^{-2/3}. \quad (\text{Eq.140})$$

The average energy of an eddy of size D_e has been defined as

$$e = 0.43\rho\pi D_e^{11/3} \varepsilon^{2/3}. \quad (\text{Eq.141})$$

The activation energy E_c , is defined to be the minimum energy needed for breakup to occur is defined as

$$E_c = \frac{\pi\sigma}{2} \left[2 \left(\frac{D}{2^{1/3}} \right)^2 + D_{max}^2 + D_{min}^2 - 2D^2 \right], \quad (\text{Eq.142})$$

where D_{min} is the minimum particle size and $D_{max} = (D^3 - D_{min}^3)^{1/3}$ is the complementary particle size.

Finally the rearranged expression for the breakup frequency is

$$\begin{aligned} f_b(D) &= C_{T1} F(\alpha) \int_{2/D}^{2/D_{min,e}} k^2 \left(D + \frac{2}{k} \right)^2 \left(1.07 D^{2/3} \right. \\ &\quad \left. + \frac{8.2}{k^{2/3}} \right)^{1/2} \exp \left(-C_{T2} \frac{\pi\sigma \left[2 \left(\frac{D}{2^{1/3}} \right)^2 + D_{max}^2 + D_{min}^2 - 2D^2 \right]}{0.43\rho\pi D_e^{11/3} \varepsilon^{2/3}} \right) dk, \end{aligned} \quad (\text{Eq.143})$$

where $F(\alpha)$ is a turbulence damping factor due to the presence of the gas phase, α is the void fraction and $D_{min,e}$ is an **arbitrarily defined minimum eddy size**. Tsouris and Tavlarides concluded that the breakup frequency is independent from the integration limits. Lasheras et al. [Lasheras et al. 2002] demonstrated that this does not hold true and that the choice of the lower limit of integration strongly affects the breakup frequency calculation. In Figure 23, the breakup frequency as a function of the bubble diameter is obtained using the Tsouris and Tavlarides model for different values of the lower limit of the integration. The surface tension, the liquid density and the turbulence eddy dissipation values have been kept constant and are $\sigma = 0.072 \text{ N/m}^{-1}$, $\rho = 1000 \text{ kg/m}^3$ and $\varepsilon = 1 \text{ m}^2/\text{s}^3$ respectively.

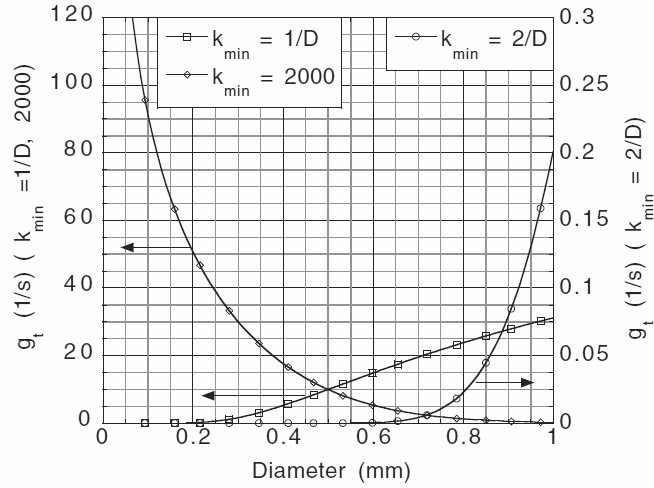


Figure 23: Breakup frequency calculated as Tsouris and Tavlarides 1994 model for different values of the lower integration limit as a function of the bubble diameter [Lasheras et al. 2002]

6.1.5 Luo and Svendsen Model

Luo and Svendsen [Luo and Svendsen 1996] proposed a model based on the kinetic theory of ideal gases. The breakup frequency is calculated considering a collision frequency between eddies of size D_e and particles of size D and a collision efficiency.

The breakup collision frequency is expressed as

$$f_{b,coll}(D) = \frac{\pi}{4} (D + D_e)^2 (\overline{\Delta u_{D_e}^2})^{1/2} \frac{dn_e}{dD_e}, \quad (\text{Eq.144})$$

where

$$\overline{\Delta u_{D_e}^2} = 2.045(\varepsilon D)^{2/3} \quad (\text{Eq.145})$$

and

$$\frac{dn_e}{dD_e} = \frac{0.822(1 - \alpha)}{D_e^4} \quad (\text{Eq.146})$$

with α being the void fraction.

The breakup efficiency η_b has been written as

$$\eta_b = \exp\left(-\frac{\overline{E_c}(D)}{\bar{e}(D_e)}\right), \quad (\text{Eq.147})$$

where $\bar{e}(D_e)$ is the mean kinetic energy of an eddy of size D_e

$$\bar{e}(D_e) = \frac{2.045\pi\rho}{12} D_e^{11/3} \varepsilon^{2/3}, \quad (\text{Eq.148})$$

and $\overline{E}_c(D)$ is the increase in surface energy if a particle of diameter D is broken into particles of size D_1 and $(D^3 - D_1^3)^{1/3}$

$$\overline{E}_c(D) = \pi\sigma(D_1^2 + (D^3 - D_1^3)^{2/3} - D^2). \quad (\text{Eq.149})$$

Finally, in dimensionless form, considering $\xi = D_e/D$, $f_v = D_1^3/D^3$, $0 \leq C_f = f_v^{2/3} + (1 - f_v)^{2/3} - 1 \leq 0.26$ depending on the daughter drop diameter and $\xi_{min} = D_{min,e}/D$, the bubble breakup frequency of a particle of diameter D can be expressed as

$$f_b(D) = \frac{1}{2} \int_0^1 \left(0.923(1 - \alpha) \left(\frac{\varepsilon}{D^2} \right)^{1/3} \int_{\xi_{min}}^1 \frac{(1 + \xi)^2}{\xi^{11/3}} \exp\left(-\frac{12C_f\sigma}{2.045\rho\varepsilon^{2/3}D^{5/3}\xi^{11/3}}\right) d\xi \right) df_v. \quad (\text{Eq.150})$$

Lasheras et al [Lasheras et al. 2002] found the model of **Leo and Svendsen very sensitive to the upper limit of integration**. In Figure 24, the breakup frequency as a function of the bubble diameter is obtained using the Luo and Svendsen model for different values of the upper limit of the integration. The surface tension, the liquid density and the turbulence eddy dissipation values have been kept constant and are $\sigma = 0.072 \text{ N/m}^{-1}$, $\rho = 1000 \text{ kg/m}^3$ and $\varepsilon = 1 \text{ m}^2/\text{s}^3$ respectively.

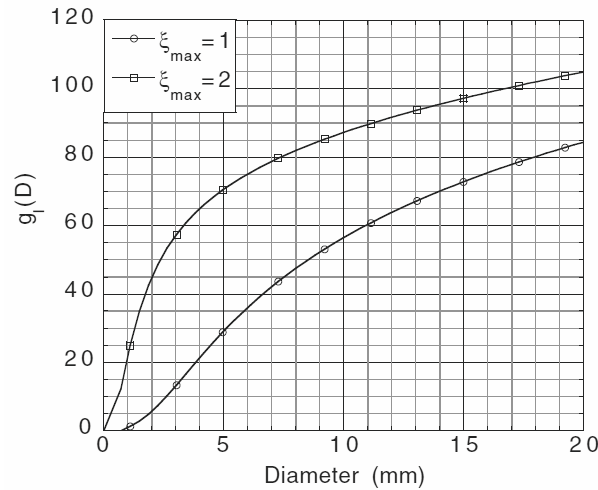


Figure 24: Breakup frequency calculated as Luo and Svendsen 1996 model for different values of the upper integration limit as a function of the bubble diameter [Lasheras et al. 2002]

6.1.6 Martinez Bazán Model

Martinez Bazán [Martinez Bazan 1998], proposed a model based only on kinematic ideas with a limited influence from empirical parameters. The premise of his model is that “for a particle to break, its surface has to be deformed and the deformation energy

must be provided by the turbulent stresses produced by the surrounding fluid” [Martinez Bazan 1998]. It means also that no bubble breakup frequency model is needed if this approach is considered.

The minimum energy provided to a bubble immersed in a surrounding liquid to deform is [Martinez Bazan 1998]:

$$E_s(D) = \pi\sigma D^2. \quad (\text{Eq.151})$$

Assuming that the viscous forces are negligible in comparison with the surface tension forces, the surface energy per unit volume, namely the surface restoring pressure, is:

$$\tau_s(D) = \frac{6E_s}{\pi D^3} = 6 \frac{\sigma}{D}. \quad (\text{Eq.152})$$

The average deformation energy per unit volume produced by turbulent stresses due to velocity fluctuations existing in the liquid between two points at a distance D can be estimated as:

$$\tau_t(D) = \frac{1}{2} \rho \overline{\Delta u^2}(D). \quad (\text{Eq.153})$$

Martinez Bazán proposed that when $\tau_t(D) > \tau_s(D)$ then the bubble deforms and eventually breaks up. The bubble deformation equation is then:

$$a_b = \frac{u_b}{t_b} = \frac{\sum F_{ext}}{Mass} = \frac{1}{2} \frac{\overline{\Delta u^2}(D)}{D} - 6 \frac{\sigma}{\rho D^2}, \quad (\text{Eq.154})$$

where a_b , u_b , t_b are the characteristic acceleration, velocity and time of the bubble break-up and F_{ext} are the external forces acting on the bubble of Diameter D.

Since $u_b \propto D/t_b$ it is possible to write the bubble frequency as

$$f_b \propto \frac{\sqrt{\overline{\Delta u^2}(D) - 12 \frac{\sigma}{\rho D^2}}}{D}. \quad (\text{Eq.155})$$

It is possible to determine the mean value of the velocity fluctuation $\overline{\Delta u^2}(D)$ by the mean of (Eq.25) considering a value for the Kolmogorov constant α equal to 1.7 (valid for the special case of submerged jets). The result for β is then 8.2. It is worth to remember that contribution of the whole turbulence spectrum energy scales while determining $\overline{\Delta u^2}(D)$ is take into account.

Finally one can write

$$f_b = K_b \frac{\sqrt{\beta(\varepsilon D)^{2/3} - 12 \frac{\sigma}{\rho D^2}}}{D}, \quad (\text{Eq.156})$$

with K_b is equal to 0.25 [Martinez Bazan 1998]. It corresponds to the value in millimeters at which the turbulent stresses are equivalent to the surface tension stresses.

In his experiment air was injected along the centerline of a submerged water jet. In that case the fixed value of 0.25 was obtained by “best fitting the transient volume probability density functions while solving the inverse problem of calculating the daughter probability density function” [Martinez Bazan 1998].

Varying K_b is equivalent to modifying the breakup frequency. It has a strong influence in cases where the value of ε is changing significantly along the flow path like the case of his experiment [Martinez Bazan 1998]. Adjusting the parameter K_b influences the results of the bubble frequency so that the final bubble size distribution is reached faster as f_b increases.

A dimensionless formulation of the bubble breakup frequency is given by Martinez Bazán et al. [Martinez Bazan et al. 2010]:

$$f_b^* = \frac{f_b D^{2/3}}{\varepsilon^{1/3}} = K_b \beta^{1/2} \sqrt{1 - \frac{1}{We_t}}, \quad (\text{Eq.157})$$

where the $We_t = (\rho \beta \varepsilon^{2/3} D^{5/3}) / (12\sigma)$.

It is then possible to change the value of β in the model and this is equal to modifying the value of the critical turbulent Weber number We_{tc} . In case of (Eq.156) the formulation is equivalent to set the number of the We_{tc} equal to 1 due to the given definition of the turbulent and the confinement stresses acting on the bubbles.

Finally, an even more general expression for the dimensionless formulation of the bubble breakup frequency is [Martinez Bazan et al. 2010]:

$$f_b^* = \frac{f_b D^{2/3}}{\varepsilon^{1/3}} = C_b \sqrt{1 - \frac{We_{tc}}{We_t}} \quad (\text{Eq.158})$$

where C_b is a constant.

6.2 Physical Models for the Determination of the Coalescence Frequency

The bubble coalescence frequency is calculated from the collision frequency and the coalescence efficiency. Liao and Lucas [Liao and Lucas 2010] operated a categorization and summarized all the models present in literature in the scheme of Figure 25. Of interest for our purposes are the physical models for the evaluation of the collision frequency and the coalescence efficiency for the case of the turbulent random motion-induced collisions only.

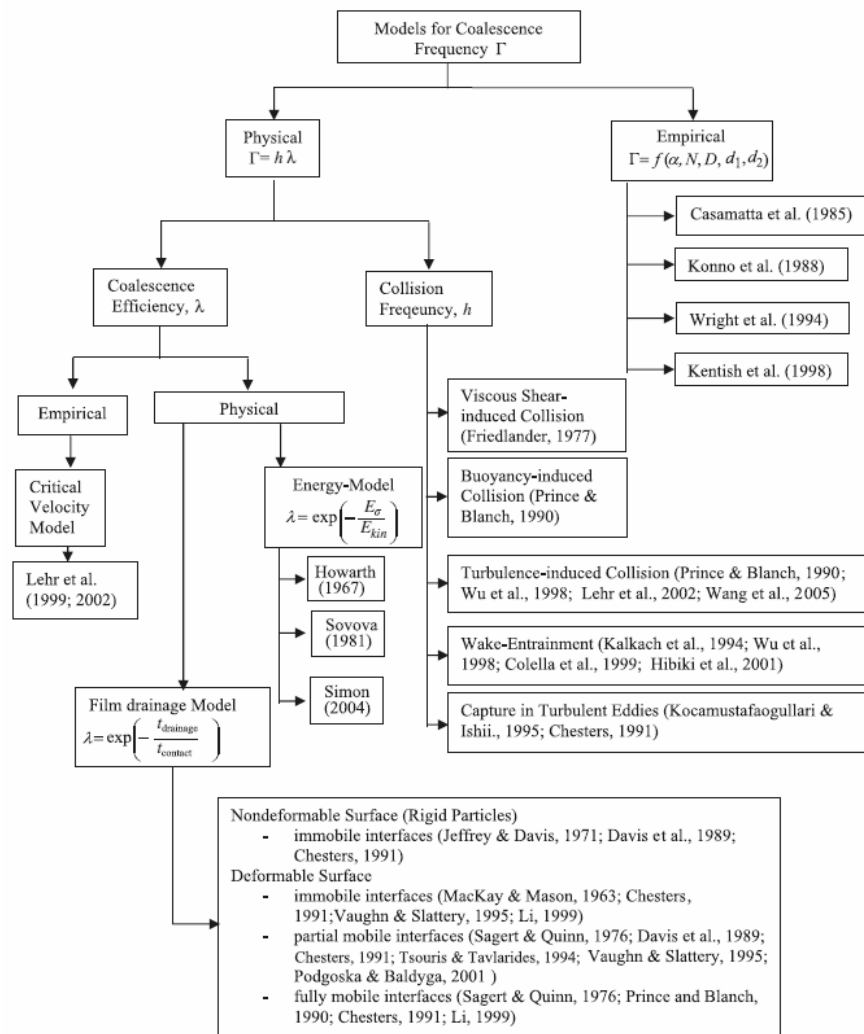


Figure 25: Classification of theories and models for the evaluation of the coalescence frequency in literature [Liao and Lucas 2010]

The calculation of the collision frequency, considering different mechanisms, relies on arbitrary assumptions and empirical correlations. In general, given the complicated fact

of taking different phenomena into account, most models assume arbitrarily dominant mechanisms and neglect other without further validation [Liao and Lucas 2010].

6.2.1 Collision frequency

As already discussed in the previous paragraph, a variety of mechanisms that promote collisions among bubbles exists. Liao and Lucas [Liao and Lucas 2010] list five of them, but of interest for the one-group interfacial area density transport equation is that of the turbulent random motion-induced collisions.

In this case, collisions of bubbles are caused by the fluctuating turbulent velocity of the liquid surrounding the bubble. Also in this case, similarly to the breakup case, the random motion of the particles in the fluid is assumed to be similar to the movement of the gas molecules in the gas kinetic theory and the concepts of collision cross sectional area S_{12} (the subscripts 1 and 2 denotes the two particles taking part in the collision process) and particle relative velocity u_{rel} are of primary importance. Kennard [Kennard 1938], in 1938 interpreted the collision frequency as the effective volume swept by the particle in a unit time:

$$f_{coll} = S_{12}u_{rel} , \quad (\text{Eq.159})$$

where

$$S_{12} = \frac{\pi}{4} (D_1 + D_2)^2 . \quad (\text{Eq.160})$$

Several authors like Coualoglou and Tavlarides [Coualoglou and Tavlarides 1977], Lee et al. [Lee et al. 1987a, b], Prince and Blanch [Prince and Blanch 1990] and Luo and Svendsen [Luo and Svendsen 1996] in order to determine the approach velocity u_{rel} , assumed for the colliding bubbles the velocity of an equal sized eddy so that:

$$u_{rel} = (u_{t1}^2 + u_{t2}^2)^{1/2} , \quad (\text{Eq.161})$$

where u_t is the velocity of the equal sized eddy that is calculated as reported in (Eq.26) as:

$$u_t \propto (\varepsilon D)^{2/3} . \quad (\text{Eq.162})$$

It is possible to express f_{coll} as follows:

$$f_{coll} \propto \frac{\pi}{4} (D_1 + D_2)^2 \left(D_1^{2/3} + D_2^{2/3} \right)^{1/2} \varepsilon^{1/3} . \quad (\text{Eq.163})$$

Essentially three modification factors can be applied to (Eq.163): C , γ and Π . The first takes into account the effect of the size ratio between bubbles and eddies [Colin et al. 2004], the second considers the existence of bubbles that reduces the free space for

bubble movement and causes an increase in the collision frequency [Wu et al. 1998] [Hibiki and Ishii 2000a] [Lehr and Mewes 1999] [Lehr et al. 2002] [Wang et al. 2003]. The third is about the ratio of the mean distance between bubbles to their average relative turbulent path length [Wu et al. 1998] [Wang et al. 2003].

Applying these modification factors (Eq.163) becomes

$$f_{coll} = C\gamma\Pi\frac{\pi}{4}(D_1 + D_2)^2 \left(D_1^{2/3} + D_2^{2/3}\right)^{1/2} \varepsilon^{1/3} . \quad (\text{Eq.164})$$

Liao and Lucas [Liao and Lucas 2010] report that the need for the modification factor Π and the formulation of Π and γ demands further investigation. The main differences in the models present in the literature lie in the calculation of the relative velocity u_{rel} and in the formulation of the factors γ and Π . For example, Chesters [Chesters 1991] uses for the relative velocity, the proportionality

$$u_{rel} \propto (D_1 + D_2)^{1/3} , \quad (\text{Eq.165})$$

while others use

$$u_{rel} \propto \left(D_1^{2/3} + D_2^{2/3}\right)^{1/2} . \quad (\text{Eq.166})$$

Other discrepancies lie in the definition of the proportionality factor in the expression of the eddy velocity u_t .

The results of the collision frequency as a function of the bubble diameter for different models in literature are summarized in Figure 26. The parameters that have been kept constant and their values are shown in the diagram.

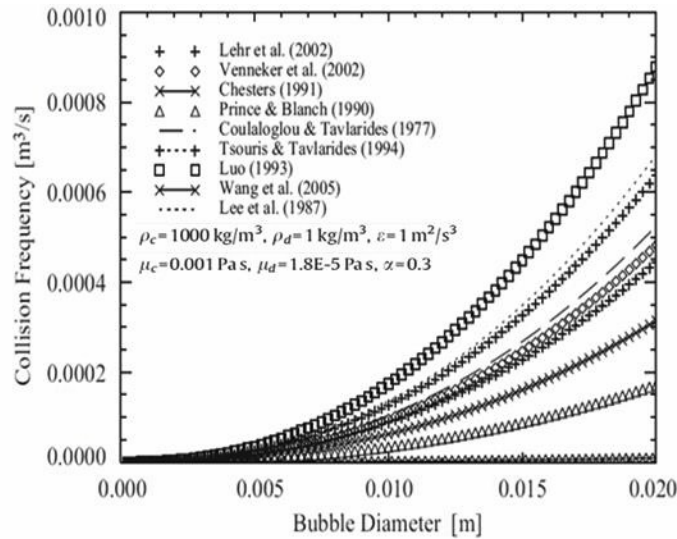


Figure 26: The dependency of the turbulent collision frequency on the bubble size [Liao and Lucas 2010].

6.2.2 Coalescence Efficiency

Liao and Lucas [Liao and Lucas 2010] report that a number of experiments show that only a fraction of collisions lead to coalescence while most of the colliding particles separate apart after collision. Based on this consideration, it is reasonable to introduce an efficiency for the description of the coalescence process. In literature three models have been used for the calculation of the coalescence efficiency [Liao and Lucas 2010]:

- Energy model,
- Critical approach velocity model,
- Film drainage model.

6.2.2.1 Energy Model

The energy model has been proposed by Howart [Howart 1967] and later has been confirmed experimentally by Kuboi et al. [Kuboi et al. 1972b] and Park and Blair [Park and Blair 1975]. They found out that a significant fraction of collisions results in immediate coalescence and the probability increases with increasing energy.

Following these considerations Sovova [Sovova 1981] wrote the following expression to link the surface energy E_σ with the kinetic collision energy E_{Kin} :

$$\eta_c = \exp\left(-C \frac{E_\sigma}{E_{Kin}}\right). \quad (\text{Eq.167})$$

Later on this approach has been used by Simon [Simon 2004]. Sovova and Simon's models are different in the manner in which they express the kinetic collision energy.

Sovova assumed E_{Kin} to be proportional to an "average" volume and to the relative velocity of two colliding bubbles:

$$E_{Kin} = \frac{1}{2} \rho_d \frac{V_1 V_2}{V_1 + V_2} u_{rel}^2. \quad (\text{Eq.168})$$

Simon calculated the E_{Kin} from a momentum balance during collision:

$$E_{Kin} = \rho_d \varepsilon^{2/3} \left(V_1^{11/9} + V_2^{11/9} \right). \quad (\text{Eq.169})$$

Both used the same expression for the surface energy E_σ and considered it as proportional to the surface tension:

$$E_\sigma = \sigma \left(V_1^{2/3} + V_2^{2/3} \right). \quad (\text{Eq.170})$$

6.2.2.2 Critical Approach Velocity Model

Based on the observation of Doubliez [Doubliez 1991] and Duineveld [Duineveld 1994], that demonstrated that coalescence is more probable in case of gentle collisions, Lehr et al. [Lehr et al. 2002] and Lehr and Mewes [Lehr and Mewes 1999] wrote an expression to link the coalescence efficiency to the bubble relative velocity:

$$\eta_c = \max\left(\frac{u_{crit}}{u_{rel}}, 1\right), \quad (\text{Eq.171})$$

where the value of the u_{crit} has to be determined experimentally.

6.2.2.3 Film Drainage Model

Following the work of Ross [Ross 1971], Coualoglou [Coualoglou 1975] wrote the following simplified expression for the collision efficiency:

$$\eta_c = \exp\left(-\frac{t_{contact}}{t_{drainage}}\right). \quad (\text{Eq.172})$$

Liao and Lucas [Liao and Lucas 2010] report that even if little criticism appears in the literature regarding the validity of the two timescales, the film drainage model is up to now the most popular model and has been used as starting point for almost all subsequent models. The models differ in the expressions used for the drainage and contact time.

For the calculation of the drainage time $t_{drainage}$, the following cases in the literature have been classified by Liao and Lucas [Liao and Lucas 2010]:

- *Non deformable rigid spheres*

Particles/bubbles are very viscous compared to the continuous phase or very small

- *Deformable particles with immobile interfaces*

When two bubbles approach, the liquid film trapped between the interfaces is expelled by a laminar flow with no slip at the interfaces. Coualoglou and Tavlarides [Coualoglou and Tavlarides 1977] used this approach for their model. This approximation is only applicable to extremely dispersed phase viscosity.

- *Deformable particles with partially mobile interfaces*

The drainage is assumed to be controlled by the motion of the liquid surface. Chesters [Chesters 1991] developed his model following this approach (see Chapter 10).

- *Deformable particles with fully mobile interfaces*

This is the most complicated closure model and the drainage process is controlled by both inertia and viscous forces. In order to simplify the problem the drainage time has been written for **high viscous liquids**, where the film is thinning viscously and the drainage velocity is independent from the film size, or for **inertia-controlled thinning**, for example in case of bubbles in turbulent flow.

Expressions for the determination of the drainage time $t_{drainage}$ and for the contact time $t_{contact}$ will be introduced in the next chapters.

Chapter 7

Review of Most Important Constitutive Models for the One-Group Interfacial Area Transport Equation

In this chapter the review of the most important constitutive models for the one-group interfacial area transport equation is presented. The models are critically analyzed and the collision and breakup rates and the coalescence and breakup efficiencies obtained by using these models are compared.

7.1 Wu, Ishii and Kim – 1998

Wu et al. [Wu et al. 1998] developed bubble interaction mechanism terms for the one-group interfacial area transport equation by considering the contribution of the bubbles' random collisions, bubble wake entrainment and turbulence impact of the eddies against the bubbles. To identify the adjustable parameters in the source and sink terms presented in the models of the constitutive relationships for the interaction mechanisms, experimental data of a steady air-water cocurrent upward flow in a 50.8 mm diameter pipe have been used. For more detailed information about the fitting procedure for the different regions of the bubbly flow regime see Wu et al. [Wu et al. 1998].

7.1.1 Modeling of Bubble Coalescence Due to Random Collision

The bubble coalescence rate modeled by Wu et al. [Wu et al. 1998] based on the bubble random collision induced by turbulence in the continuous medium can be summarized as follows:

$$\Phi_{RC} = -12\pi \left(\frac{\alpha}{a_i}\right)^2 f_{coll} n \eta_c . \quad (\text{Eq.173})$$

The collisions are postulated to occur only between neighboring bubbles. In this case the collision frequency is considered to be:

$$f_{coll1} = \frac{u_t}{\bar{L}} \propto \frac{(\varepsilon D)^{1/3}}{\frac{D}{\alpha^{1/3}} \left(\frac{\alpha_{max}^{1/3} - \alpha^{1/3}}{\alpha_{max}^{1/3}} \right)}, \quad (\text{Eq.174})$$

where u_t is the root-mean-square approaching velocity of the two bubbles, and \bar{L} represents the mean travelling distance between the two bubbles for one collision. The value of α_{max} is 0.74 and is the value of the dense packing limit by definition.

The expression is then multiplied by a modification term p_{coll} . This takes into consideration two separate effects: the first is that not always the bubbles are moving towards each other and the second to take into account that no matter how far away the bubbles are, the collision would occur as long as there is a finite approaching velocity:

$$p_{coll} \propto \left(\frac{\alpha}{\alpha_{max}} \right)^{2/3} \left[1 - \exp \left(-C \frac{\alpha_{max}^{1/3} \alpha^{1/3}}{\alpha_{max}^{1/3} - \alpha^{1/3}} \right) \right]. \quad (\text{Eq.175})$$

The final expression for the bubble collision frequency obtained by Wu et al [Wu et al. 1998], except for a proportionality constant, is:

$$f_{coll} = f_{coll1} p_{coll} \propto \frac{(\varepsilon D)^{1/3}}{\frac{D}{\alpha^{1/3}} \left(\frac{\alpha_{max}^{1/3} - \alpha^{1/3}}{\alpha_{max}^{1/3}} \right)} \left(\frac{\alpha}{\alpha_{max}} \right)^{2/3} \left[1 - \exp \left(-C \frac{\alpha_{max}^{1/3} \alpha^{1/3}}{\alpha_{max}^{1/3} - \alpha^{1/3}} \right) \right]. \quad (\text{Eq.176})$$

It is worth noting that the authors decided not to implement a coalescence efficiency model. This is due to the fact that the coalescence rate decreases exponentially with respect to the turbulent fluctuating velocity. This decreasing trend is, following Wu et al. [Wu et al. 1998] very strong and caused, while tuning the model, tremendous discrepancies for different liquid flow conditions. Wu et al [Wu et al. 1998], in order to depict the randomness of the coalescence phenomenon after each collision decided then to use a constant coefficient for the collision frequency η_c in (Eq.173). The value of this coefficient is **not explicitly given** in the work, but it is contained in the constant C_{RC} . This coefficient summarizes also other proportionality constants present in the model but not reported explicitly. The final form for the interfacial area change rate due to random collision considering spherical bubbles is:

$$\begin{aligned}
\Phi_{RC} &= -12\pi \left(\frac{\alpha}{a_i}\right)^2 f_{coll} n \eta_c \\
&= -12\pi \left(\frac{\alpha}{a_i}\right)^2 C_{RC} \frac{(\varepsilon D)^{1/3}}{\frac{D}{\alpha^{1/3}} \left(\frac{\alpha_{max}^{1/3} - \alpha^{1/3}}{\alpha_{max}^{1/3}}\right)} \left(\frac{\alpha}{\alpha_{max}}\right)^{2/3} \left[1 \right. \\
&\quad \left. - \exp\left(-C \frac{\alpha_{max}^{1/3} \alpha^{1/3}}{\alpha_{max}^{1/3} - \alpha^{1/3}}\right) \right] \left(\frac{6\alpha}{\pi D^3}\right)
\end{aligned} \tag{Eq.177}$$

where the value of C is 3. The value of C_{RC} has been found empirically, by fitting a large set of experimental data, to be equal to 0.0565.

7.1.2 Modeling of Bubble Coalescence Due to Wake Entrainment

The bubble coalescence rate modeled by Wu et al. [Wu et al. 1998] based on the bubble wake entrainment can be summarized as follows:

$$\Phi_{WE} = -12\pi \left(\frac{\alpha}{a_i}\right)^2 f_{we} n \eta_{we}. \tag{Eq.178}$$

In order to define the expression of the bubble coalescence frequency f_{we} , the value of the volume of the wake region V_w has to be defined:

$$V_w = \frac{1}{4} \pi D^2 \left(L_w - \frac{D}{2}\right), \tag{Eq.179}$$

where L_w is the wake region length. In this volume the following bubbles may collide with the leading one.

Assuming the effective number of bubbles in the wake region as $N_w = nV_w$ and assuming Δt , the collision time interval, the collision frequency would be:

$$f_{we} = \frac{1}{2} \frac{N_w}{\Delta t} = \frac{1}{8} \pi D^2 \frac{\left(L_w - \frac{D}{2}\right)}{\Delta t} n = \frac{1}{8} \pi D^2 (\overline{u_{rw}}) n, \tag{Eq.180}$$

where $\overline{u_{rw}}$ is the average relative velocity between the leading bubbles and the bubbles in the wake region. It is given by:

$$\overline{u_{rw}} = u_r F\left(\frac{D}{L_w}\right), \tag{Eq.181}$$

where u_r is the bubble terminal velocity and F is a function to describe the form of the bubble wake region. Its analytic form is not relevant, since the bubble region may not be fully established. Tsuchiya et al. [Tsuchiya et al. 1989] defined the ratio L_w/D to be around 5 to 7 for air-water systems. F , for our purposes, can be treated as a constant.

Wu et al. [Wu et al. 1998] defined the bubble terminal velocity following Ishii and Chawla [Ishii and Chawla 1979]. The expression is based on the balance between the buoyancy force and drag force in a two-phase bubbly flow:

$$u_r = \left[\frac{Dg(\rho_l - \rho_g)}{3C_D\rho_l} \right]^{1/2}, \quad (\text{Eq.182})$$

where C_D is the interfacial drag coefficient.

The final form for the interfacial area change rate due to wake entrainment considering spherical bubbles is:

$$\Phi_{WE} = -12\pi \left(\frac{\alpha}{a_i} \right)^2 f_{we} n \eta_{we} = -12\pi \left(\frac{\alpha}{a_i} \right)^2 C_{WE} \pi D^2 (u_r) n, \quad (\text{Eq.183})$$

where C_{WE} is an adjustable constant to summarize several parameters in the equations above. It is mainly determined by the ratio of the effective wake length to the bubble size and the coalescence efficiency. Wu et al. [Wu et al. 1998] set it equal to 0.151.

7.1.3 Modeling of Bubble Breakup Due to Turbulence Impact

The bubble breakup is considered to occur due to the impact of turbulent eddies in the continuous medium. Their formulation can be in general summarized as follows:

$$\Phi_{TI} = 12\pi \left(\frac{\alpha}{a_i} \right)^2 f_{b,coll} n \eta_b. \quad (\text{Eq.184})$$

The expression of the bubble-eddies collision frequency is based on a momentum balance approach, considering that only the eddies of the same order of magnitude of the bubble size can break it. For more detail see Wu et al. [Wu et al. 1998]

The proportionality for the bubble-eddies collision frequency is

$$f_{b,coll} \propto \frac{(\varepsilon D)^{1/3}}{D} \left(1 - \frac{We_{cr}}{We} \right)^{1/2} \quad We = \frac{\rho_l u_t^2 D}{\sigma} > We_{cr}. \quad (\text{Eq.185})$$

In homogeneous turbulent flow, the probability for a bubble to collide with an eddy that has sufficient energy to break the bubble is approximately:

$$\eta_b = \exp\left(-\frac{We_{cr}}{We}\right) \quad We > We_{cr}. \quad (\text{Eq.186})$$

The final form of the interfacial area change rate due to turbulent impact is:

$$\Phi_{TI} = 12\pi \left(\frac{\alpha}{a_i} \right)^2 C_{TI} \frac{(\varepsilon D)^{1/3}}{D} \left(1 - \frac{We_{cr}}{We} \right)^{1/2} \left(\frac{6\alpha}{\pi D^3} \right) \exp\left(-\frac{We_{cr}}{We}\right). \quad (\text{Eq.187})$$

Also in this case the coefficient C_{TI} contains proportionality factors not expressed explicitly. Its value has been found empirically, by fitting a large set of experimental data, to be equal to 2. The value of the critical Weber number is 0.18.

7.2 Hibiki and Ishii – 2000

Hibiki and Ishii [Hibiki and Ishii 2000a] developed bubble interaction mechanism terms for the one-group interfacial area transport equation considering only the contribution of the bubbles random collision and turbulence impact of the eddies against the bubbles. No wake entrainment was considered.

7.2.1 Modeling of Bubble Coalescence Due to Random Collision

The bubble coalescence is considered to occur due to bubble random collision induced by turbulence in the liquid phase. Their formulation can be in general summarized as follows:

$$\Phi_{RC} = -12\pi \left(\frac{\alpha}{\alpha_i}\right)^2 f_{coll} n \eta_c. \quad (\text{Eq.188})$$

The bubble collision frequency f_{coll} , assuming that the bubbles behave as ideal gas molecules, can be expressed considering the bubble velocity $\overline{u_c}$ as a function of the surface S_c and the volume V_c available for collision. Due to the fact that a part of the system volume is inaccessible to the bubbles because of the other bubbles already present in it, the concept of “excluded volume” should be introduced to calculate the V_c available for collision. Taking into account the excluded volume for bubbles, the final form of the bubble collision frequency is:

$$f_{coll} = \frac{\gamma'_c \alpha \varepsilon^{1/3}}{D^{2/3} (\alpha_{max} - \alpha)}, \quad (\text{Eq.189})$$

where γ'_c is an adjustable constant tuned on experimental data. The turbulent energy dissipation ε , in this special case is obtained from the mechanical energy equation using this expression:

$$\varepsilon = \frac{\langle j \rangle}{\rho_m} \left(-\frac{dP}{dz} \right)_F, \quad (\text{Eq.190})$$

where j is the mixture volumetric flux, ρ_m is the mixture density and $(-dP/dz)_F$ is the gradient of pressure caused by the frictional losses along the flow direction.

The value of α_{max} is 0.52 and was given by Taitel et al. [Taitel et al. 1980] as the finely dispersed bubbly to slug flow transition limit.

Hibiki and Ishii [Hibiki and Ishii 2000a] based the formulation of the collision efficiency on the work of Coulaloglou and Tavlarides [Coulaloglou and Tavlarides 1977]. Their formulation is a function of the time required for coalescence t_c and the contact time t_i and can be expressed as:

$$\eta_c = \exp\left(-\frac{t_c}{t_i}\right) = \exp\left(-K_c \sqrt[6]{\frac{D^5 \rho_l^3 \varepsilon^2}{\sigma^3}}\right). \quad (\text{Eq.191})$$

In this expression K_c is coefficient and its value is found to be 1.29. This value is also obtained based on assumptions for the liquid initial and critical film thickness at the point where film rupture occurs.

Substituting expression (Eq.189) and (Eq.191) in (Eq.188), the final expression for the interfacial area change rate due to random collision obtained by Hibiki and Ishii [Hibiki and Ishii 2000a] is:

$$\Phi_{RC} = -\frac{72\gamma'_c}{\Gamma_c} \left(\frac{\alpha}{a_i}\right)^2 \frac{\alpha^2 \varepsilon^{1/3}}{D^{11/3}(\alpha_{max} - \alpha)} \exp\left(-K_c \sqrt[6]{\frac{D^5 \rho_l^3 \varepsilon^2}{\sigma^3}}\right), \quad (\text{Eq.192})$$

where Γ_c is set by the authors to be 0.188, γ'_c is then around 0.00261.

7.2.2 Modeling of Bubble Breakup Due to Turbulence Impact

The bubble breakup is considered to occur due to the collision of the turbulent eddies with the bubbles. Their formulation can be in general summarized as follows:

$$\Phi_{TI} = 12\pi \left(\frac{\alpha}{a_i}\right)^2 f_{b,coll} n_e \eta_b. \quad (\text{Eq.193})$$

The formulation of the bubble-eddy collision frequency $f_{b,coll}$ is based on the concept that only eddies with characteristic length of the same order of magnitude of the bubble diameters have enough energy to break it but not so much to only transport it. The eddy number density will be obtained referring to the volume of the liquid phase based on the work of Azbel and Athanasios [Azbel and Athanasios 1983]. The bubble-eddy collision frequency $f_{b,coll}$ is calculated by assuming that the bubbles behave as ideal gas molecules. Assuming the same bubbles velocity $\overline{u_b}$ as a function of the surface S_b and the volume V_b available to collision and taking into account the excluded volume for bubbles, the final form of the bubble-eddy collision frequency is:

$$f_{b,coll} = \frac{\gamma'_b \alpha \varepsilon^{1/3}}{D^{2/3}(\alpha_{max} - \alpha)}, \quad (\text{Eq.194})$$

where γ'_b is an adjustable constant tuned on experimental data. Again the value considered for α_{max} is 0.52.

In order to obtain the value of the breakup rate, the breakup efficiency is calculated based on the considerations of Tsouris and Tavlarides [Tsouris and Tavlarides 1994] on the energy content of a single eddy in the flow.

The final expression of the bubble breakup efficiency is expressed in terms of an exponential function of the ratio between of the energy required for breakup E_b and the energy content of a single eddy E_e multiplied by a constant η of order 1.

$$\eta_b = \exp\left(-\frac{E_b}{\eta E_e}\right) = \exp\left(-K_b \frac{\sigma}{\rho_l D^{5/3} \varepsilon^{2/3}}\right), \quad (\text{Eq.195})$$

where K_b is a constant which was determined based on the assumptions above and its value is 1.37. For detail see Hibiki and Ishii [Hibiki and Ishii 2000a].

Considering that the only eddies which have an adequate energy level to break up the bubbles have a dimension similar to that of the bubble, the number of eddies n_e in the liquid volume can be computes as:

$$n_e = \frac{6(1 - \alpha)}{\pi D^3}. \quad (\text{Eq.196})$$

Substituting (Eq.194), (Eq.195) and (Eq.196) in (Eq.193), the final expression for the interfacial area change rate due to turbulent impact of the eddies with bubbles obtained by Hibiki and Ishii [Hibiki and Ishii 2000a] is:

$$\Phi_{TI} = \frac{72\gamma'_b}{\Gamma_b} \left(\frac{\alpha}{\alpha_i}\right)^2 \frac{\alpha(1 - \alpha)\varepsilon^{1/3}}{D^{11/3}(\alpha_{max} - \alpha)} \exp\left(-K_b \frac{\sigma}{\rho_l D^{5/3} \varepsilon^{2/3}}\right), \quad (\text{Eq.197})$$

where Γ_b is set by the authors to be 0.264 and γ'_b is then around 0.00367.

7.3 Ishii and Kim – 2001

Ishii and Kim [Ishii and Kim 2001] developed in 2001 a micro four-sensor conductivity probe to obtain data of the radial distribution of the main parameters of interest for the study of two-phase flow evolution. They extended the database available for the assessment of the source and sink terms proposed by Wu at al [Wu et al. 1998] previously with such a measurement technique. The authors benchmarked the model of Wu et al. [Wu et al. 1998] against the new data averaged over the channel cross sectional area. This was done in order to simplify the evaluation procedure. In this way the covariance of the terms under study is negligible, since all parameters are assumed to have uniform profiles along the radial direction [Ishii and Kim 2001].

They proposed a new set of empirical coefficient as given below:

$$C_{TI} = 0.085 \quad C_{RC} = 0.004 \quad C = 3.0$$

$$C_{WE} = 0.002 \quad We_{cr} = 6.0 \quad \alpha_{max} = 0.75$$

7.4 Yao and Morel – 2004

Yao and Morel [Yao and Morel 2004] developed bubble interaction mechanism terms for the one-group interfacial area transport equation considering only the contribution of the bubbles random collision and the turbulence impact of the eddies against the bubbles.

The main modification introduced by Yao and Morel regarding the contributions analyzed previously regarding the bubble coalescence and breakup is:

- 1) The bubble and coalescence time is split into two contributions (free travelling time and interaction time).
- 2) The breakup interaction time is modeled according to the bubble-eddy resonance mechanism.

Yao and Morel used their coalescence and breakup models in combination to the bubble induced turbulence model explained in section 4.2.2.2.

7.4.1 Modeling of Bubble Coalescence Due to Random Collision

Yao and Morel based the expression of the collision frequency considering the contributions of the free travelling time t_{cf} and interaction time t_{ci} .

$$f_{coll} = \frac{1}{t_{cf} + t_{ci}} \quad (\text{Eq.198})$$

The free travelling time t_{cf} represents the time needed for a bubble to cover the mean distance between two bubbles and collide. The interaction time t_{ci} is the time needed for coalescence to occur after a collision has taken place and the film rupture has concluded.

The collision frequency, on which the calculation of the free travelling time is based, derives from the formula of Prince and Blanch [Prince and Blanch 1990]. This formula for the case of bubbles of different group sizes (i, j) is:

$$f_{ij}^T = n_i n_j S_{ij} (u_i^2 + u_j^2)^{1/2} \quad (\text{Eq.199})$$

where the effective cross sectional area is given by

$$S_{ij} = \frac{\pi}{4} (r_i + r_j)^2 \quad (\text{Eq.200})$$

As already mentioned for Prince and Blanch (see paragraph 6.1.3) also Yao and Morel claim that they derived the cross-sectional collision area from the kinetic theory of gases. Nevertheless, their definition of the cross-sectional collision area yields results four times smaller than (Eq.132) without any further explanation.

Formulating (Eq.199) and (Eq.200) with respect to a single bubble size and considering a collision event for each two bubbles, it is now possible to write:

$$f_{cf} = \frac{1}{2} n^2 \frac{\pi}{4} D^2 \sqrt{2} u = C_c \frac{\varepsilon^{1/3}}{D^{11/3}} \alpha^2 \quad (\text{Eq.201})$$

if

$$u = \sqrt{2} \varepsilon^{1/3} D^{1/3} . \quad (\text{Eq.202})$$

C_c is a coefficient and its value is 2.86.

The total collision frequency f_{cf} between bubbles is expressed in this way per unit time and volume. For only one bubble the mean average free travelling time can be obtained as:

$$t_{cf} = \frac{n}{2} f_{cf} = \frac{1}{3} \frac{D^{2/3}}{\alpha \varepsilon^{1/3}} . \quad (\text{Eq.203})$$

Considering a term for the modification of the average free travelling time when the value of α reaches $\alpha_{max} = 0.52$ (Eq.203) becomes:

$$t_{cf} = \frac{1}{3} \frac{D^{2/3}}{\alpha \varepsilon^{1/3}} g(\alpha) = \frac{1}{3} \frac{D^{2/3}}{\alpha \varepsilon^{1/3}} \left(\frac{\alpha_{max}^{1/3} - \alpha^{1/3}}{\alpha_{max}^{1/3}} \right) . \quad (\text{Eq.204})$$

Regarding the interaction time t_{ci} the film thinning model is used [Kirkpatrick and Lockett 1974]. The model assumes that two bubbles will coalesce if the contact time between them is larger than the liquid film drainage time. Yao and Morel [Yao and Morel 2004] considered the interaction time t_{ci} to be equal to the drainage time t_c .

$$t_{ci} = t_c = 0.814 \sqrt{\frac{\rho_l D^3}{\sigma}} . \quad (\text{Eq.205})$$

The constant 0.814 has been derived analytically assuming constant typical values for the initial and critical film thickness. For more detailed information consider to read Yao and Morel [Yao and Morel 2004].

Substituting (Eq.204) and (Eq.205) in (Eq.198), it is possible to obtain the collision frequency:

$$f_{coll} = \frac{1}{\frac{1}{3} \frac{D^{2/3}}{\alpha \varepsilon^{1/3}} \left(\frac{\alpha_{max}^{1/3} - \alpha^{1/3}}{\alpha_{max}^{1/3}} \right) + 0.814 \sqrt{\frac{\rho_l D^3}{\sigma}}}. \quad (\text{Eq.206})$$

Following Kim and Lee [Kim and Lee 1987], the bubble coalescence efficiency is estimated to be:

$$\eta_c = \exp\left(-\frac{t_c}{\tau_c}\right) = \exp\left(-\frac{0.814 \sqrt{\frac{\rho_l D^3}{\sigma}}}{\frac{R^{2/3}}{\varepsilon^{1/3}}}\right), \quad (\text{Eq.207})$$

where τ_c is the contact time and is given by the characteristic time of the eddies having the same radius R of the bubbles [Yao and Morel 2004].

The final form for the interfacial area change rate due to random collision considering spherical bubbles is:

$$\begin{aligned} \Phi_{RC} &= -12\pi \left(\frac{\alpha}{a_i}\right)^2 f_{coll} n \eta_c \\ &= -12\pi \left(\frac{\alpha}{a_i}\right)^2 K_{c1} \frac{\varepsilon^{1/3} \alpha^2}{D^{11/3}} \frac{1}{g(\alpha) + K_{c2} \alpha \sqrt{We/We_{cr}}} \exp\left(-K_{c3} \sqrt{\frac{We}{We_{cr}}}\right), \end{aligned} \quad (\text{Eq.208})$$

where the values of the constants K_{c1} , K_{c2} , K_{c3} are respectively: 2.86, 1.922 and 1.017. The value of the We_{cr} is 1.24.

7.4.2 Modeling of Bubble Breakup Due to Turbulence Impact

Yao and morel based the expression of the bubble breakup due to turbulence impact on the bubble-eddy resonance mechanism.

The bubble-eddy collision frequency takes into account the contributions of the free travelling time t_{bf} and interaction time t_{bi} .

Similarly to the coalescence case, the free travelling time t_{bf} represents the time needed for an eddy or a bubble to cover the mean distance between the them to collide. The interaction time t_{bi} is the time needed for breakup to occur after collision has taken place and the bubble rupture concluded.

$$f_{b,coll} = \frac{1}{t_{bf} + t_{bi}} \quad (\text{Eq.209})$$

For a detailed overview on the derivation of the expression of the free travelling time and the breakup characteristic time the reading of Yao and Morel [Yao and Morel 2004] is advised.

In order to calculate the collision frequency between eddies and bubbles, similarly to (Eq.136) an integral formulation is proposed. In order to make the solution of the integral possible, the integration range has to be limited and the lower and upper integration limits need to be set. It is important to pay attention to the fact that **these values are not universal** and were chosen by the authors **to better fit the bubble diameters of the DEBORA experiment** [Yao and Morel 2004]. Even if Yao and Morel claim that the model is not parameter dependent it does strongly depend on the lower and upper limits of integration chosen *ad hoc* by the authors.

The bubble average free travelling time t_{bf} is:

$$t_{bf} = C_{bf} \frac{D^{2/3}}{\varepsilon^{1/3}(1-\alpha)} \quad C_{bf} = 1.194. \quad (\text{Eq.210})$$

The bubble breakup characteristic time t_{bi} is based on the concept of resonance of bubble oscillations with turbulent eddies and has been derived by Yao and Morel [Yao and Morel 2004] to be:

$$t_{bi} = 0.64 \sqrt{\frac{\rho_l D^3}{\sigma}}. \quad (\text{Eq.211})$$

The bubble breakup frequency is:

$$f_{b,coll} = \frac{1}{t_{bf} + t_{bi}} = \frac{1}{C_{bf} \frac{D^{2/3}}{\varepsilon^{1/3}(1-\alpha)} + 0.64 \sqrt{\frac{\rho_l D^3}{\sigma}}}. \quad (\text{Eq.212})$$

The bubble breakup efficiency is expressed similarly to Wu et al. [Wu et al. 1998] as:

$$\eta_b = \exp\left(-\frac{We_{cr}}{We}\right). \quad (\text{Eq.213})$$

The final form for the interfacial area change rate due to bubble-eddy turbulent impact and considering spherical bubbles is:

$$\begin{aligned} \Phi_{TI} &= 12\pi \left(\frac{\alpha}{a_i}\right)^2 f_{b,coll} n_e \eta_b \\ &= 12\pi \left(\frac{\alpha}{a_i}\right)^2 K_{b1} \frac{\varepsilon^{1/3} \alpha (1-\alpha)}{D^{11/3}} \frac{1}{1 + K_{b2} (1-\alpha) \sqrt{We/We_{cr}}} \exp\left(-\frac{We_{cr}}{We}\right), \end{aligned} \quad (\text{Eq.214})$$

where n_e is the eddies number density and has been obtained in a similar way as in Hibiki and Ishii [Hibiki and Ishii 2000a] following Azbel and Athanasios [Azbel and Athanasios 1983]. The value of the constants K_{b1} and K_{b2} are, respectively, 1.6 and 0.42.

7.5 Wang – 2010

Wang in 2010 [Wang 2010] applied the models of Wu et al. [Wu et al. 1998] to 3D simulations of vertical concurrent upward two-phase flow in pipes using the CFD code Fluent. In his work, Wang tested the model with Wu et al. original coefficients and proposed a new set of them for 3D simulations based on the following considerations.

Wang reported that there are two possible issues when a calibrated one dimensional IATE model is used for three-dimensional analysis.

The first issue is attributed to the averaging process used to obtain the one-dimensional IATE model from the three-dimensional IATE model. In the averaging process, the covariance term representing the difference between the average of the product of two variables and the product of two averaged variables was neglected [Kim 1999]. In case of one-dimensional simulation this had no influence on the applicability of the model to the calculation of the area-averaged source and sink terms [Wu et al. 1998]: “The exact mathematical expressions for the area-averaged source and sink terms would involve many covariances that may further complicate the one-dimensional problem. However, since these local terms were originally obtained from a finite volume element of the mixture, the functional dependence of the area-averaged source and sink terms on the averaged parameters should be approximately the same if the hydraulic diameter of the flow path is considered as the length scale of the finite element.”

The other issue is related to the source term of the interfacial area transport equation related to pressure changes. In case of 1D simulations only the z component is taken into consideration, while in 3D simulations, also the other two components (x,y) are taken into account.

Wang proposed a new set of empirical coefficient as given below:

$$C_{TI} = 0.005 \quad C_{RC} = 0.013 \quad C = 3.0$$

$$C_{WE} = 0.006 \quad We_{cr} = 6.0 \quad \alpha_{max} = 0.75$$

The methodology for determining these coefficients is based on the experimental observations that the different bubble interaction mechanisms are predominant in different flow conditions [Wang 2010]. Following this idea Wang claims that it is possible to estimate quasi-independently each of the coefficients, if for certain flow

conditions, its related term in the equation is significant, and the influence of the others is either known or negligible.

The calibration procedure has been performed by following the steps below [Wang 2010]:

- 1) Estimation of C_{WE} for low j_G and j_L
- 2) Estimation of C_{RC} for high j_G and low j_L
- 3) Estimation of C_{TI} for high j_G and j_L
- 4) Check for all flow conditions
- 5) **Adjust the coefficient iteratively until the relative errors between predictions and experimental data approach their minimum.**

7.6 Comparison of the Bubble Coalescence and Breakup

Frequency and Efficiency Terms

For the evaluation of the diagrams presented in the next sections the turbulence eddy dissipation ε has been selected as the only variable parameter. The flow parameters presented in the formulas presented in the previous sections of this chapter for the evaluation of the interaction mechanisms frequency and efficiency have been kept constant and their values are:

$$\alpha = 0.2 [-] \quad D = 0.003 [m] \quad \rho_l = 997 [kg/m^3]$$

$$\rho_g = 1.185 [kg/m^3] \quad \sigma = 0.0727 [N/m]$$

7.6.1 Bubble Coalescence Due to Random Collision

In the case of the random collision coalescence terms, it is not possible to compare all the above reported models together. This is due to the fact that, on one side, Hibiki and Ishii [Hibiki and Ishii 2000a] and Yao and Morel [Yao and Morel 2004] are furnishing an expression for the calculation of the bubble coalescence efficiency and are treating it separately from the bubble collision frequency. On the other side, the model of Wu et al. [Wu et al. 1998] and the others derived from it, (Ishii and Kim [Ishii and Kim 2001] and Wang [Wang 2010]) do not consider the bubble coalescence frequency separately, as Wu et al. decided to use a **constant coefficient** for the collision frequency η_c in (Eq.173). The value of this coefficient is **not explicitly given** in the work, but it is contained in the constant C_{RC} .

For this reason it is not possible to separate the effects of the two components and it is not possible to perform a comparison.

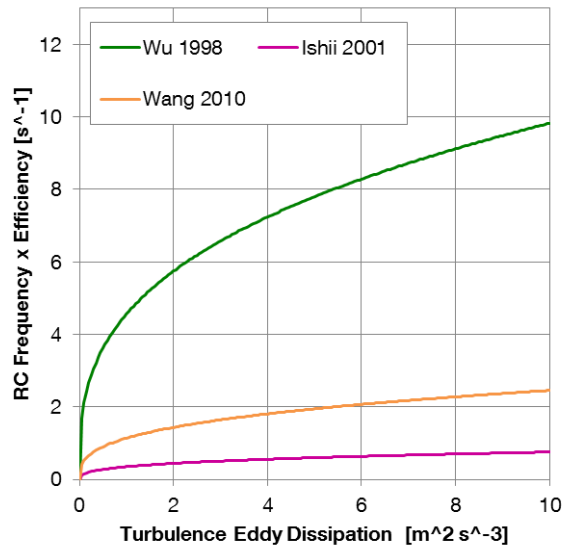


Figure 27: Trend of the Random Collision Frequency x Efficiency as a function of the Turbulence eddy dissipation

In Figure 27, it is possible to see how the different proportionality coefficients chosen by Wu et al. [Wu et al. 1998], Ishii and Kim [Ishii and Kim 2001] and Wang [Wang 2010], affect the trend of the random collision frequency multiplied by a constant coalescence efficiency as a function of the turbulence eddy dissipation. The highest values are obtained by the model proposed by Wu et al. [Wu et al. 1998]. The slope of the curve is very high for very low values of the energy dissipation. The lowest values are those obtained by Ishii and Kim [Ishii and Kim 2001].

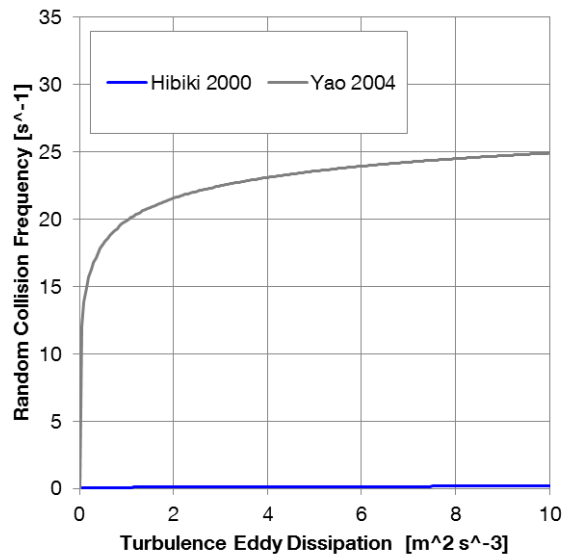


Figure 28: Trend of the Random Collision Frequency as a function of the Turbulence eddy dissipation

In Figure 28, the random collision frequency model of Hibiki and Ishii [Hibiki and Ishii 2000a] is compared to that of Yao and Morel [Yao and Morel 2004]. This last model delivers results in the order of two orders of magnitude higher than the Hibiki and Ishii model even at very high values of the energy dissipation.

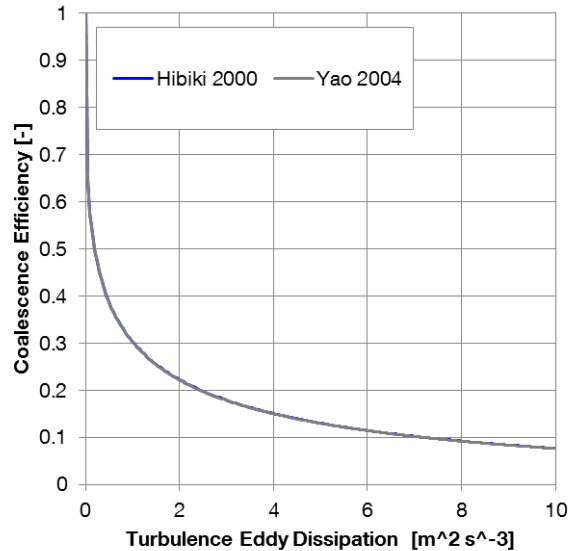


Figure 29: Trend of the Coalescence Efficiency as a function of the Turbulence eddy dissipation

In Figure 29, the trend of the coalescence efficiency as a function of the turbulence eddy dissipation is shown. The model of Hibiki and Ishii [Hibiki and Ishii 2000a] and the model of Yao and Morel [Yao and Morel 2004] are delivering essentially the same results.

7.6.2 Bubble Breakup Due to Turbulence Impact

In case on the impact of turbulent eddies against the bubbles, it is possible to compare all the available models for the bubble-eddy collision frequency and for the efficiency since the expressions for the calculation and almost all coefficients have been given explicitly in the respective works. In case of a coefficient have not been given separately for each effect, it has been possible to separate it from other constants for the comparison. These coefficients have been given in the preceding chapter.

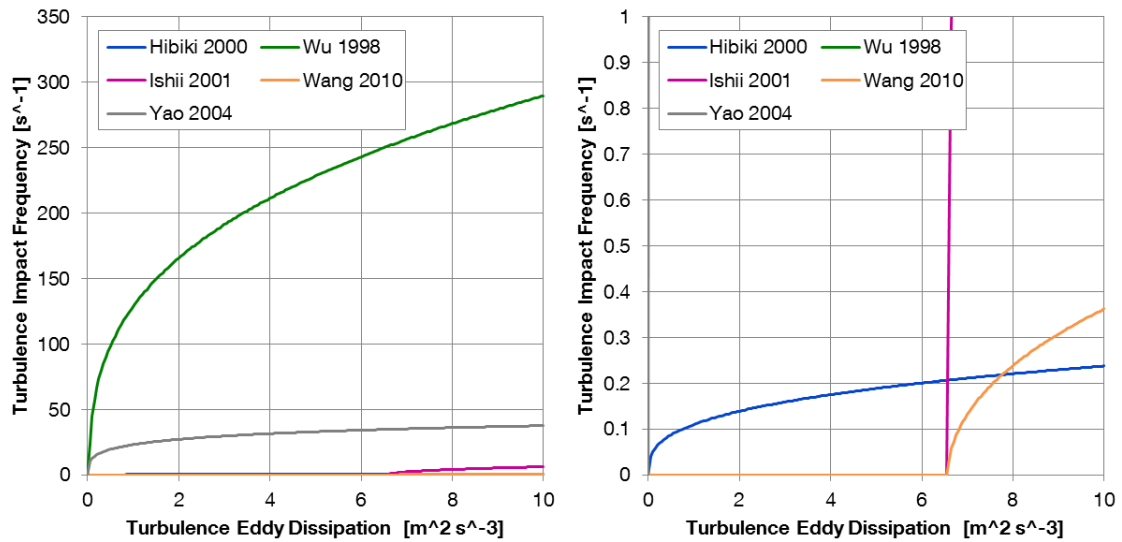


Figure 30: Trend of the Turbulence Impact Frequency as a function of the Turbulence eddy dissipation: whole frequency scale range (left), reduced frequency scale range (right)

In Figure 30, the turbulent impact frequency models have been compared. The highest values are obtained by using the Wu et al. [Wu et al. 1998], model as already seen for the coalescence frequency. The second highest values are obtained using the Yao and Morel [Yao and Morel 2004] model.

In order to appreciate the trend of the Wang 2010 and Hibiki and Ishii 2000 models, a scale range reduction is needed (Figure 30 right). In this figure it is possible to see that the Wang and Ishii and Kim models do not present breakup events at all up to a critical value of the turbulence eddy dissipation. This value in this special case lies between 6 and 7 [$\text{m}^2 \text{s}^3$].

The Hibiki and Ishii [Hibiki and Ishii 2000a] model delivers in general the lowest results of the collision frequency caused by the turbulent impact of the eddies against the bubbles.

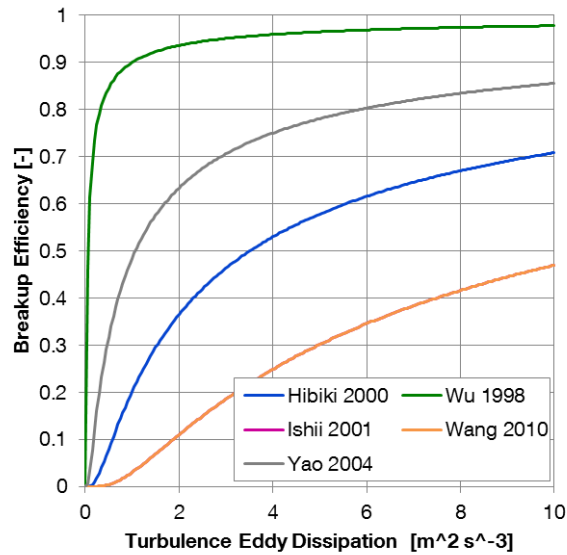


Figure 31: Trend of the Breakup Efficiency as a function of the Turbulence eddy dissipation

In Figure 31, the breakup efficiency models as a function of the turbulence eddy dissipation have been compared. The highest value is obtained again using the Wu et al. model. The lowest value of the breakup efficiency is obtained using the model of Wu et al. with coefficients from Wang.

It is worth of notice the fact that the same trend is appreciable both for the breakup and coalescence cases: Wu et al. model is delivering the highest coalescence and breakup rates. The model delivering the second highest rates is that proposed by Yao and Morel; both for bubble breakup and coalescence case. The model delivering the lowest bubble interaction rates is that proposed by Hibiki and Ishii. However, the absolute value assumed by the models is not so relevant to the evaluation of the capability of a model. In fact, the source and sink terms explained in the previous sections are applied together, for each author, to modify the transported value in the interfacial area transport equation. For this reason the important is the resultant value from the balance between creation and destruction of bubbles and not the values of the single interaction terms considered alone.

Chapter 8

Implementation of the One-Group Interfacial Area Transport Equation in ANSYS CFX

In this chapter, the two-phase simulation methods available in the general CFD commercial code ANSYS CFX are presented. The differences in the theoretical form of the interfacial area transport equation and that of the additional transport equation to be implemented in the code are shown. A solution to reduce the numerical diffusion and to implement the source and sink terms in the correct form in the code has been proposed.

8.1 The Computational Fluid Dynamics Code ANSYS CFX

ANSYS CFX is a general purpose CFD (Computational Fluid Dynamics) software suite that combines a solver with pre- and post-processing capabilities.

Computational fluid dynamics is the analysis of engineering systems involving fluid flow, heat transfer and associated phenomena, by means of computer-based simulations, solving equations for mass, momentum, energy, turbulence and concentration with specified conditions on the boundary of that region. In CFD codes one of the most common used solution methods is known as the finite volume technique. In this technique, the region of interest is divided into small sub-regions, called control volumes. The equations are discretized and solved iteratively for each control volume. As a result, an approximation of the value of each variable at specific points throughout the domain can be obtained [Ansys 2009].

As shown in Figure 32 ANSYS CFX is a suite composed of several packages. They are essentially three. The “pre-processor” to define computational regions, the initial and boundary conditions, materials properties, the physical models and the numerical schemes. The “solver” used to solve the variables of the problem and to manage

partitioning and memory allocation. The “post-processor” to create 2D or 3D plots of the main significant variables of the problem and to export the data for further analysis.

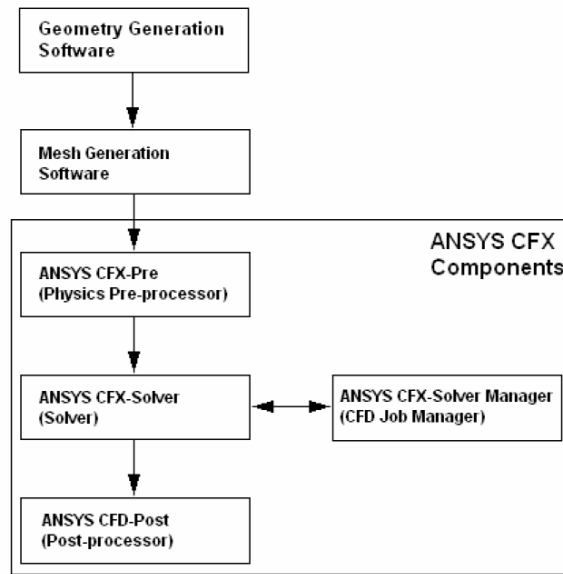


Figure 32: Overview of ANSYS CFX code structure [Ansys 2009]

8.2 Two-phase Flow Solution Methods

By default, Ansys CFX is able to solve a two-phase flow problem by using the Eulerian-Eulerian model or the Lagrangian Particle Tracking model. Of interest for this work is the Eulerian-Eulerian approach. Within the Eulerian-Eulerian formulation certain interphase transfer terms used in the momentum, heat and other interphase transfer models can be modeled using the [Ansys 2009]:

- Particle Model.
- Mixture Model.
- Free Surface Model.

Also the interfacial area density, for the inhomogeneous transfer between a pair of fluids, is calculated according to one of the three models above listed [Ansys 2009]. The simulation is based on a two-fluid approach, already introduced in chapter 4.1. If the Particle Model is used, then the two phases are considered to be one continuous and other dispersed. The dispersed phase can be considered as:

- Mono-dispersed
- Poly-dispersed (MUSIG Multiple Size Group)

If the gas is considered to be the dispersed phase, in the **monodispersed** approach, all the bubbles are supposed to have the same spherical form and the same average

diameter. Their common diameter can be a constant or an expression dependent on local parameters. Furthermore, they share the same dispersed phase velocity field. In this case for a two-fluid system, the equations to be solved are in total **11** divided as follows:

- Momentum of the liquid phase: 3
- Momentum of the gas phase: 3
- Pressure: 1
- Mass of liquid: 1
- Mass of gas: 1
- Turbulence in the liquid phase: 2

In the **polydispersed** approach, if the gas is supposed to be the dispersed phase, all the bubbles present in the system are supposed to share the same spherical form, but not the same average diameter. In this case, the bubbles are divided in classes and the initial bubble size distribution is defined as a boundary condition. The bubble groups can share the same velocity field or they can be associated to different velocity field. The first case refers to the homogeneous model where as the second case refers to the inhomogeneous model. The intergroup bubble transfer is simulated as explained previously in chapter 4 by means of coalescence and breakup source and sink terms. They determine the changes in the bubble group size fractions as a result of break-up and coalescence process. In the case of a **two-fluid** system (homogeneous MUSIG) considering n bubble size groups the equations to be solved are in total **11+n** divided as follows:

- Momentum of the liquid phase: 3
- Momentum of the gas phase: 3
- Pressure: 1
- Mass of liquid: 1
- Mass of gas: 1
- Turbulence in the liquid phase: 2
- Bubble group size fraction: n

If also cap bubbles or slugs exist, then a third fluid (gas) needs to be introduced with adequate transfer terms between with the other two. In fact, when the flow conditions are changing and bubbles of different diameters and shapes are formed, the definition of a second gas flow is justified because the interfacial structures in different flow regimes change dramatically [Ishii and Hibiki 2006]. Furthermore, the bubble

interaction mechanisms in such flow conditions, driven by two bubble types, can be quite different compared with those considered by the other gas flow.

In the case of such a **three-fluid system** (inhomogeneous MUSIG) considering n bubble size groups (they can be even more than the previous case) the equations to be solved are in total **15+n** divided as follows:

- Momentum of the liquid phase: 3
- Momentum of the first gas phase: 3
- Momentum of the second gas phase: 3
- Pressure: 1
- Mass of the liquid phase: 1
- Mass of the first gas phase: 1
- Mass of the second gas phase: 1
- Turbulence of the liquid phase: 2
- Bubble group size fractions: n

The limit of the monodispersed approximation is that the average bubble size needs to be known “a priori” and the shape of the bubbles needs to be nearly spherical. Furthermore, this approach is suitable for weak interacting flows with a particle size distribution concentrated around the average value. Of course, the bubble size can be defined as an algebraic expression related to local variables as, for example, the elevation. In this way it is possible to take into account the bubble expansion due to the decrease of hydrostatic pressure (the bubble rise in a bubble column or in a vertical upward pipe flow).

In case of the polydispersed approximation, it is possible to obtain very precise results depending on the quality of the interaction mechanism models used for the simulation. In practice, more than 15 bubble groups are needed to describe the flow accurately. This aspect is relevant because, if, on one side, the accuracy of the results increases compared to monodispersed simulation, on the other side, also the computational effort raises dramatically.

A good compromise between the monodispersed and polydispersed (homogeneous or inhomogeneous) methods is represented by the Interfacial Area Transport Equation approach. This allows to keep the computational effort as low as possible (essentially equal to the monodispersed case if only one additional transport equation is added), while taking into consideration the local bubble interaction mechanisms. Furthermore,

if assumptions concerning the form of the bubbles present in the system are made, it is possible to calculate a local value for the bubble mean diameter. This is done by using simple algebraic relations between the volume and the interfacial area in each computational node.

This last simulation strategy is not, by default, included in Ansys CFX. However, it is possible for the user to define an additional transport equation associated to a user defined interfacial area variable. Furthermore, it is possible to define source and sink terms to modify the value of the transported quantity along the path.

One or two additional transport equations can be added to the original ANSYS CFX solver (that of the monodispersed approach) to implement the **one- or two-groups** interfacial area transport equations. In the **first** case **12** equations need to be solved:

- Momentum of the liquid phase: 3
- Momentum of the gas phase: 3
- Pressure: 1
- Mass of liquid: 1
- Mass of gas: 1
- Turbulence of the liquid phase: 2
- One-group interfacial area density: 1

In the **second** case **17** equations are considered. This is due to the fact that the second bubble groups is not sharing the same velocity field with the first one:

- Momentum of the liquid phase: 3
- Momentum of the first gas phase: 3
- Momentum of the second gas phase: 3
- Pressure: 1
- Mass of the liquid phase: 1
- Mass of the first gas phase: 1
- Mass of the second gas phase: 1
- Turbulence of the liquid phase: 2
- One-group interfacial area density: 1
- Two-group interfacial area density: 1

8.3 Additional Variable for the Interfacial Area Density Under the Form of a Transport Equation in ANSYS CFX

The one-group interfacial area transport equation is solved by using a user defined additional variable under the form of a transport equation offered by ANSYS CFX. In fact the software allows defining a transport equation for any scalar quantity transported by a field velocity. The general form of the transport equation for the interfacial area density a_i in multiphase flow calculations that is possible to implement in the code is

$$\frac{\partial \alpha a_i}{\partial t} + \nabla \cdot (\alpha a_i \vec{v}_g) - \nabla \cdot \left[\alpha \left(D_g^{a_i} + \frac{\mu_{t,g}}{Sc_{t,g}} \right) \nabla a_i \right] = S_{a_i} + T_{a_i}. \quad (\text{Eq.215})$$

If the additional transport equation is associated to the gas phase:

- a_i is the conserved quantity: interfacial area density per unit volume of the actual phase.
- α is the void fraction.
- $D_g^{a_i}$ is the kinematic diffusivity for the scalar to be transported and can be set freely by the user.
- $Sc_{t,g}$ is the Turbulent Schmidt number (per default equal to 0.9).
- $\mu_{t,g}$ is the Turbulent eddy viscosity.
- S_{a_i} is the external volumetric source term.
- T_{a_i} is the total source due to inter-phase transfer across interfaces with other phases and is not considered in the adiabatic case.

The first term on the LHS of (Eq.215) is the term taking into account the time changes of the interfacial area density, the second is the convective term and the third is the diffusive term.

(Eq.215) differs from (Eq.114) because of the presence of the diffusive term and of the void fraction inside the derivative terms. In a previous work, also Prabhudharwadkar et al. [Prabhudharwadkar et al. 2009] suggested a possible strategy to overcome the constraints of the software since the form of (Eq.215) cannot be modified by the user.

8.3.1 The Elimination of the Diffusion Term

Three different attempts have been carried out to reduce or eliminate the influence of the diffusive term:

1. define the Turbulent Schmidt number as follows:

$$Sc_{t,g} = -\frac{\mu_{t,g}}{D_g^{a_i}}, \quad (\text{Eq.216})$$

in order to obtain a constant value of zero inside the divergence of the diffusive term.

2. implement the complete diffusive term on the RHS of (Eq.215) by means of “User CELs” (For a brief explanation on “User CELs” refer to the next section).
3. reduce the influence of the diffusive term without eliminating it, as suggested by Prabhudharwadkar et al. [Prabhudharwadkar et al. 2009] and by the Customer Support of ANSYS, by setting a low value for the kinematic diffusivity $D_g^{a_i} = 1E - 15$ and a sufficient high value for the $Sc_{t,g} = 1000$ or above.

The first two attempts caused the solver to become very unstable and it has not been possible to reach convergence for any of the cases tested. Overflows have also been experienced.

The strategy of point three ended up being the only viable way to reduce the influence of the diffusion term. In Figure 33, the sensitivity of the interfacial area concentration radial profile on the Schmidt number (left) and the kinematic diffusivity (right) is shown. Regarding the Schmidt number, no appreciable difference can be noticed between the cases with $Sc_{t,g} = 1000$ and $Sc_{t,g} = 10000$. For the kinematic diffusivity, there are almost no differences between the cases $D_g^{a_i} = 1E - 8$ and $D_g^{a_i} = 1E - 15$.

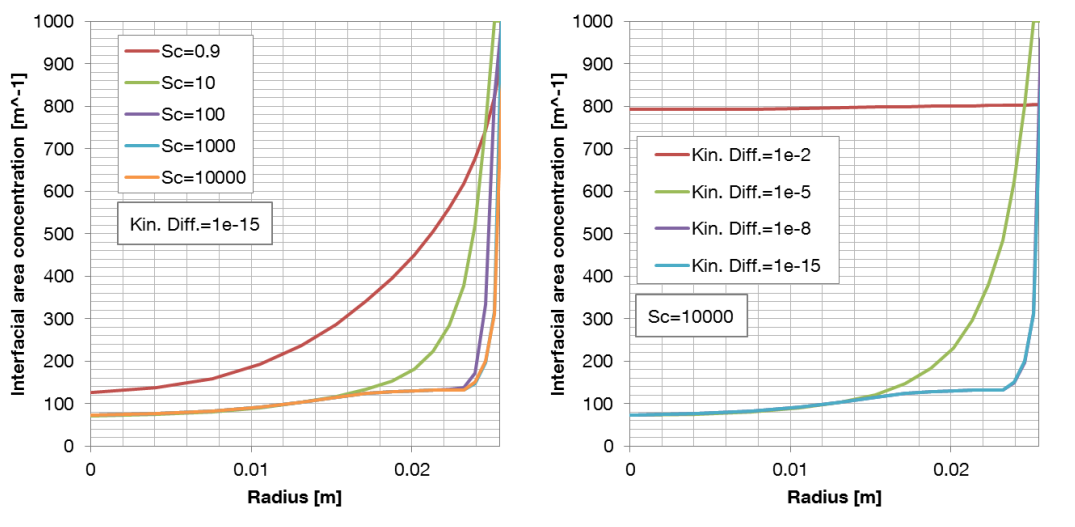


Figure 33: Sensitivity analysis of the interfacial area concentration radial profile on the Schmidt number (left) and on the kinematic diffusivity (right).

8.3.2 Calculation of the Derivatives in the Source and Sink Terms

In order to calculate gradients and divergences, a set of FORTRAN subroutines have been written and implemented. The set is composed by only “User CELs” and make use of the internal command of the software. They are needed since it is not possible to access derivative operators from the GUI of ANSYS CFX. “User CEL” functions allow to create functions in addition to the predefined CELs already defined in the code (sin, cos, min, max, etc.). A “User CEL” function passes an argument list to a subroutine, and then uses the returned values from the subroutine to set values for the quantity of interest [Ansys 2009].

8.3.3 The Transformation of the Source and Sink Terms

The presence of the void fraction multiplied by the transported variable in (Eq.215) leads to the necessary implementation of a supplementary term on the RHS. This term takes into account the presence of mixed derivative terms in (Eq.215) with respect of (Eq.114).

For the time derivative term, the following decomposition is applied:

$$\frac{\partial \alpha a_i}{\partial t} = a_i \frac{\partial \alpha}{\partial t} + \alpha \frac{\partial a_i}{\partial t}. \quad (\text{Eq.217})$$

For the convective term, the divergence term $\nabla \cdot (\alpha a_i \vec{v}_g) = \nabla \cdot (\vec{W})$ is expanded as follows:

$$\vec{W} = \begin{pmatrix} W_x \\ W_y \\ W_z \end{pmatrix} = \begin{pmatrix} \alpha a_i v_{g,x} \\ \alpha a_i v_{g,y} \\ \alpha a_i v_{g,z} \end{pmatrix}, \quad (\text{Eq.218})$$

so that

$$\nabla \cdot (\vec{W}) = \frac{\partial W_x}{\partial x} + \frac{\partial W_y}{\partial y} + \frac{\partial W_z}{\partial z} = \frac{\partial \alpha a_i v_{g,x}}{\partial x} + \frac{\partial \alpha a_i v_{g,y}}{\partial y} + \frac{\partial \alpha a_i v_{g,z}}{\partial z}. \quad (\text{Eq.219})$$

Each of the terms in (Eq.219) can be further expanded and then rearranged:

$$\begin{aligned} \frac{\partial \alpha a_i v_{g,x}}{\partial x} &= a_i v_{g,x} \frac{\partial \alpha}{\partial x} + \alpha v_{g,x} \frac{\partial a_i}{\partial x} + \alpha a_i \frac{\partial v_{g,x}}{\partial x} \\ &= a_i v_{g,x} \frac{\partial \alpha}{\partial x} + \alpha \left(v_{g,x} \frac{\partial a_i}{\partial x} + a_i \frac{\partial v_{g,x}}{\partial x} \right), \end{aligned} \quad (\text{Eq.220})$$

$$\begin{aligned} \frac{\partial \alpha a_i v_{g,y}}{\partial y} &= a_i v_{g,y} \frac{\partial \alpha}{\partial y} + \alpha v_{g,y} \frac{\partial a_i}{\partial y} + \alpha a_i \frac{\partial v_{g,y}}{\partial y} \\ &= a_i v_{g,y} \frac{\partial \alpha}{\partial y} + \alpha \left(v_{g,y} \frac{\partial a_i}{\partial y} + a_i \frac{\partial v_{g,y}}{\partial y} \right), \end{aligned} \quad (\text{Eq.221})$$

$$\begin{aligned}\frac{\partial \alpha a_i v_{g,z}}{\partial z} &= a_i v_{g,z} \frac{\partial \alpha}{\partial z} + \alpha v_{g,z} \frac{\partial a_i}{\partial z} + \alpha a_i \frac{\partial v_{g,z}}{\partial z} \\ &= a_i v_{g,z} \frac{\partial \alpha}{\partial z} + \alpha \left(v_{g,z} \frac{\partial a_i}{\partial z} + a_i \frac{\partial v_{g,z}}{\partial z} \right).\end{aligned}\quad (\text{Eq.222})$$

In simplified form equation (Eq.220), (Eq.221) and (Eq.222) can be written as:

$$\nabla \cdot (\alpha a_i \vec{v}_g) = a_i (\nabla \alpha \cdot \vec{v}_g) + \alpha \nabla \cdot (a_i \vec{v}_g). \quad (\text{Eq.223})$$

Combining (Eq.215), without taking into consideration the diffusive term, with (Eq.217) and with (Eq.223) leads to:

$$\begin{aligned}\frac{\partial \alpha a_i}{\partial t} + \nabla \cdot (\alpha a_i \vec{v}_g) &= a_i \frac{\partial \alpha}{\partial t} + \alpha \frac{\partial a_i}{\partial t} + a_i (\nabla \alpha \cdot \vec{v}_g) + \alpha \nabla \cdot (a_i \vec{v}_g) \\ &= \alpha \left[\frac{\partial a_i}{\partial t} + \nabla \cdot (a_i \vec{v}_g) \right] + a_i \left(\frac{\partial \alpha}{\partial t} + \vec{v}_g \cdot \nabla \alpha \right),\end{aligned}\quad (\text{Eq.224})$$

where the term in the square bracket is the interfacial area density transport equation as expressed in (Eq.114) and the other is the transport equation for the void fraction.

The final form of the source term to be implemented in equation (Eq.215) is:

$$S_{a_i} = \alpha \left\{ 12\pi \left(\frac{\alpha}{a_i} \right)^2 \sum_j R_j + \frac{2}{3} \left(\frac{a_i}{\alpha} \right) \left[\frac{\partial \alpha}{\partial t} + \nabla \cdot (\alpha \vec{v}_g) \right] \right\} + a_i \left(\frac{\partial \alpha}{\partial t} + \vec{v}_g \cdot \nabla \alpha \right). \quad (\text{Eq.225})$$

Under steady state conditions (Eq.225) becomes:

$$S_{a_i} = \alpha \left\{ 12\pi \left(\frac{\alpha}{a_i} \right)^2 \sum_j R_j + \frac{2}{3} \left(\frac{a_i}{\alpha} \right) [\nabla \cdot (\alpha \vec{v}_g)] \right\} + a_i (\vec{v}_g \cdot \nabla \alpha). \quad (\text{Eq.226})$$

The first term of the RHS is implemented in ANSYS CFX as “Source”. It means that it is applied to the bulk fluid and then multiplied by the void fraction automatically by the code by default. The second term, outside curly brackets, is defined as “Fluid Source” and is applied directly to the gas phase without being multiplied by the void fraction automatically by the code by default.

In Appendix A it is possible to find the source code of the set of FORTRAN subroutines that have been written for the implementation of the terms (divergence and gradient) explained above.

Chapter 9

Simulation of Upward Adiabatic Bubbly Flow with the State of the Art Available Models with ANSYS CFX 12.1

In this chapter, the PUMA experimental facility and the data used for validation are described. The computational domain, the boundary conditions and mesh sensitivity analysis are presented. Furthermore, simulation results using the state of the art simulation methods and models for upward adiabatic turbulent bubbly flow are reported.

9.1 Upward Turbulent Adiabatic Bubbly Flow Experimental Data from Santos Mendez 2008

The results of the simulations presented in the next paragraphs have been compared against the experimental data of Santos Mendez [Santos Mendez 2008]. These data have been collected with the main goal of making available experimental data for the interfacial area density models validation. The data have been measured in a moderate diameter vertical test section. The flow area affects the interaction mechanisms [Hibiki et al. 2001a]; thus the dominant mechanisms are not the same for moderate as for large diameter pipes. Data of the MTLOOP (now out of order) and of the TOPFLOW experiments carried out at the Helmholtz-Zentrum Dresden-Rossendorf (HZDR) has also been made available by the authors. Unfortunately, we did not have access unprocessed data. The processed version of the experimental results have been prepared to make feasible the study and validation of models essentially, for monodispersed flow (MTLOOP), for the assessment of the interfacial forces models in moderate diameter pipes and, for polydispersed flows (TOPFLOW), for the study of the bubbly interaction mechanisms and transition to slug flow in large diameter pipes. Furthermore, the possibility of using sets of data from the literature has been investigated. It has not been possible to use data from the literature to carry out

simulations mostly because of the lack of details and completeness of the information available.

9.1.1 Description of the Experimental Facility

The set-up of the experimental facility PUMA [Santos Mendez 2008] built and operated at the University of Valencia is illustrated schematically in Figure 34.

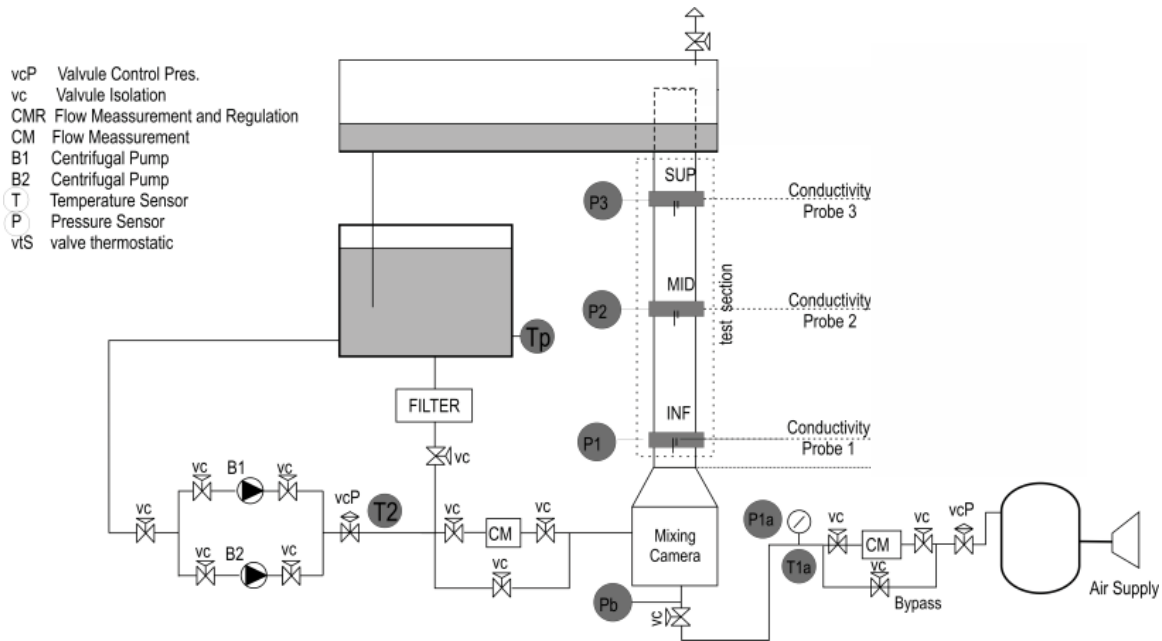


Figure 34: Setup of the PUMA experiment [Santos Mendez 2008]

In the PUMA experiment, operated with water as continuous fluid and air as the dispersed one, water entered at atmospheric pressure and at 20°C and adiabatic conditions have been maintained. The pipe internal diameter was 52 mm and the test section around 3000 mm long. The flow conditions covered most of the bubbly flow region, including finely dispersed bubbly flow and bubbly-to-slug transition flow.

The average radial profiles of the void fraction, as well as the gas velocity and the interfacial area, were measured at three specific axial locations ($z/D=2$, $z/D=36$, $z/D=56$) and at 15 radial locations ($r/R= 0$ to 0.95) in upward water air two-phase flow using four-sensor conductivity probes (see Figure 35) designed jointly with the University Jaume I, Spain. From these quantities, the radial profiles of the Sauter Mean Diameter were derived.

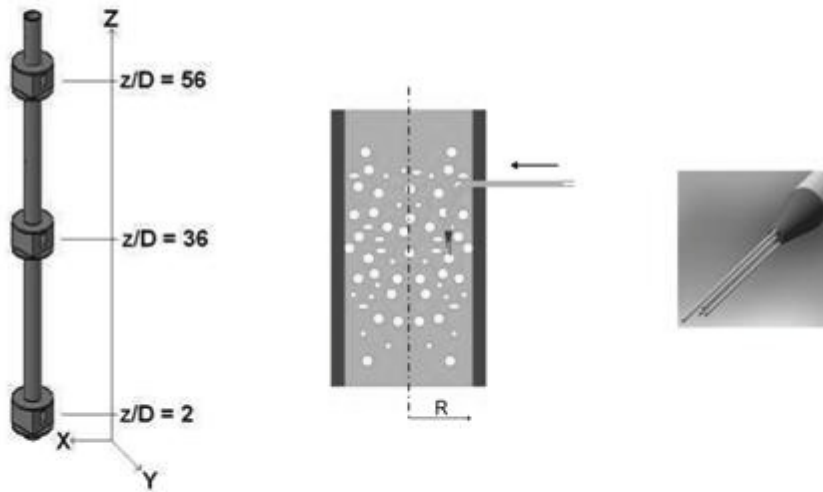


Figure 35: Positions of the measuring ports (left), scheme of the measuring principle in the flow (center), a particular of the four-sensor probe (right)

9.1.2 The Experimental Matrix

The experimental points considered in the calculations presented in the next paragraphs and their superficial velocities are indicated in Figure 36. The data have been collected at a pressure about 1 atm and a temperature of 20°C.

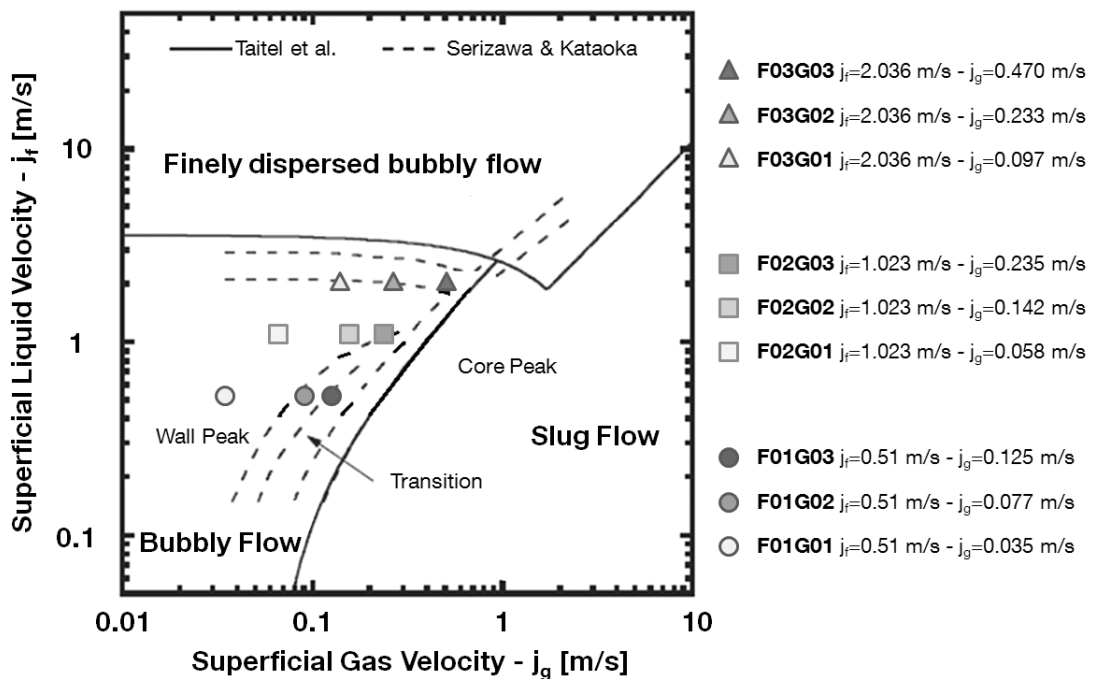


Figure 36: Maps of phase distribution patterns at $z/D=56$

9.2 The ANSYS CFX Model

During the work several 3D grids (45° wedge section) and nearly 2D grids (5° wedge section) were tested in order to set up the computational domain. In this last case, the results showed practically no differences between them. Sari et al. [Sari et al. 2009] and Liao et al. [Liao et al 2011] already used the quasi-2D approach to simulate experiments related to upward vertical bubbly flow conditions. The nearly 2D calculation mesh has been selected for calculations.

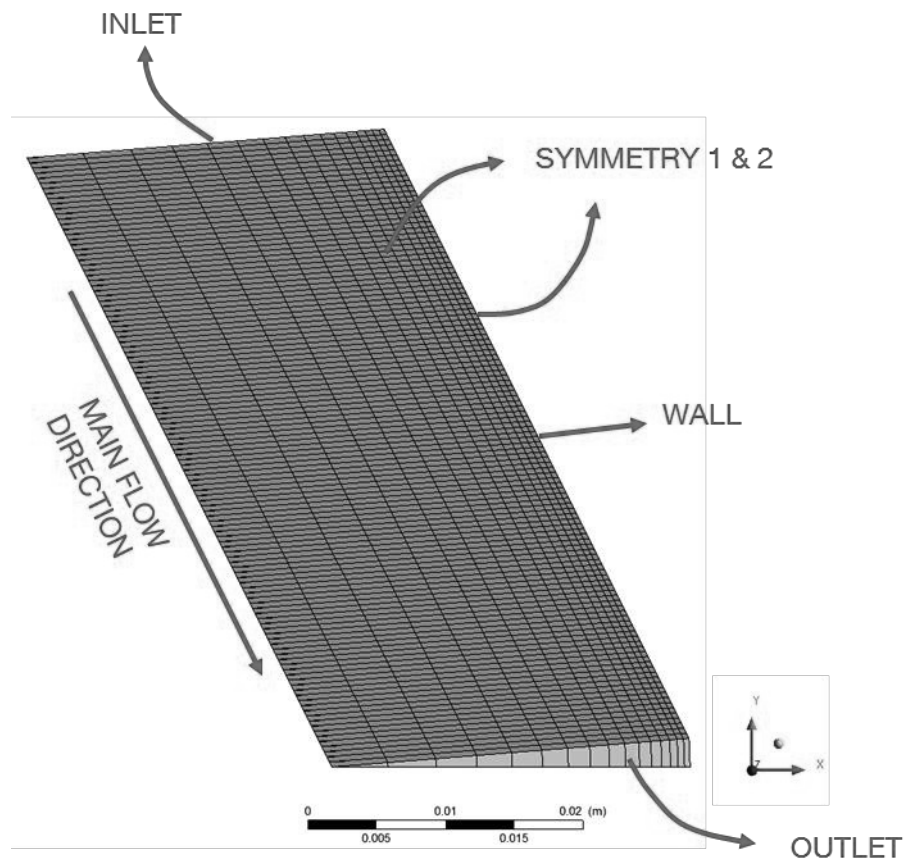


Figure 37: Nearly 2D grid used for the definition of the computational domain;
View downstream the main flow direction; the domain boundaries have been named

9.2.1 Definition of the Boundary Conditions and Fluid Domain Models

The ANSYS CFX computational model consists of five 2D primitives and one fluid domain.

The boundary conditions at the boundaries have been set as follows

- **Inlet:** the experimental radial profiles measured at the entrance of the PUMA experiment have been set as inlet conditions for the following variables:
 - Gas Volume Fraction
 - Gas Velocity
 - Gas Liquid Interfacial Area Density (when needed)
 - Liquid Volume Fraction (1-Gas Volume Fraction)
 - Liquid Velocity

The experiments only provided a value of the mass flow rate whose average velocity has been calculated and applied to a fully developed turbulent flow profile in order to obtain the inlet data.
- **Outlet:** the value of the relative pressure has been set here equal to zero. It means that the system pressure equals the atmospheric pressure at this point.
- **Wall:** the non-slip boundary condition has been set for the liquid-phase and the free slip for the gas phase.
- **Symmetries:** no particular model has been set at the symmetry planes.

The fluid domain models used for the calculation have been explained in detail in Chapter 4. The values chosen for the model coefficients and their assessment will be explained in the next sections.

A Reynolds Averaged Navier Stokes (RANS) turbulence model, based on the SST model already introduced in 4.2.1, for the liquid phase has been used as explained in paragraph 3.6. A zero equation turbulence model for the gas phase is considered because is simple to implement and use and can produce approximate results very quickly. The turbulence data used for further calculation in the next paragraphs are those related to turbulence in the liquid phase and not in the gas phase. The bubble induced turbulence has been taken into account based on two different approaches (sections 4.2.2.1 and 4.2.2.2); the effect of the two-phase flow turbulence modeling on the simulation results is also the object of the analysis.

If the monodispersed approach is used, the bubble interaction mechanisms are not taken into account and the bubble diameter is set by the user. In the simulation presented in this work, the value of the average Sauter diameter is elevation dependent: the diameter is varying linearly between the values measured at the lower and upper measuring port of the PUMA experiment. In this case the effect of the gas expansion due to the elevation change is taken into account.

If the interfacial area density approach is used, then, as introduced in Chapter 5, the interfacial area density is calculated by means of a transport equation and its boundary value at the inlet is set similarly to the other transported variables. The interfacial area density changes are calculated by means of the constitutive models for bubble interaction mechanisms. As result the Sauter mean diameter of the dispersed phase is explicitly calculated.

The residuals convergence criteria for all calculations have been set to a RMS value of 1E-4. This value has been considered a good compromise between accuracy of the results and the speed-up of the calculation process.

9.3 Mesh Sensitivity Analysis

Several grid configurations have been prepared in order to study the influence of the spatial discretization on the numerical results. They have been tested for the case defined as F02G02 (see Figure 36). This case has been selected among those presented in Figure 36, given its position in the middle of the other experimental data available

Concerning the grid requirements, the mesh sensitivity analysis has been performed following the recommendations proposed by the “Best Practice Guidelines for the use of CFD in Nuclear Reactor Safety Application” [NEA 2007].

- Angles below 20° and above 160° have been avoided except for the node at the symmetry axis but this showed no particular numerical influence on the results with the 5° wedge section.
- The grid lines are aligned with the flow direction.
- The aspect ratio has been kept between 10 and 50.
- A finer grid has been placed in the wall near region.

In Table 1 and Table 2 the details of the mesh resolution are summarized.

Table 1: Mesh Information – Axial node number variation

	Nodes (z)	Nodes (r)	Nodes	Calc. Time
	[-]	[-]	[-]	[s]
Mesh A	120	17	3960	6162
Mesh B	240	17	7920	9037
Mesh C	360	17	11880	10597
Mesh D	480	17	15840	12555

Table 2: Mesh Information – Radial node number variation

-	Nodes (z) [-]	Nodes (r) [-]	Nodes [-]	Calc. Time [s]
Mesh E	120	10	2280	4205
Mesh A	120	17	3960	6162
Mesh F	120	34	8040	10205
Mesh G	120	51	12120	22727
Mesh H	120	68	16200	69157

In Figure 38, Figure 39 and Figure 40 the effect of the different grids on the calculation results and on the calculation time is shown. The data plotted have been extracted at a height of 2.9 m and they represent the behavior at any other axial point. It is worth of notice the fact that regarding the axial node number variation (Figure 38), no differences between the tested configurations can be appreciated.

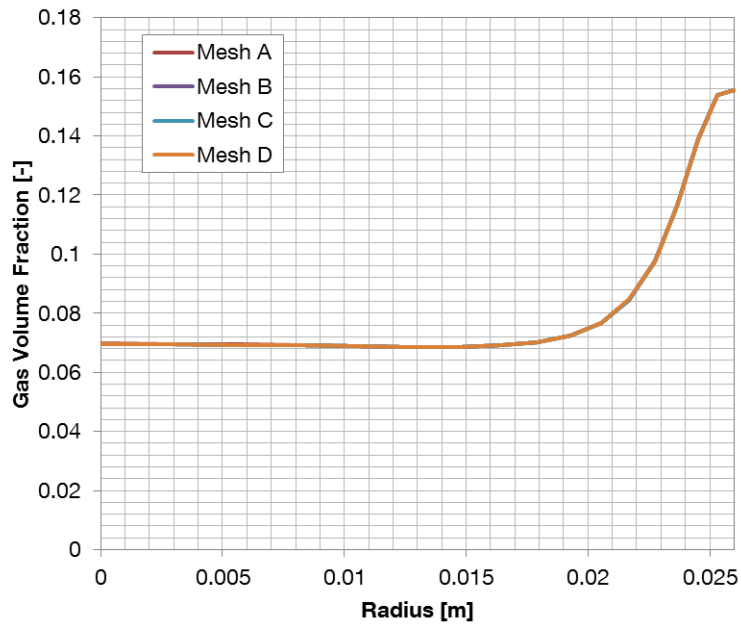


Figure 38: Influence of the axial node distribution on the gas volume fraction radial profile (case F02G02)

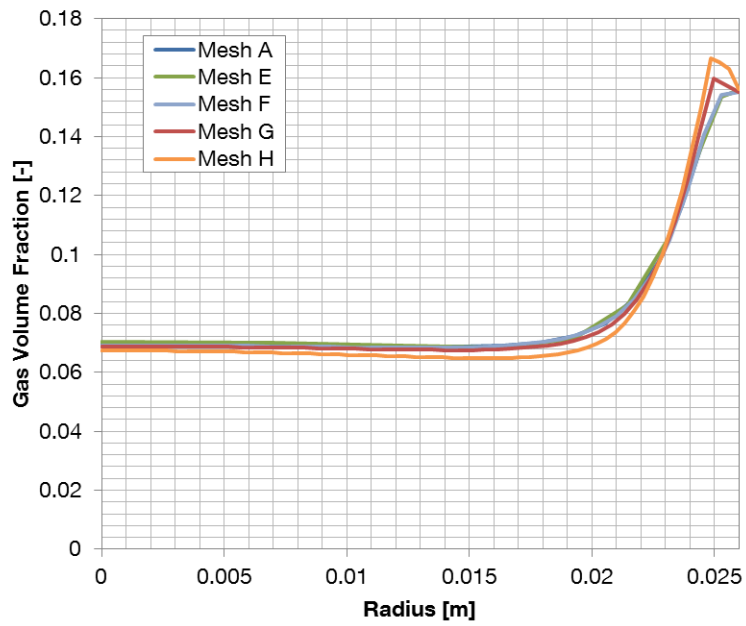


Figure 39: Influence of the radial node distribution on the gas volume fraction radial profile (case F02G02)

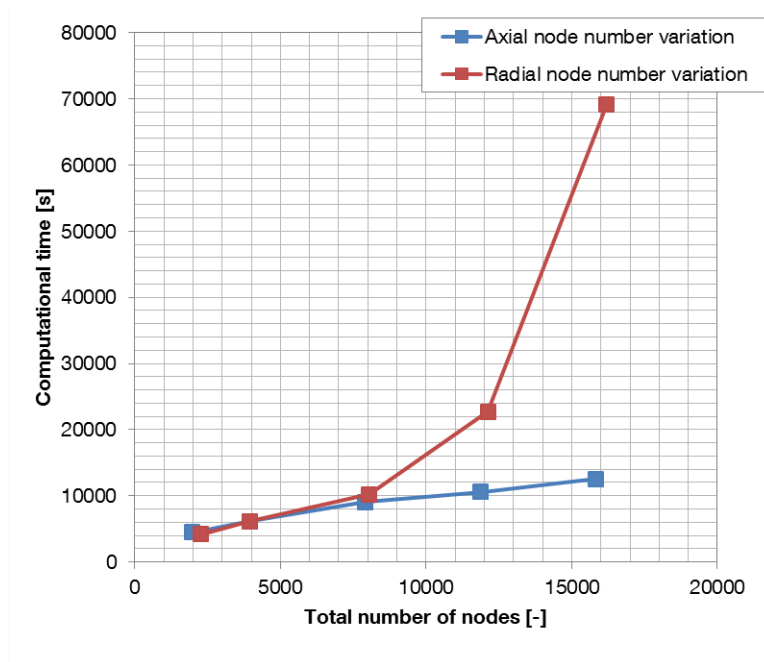


Figure 40: Computational time for the meshes of Table 1 and Table 2 in case of serial calculations for the case F02G02

After the mesh sensitivity analysis has been conducted the best combination between acceptability of the results and computational time is assured the Mesh A in Table 1. The model is built by ca. 4000 nodes that represents a 5° wedge section of the vertical test rig of the PUMA installation using symmetric boundary conditions for both axially cut planes.

The distance of the first node at the wall in order to ensure a value of the y^+ around 30 have been set equal to 0.4 mm for all the cases shown in Figure 36. The choice of a high value of the y^+ , if compared to a single phase simulation, has been determined by convergence and stability issues that have been encountered during the work.

9.4 Analysis of the Effects on the Simulation Results of the Interfacial Forces Models

As already discussed in the paragraph 4.3.2, several forces have an influence on the dynamics of the gas phase. In the next sections, several models for the drag, lift and wall lubrication force as also for the turbulent dispersion force have been tested in monodispersed conditions. Furthermore, different values for various interfacial non-drag forces have been considered. This has been done in order to find a good balance of the forces able to perform reliable simulations for a wide spectrum of cases in the bubbly flow regime.

Also in this case, the F02G02 conditions have been taken as reference for the analysis. A similar behavior has been observed for the other gas and liquid superficial velocities conditions. The set of models that has been selected as a basis to perform the differential analysis based on our previous experience is:

- Drag force: Grace
- Lift force: Tomiyama 1998
- Wall lubrication force: Antal with coefficients -0.0064, 0.016
- Turbulent dispersion force: FAD
- Turbulence model: SST
- Bubble induced turbulent model: Sato

The analysis will then proceed by systematically changing the force models with those we want to evaluate.

The results shown in the next sections have been compared with experimental data radial profiles obtained at the upper measuring port of the installation PUMA (around 2.9 m).

9.4.1 Drag Force

The effect on the radial profile of the gas volume fraction produced by the use of different drag force models has been investigated and the results are shown in Figure 41.

The drag force, see (Eq. 71), accounts for the drag of one phase onto the other. It is a function of the following variables:

$$\vec{F}_D = f(C_D, \alpha, \rho_l, D^{-1}, u_g, u_l).$$

The drag coefficient C_D is a function of the terminal velocity of the dispersed phase and of the dispersed phase bubble diameter. The terminal velocity is Eötvös and Morton number dependent and for its determination experimental correlations are needed.

The simulations discussed differ only in the procedure for the determination of the drag coefficient, while the expression for the drag force remains unvaried.

The differences in the results for the different drag coefficient models (see Figure 41), in the investigated gas and liquid superficial velocity range show very small differences in the radial distribution of the void fraction. The differences are concentrated in the near wall region (from 0.02 m to 0.026 m).

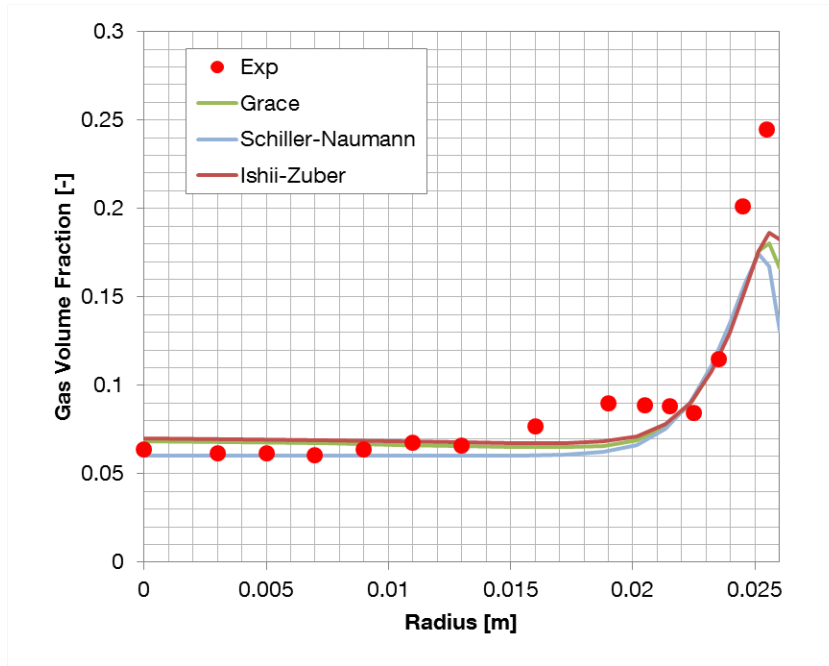


Figure 41: Effect on the results various drag coefficient models for the case F02G02

The C_D model selected for further calculation is that of Grace (see subsection 4.3.2.1). This model has been formulated for flow past a single bubble and it is suitable in case of small volume fractions. It considers the bubble having a distorted form similar to an ellipsoid. Since Grace's model has been developed from air-water data, it produces better results for air-water systems [Ansys 2009].

9.4.2 Lift force

The effect on the Gas volume fraction radial distribution of the use of several lift force models and coefficients has been investigated and the results are shown in Figure 42.

The lift force, see (Eq.79), is a function of the following variables:

$$\vec{F}_L = f(C_L, \alpha, \rho_l, D^{-1}, u_g, u_l).$$

The lift coefficient C_L significantly influences the direction and the intensity of the lift force \vec{F}_L as it can take depending on the flow and bubble conditions, a very wide spectrum of values. C_L is dependent on the bubble Reynolds number (and then of the gas terminal velocity), the Eötvös number (square value of the bubble diameter) and the Morton number (only physical properties dependent).

The simulations discussed below differ only in the model used for the determination of the lift coefficient, while the expression of the lift force remains unvaried.

The model of Tomiyama 1998 has been compared against the prediction with constant C_L values and those with the Magnaudet model (the other model implemented per default in Ansys CFX). The applicability range of this last model is for bubble Reynolds number up to 500. The first constant C_L of 0.288 is obtained by calculating it through the Tomiyama 1998 formulation with a maximum horizontal diameter correlation proposed by Wellek et al. [Wellek et al. 1966]. The second C_L is much lower and is of the same order of magnitude of the value proposed by Lopez de Bertodano and Prabhudharwadkar [Lopez de Bertodano and Prabhudharwadkar 2010] as a better value for calculation of upward turbulent adiabatic bubbly flow. The value of 0.06 has been derived calculating the lift coefficient using the Tomiyama 1999 formulation with the maximum horizontal diameter calculated as explained at page 55 with air-water bubble distortion data from Aybers and Tapucu [Aybers and Tapucu 1969].

Magnaudet’s model seems to deliver the best results for the case F02G02 but its range of applicability make its use limited. Tomiyama and the fixed coefficient 0.288 deliver both the same results as expected. Finally, the coefficient 0.06, in combination with the Sato Bubble Induced Turbulence model, does not reproduce at all the gas volume fraction peak at the wall as the other models do.

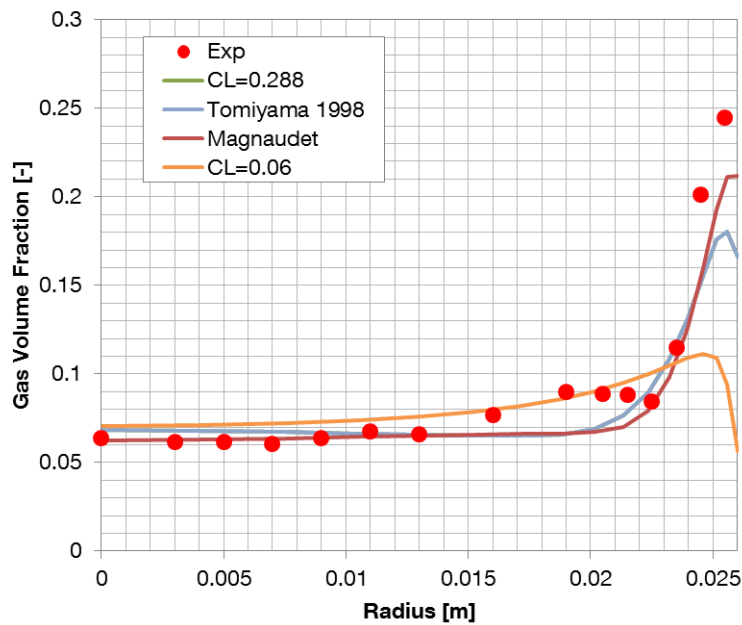


Figure 42: Effect on the results various lift coefficient models and coefficients for the case F02G02

9.4.3 Wall Lubrication Force

The effect on the results of the use of several wall lubrication force models has been investigated and the results are shown in Figure 43.

The wall lubrication force, see (Eq.90), is perpendicular to the wall tangential plane, and it is directed away from it.

$$\vec{F}_{WL} = f(C_{WL}, \alpha, \rho_l, D, u_{\parallel}^2), \vec{n}_w.$$

The wall lubrication force coefficient C_{WL} is inversely dependent on the dispersed phase bubble diameter and at different grades, depending on the models, on the inverse on the distance to the nearest wall. In the expression of the C_{WL} tuning parameters are present to adjust its range of influence and its absolute.

The simulations discussed below differ only in the model for the calculation of C_{WL} while the expression of the wall lubrication force \vec{F}_{WL} remains unchanged.

On page 60 in Figure 19, it has been shown that the highest value of the wall lubrication force coefficient is derived from Frank's model [Frank et al. 2008] with original coefficients 10, 6.8, 1.7. As already commented, the Frank's model is based on the Tomiyama's model [Tomiyama 1998] and resolves the issues related to its dependency on the pipe diameter. The results produced by these two models are very similar and the absolute values in their radial void fraction profiles are of the same order of magnitude. Other two sets of coefficients for the Frank's model have been tested with the aim of reducing the intensity of its effect; they are: 10, 6.8, 1.2 and 8, 8, 1.2 with similar results. In fact, the last of the three coefficients (coefficient "p") is the dominating one. Also for the case of Antal's formulation (see (Eq.91)) two different sets of coefficient have been tested. This has been done in order to understand its effect on the modeling of the void fraction peak at the near wall region. The most suitable model used for the calculation, when compared to experimental data, has been the Antal's formulation with coefficient -0.0064,0.016 as suggested by Krepper et al. [Krepper et al. 2005].

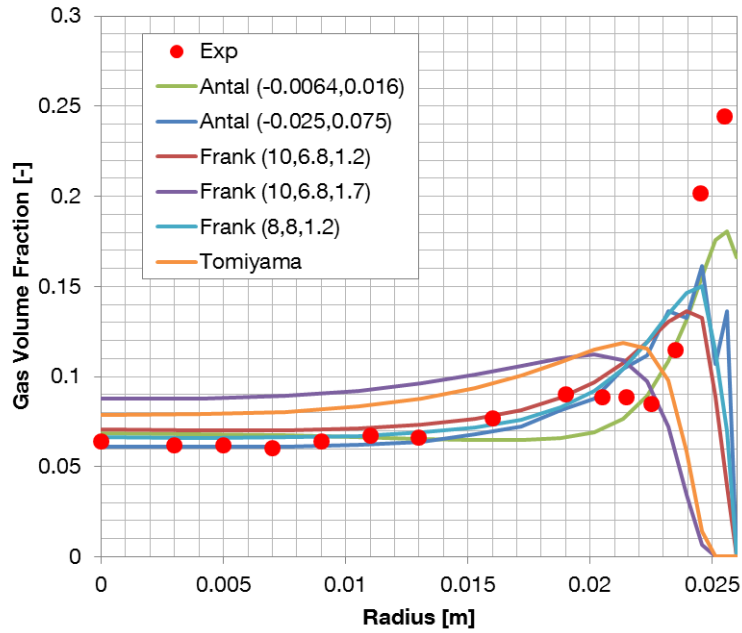


Figure 43: Effect on the results of various wall lubrication force models and coefficients for the case F02G02

A large influence of the effect of the wall lubrication force model on the results can be found in the selection of the location of the first node near the wall. This parameter determines how large the value of the coefficient in the near wall region is (see Figure 19). In the present calculations the value of the distance of the first node at the wall has been set at 0.4 mm. in order to achieve a good balance between the resolution of the near wall turbulence and the numerical stability of the simulation.

9.4.4 Turbulent Dispersion Force

The effect on the results of the use of the turbulence dispersion force has been investigated and the results are shown in Figure 44.

The turbulent dispersion force is responsible for the displacement of the dispersed phase from areas with higher to those with lower concentration. Turbulent fluctuations are the driving mechanism and the force is the result of the combination of the effect of turbulent eddies on the dispersed phase and of the drag between the phases. The force, see (Eq.92), is dependent on:

$$F_{TD} = f(C_{TD}, \alpha, \nabla\alpha).$$

The proportionality constant to adjust the absolute value of the force is the so called turbulent dispersion force coefficient C_{TD} .

Practically, the effect of the turbulent dispersion is that of smoothing out the presence of the phase from areas with higher to those at lower concentration and gradients. It is the only force counterbalancing the effect of the lift force in the regions not in the vicinity of the wall. There are two models to calculate the turbulence dispersion force in Ansys CFX, namely FAD and Lopez de Bertodano's model. Modulating the coefficient of the FAD turbulent dispersion force from 0 to 1 would have the effect to obtain results between the two curves shown in Figure 44. Also the Lopez de Bertodano's model has been tested with two different coefficients: 0.5 and 1. For the monodispersed case, this model, in combination with the bubble induced turbulence model of Sato (see (Eq. 61)) leads, in general, to better results than the FAD model.

The effect of the turbulent dispersion force is of primary importance because it reduces and rounds the shape of the gas volume fraction wall peak.

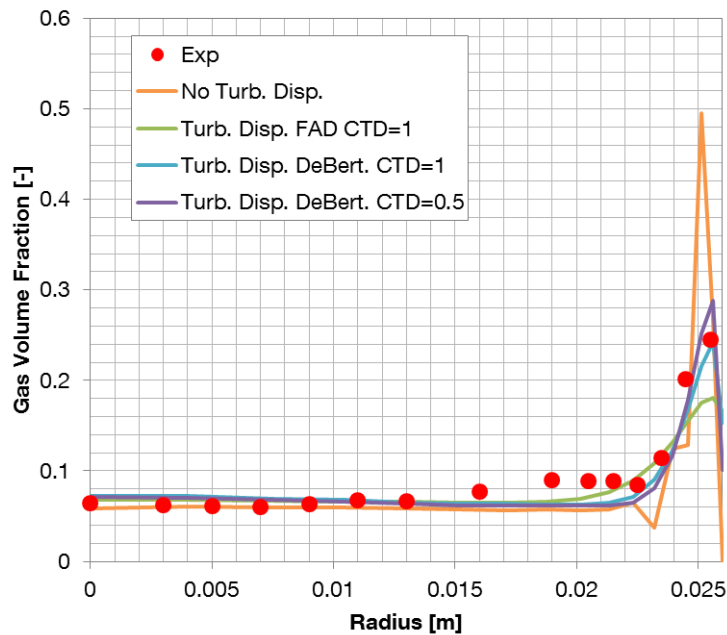


Figure 44: Effect of the turbulent dispersion force on the results for the case F02G02

9.5 Analysis of the Effects on the Simulation Results of the Bubble Induced Turbulence (BIT) Modeling

The effect of using two different approaches presented in paragraphs 4.2.2.1 and 4.2.2.2 to take into account the bubble induced turbulence modeling has been investigated in this subsection. Essentially the difference between the two models lays in the degree of coupling of the system equations that is possible to observe from the results. In the case of the additional viscosity term (4.2.2.1) there is no direct coupling

between the turbulence equations and those of the continuity and momentum. A direct coupling of the mass and momentum quantities with the turbulence quantities is realized if an additional source terms in the turbulence equations is introduced to take into account the turbulent enhancement produced by one phase on the other. For more detail see equation (Eq. 62), (Eq. 63) and (Eq. 64).

In Figure 45 and Figure 46, the results of monodispersed simulation of radial profiles of the turbulence eddy dissipation at 2.9 m from the inlet are shown. In Figure 45 results for all the cases presented in Figure 36 are reported. In general, the intensity of the turbulence eddy dissipation obtained by using the Sato model is much lower than that obtained by using the Yao and Morel’s model [Yao and Morel 2004]. Sato’s model produces an increase in the turbulence eddy dissipation only in the near wall region. Morel’s model is able to reproduce the effect of the presence of the bubbles, everywhere along the pipe radius.

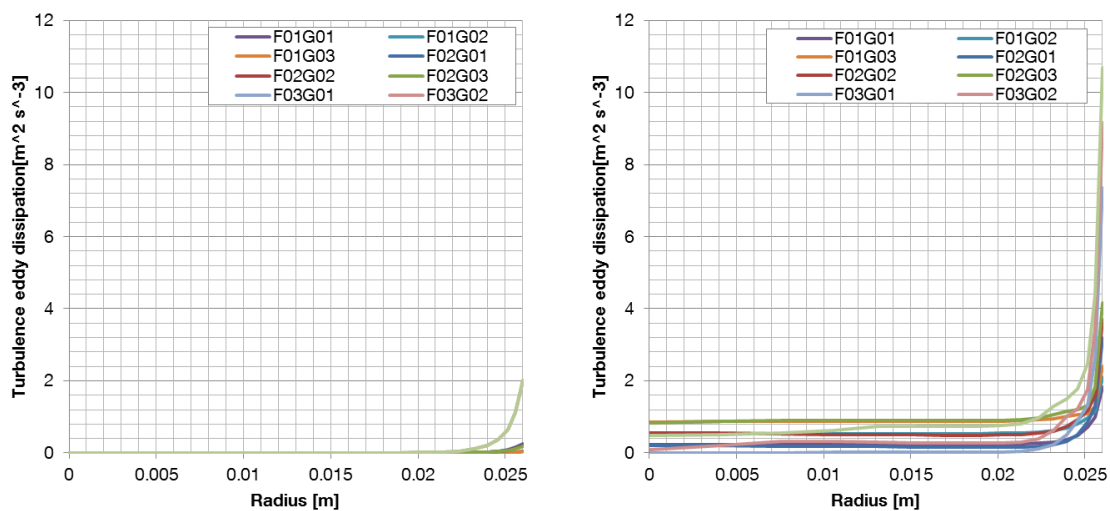


Figure 45: Radial profiles of the turbulence eddy dissipation for several liquid and gas superficial velocities: Sato model (left), Morel model (right).

In Figure 46 only the results for the case corresponding to the liquid superficial velocity around 1 m/s are presented. This has been done to give a better overview of the differences between the effects of the two bubble induced turbulence models. In the image on the left, almost no difference can be appreciated on the turbulence distribution along the radius as the gas superficial velocity increases, with consequent amount of gas in the test section. On the right, the turbulence eddy dissipation is higher as the amount of gas in the pipe section increases.

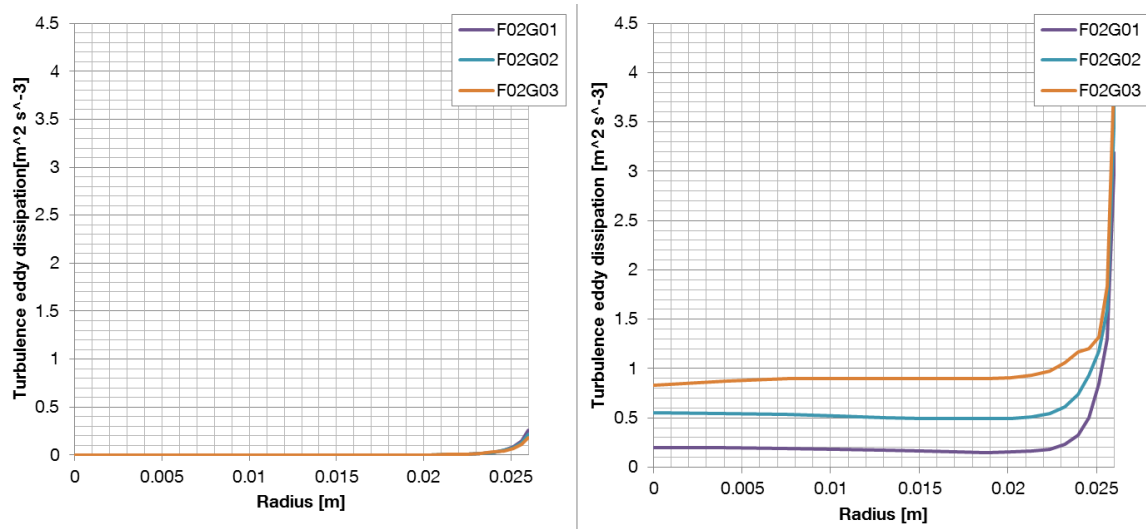


Figure 46: Radial profiles of the turbulence eddy dissipation for the cases F02G01, F02G02, F02G03: Sato model (left), Morel model (right).

If the monodispersed calculation method is used, no bubble interaction models are used for the simulation. Then, the bubble induced turbulence model has a relatively low influence on the simulation results. On the contrary, when the interfacial area transport equation is used, it will have a primary importance for the determination of the breakup and coalescence rates.

The two-phase flow turbulence modeling has a major impact also on the void fraction and on the interfacial area density radial profiles. If the Morel's [Yao and Morel 2004] model for BIT is used (see Figure 47) the lift coefficient obtained using the maximum horizontal diameter correlation from Wellek et al. is too high and the effect is that the gas phase is pushed toward the wall reaching a volume fraction peak value of around 0.5. If a lower lift coefficient is used, as proposed in section 4.3.2.2, the lift force achieves a lower value and the void fraction and interfacial area radial profiles yield values in good agreement with the experimental data.

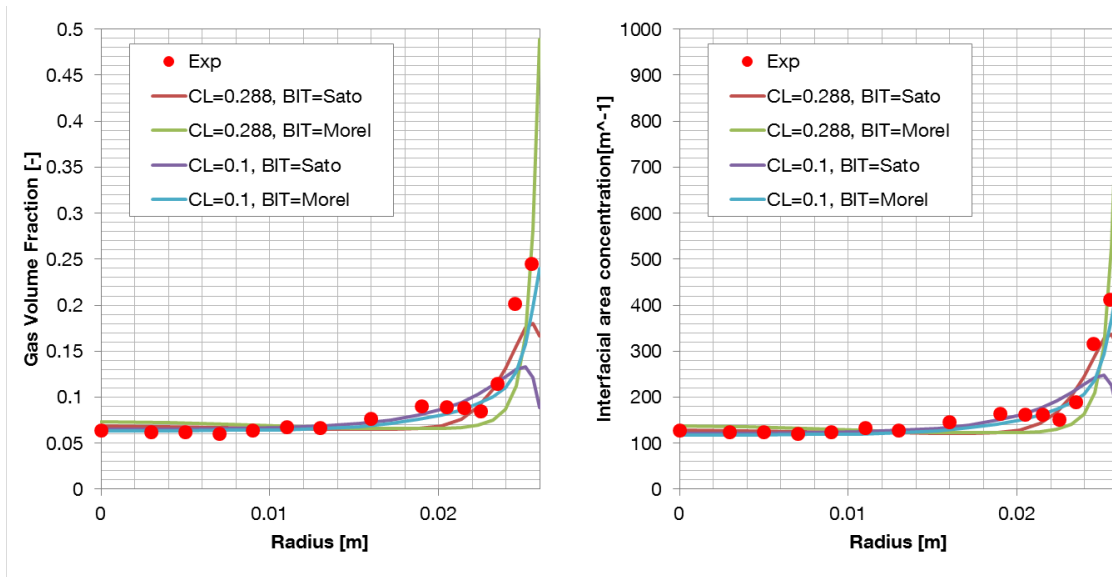


Figure 47: Effect of the lift coefficient and of the turbulent dispersion model on the void fraction and interfacial area density results for the case F02G02

9.6 Analysis of the Combined Effect on the Results of the Lift Force Coefficient and the Bubble Induced Turbulence Model

In the next sections the results for the cases F02G02, F03G02 and F03G03 simulated by using the monodispersed approach are shown. These cases have been selected in order to give an overview of the effect on the results produced by the modifications of the liquid superficial velocity (F02G02 to F03G02) and of the increase of the gas superficial velocity (F03G02 to F03G03).

The results are shown for the two different approaches of the BIT already presented (Sato and Morel) with two different lift coefficients: 0.288 and 0.1.

In general, in combination with the monodispersed approach, the Morel BIT model tends to over predict the value of the volume fraction peak at the wall. It is possible to reduce it by lowering the lift coefficient taking into account the bubble distortion as already explained in section 9.5. Using the BIT model of Sato in combination with a constant lift coefficient of 0.288 yields results with an acceptable agreement over the range of flow conditions covered by the three experimental data sets in Figure 48. Using a value for the lift coefficient equal to 0.1 in combination with the Sato BIT model tends to under-predict the experimental profiles.

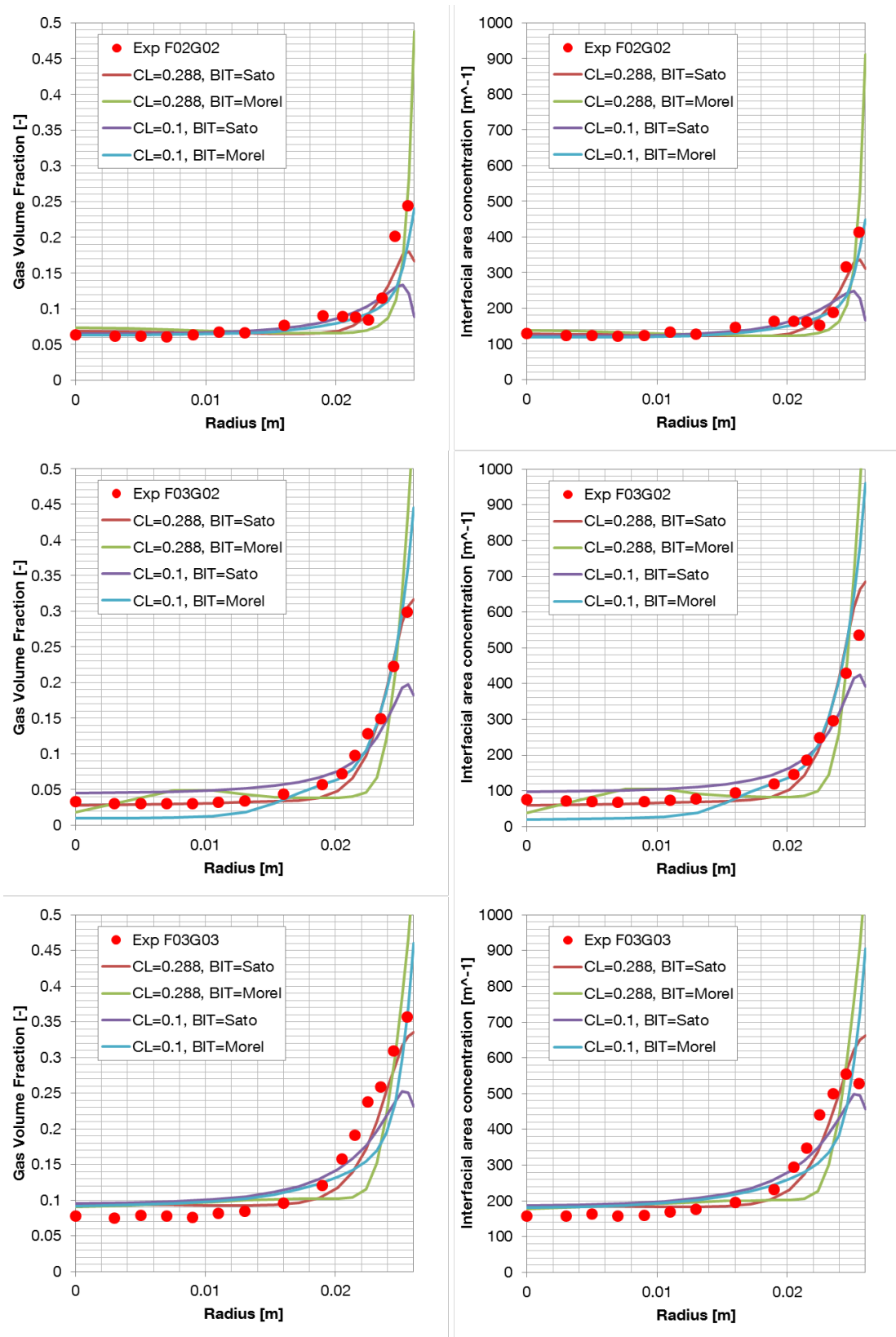


Figure 48: Radial profiles of the gas volume fraction (left) and interfacial area concentration (right) for the cases F02G02 (up), F03G02 (middle) and F03G03 (right)

In Figure 49 the results of the gas velocity radial profiles are shown. There is almost no difference between the results obtained changing the BIT model. If the liquid superficial velocity is increased then, a slightly better reproduction of the velocity profile at the pipe centerline is obtained using a lift coefficient equal to 0.1.

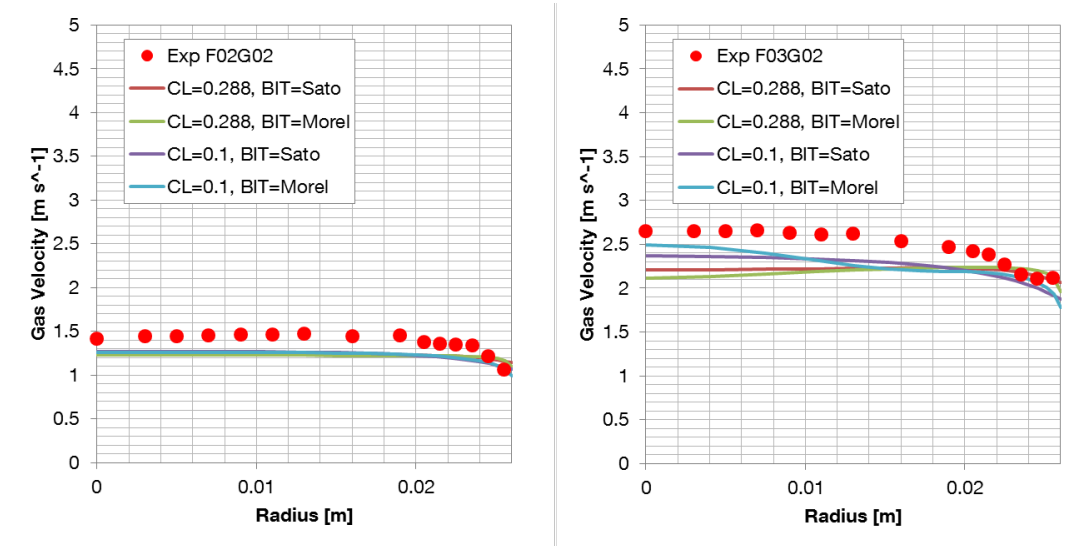


Figure 49: Radial profiles of the gas velocity F02G02 (left) and F03G02 (right)

Considering the results of the simulations above, in case of a monodispersed simulation for air water upward turbulent bubbly flow, good results can be obtained if the Sato BIT model is used in combination with the following interfacial non-drag forces models:

- Lift force: Tomiyama 1998
- Wall lubrication force: Antal (with coefficients -0.0064,0.016)
- Turbulent dispersion force: FAD (with coefficient 1)

9.7 Analysis of the Simulation Results Using the Interfacial Area Density Transport Equation and the State of the Art Coalescence and Breakup Models

The constitutive models for the source and sink terms introduced in chapter 7 for the interfacial area transport equation have been implemented in Ansys CFX as explained in section 8.3.3.

In the previous sections of this chapter, a great influence of interfacial non-drag forces on the results has been noticed. For this reason for the case F02G02 the effects of

several combinations of models and coefficients have been investigated. The radial profiles for the gas volume fraction and interfacial area concentration for Hibiki and Ishii 2001 and Yao and Morel 2004 models (Figure 50) and for Wu et al. 1998, Ishii and Kim 2001 and Wang 2010 (Figure 51) are shown. These models have been introduced and analyzed in detail in sections 7.1 to 7.5.

In general, the five models listed above, are able to reproduce with good agreement the gas volume fraction radial profile and their differences are limited (Figure 50 and Figure 51). This happens except if Sato BIT model is used in combination with a lift coefficient equal to 0.1. A similar behavior has been observed in Figure 42 in case of monodispersed simulations.

The gas volume fraction is in good agreement with the experimental data in almost all conditions and interfacial area density models tested. This is not valid, however, for the interfacial area density radial profile. This variable is in relative good agreement with the experimental data in the central region of the pipe. On the contrary, in the near wall region the discrepancies are much higher and in most of the cases models are not able to predict the interfacial area density adequately.

For the case F02G02, shown in Figure 50, results in good agreement with the experimental data have been obtained with the Yao and Morel 2004 model (up to the last node at the wall where the value over-predicts the experimental data) using the lift coefficient $C_L = 0.288$, the wall lubrication coefficient $C_{WLF} = \text{Antal} (-0.01, 0.05)$ and the turbulent dispersion force FAD with coefficient equal to 1.

This is not surprising as the authors suggested the use of a high lift coefficient (0.5) in combination with a high value of turbulent dispersion force coefficient [Yao and Morel 2004]. Furthermore, their model for the calculation of eddies-bubbles collision frequency has been opportunely tuned to better approximate the case of upward turbulent bubbly flow in pipe of moderate diameter [Yao and Morel 2004] in conditions very similar to those of the PUMA experiment. These tuned values are not valid universally, however.

In order to reduce the high value of the interfacial area density in the near wall region a lift coefficient equal to 0.288 and the Lopez de Bertodano turbulent dispersion force with coefficient equal to 1 has been also tested. In this case, the results under-predict the interfacial area density in the near wall region since the Lopez de Bertodano's model delivers a too high turbulent dispersion force. Tests have also been performed

to reduce the turbulent dispersion force by reducing its coefficient. This had the effect to make the simulations unstable. Overflows have been experienced without the possibility to write the results to file.

The experimental results are over-predicted when the Wu et al. 1998, Ishii and Kim 2001 and Wang 2010 models are used (Figure 51). In general it has not been possible to lower the peak of the interfacial area density at the wall under the level of 1000 m^{-1} . It is worth to notice, that the value of the interfacial area density has been limited to 1000 m^{-1} for calculation stability purposed. Without limiter, the peak at the wall would have reached much higher values up to 30000 m^{-1} .

As an example, in Figure 52 the Sauter mean diameter (left) and the gas velocity (right) radial profiles for the lift coefficient $C_L = 0.288$, the wall lubrication coefficient $C_{WLF} = \text{Antal}(-0.01, 0.05)$ and the turbulent dispersion force FAD with coefficient equal to 1 are shown. Similarly to the limiter set for the interfacial area concentration, the value of the Sauter Diameter has been constraint between 0.3 and 3 times the value of the Sauter diameter average value measured for each case at the lower measuring port of the PUMA facility. In general, the calculation of the Sauter mean diameter presents oscillations as it depends on a calculated (gas volume fraction) and a transported variable (interfacial area concentration). If the results of these variables are not well coupled, the ratio can deliver, point-wise, results far away from the experimental values. If the interfacial area concentration is overestimated, the Sauter mean diameter will deliver values lower than the experimental results. The radial profiles of the Sauter mean diameter is in good agreement with the experimental results if the Morel model is used.

In general, for other gas and liquid superficial velocity values, different to those in the case F02G02, the experimental data for are under predicted for all the closure models used.

The results of the Interfacial Area Concentration (IAC) change rate due to the bubble interaction mechanisms are shown in Figure 53 (left) for the Random Collision (RC) and (right) for the Weak Entrainment (WE) and in Figure 54 for the Turbulent Impact (TI). For both coalescence and breakup, the model of Wu et al. 1998 predicts the highest effects. Wang 2010 and Ishii and Kim 2001 yield similar results but the order of magnitude is lower, because of lower values for the tuning coefficients in the model.

The Hibiki and Ishii 2000 model delivers in general the smallest results. Yao and Morel produces results in the order of magnitude of Wu et al. 1998, but the curves in Yao and Morel's case are much more regular and the values are not diverging in the near wall region as much as Wu's model does.

This page has been intentionally left blank.

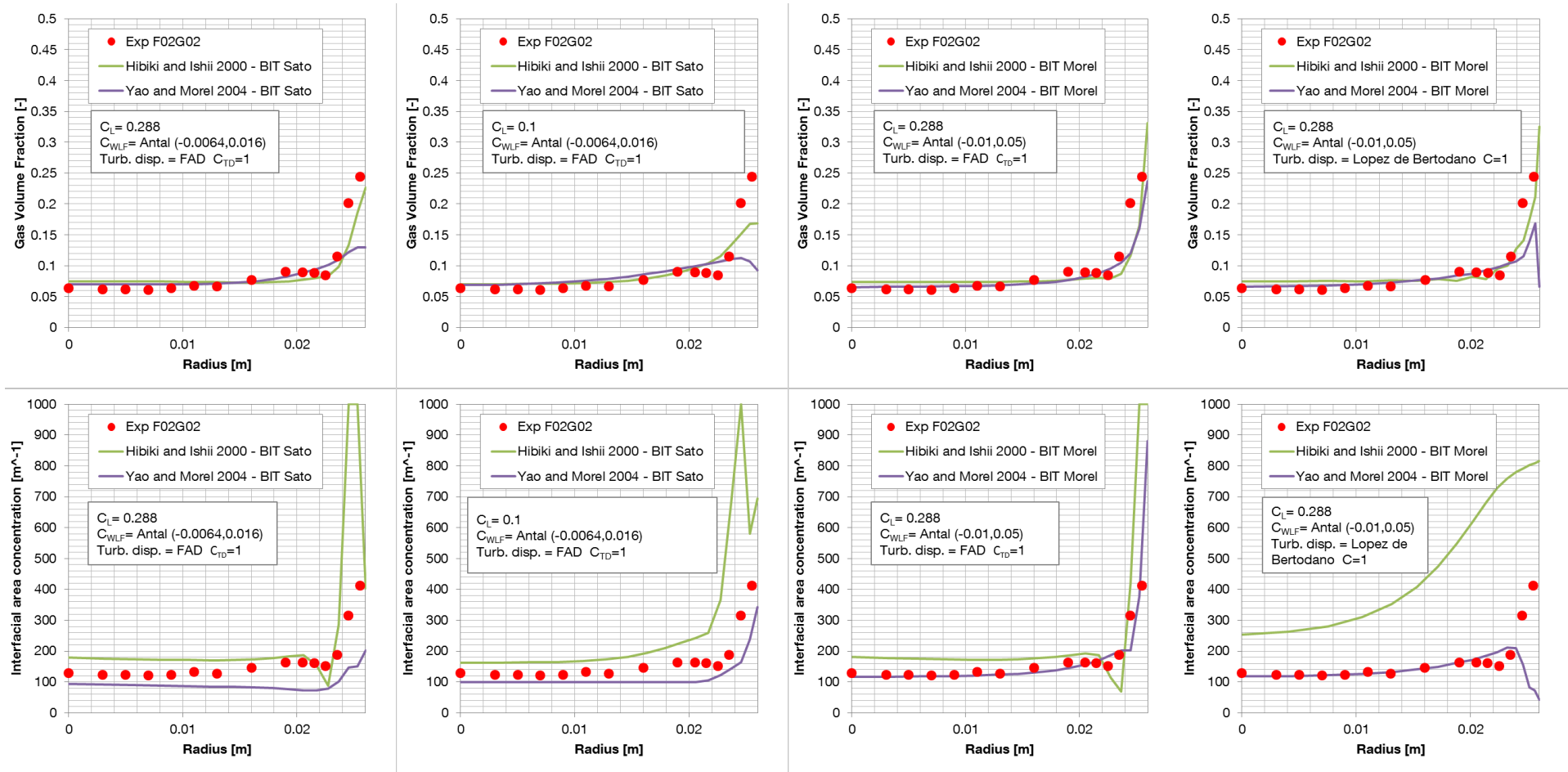


Figure 50: Radial profiles for the volume fraction (up) and for the interfacial area concentration (down) for various domain models combinations for the case F02G02 with the Hibiki and Ishii 2000 and Yao and Morel 2004 models.

This page has been intentionally left blank.

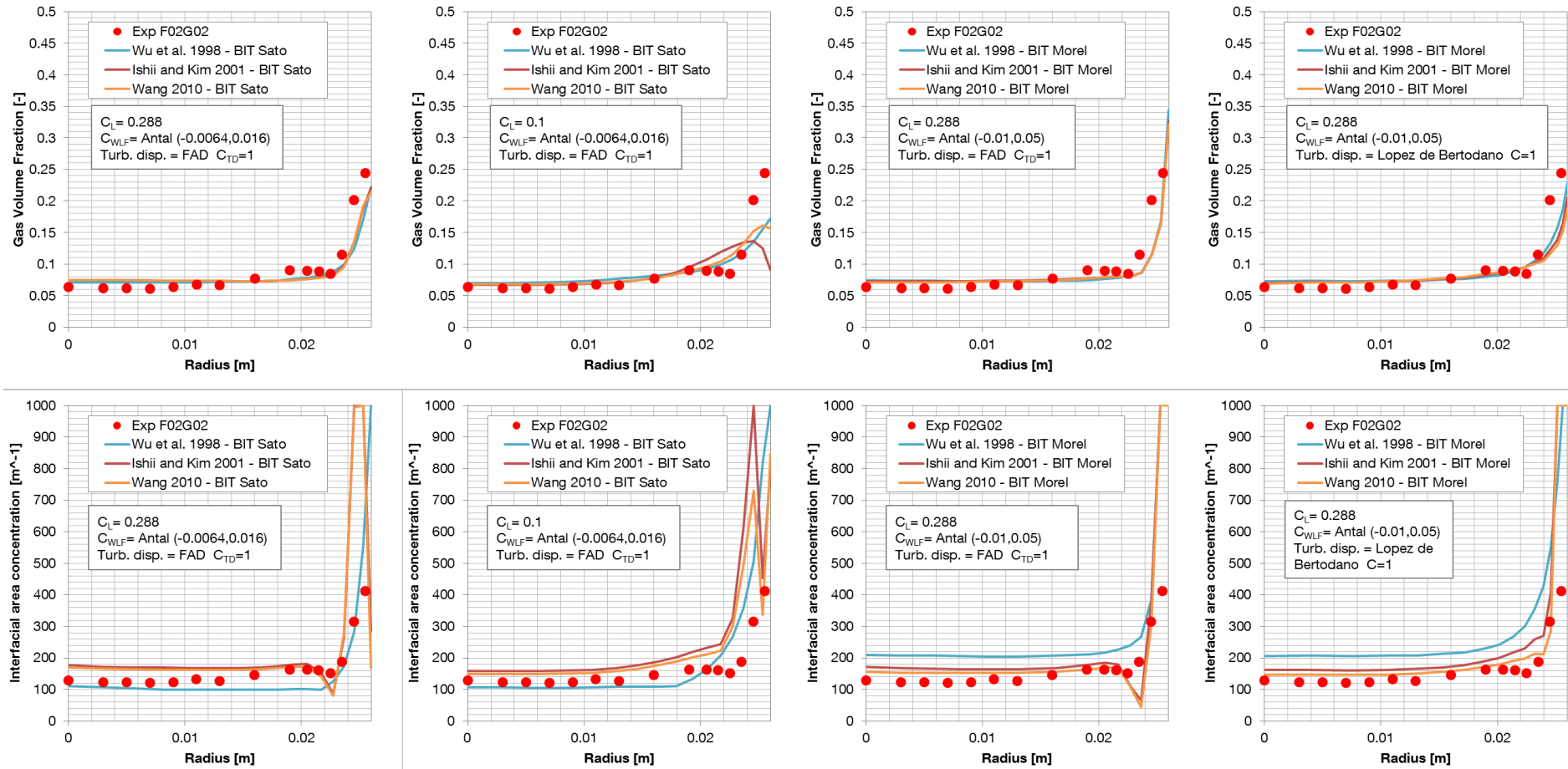


Figure 51: Radial profiles for the volume fraction (up) and for the interfacial area concentration (down)

for various domain models combinations for the case F02G02 with the Wu et al. 1998, Ishii and Kim 2001 and Wang 2010 models.

This page has been intentionally left blank.

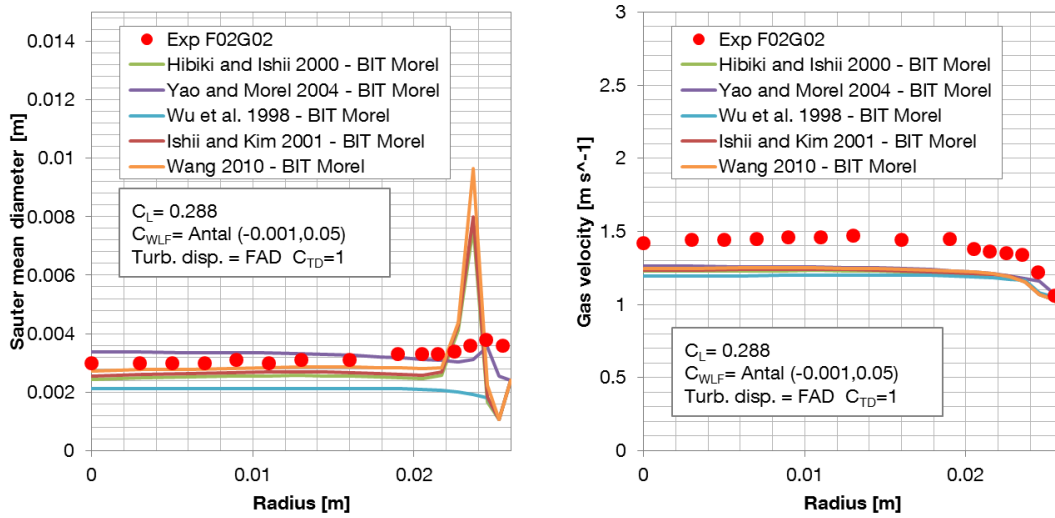


Figure 52: Radial profiles for the Sauter mean diameter (left) and gas velocity(right) for the case F02G02 with the Hibiki and Ishii 2000, Yao and Morel 2004 Wu et al. 1998, Ishii and Kim 2001 and Wang 2010 models.

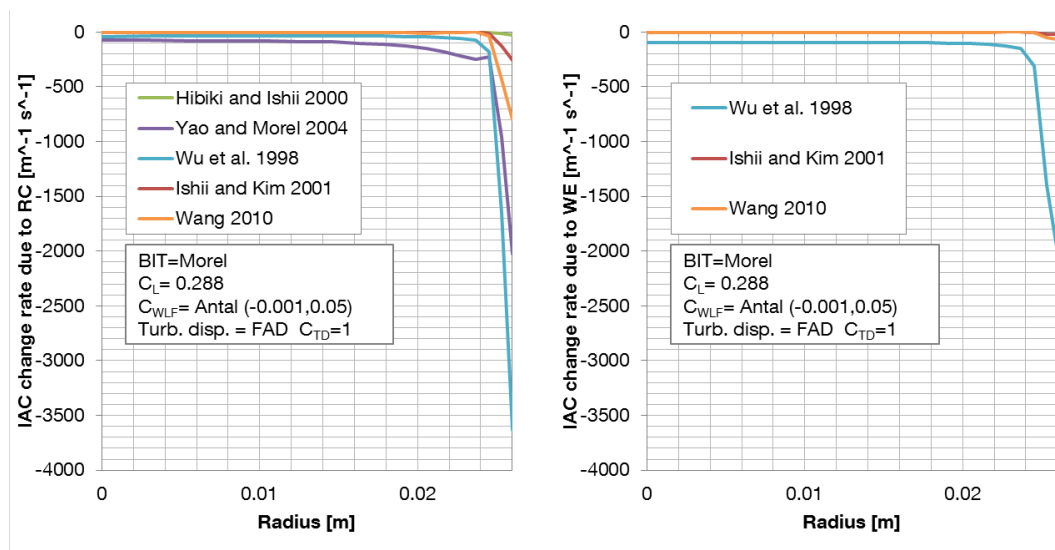


Figure 53: Radial profiles for the IAC change rate due to Random Collision (left) and Weak Entrainment (right) for the case F02G02 with the Hibiki and Ishii 2000, Yao and Morel 2004 Wu et al. 1998, Ishii and Kim 2001 and Wang 2010 models.

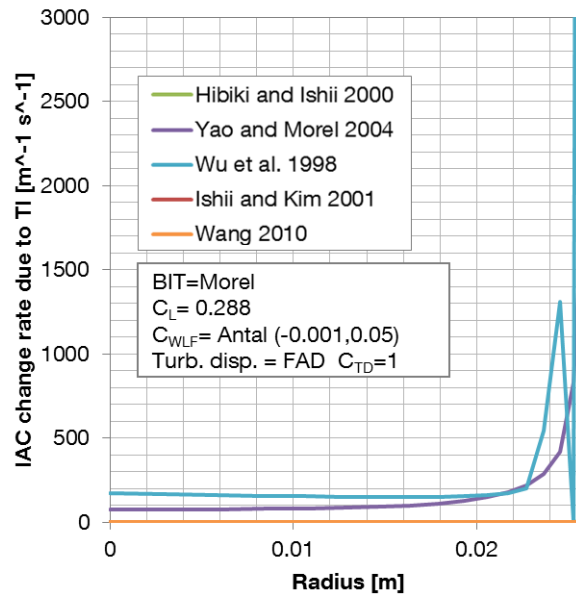


Figure 54: Radial profiles for the IAC change rate due to Turbulent Impact for the case F02G02 with the Hibiki and Ishii 2000, Yao and Morel 2004 Wu et al. 1998, Ishii and Kim 2001 and Wang 2010 models.

Results for the experimental conditions F03G02 and F03G03 using the Morel’s BIT model and the lift coefficient $C_L = 0.288$, the wall lubrication coefficient $C_{WLF} = \text{Antal} (-0.01, 0.05)$ and the turbulent dispersion force FAD with coefficient equal to 1 are shown in Figure 55. In case of the experiment F03G03 only the results of the Hibiki and Ishii 2000 and Yao and Morel 2004 have been reported since for the other models it has not been possible to write results to files due to overflow in the calculations.

The gas volume fraction is in both cases over-predicted near the wall delivering results up to 0.6. The models of Wu et al. 1998, Ishii and Kim 2001 and Wang 2010 showed a strange behavior in the central pipe region as the interfacial area density is increasing up to value between 300 and 400 m^{-1} . Yao and Morel 2004 produced results in acceptable agreement with the interfacial area experimental results in the bulk liquid but the model over-predicted the experimental values at the vicinity of the wall. This is valid both for the cases F03G02 and F03G03. In general, the calculation of the Sauter mean diameter presents oscillations as already observed for the simulations of case F02G02. The maximum and minimum value of the Sauter diameter have been limited also for these simulations between 0.3 and 3 times the value of the average Sauter diameter measured for each case at the lower port of the PUMA facility. The radial

profiles are in good agreement with the experimental results if Yao and Morel's model is used. Also in this case oscillations occur at the vicinity of the wall.

This page has been intentionally left blank.

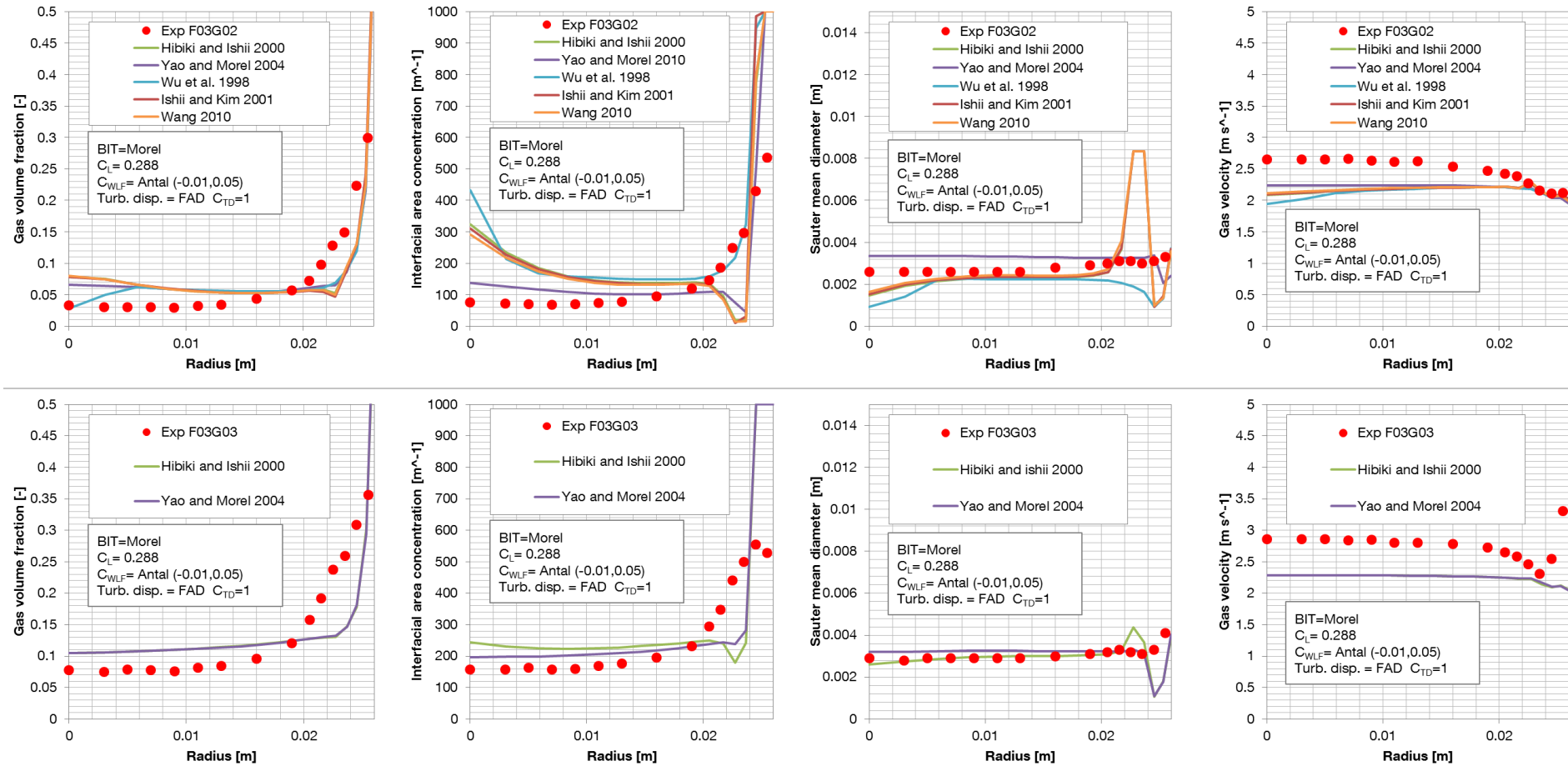


Figure 55: Radial profiles of the gas volume fraction, interfacial area concentration, Sauter mean diameter and gas velocity for the cases F03G02 (up) and F03G03 (down) for several interfacial area density breakup and coalescence terms.

9.8 Conclusions of the Analysis

In chapter 4 we have seen that several forces have an influence on the dynamics of the gas phase. In chapter 5 it has been explained that the interfacial transfer of mass, momentum and energy are proportionally related not only to the interfacial forces described above but also to the interfacial area density.

For these reasons, in this chapter the analysis of two different simulation approaches and of the effects of the interfacial forces models for the upward turbulent bubbly flow in adiabatic conditions has been carried out for:

- 1) Monodispersed simulation
- 2) Monodispersed + Interfacial area transport simulation (state of the art models)

9.8.1 Main Conclusions for the Monodispersed Simulations

In this analysis several models for the drag, lift and wall lubrication forces as also for the turbulent dispersion force have been tested. Different values for various interfacial forces have been considered in order to find a good balance of the forces able to perform reliable simulations for a wide spectrum of cases in the bubbly flow regime. No bubble interaction mechanisms have been taken into account.

The accurate analysis of the simulation results carried out for monodispersed simulation has shown that a reliable simulation of upward turbulent bubbly flow in adiabatic conditions is possible with the code Ansys CFX using the following set of interfacial drag and non-drag forces and turbulence models:

- Drag force: Grace
- Lift force: Tomiyama 1998
- Wall lubrication force: Antal with coefficients -0.0064, 0.016
- Turbulent dispersion force: FAD
- Turbulence model: SST
- Bubble induced turbulent model: Sato

The monodispersed simulation approach does not take into consideration the effect of the bubble interaction mechanisms to determine the dynamic of the two-phase flow. For this reason, in the literature concerning monodispersed simulations of upward turbulent bubbly flow in adiabatic conditions, the effect of the turbulence generated by the presence of the gas on the liquid phase has not been considered as a critical issue. In fact, the attention has been concentrated more on the assessment of the coefficient

for the determination of the non-drag forces empirical coefficients for a reliable determination of the radial profile of the phases distribution.

In this chapter two different models for the determination of the Bubble Induced Turbulence (BIT) have been tested as explained in subsection 4.2.2. In that subsection several BIT models has been compared against DNS simulation of bubbles rising in a channel [Wörner et al. 2004]. The BIT model of Yao and Morel [Yao and Morel 2004] with results in good agreement with the DNS simulation has been selected for further use in this work. The radial distributions of the turbulence eddy dissipation obtained using the Sato's BIT model [Ansys 2009] for increasing content of the gas phase in the duct showed no appreciable differences between the cases examined. On the contrary, when the BIT Yao and Morel's model was used, a significant increase in the level of the turbulence eddy dissipation along the pipe radius was noticed for increasing gas superficial velocity.

During the analysis, a strong coupling between the BIT model and the value of the lift force coefficient has also been observed. The use of the more accurate Yao and Morel's BIT model demanded the use of a value for the lift force coefficient much smaller (around 0.1) than that used in case of simulation using the Sato's BIT model (around 0.288). These considerations are supported also by the work of Lopez de Bertodano and Prabhudharwadkar [Lopez de Bertodano and Prabhudharwadkar 2010]. The simulations carried out using the smaller constant value equal to 0.1 for the lift coefficient combined with the more realistic Yao and Morel's BIT model delivered results in better agreement with the experimental data of the radial distribution of the void fraction. Nevertheless, a unique constant value of the lift coefficient has not been found suitable to perfectly reproduce the experimental conditions under study. For this reason further study is needed to develop dynamic correlations to calculate the bubble distortion depending on the flow conditions for the determination of the lift coefficient.

9.8.2 Main Conclusions for the Monodispersed Simulations Together with the Interfacial Area Transport Equation and the State of the Art Bubble Interaction Models

A better manner to model the interfacial area concentration than an algebraic approximation is to do it directly by means of a transport equation, especially for the three-dimensional formulation of two-phase flow. The accurate determination of the interfacial area is important to achieve both good local and global prediction of two-

phase flow characteristics. This approach is also able to reproduce dynamic and transient phenomena such as phase change or flow regime transitions that cannot be simulated by the monodispersed approach alone.

In this Thesis the monodispersed approach together with the self-implemented additional interfacial area transport equation and several constitutive models for bubble breakup and coalescence from the literature have been tested.

The main goals of this analysis were to validate the correct implementation of the additional transport equation and to analyze the influence of its state-of-the-art constitutive models on the results and try to find their limits. Thus, formulations describing different aspects of bubble dynamics from Hibiki and Ishii 2001, Yao and Morel 2004, Wu et al. 1998, Ishii and Kim 2001 and Wang 2010 have been implemented in the code and tested. These models have been described and discussed in detail in sections 7.1 to 7.5.

In general, the five models listed above are able to reproduce with good agreement the gas volume fraction radial profile and their differences with the experimental measurements are small (Figure 50 and Figure 51). This happens except when, in combination with all the five Interfacial Area Transport Equation constitutive models, the Sato's Bubble Induced Turbulence model is used in combination with a lift force coefficient equal to 0.1 (similarly to Figure 42 in case of monodispersed simulations).

Problems arise if the interfacial area density or the Sauter mean bubble diameter radial distributions are considered though. For instance, the interfacial area concentration is in relative good agreement with the experimental data in the central region of the pipe whereas, in the near wall region the discrepancies are much larger and, in most cases, the models are not able to predict the interfacial area density or the Sauter mean diameter of the bubbles adequately.

The best agreement with the experimental data has been obtained with the Yao and Morel's constitutive model for the interfacial area transport equation in combination with the following set of interfacial drag and non-drag forces and turbulence models:

- Drag force: Grace
- Lift force: Tomiyama 1998 with constant $C_L = 0.288$
- Wall lubrication force: Antal with coefficients (-0.01,0.05)
- Turbulent dispersion force: FAD (coefficient 1)
- Turbulence model: SST

- Bubble induced turbulent model: Yao and Morel

Nevertheless, the interfacial area constitutive models tested in this chapter contain a number of empirical coefficients. For Wu et al. 1998 and Ishii and Kim 2001 and Hibiki and Ishii 2001 the empirical coefficients have been tuned to fit the 1D vertical evolutions of the main flow parameters. In case of Wang 2010, the set of coefficients has been obtained through a very time and resource intensive calibration procedure for three-dimensional calculations. This means that they are not universal and that modifying the flow conditions or the geometry of the system under exam can lead to the need to calibrate the model coefficients again.

Furthermore, Yao and Morel [Yao and Morel 2004] do not explain a coefficient in their formula for the determination of the cross sectional area for bubble collisions (see (Eq.200)). Finally, both in Hibiki and Ishii 2001, as also in Yao and Morel 2004 the expressions for the determination of the energy content of the eddies that can break the bubble are difficult to be validated against experimental data [Liao and Lucas 2009] (Hibiki and Ishii 2001 and Yao and Morel 2004) or have been selected *ad hoc* to better fit upward vertical turbulent bubbly flow experiments [Yao and Morel 2004], thus they are not universally applicable.

Based on these last considerations, the need for the development of new bubble interaction terms for the one-group interfacial area transport equation is clear. In chapter 10 the inconsistencies in the use of the 1D definition of the bubble interaction terms for 3D simulations are explained and a new local mechanistic formulation of bubble interaction models for coalescence and breakup is developed and presented. In chapter 11 the effect on the simulation results of various model parameters and coefficient is shown in detail. Furthermore, radial profiles of the main variables are presented in order to explain the behavior of the newly developed models. Several set of experimental data have been simulated in order to test the model for a wide range of conditions.

Chapter 10

Development of New Bubble Interaction Terms for the One-Group Interfacial Area Transport Equation

In this chapter, the inconsistencies in the use of the 1D definition of the bubble interaction terms for 3D simulations are explained. A new local mechanistic formulation of bubble interaction models for coalescence and breakup is developed and presented.

The most important parameter in the breakup and coalescence terms developed for both 1D and for the 3D local formulation is the turbulence energy dissipation ε . This parameter in case of 1D codes can be evaluated by means of relatively simple algebraic expressions obtained from the mechanical energy equation and among all function of the pressure losses caused by wall and interfacial friction along the flow directions [Hibiki and Ishii 2000a]:

$$\varepsilon = \frac{\langle j \rangle}{\rho_m} \left(-\frac{dp}{dz} \right)_F. \quad (\text{Eq.227})$$

In case of ANSYS CFX the turbulence energy dissipation ε is a result of the turbulence modeling and comes directly from the differential transport equation for the turbulence dissipation rate [Ansys 2009].

The breakup and coalescence models used in chapter 9 by ANSYS CFX to calculate the interfacial area transport equation presented in chapter 7 are those proposed by Hibiki and Ishii [Hibiki and Ishii 2000a], Wu et al. [Wu et al. 1998] (this case also with coefficients proposed later by Ishii and Kim [Ishii and Kim 2001] and Wang [Wang 2010]) and Yao and Morel [Yao and Morel 2004]. Hibiki and Ishii's and Wu et al.'s models have been developed for 1D applications and have been established through mechanistic modeling of the major particle interactions that take part in the change of a_i . The fluid dependent parameters needed for the evaluation are intended as

averaged values along the radial direction. The distortion caused by this assumption has been adjusted by the means of tuning parameters in the final expressions of the terms [Hibiki and Ishii 2000a]. This modeling strategy yields the best agreement with the axial evolution of the flow parameters. This is due to the limited variation of the main flow parameters along the axis (see Figure 56).

In Figure 56, the evolution of the turbulence eddy dissipation along the flow axis (left) and the radius (right) is shown for the case F03G02 using both Sato's and Morel's BIT models. Any other of the experimental conditions analyzed replicated the same behavior.

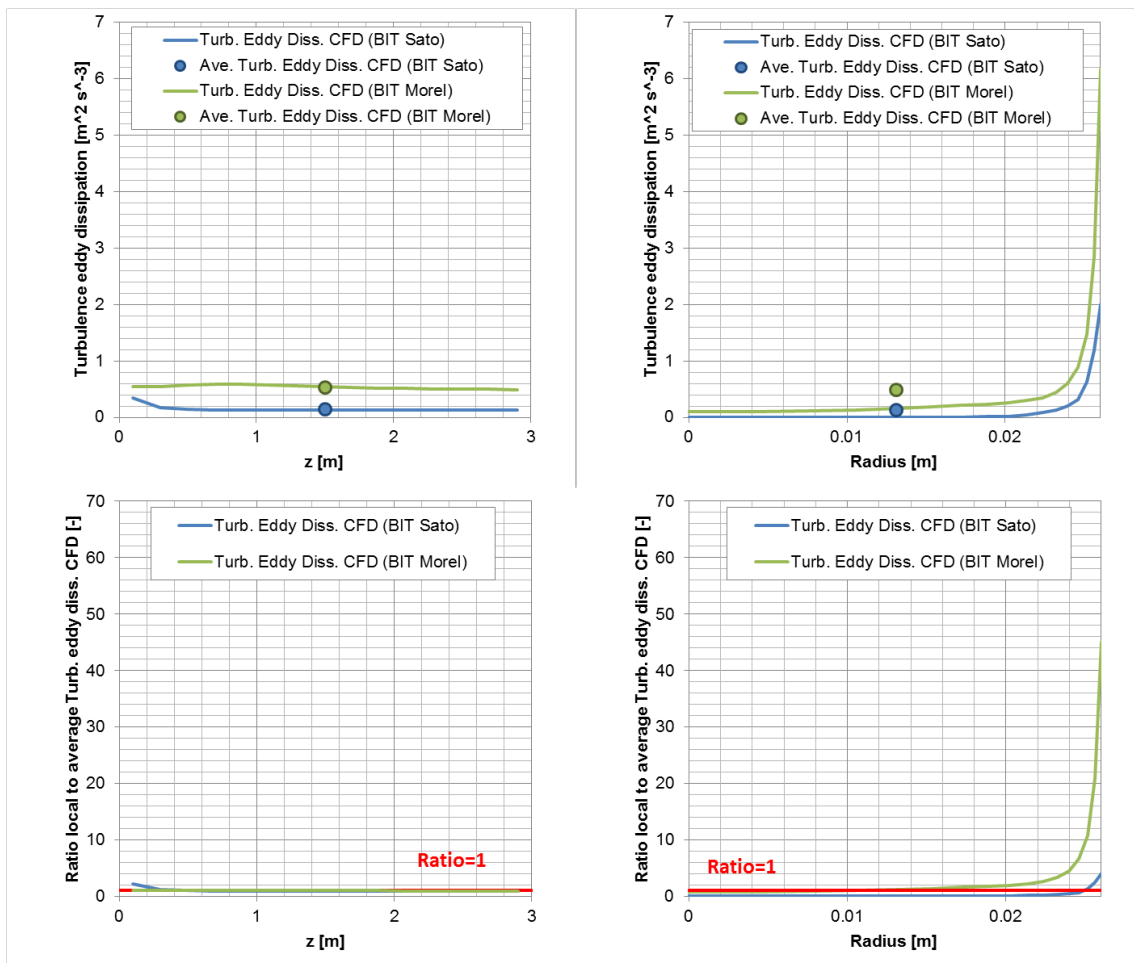


Figure 56: Comparison between local and average values of turbulence eddy dissipation: axial (left) and radial profiles at 2.9 m (right); eddy dissipation (up) and ratio local to average values (down).

The axial profile variation of the turbulence eddy dissipation is less pronounced than the radial one. Concerning the axial evolution, both BIT models deliver results for the local values very near to the radial average. If the radial profiles are considered and the

Morel BIT model is used, the values in the near wall region reach valued 10 to 40 times the average.

Considering the radial evolution of the energy dissipation, such a large difference between the local data and the average value will bring inadequate results in the near wall region and in the inner pipe region. For this reason, it seems inconsistent to apply the actual 1D formulation of the constitutive models for bubble interaction mechanisms to 3D CFD calculations.

10.1 Constitutive Models

Jo and Revankar [Jo and Revankar 2011a] investigated several bubble breakup and coalescence models to develop bubble interaction terms for polydispersed flow calculations in packed bed reactors. A packed bed reactor among other forms could be a vessel that is filled with a packing material with the typical purpose to improve contact between two phases in a chemical or similar process. Jo and Revankar found out that no one of the investigated models has been found as really appropriate for their particular configuration and they proposed possible modification for packed bed reactors. The unmodified model that delivered the best predictions for both coalescence and breakup predominant flows has been shown to be a combination of the Martinez Bazán [Martinez Bazan 1998] for breakup and Chester [Chesters 1991] model for coalescence.

The expressions presented by Martinez Bazán and Chesters have been derived mechanistically, have a local formulation and the presence of empirical parameters is strongly reduced to make them as independent as possible from the geometry and flow conditions. They can be used to resolve locally the breakup and coalescence rate respectively.

10.1.1 Bubble Breakup

Martinez Bazán [Martinez Bazan 1998] proposed a model based only on kinematic ideas with a limited influence from empirical parameters [Lasheras et al. 2002]. The model has been developed based on observations of breakup of air bubbles immersed in highly turbulent water flow.

This model has been explained in detail in section 6.1.6. Its main premise is that “for a particle to break, its surface has to be deformed and the deformation energy must be provided by the turbulent stresses produced by the surrounding fluid” [Martinez Bazan

1998]. It means also that no bubble breakup frequency model is needed if this approach is considered.

The coefficients calculated by Martinez Bazán need to be changed to match the different turbulence intensity and conditions of the PUMA experiment (upward turbulent bubbly flow in pipes with velocity below 5 m/s and bubble sizes below 10 mm). In Figure 57 the turbulent and surface tension stresses are plotted for the present case and for that of Martinez Bazán. Given a surface tension equal to $\sigma = 0.072 \text{ N/m}^{-1}$ (characteristic at room temperature and atmospheric pressure), and a turbulent energy dissipation $\varepsilon = 2 \text{ m}^2/\text{s}^3$ (much lower than the values encountered by Martinez Bazán in his experiment and more similar to those in case of upward vertical turbulent bubbly flow) the results for the breakup coefficient K_b in (Eq.156) would be one order of magnitude bigger than in the case of Martinez Bazan and its value would be around 3. Jo and Revankar defined K_b to be equal to the diameter in millimeters for which the turbulent stresses are equal to the surface tension stresses [Jo and Revankar 2011b].

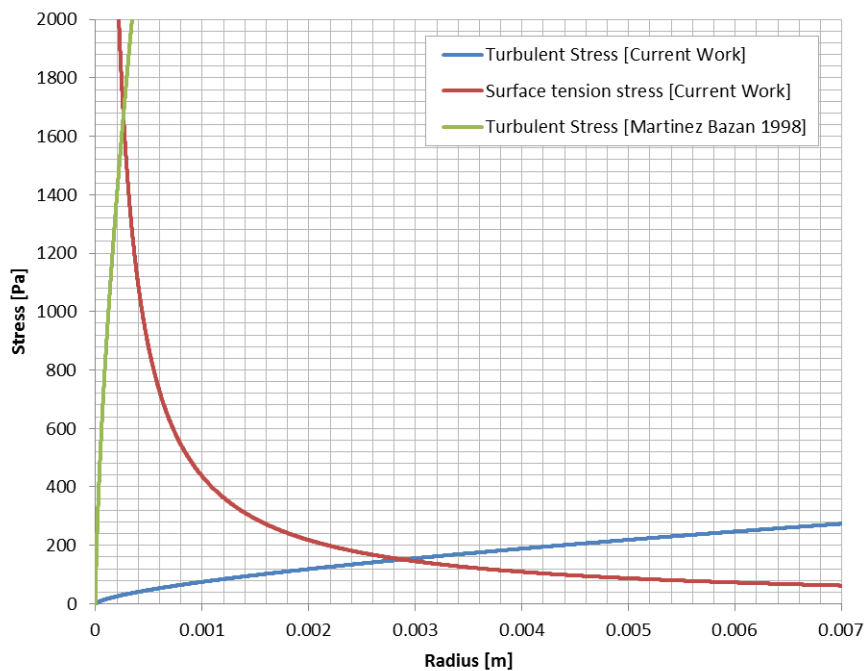


Figure 57: Plot of turbulent and surface tension stresses

The value of the coefficient β in (Eq.156) is, for turbulent flows in pipes, around 9.45 as already discussed in section 3.8.

10.1.1.1 Interfacial Area Change Rate Due to Bubble Breakup

The interfacial area change rate due to breakup Φ_B is equal to the bubble number change rate multiplied by a factor that takes into account the definition of the bubble number density n as a function of the interfacial are density a_i and the volume fraction α , and of the bubble shape factor ψ [Hibiki and Ishii 2006]. If the bubble is considered spherical, that is $\psi = 1/36\pi$, the modification factor, as already seen in (Eq.114), is:

$$f_{IATE} = \frac{1}{3\psi} \left(\frac{\alpha}{a_i} \right)^2 = 12\pi \left(\frac{\alpha}{a_i} \right)^2. \quad (\text{Eq.228})$$

Based on the mechanistic considerations expressed in the previous paragraph, it is possible to use the Martinez Bazán bubble breakup frequency formula to express the interfacial area change rate due to particles breakup as follows:

$$\Phi_B = f_{IATE} f_b n = \frac{1}{3\psi} \left(\frac{\alpha}{a_i} \right)^2 \left(K_b \frac{\sqrt{\beta(\varepsilon D)^{2/3} - 12 \frac{\sigma}{\rho D^2}}}{D} \right) \left(\frac{6\alpha}{\pi D^3} \right), \quad (\text{Eq.229})$$

with f_{IATE} , K_b and β a function of the bubble distortion and the turbulence field conditions, which need to be simulated as discussed in section 10.1.1.

10.1.2 Bubble Coalescence

The coalescence model proposed by Chesters is restricted to flow-driven collisions [Chesters 1991]. In its work, Chesters, is more concentrated on the processes of collision and coalescence rather than on available correlations to describe these phenomena. The result is the setup of a mechanistic and geometry independent set of expressions describing the coalescence probability and particle collision (frequency and duration).

In his review, Chesters divided the models following the scheme of the sub processes of interest to reach coalescence. Namely: collision, film drainage and rupture. The first is of interest for the definition of an expression for the collision **frequency**, while the second and the third are relevant for the definition of the coalescence **efficiency**.

10.1.2.1 Collision Frequency

Kuboi et al. [Kuboi et al. 1972b] derived an expression for collision and coalescence of dispersed drops in turbulent flows. They based their formulation on experimental observations of collision and coalescence of drops in random turbulent motion [Kuboi et al. 1972a]. Under several assumptions such the independent movement of the

particles, a uniform drop diameter and that the number of particles per unit volume is constant and they are not densely packed, they developed an expression for the collision frequency **per unit volume**.

Based on the assumptions above and from considerations derived from gas kinetic theory, Kuboi et al. [Kuboi et al. 1972b] wrote:

$$\hat{f}_c = \frac{\sqrt{2}}{2} \pi D^2 n^2 \bar{u} , \quad (\text{Eq.230})$$

where the reductive coefficient in front of the cross sectional collision area has been introduced to take into consideration the fact that in reality the bubbles are not spherical. No further information is given about the actual value chosen by the authors. Interesting is the choice of the reductive coefficient around 0.7 adopted for the case of drops in liquids where no significant distortion takes place (see Figure 16). \bar{u} is the characteristic collision velocity.

The turbulence velocity component of particles is not a uniform but a random quantity whose three-dimensional distribution function can be expressed by a Maxwell distribution as [Kuboi et al. 1972a]:

$$P(u) = 4\pi \left(\frac{3}{2\pi\bar{u}^2} \right)^{3/2} u^2 \exp\left(-\frac{3u^2}{2\bar{u}^2} \right) \quad (\text{Eq.231})$$

where, similarly to (Eq.26) the difference of fluctuation velocities at two neighboring points in the fluid can be calculated as

$$\overline{u^2} \approx 2(\varepsilon D)^{2/3} . \quad (\text{Eq.232})$$

The characteristic collision velocity in (Eq.230) can then be calculated as follows

$$\bar{u} = \int_0^\infty u P(u) du = \dots = \sqrt{\frac{8\pi}{3}} \sqrt{\overline{u^2}} . \quad (\text{Eq.233})$$

Considering equation (Eq.233), Kuboi et al. [Kuboi et al. 1972b] rewrote equation (Eq.230) as

$$\hat{f}_c = \frac{\sqrt{2}}{2} D^2 n^2 \frac{4}{\sqrt{3\pi}} (\varepsilon D)^{1/3} . \quad (\text{Eq.234})$$

This is the general equation for collision frequency **per unit volume** of drops or particles in turbulent flow under the hypothesis of local isotropy and random motion.

Finally, for **one bubble** the average bubble collision frequency can be written as:

$$f_c = K_c D^2 n C_c (\varepsilon D)^{1/3} , \quad (\text{Eq.235})$$

where K_c and C_c are coefficient to take into account the cross-sectional collision area and the difference of fluctuation velocities at two neighboring points in the flow. Their values will be determined later.

Furthermore, the expression of the bubble collision frequency should contain a term γ to take into account the excluded volume. The excluded volume of a particle is the volume that is inaccessible to other particles in the system as a result of the presence of the first one. The maximum volume that the particles can occupy is set by the maximum dense packing limit α_{max} . The expression for γ following Wang et al. [Wang et al. 2005a] is

$$\gamma = \frac{\alpha_{max}}{\alpha_{max} - \alpha} \quad (\text{Eq.236})$$

The value of α_{max} is given by the physical dense packing limit of spheres of equal diameter. In case of cubic or hexagonal close packing with several layer stacking sequences in which each sphere is surrounded by 12 other spheres, its value is around 0.74. It is the highest density amongst all possible lattice packings [Gauss 1876].

The trend of the coefficient γ with $\alpha_{max} = 0.74$ as a function of the volume fraction is shown in Figure 58.

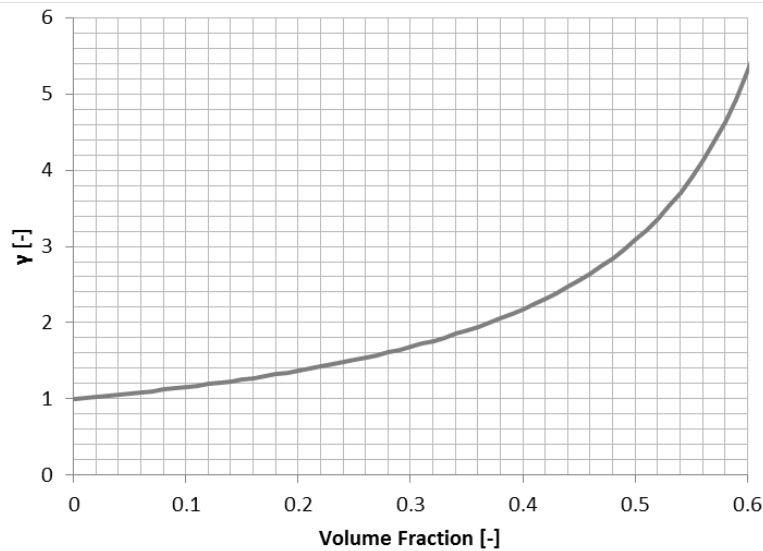


Figure 58: Trend of the coefficient γ with $\alpha_{max} = 0.74$ as a function of the volume fraction

A second modification factor Π for f_c takes into account the fact that collisions do not occur when the mean distance between particles is larger than the eddy size. This is due to the fact that the range of the relative motion for collisions between the

neighboring bubbles is limited by an eddy size comparable to the bubble size [Wu et al. 1998].

Following Wang et al. [Wang et al. 2005a] the general expression for Π is

$$\Pi = \exp\left(-\left(\frac{h}{l_{bt12}}\right)^6\right), \quad (\text{Eq.237})$$

where l_{bt} is the mean turbulent path length of a bubble of size d that is of the same order of magnitude of the bubble diameter D .

Considering two approaching bubbles having the same diameter

$$l_{bt12} \approx (l_{bt1}^2 + l_{bt2}^2)^{1/2} = \sqrt{2}D, \quad (\text{Eq.238})$$

h is the mean distance between bubbles that can be calculated by means of geometric considerations as expressed by Wu et al. [Wu et al. 1998] as

$$h \approx \frac{D}{\alpha^{1/3}} \left(1 - \left(\frac{\alpha}{\alpha_{max}}\right)^{1/3}\right). \quad (\text{Eq.239})$$

Substituting (Eq.238) and (Eq.239) in (Eq.237) leads to

$$\Pi \approx \exp\left(-\left(\frac{\frac{D}{\alpha^{1/3}} \left(1 - \left(\frac{\alpha}{\alpha_{max}}\right)^{1/3}\right)}{\sqrt{2}D}\right)^6\right). \quad (\text{Eq.240})$$

The trend of the coefficient Π with $\alpha_{max} = 0.74$ and $D = 3 \text{ mm}$ as a function of the volume fraction is shown in Figure 59.

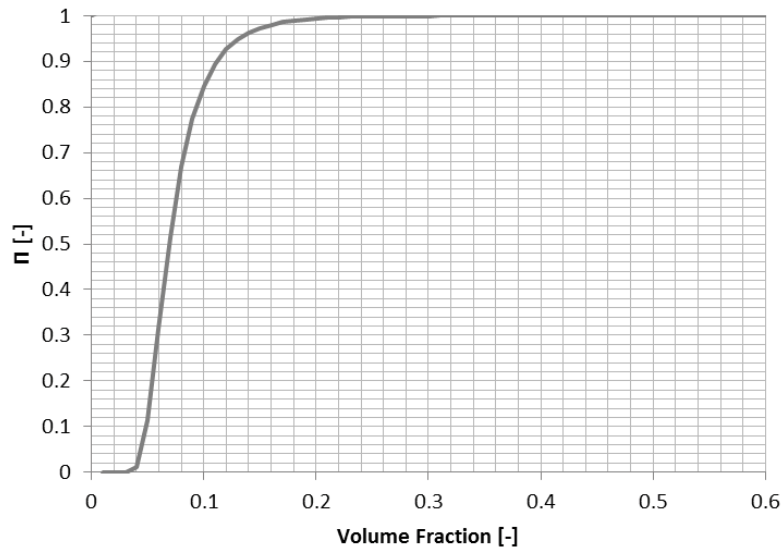


Figure 59: Trend of the coefficient Π as a function of the volume fraction

Finally, the modified average bubble collision frequency is

$$\begin{aligned}
f_c &= K_c D^2 n C_c (\varepsilon D)^{1/3} \gamma \Pi \\
&= K_c D^2 n C_c (\varepsilon D)^{1/3} \frac{\alpha_{max}}{\alpha_{max} - \alpha} \exp \left(- \left(\frac{\frac{D}{\alpha^{1/3}} \left(1 - \left(\frac{\alpha}{\alpha_{max}} \right)^{1/3} \right)}{\sqrt{2} D} \right)^6 \right). \quad (\text{Eq.241})
\end{aligned}$$

K_c is the coalescence coefficient that is defined to account for the uncertainties introduced in the previous equations while determining the cross sectional collision area and the turbulence related quantities. C_c is a constant of order unity.

10.1.2.2 Collision Efficiency

For a reliable estimation of the probability of coalescence during collision of particles it is necessary to provide a formulation depending only on the given local flow conditions.

Chesters presented a formulation based on the consideration that coalescence (film rupture) will occur if the interaction time t_i exceeds the drainage time t_c , that is the time required for drainage up to the thickness h_c .

$$\eta_c = \exp \left(- \frac{t_c}{t_i} \right). \quad (\text{Eq.242})$$

The formulation tends to zero for large values of the ratio t_c/t_i and to 1 for small ones.

Bubbles in turbulent flows are in general much larger than the scale of the Kolmogorov eddy size and the corresponding values of the bubble Reynolds number are consequently high. Under these conditions and the fact that the shear stress exerted by the gas phase is negligible, Chesters and Hoffman [Chesters and Hoffman 1982] applied the drainage model based on full interfacial mobility and inertial control (instead of viscous) in order to determine an expression for the **drainage time**:

$$t_c \cong 0.5 \frac{\rho_l V R^2}{\sigma}, \quad (\text{Eq.243})$$

where V is the relative velocity of centers of colliding particles.

During collisions, particles move towards each other driven by the flow, rotate around each other and then, if coalescence has not occurred, separate again. During this phase, in absence of viscous dissipation, the kinetic energy is converted into surface energy during the film formation [Chesters 1991] and if coalescence does not occur is reconverted as the particle bounces away. Chesters and Hoffman express the **interaction time** from the onset of surface flattening up to the point at which the particle motion is arrested, as

$$t_i \cong \left[\left(\frac{4\rho_g}{3\rho_l} + 1 \right) \frac{\rho_l R^3}{2\sigma} \right]^{1/2}. \quad (\text{Eq.244})$$

Chesters [Chesters 1991] reports that in case of turbulence induced coalescence, if the bubbles are smaller than the size of the energy-containing eddies, the relative velocity of centers of colliding particles may be supposed to be calculated with

$$V \propto (\varepsilon D)^{1/3}. \quad (\text{Eq.245})$$

In this case (Eq.242), approximating for air-water mixtures the term into round bracket in (Eq.244) to 1, becomes:

$$\eta_c = \exp \left[-C_c \left(\frac{We}{2} \right)^{1/2} \right], \quad (\text{Eq.246})$$

where, again, C_c is a constant of order unity which includes the ratio of fluctuating to continuous phase velocity that has to be defined in order to be able to calculate the relative velocity of centers of colliding particles consistently with (Eq.235). The Weber number is expressed as:

$$We = \frac{\rho_l D (\varepsilon D)^{2/3}}{2\sigma}. \quad (\text{Eq.247})$$

10.1.2.3 Interfacial Area Change Rate Due to Bubble Coalescence

The interfacial area change rate due to coalescence Φ_c is equal to the bubble number change rate due to coalescence multiplied by a factor that takes into account the definition of the bubble number density n (as a function of the interfacial are density a_i and the volume fraction α) and the bubble shape factor [Ishii and Hibiki 2006]. The modification factor is:

$$f_{IATE} = \frac{1}{3\psi} \left(\frac{\alpha}{a_i} \right)^2. \quad (\text{Eq.248})$$

If the bubble is considered spherical $\psi = 1/36\pi$.

Based on the mechanistic considerations expressed in the previous paragraph it is possible to express the interfacial area change rate due to particle coalescence as follows:

$$\Phi_C = -\frac{1}{2} f_{IATE} f_c n \eta_c = -\frac{1}{3\psi} \left(\frac{\alpha}{a_i}\right)^2 \left(\frac{1}{2}\right) K_c D^2 C_c (\varepsilon D)^{1/3} \frac{\alpha_{max}}{\alpha_{max} - \alpha} \exp\left(-\left(\frac{\frac{D}{\alpha^{1/3}} \left(1 - \left(\frac{\alpha}{\alpha_{max}}\right)^{1/3}\right)}{\sqrt{2}D}\right)^6\right) \left(\frac{6\alpha}{\pi D^3}\right)^2 \exp\left[-C_c \left(\frac{We}{2}\right)^{1/2}\right], \quad (\text{Eq.249})$$

with f_{IATE} , K_c and C_c to be determined as a function of the bubble distortion, the turbulence field conditions and the bubbles approaching angle, whose randomness is taken into account by means the Maxwell distribution introduced in equation (Eq.231). The factor 1/2 has been introduced to avoid counting the coalescence events between the same bubble pair twice.

Calculating the bubble relative velocity based on (Eq.26), and applying the Maxwell distribution function as expressed in (Eq.231), to consider the randomness of collisions, the value of the constant C_c becomes

$$C_c = 2.093 \quad (\text{Eq.250})$$

In reality, the minimum value of the constant C_c is 0 which is when the bubble approaching angle is equal to zero. It means when the two bubbles are travelling in the same direction with the same characteristic velocity and no collision occurs.

As already introduced before the coefficient K_c is used to correct the uncertainties introduced when determining the cross sectional collision area and the turbulence related quantities.

The cross section area, for instance, is based on that the “collision tube” model derived from the ideal gases kinetic theory is valid for rigid spherical particles. This model should not be applied directly to non-spherical bubbles with a moving interface and highly variable form.

Other authors like Prince and Blanch [Prince and Blanch 1990] and Yao and Morel [Yao and Morel 2004] take K_c equal to 0.25 given their definition (no further explained) of the collision cross section. Furthermore, the value of this coefficient should not be a constant valid for all flow conditions. As already mentioned for the lift force coefficient in section 4.3.2.2, it is dependent on the bubble form and distortion which is itself dependent on a number of additional flow conditions.

At this moment aspects regarding this argument are still a matter of investigation and are not fully understood.

10.2 Main Conclusions of this Chapter

In chapter 9, the five state-of-the-art constitutive models for the simulation of the bubble interaction mechanisms suitable for the one-group interfacial area transport equation have been demonstrated not to deliver a good prediction of the interfacial area concentration radial profile. The best results in agreement with the experimental data have been obtained with the Yao and Morel's model [Yao and Morel 2004]

In this chapter the inconsistencies in the use of the 1D definition of the bubble interaction terms for 3D simulations have been explained. In 1D calculation, the fluid dependent parameters needed for the evaluation are intended as averaged values along the radial direction. The distortion caused by this assumption has been adjusted by means of "*tuning*" parameters in the final expressions of the terms [Hibiki and Ishii 2000a]. This modeling strategy yields the best agreement with the axial evolution of the flow parameters. The axial profile variation of the turbulence eddy dissipation is much less pronounced than the radial one (see Figure 56). If the radial profiles are considered and the Yao and Morel's BIT model is used, the values in the near wall region reach valued 10 to 40 times the average.

Based on the conclusion of chapter 9, in order to overcome the limits of the current formulation, we have performed several analytical studies that have provided us with the insights regarding the modeling of bubble breakup and coalescence and new local mechanistic formulations have been developed and presented in this chapter.

In chapter 11 these models have been tested and the effect on the simulation results of various model parameters and coefficient is shown in detail. Furthermore, radial profiles of the main variables are presented in order to explain the behavior of the newly developed models. Several set of experimental data have been simulated in order to test the model for a wider range of conditions.

10.2.1 Bubble Breakup

Martinez Bazán [Martinez Bazan 1998] argued that most of the models for bubble break-up in the literature are based on a theory essentially similar to the kinetic theory of gases. Furthermore, the models assume that turbulence is manifested as an array of eddies with well-defined sizes and densities. In order to obtain values from these models a collision cross section has to be defined and, from this, an eddy frequency determined. Furthermore, closure parameters that can alter significantly the model behavior, such as integration limits, have to be set (e.g. see sections 6.1.3 and 6.1.5).

By using the Martinez Bazán 1998 model for the definition of the bubble breakup frequency it is possible to overcome such problems, since no bubble eddy collision is considered and no bubble breakup efficiency has to be defined. These two aspects linked together lead to a great simplification of the breakup problem. The current Thesis represents the first attempt to model bubble breakup for the interfacial area transport equation by using the approach proposed in 1998 by Martinez Bazán.

Recently, Liao et al. [Liao et al. 2011] tried to apply the Martinez Bazán's model to the development of a general model for bubble breakup for the MUSIG approach. However, the authors didn't understand completely the ideas behind the bubble frequency model proposed in 1998 by Martinez Bazán. In fact, previously Liao and Lucas [Liao and Lucas 2010] in their review of breakup models classified erroneously this model in the category of "Turbulent kinetic energy of the hitting eddy E_e greater than a critical value E_{cr} ". Martinez Bazán in his work is never doing reference to eddies bombarding the bubble causing breakup and is also never considering a bubble-eddies relative approaching velocity. On the contrary, in his doctoral thesis Martinez Bazán is clearly speaking about a surface deformation energy that must be provided by the turbulent stresses produced by the surrounding fluid [Martinez Bazan 1998]. Of course, this concept is related to the energy applied by the turbulent surrounding fluid on the bubble surface considering its global effect. The concept of the bombarding eddies is doing reference only to a component of the turbulent stresses: the one applied normal to the bubble surface. To better understand the difference of these two approaches, in section 3.8, the difference of fluctuation velocities at two neighboring points under isotropic and homogeneous turbulent conditions had been introduced. In that section two different cases were considered. The first, it is used for the determination of the **longitudinal fluctuation velocity difference** [Rotta 1972] between two points in the fluid and it is valid for the determination of the **relative bubble approaching velocity** in case of bubbles collision. The second case, it is useful for the determination of the **absolute value of the fluctuation velocity difference** [Batchelor 1956] between two points in the fluid and it is used for the determination of the **turbulent stresses applied on the bubbles by the surrounding fluid**.

In this Thesis, the longitudinal fluctuation velocity difference [Rotta 1972] has been used, in case of coalescence modeling, for the determination of the coefficient C_c needed for the calculation of relative bubble approaching velocity. The absolute value

of the fluctuation velocity difference [Batchelor 1956], has been used, in case of break-up modeling, for the determination of the coefficient β needed for the calculation of the turbulent stresses applied on the bubbles by the surrounding fluid. Finally It is important to notice that the coefficients C_c and β are correlated and universal for a given flow condition. It means it is not possible to modify the value of one of them without consequently adjusting the value of the other.

Liao et al. [Liao et al. 2011] did not take into account the small but determinant difference in the theoretical derivation of the fluctuation velocity difference indicated by Rotta and Batchelor in their respective works. Then, they used a modified version of the bubble breakup frequency proposed by Martinez Bazán completely neglecting the important coefficient β in the formula of the bubble breakup frequency; this yields to an erroneous calculation of the turbulent stresses applied on the bubble by the surrounding liquid. In fact, the difference of fluctuation velocities at two neighboring points under isotropic and homogeneous turbulent conditions calculated taking into account the **absolute** value of the fluctuation velocity difference delivers a result almost 3.7 times higher than considering the **longitudinal** fluctuation velocity difference only.

In this chapter, the coefficients β and K_b in the formula of the bubble breakup frequency have been defined and exhaustively explained. The coefficient β is linked with the dimensionless constant α , also called the Kolmogorov constant deduced experimentally and characteristic of the actual turbulence conditions. Values of the Kolmogorov constant are considered universal for each flow type. Then following, Jo and Revankar [Jo and Revankar 2011b], the coefficient K_b has been defined to be to be equal to the diameter in millimeters for which the turbulent stresses are equal to the surface tension stresses.

In chapter 11, the sensitivity of the results to the two parameters β and K_b is shown. The radial profiles of the main variables are presented in order to explain the behavior of the model. Several set of experimental data have been simulated in order to test the model for a wide range of conditions.

10.2.2 Bubble Coalescence

In order to define the bubble coalescence frequency, physical models for the bubble collision, liquid drainage and film rupture, for the collision efficiency, have been used.

The collision model, derived from the gas kinetic theory, is based on the widely used collision of spheres behaving as ideal particles (see section 6.2.1). Coefficients are applied to take into consideration that bubbles in reality do not interact like ideal particles (coefficient K_c), that the presence of the other bubbles influences their behavior (coefficient γ) and that the ratio mean distance between particles to their average relative turbulent path needs also to be taken into account to define the collision rate (coefficient Π).

This manner of defining the bubble collision frequency is not new and other authors previously derived a general expression similar to the one presented here. In the current work attention has been concentrated, however, on consistent sub-models based on geometric consideration only and neglecting, as much as possible, considerations based on the order of magnitude of the phenomena. The only consideration based on the order of magnitude used, largely accepted in the literature, is that the eddies interacting with the bubbles have a characteristic dimension of the same order of magnitude of the bubbles present in the system.

The definition of the coefficient K_c is not trivial as it is related to the modification of the cross sectional bubble collision areas due to the non-regular form of the bubbles. K_c is a reductive coefficient that should not be considered as a constant but a variable calculated depending on the actual flow conditions. If a significant bubble distortion is taking place, the bubble aspect ratio is much smaller than 1 and the coefficient K_c : (i.e. in case of bubble aspect ratio smaller than 0.5) should assume values smaller than 0.5. In case of less bubble distortion (i.e. case of liquid drops in liquid) the coefficient takes values around 0.7 [Kuboi et al. 1972b].

Another important variable, related to the turbulence conditions in the flow, to be defined in order to determine the collision frequency is the relative velocity of bubbles that take part in a collision event. In this Thesis the coefficient C_c needed for the calculation of relative bubble approaching velocity has been calculated, in correlation with β , by applying the following considerations:

- since the longitudinal component only need to be considered in order to determine the relative velocity of two bubbles, the approach of Rotta [Rotta 1972] has been used. The multiplication coefficient in the expression of the longitudinal fluctuation velocity difference (see section 3.8) has been defined, by means of the Kolmogorov constant deduced experimentally and characteristic of the actual turbulence conditions.

- based on the consideration of Kuboi et al. [Kuboi et al. 1972a] regarding the non-uniformity of the turbulence velocity component of particles, the bubble relative approaching velocity has been expressed by a Maxwell distribution to take into consideration the randomness of the bubble approaching phenomena (e.g. approaching angle etc.)

In order to calculate the collision efficiency, the widely used film drainage model (see section 6.2.2.3) has been used. The expressions used for the definition of the interaction and drainage time to calculate the coalescence efficiency are those proposed by Chesters and Hoffman in 1982. These models have not yet been used in the literature in the definition of constitutive terms for the interfacial area density transport equation. In the expression of the drainage time, the relative velocity of the centers of colliding particles has been defined consistently with the case of bubble collision explained above.

It is worth of notice that, both for the collision frequency and for the efficiency, Chesters 1991 did not define an equation to calculate the bubble relative approaching velocity and only furnished proportionality.

In Chapter 11, the sensitivity of the results to the parameters K_c is presented. The radial profiles of the main variables are presented in order to explain the behavior of the model. Several set of experimental data have been simulated in order to test the model for a wide range of conditions.

Chapter 11

Simulation of Upward Adiabatic Bubbly Flow Using the Newly Implemented One-Group Interfacial Area Constitutive Models in ANSYS CFX 12.1

In chapter 10 a new model for the one-group interfacial area constitutive models has been developed. Then, the bubble interaction mechanisms expressions have been implemented in ANSYS CFX 12.1. In this chapter, the effect on the simulation results of the various model parameters and coefficient is shown in detail. Radial profiles of the main variables are shown in order to explain the behavior of the newly developed models. Several set of experimental data have been simulated in order to test the model for a wide range of conditions.

11.1 Analysis of the Effects of Several Parameters on the Results

The models presented in chapter 10 have been implemented in Ansys CFX and the results of simulations are shown in the next sections. A new local mechanistic formulation of bubble interaction models for coalescence and breakup has been developed. The coefficients of the formulation have been exhaustively explained in the previous chapter and their influence on the results will be studied in the next sections.

A sensitivity analysis of the influence on the results for several parameters has been performed and the results are shown for the case F03G02. In this case the level of the turbulence eddy dissipation is higher than for the other cases with lower liquid superficial velocity and the differences between the results of the simulations can be

better appreciated in the diagrams presented. On a smaller scale, the same trends have been observed for the other experimental conditions.

The relevant parameters taken into consideration to perform for the analysis are those already considered in the analysis in section 9.7. Furthermore the influence of the breakup and coalescence coefficients has been investigated.

Finally, the list of the parameters or models under study is:

- Lift force coefficient C_L (Figure 60)
- Wall lubrication force coefficient C_{WL} (Figure 61)
- Turbulent dispersion force (Figure 62)
- BIT (Figure 63)
- Intensity of the turbulence eddy dissipation (Figure 64)
- Breakup coefficient K_B (Figure 65)
- Coalescence coefficient K_C (Figure 66)
- Interfacial area factor f_{IATE} (Figure 67)

For each of the above mentioned parameters, diagrams showing the radial profiles of several variables are presented.

The set of models that have been selected as basis to perform the analysis, based on our previous experience, are:

- Drag force: Grace
- Lift force: 0.1
- Wall lubrication force: Antal with coefficients -0.0064, 0.016
- Turbulent dispersion force: FAD
- Turbulence model: SST
- Bubble induced turbulent model: Morel

The analysis will then proceed by systematically changing the force models with those we want to evaluate.

The nearly 2D computational mesh used is that introduced already in section 9.3.

In Figure 60, Figure 61 and Figure 62, the results for the sensitivity at the variation of the lift, wall lubrication and turbulent dispersion forces are shown. These three parameters have the greatest influence on the results.

The **lift force coefficient** influences the value of the void fraction in the near wall region. As it is reduced the void fraction becomes smaller and approaches the

experimental results. Also the value of the void fraction in the pipe central region is affected by the lift coefficient: the value of the void fraction in this region approaches the experimental data as the lift coefficient assumes smaller values. Also the Sauter mean diameter profile is influenced by the lift coefficient changes: the peak near the wall decreases as the lift coefficient decreases.

The **wall lubrication force** has its highest influence on the near wall region. Increasing the value of the coefficient has an effect similar to a reduction of the lift force. In fact, they are acting in opposite directions. At the wall, numerical oscillations showing the form of a chessboard pattern appear if a too high wall lubrication coefficient is used in combination of a low lift coefficient. This is the case of the Frank model (8,8,1.2) or the Antal model (-0.025,0.075) in combination with the lift coefficient equal to 0.1.

The **turbulent dispersion force** is the other parameter that has been shown to have an important effect on the results. In Figure 62, the effects of two different turbulence dispersion models have been compared with a simulation where it has not been taken into account. In this last case, an irregular form of the profiles is observed and there is not bubble redistribution operated by the force from regions of higher concentration and gradient to others. If the FAD model is compared with the Lopez de Bertodano model, the second one shows a much stronger dispersive effect. Its profiles are smoothed out and the gas volume fraction and the interfacial area density in the near wall region reach results with a much lower value.

This page has been intentionally left blank.

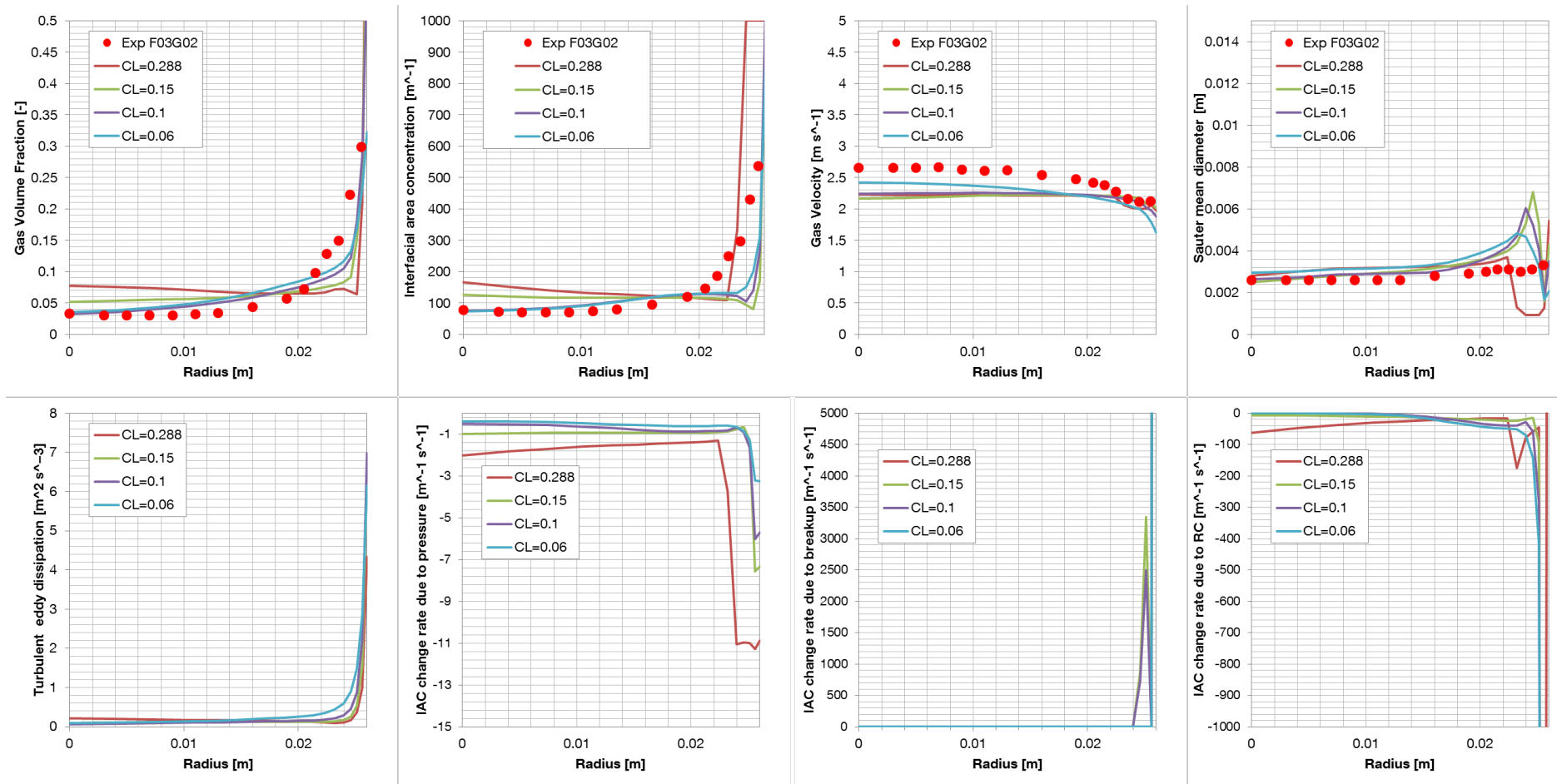


Figure 60: Effect of the lift force coefficient on the radial profiles of:
 (up from left to right) gas volume fraction, interfacial area density, gas velocity, Sauter mean diameter
 (down from left to right) turbulence eddy dissipation, IAC change rate due to pressure, due to breakup and due to coalescence.

This page has been intentionally left blank.

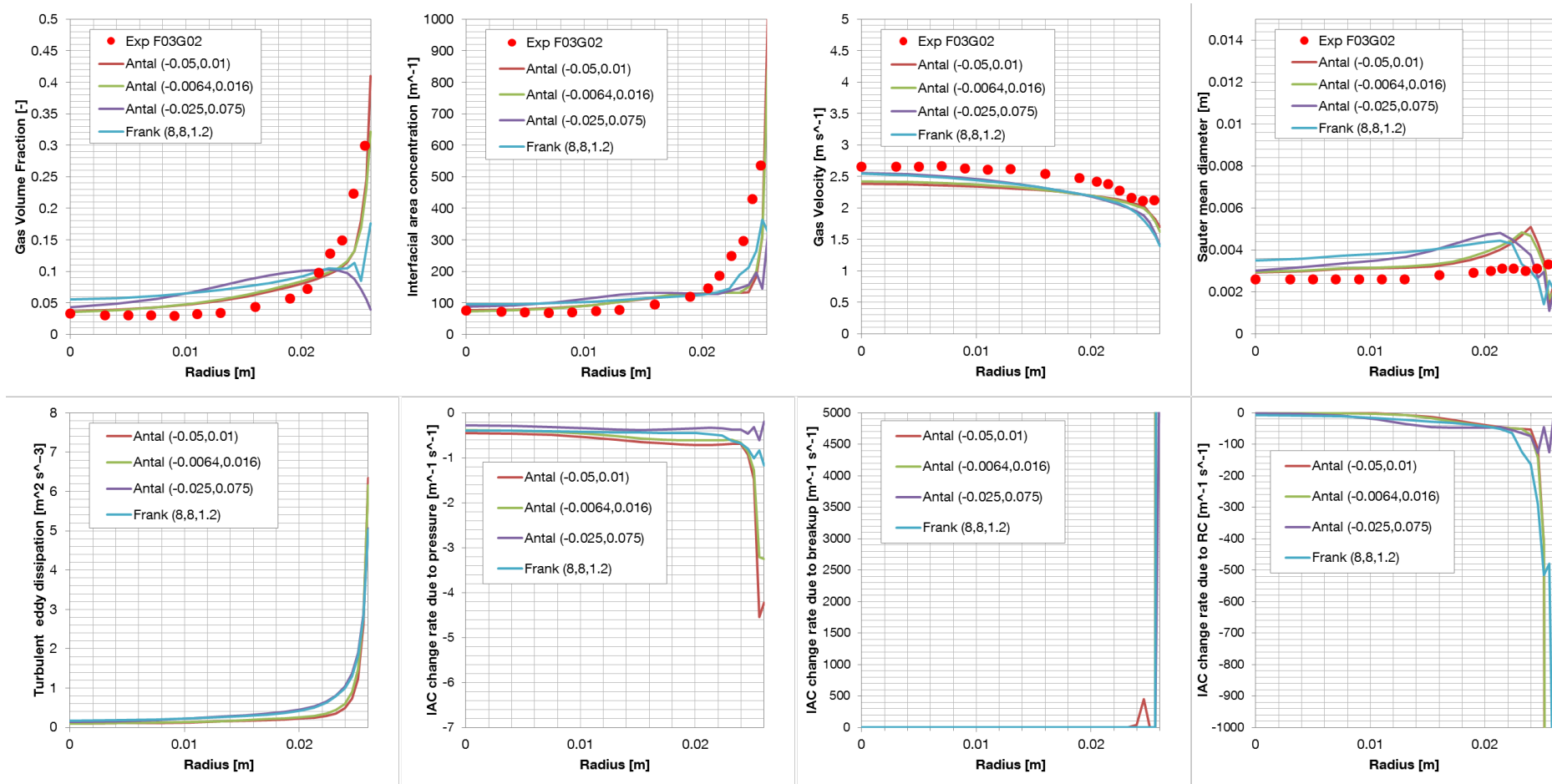


Figure 61: Effect of the wall lubrication force coefficient on the radial profiles of:
 (up from left to right) gas volume fraction, interfacial area density, gas velocity, Sauter mean diameter
 (down from left to right) turbulence eddy dissipation, IAC change rate due to pressure, due to breakup and due to coalescence.

This page has been intentionally left blank.

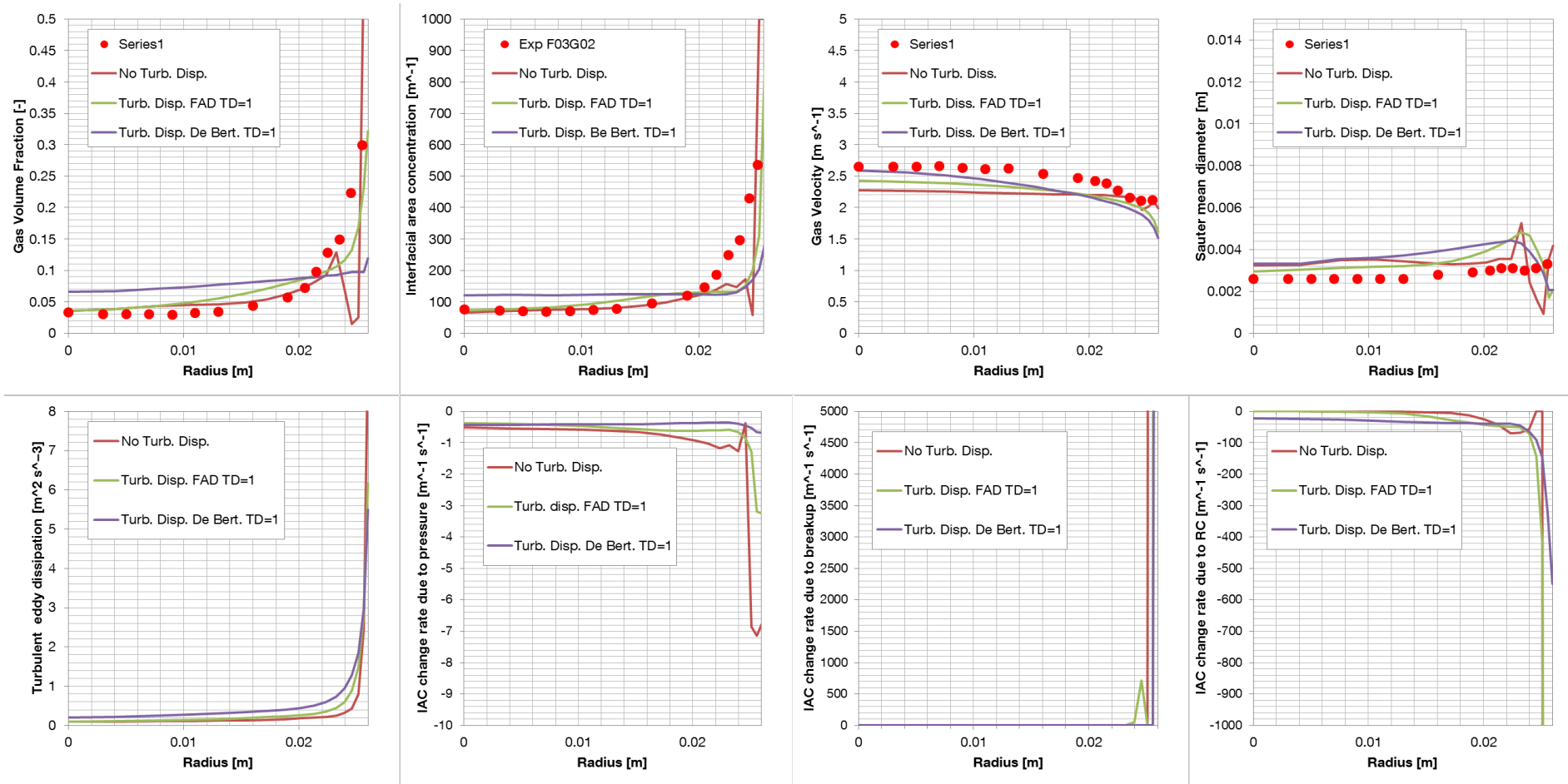


Figure 62: Effect of the turbulent dispersion force on the radial profiles of:
 (up from left to right) gas volume fraction, interfacial area density, gas velocity, Sauter mean diameter
 (down from left to right) turbulence eddy dissipation, IAC change rate due to pressure, due to breakup and due to coalescence.

This page has been intentionally left blank.

Figure 63 shows the effect of the **Bubble Induced Turbulence (BIT)** model on the simulation results. The Sato model is compared against the Morel model. In Sato's approach, the turbulence equations are not strongly coupled with the momentum and mass equations. The results are similar in the two cases but they show a more regular numerical behavior if the Morel model is used. Even if the turbulence eddy dissipation reaches higher values when Morel's model is used, it does not seem to have a major impact on the results. Overall, there is a better redistribution of the dispersed phase due to the effect of turbulence on the momentum equation. It is then possible to obtain a better agreement of the results of the gas velocity with the measured data.

The effect of the **level of the turbulence eddy dissipation** predicted by the Morel model has also been investigated (see Figure 64). A multiplying coefficient has been applied to the breakup and coalescence rate terms in the interfacial area transport equation. In this way, the influence of the turbulence prediction has been shown and seems to have a small influence on the results. More important than the absolute value of turbulence is the correct prediction of the shape turbulence eddy dissipation radial profile. In fact, by modifying the turbulence eddy dissipation radial profile different bubble coalescence and breakup rates will be calculated and the interfacial area density will be modified to better fit the experimental data.

The effects of the **breakup** (Figure 65) and **coalescence** (Figure 66) coefficients and of the **IAC factor** (Figure 67) have also been investigated.

While the breakup coefficient has shown no influence in case of steady state simulations, on the other side, the coalescence coefficient has a clear influence. It affects in a minor way the gas volume fraction and the interfacial area density profiles, but it has a much higher influence on the determination of the Sauter mean diameter. This parameter approaches the experimental data as the value of the coalescence coefficient decreases. The discrepancies could be explained by the fact that the cross collision sectional area determined thanks to the ideal gas kinetic theory **is not** suitable in case of deformed bubbles with a moving interface if a term considering bubble deformation is not taken into account.

A similar effect to that explained for the coalescence is observed if the IAC factor is taken into consideration. In general, also this coefficient has a minor influence on the results.

This page has been intentionally left blank.

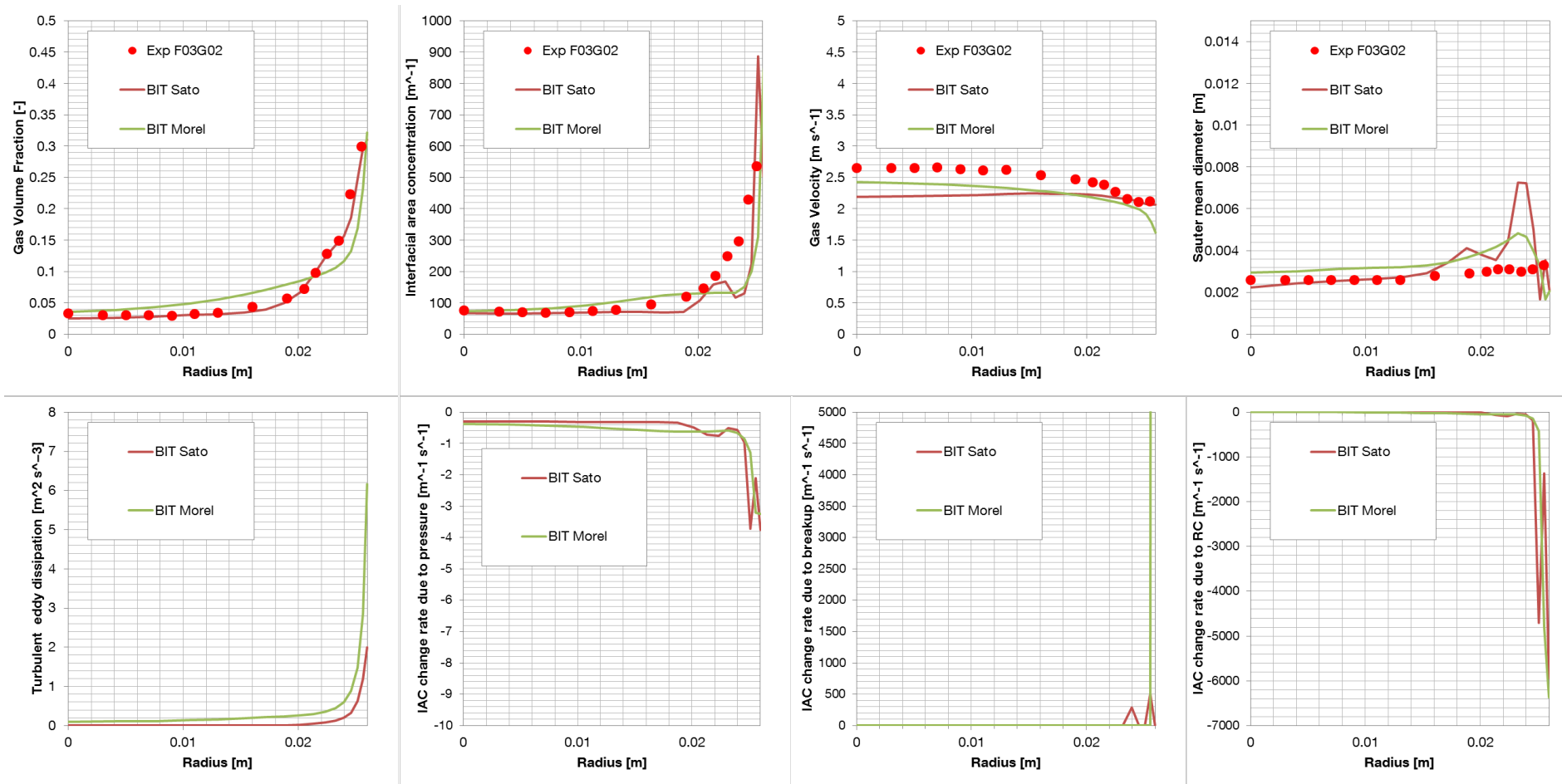


Figure 63: Effect of the BIT model on the radial profiles of:
 (up from left to right) gas volume fraction, interfacial area density, gas velocity, Sauter mean diameter
 (down from left to right) turbulence eddy dissipation, IAC change rate due to pressure, due to breakup and due to coalescence.

This page has been intentionally left blank.

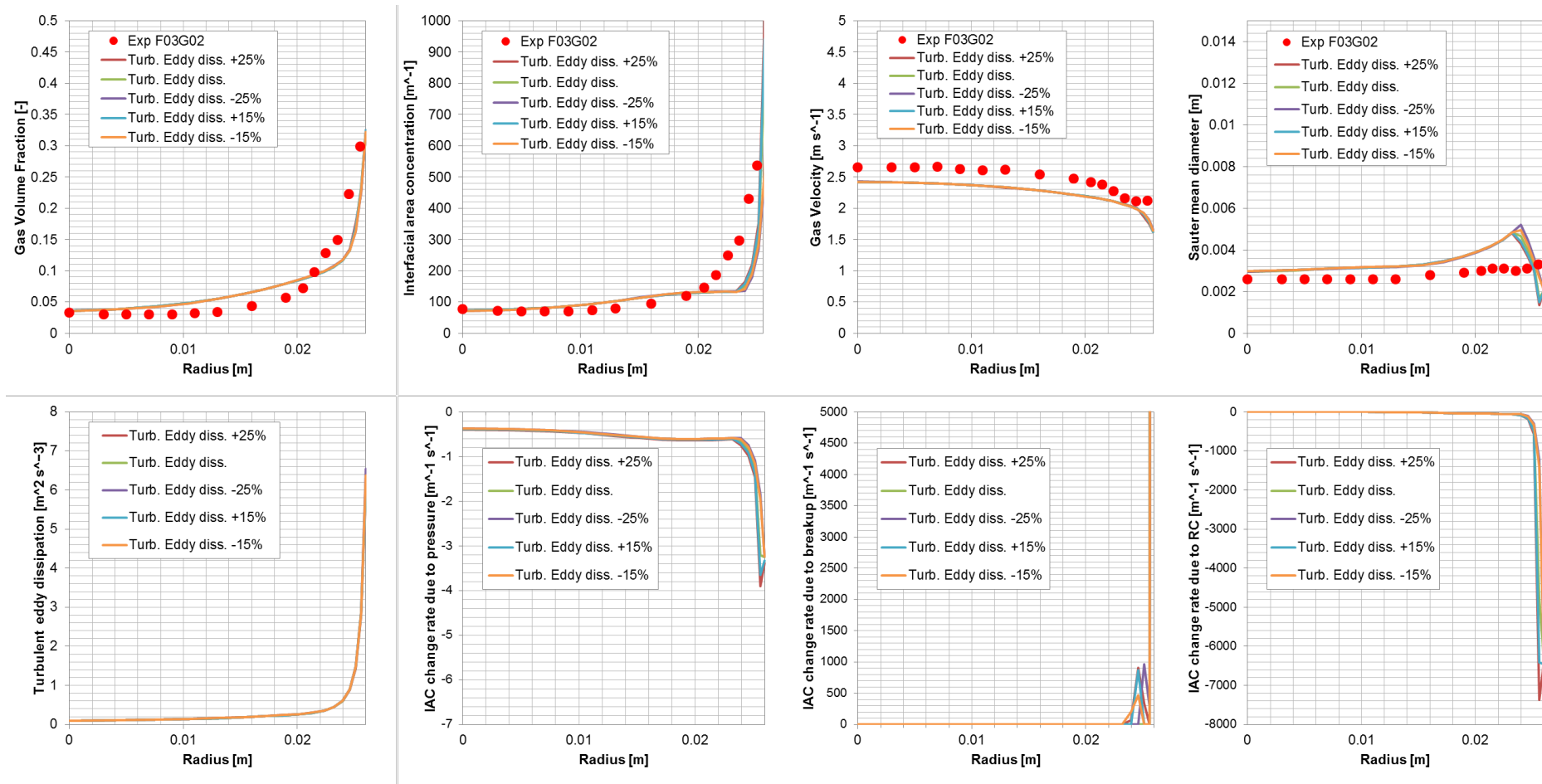


Figure 64: Effect of the turbulence eddy dissipation intensity on the radial profiles of:
 (up from left to right) gas volume fraction, interfacial area density, gas velocity, Sauter mean diameter
 (down from left to right) turbulence eddy dissipation, IAC change rate due to pressure, due to breakup and due to coalescence.

This page has been intentionally left blank.

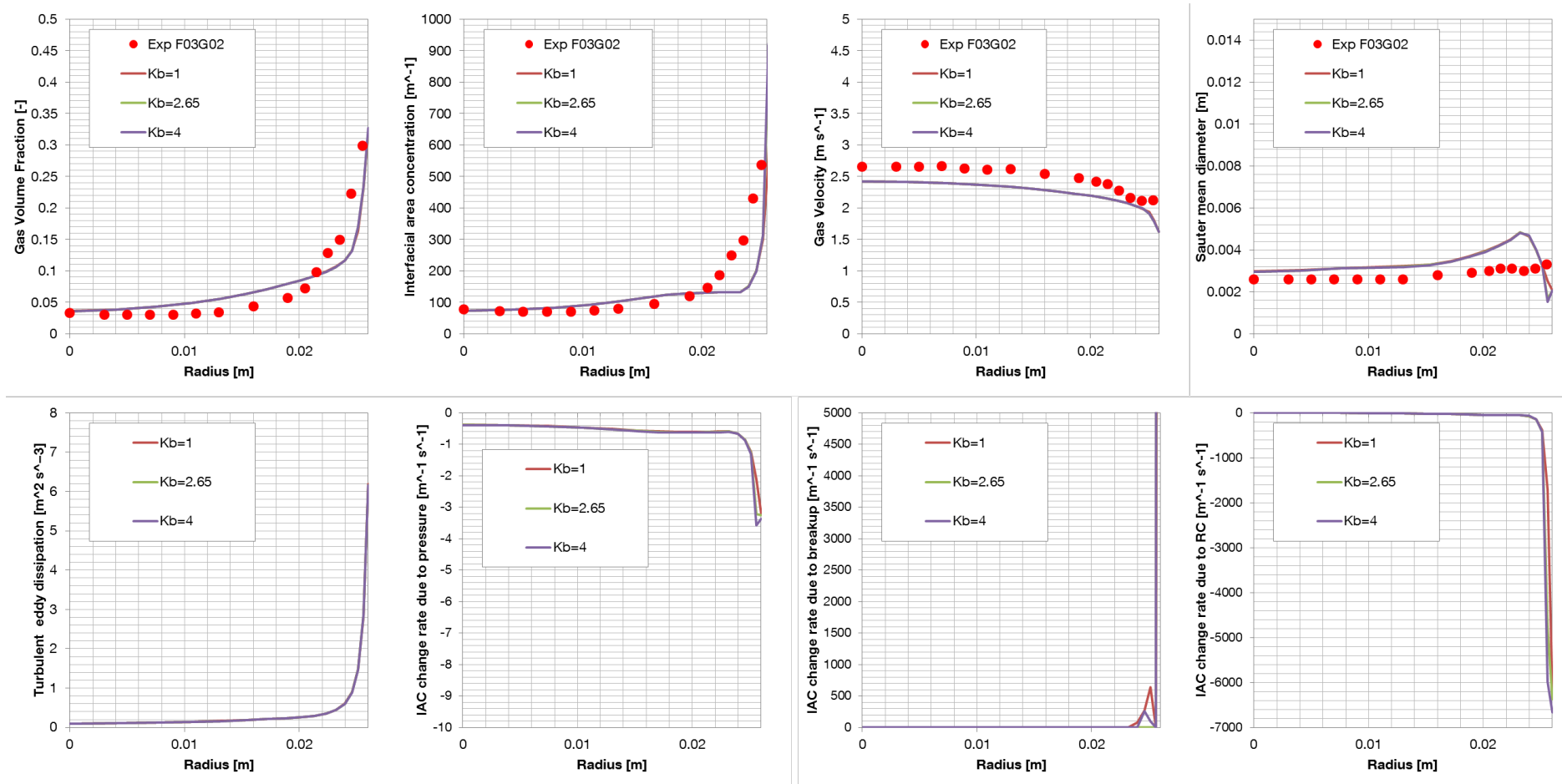


Figure 65: Effect of the breakup coefficient on the radial profiles of:
 (up from left to right) gas volume fraction, interfacial area density, gas velocity, Sauter mean diameter
 (down from left to right) turbulence eddy dissipation, IAC change rate due to pressure, due to breakup and due to coalescence.

This page has been intentionally left blank.

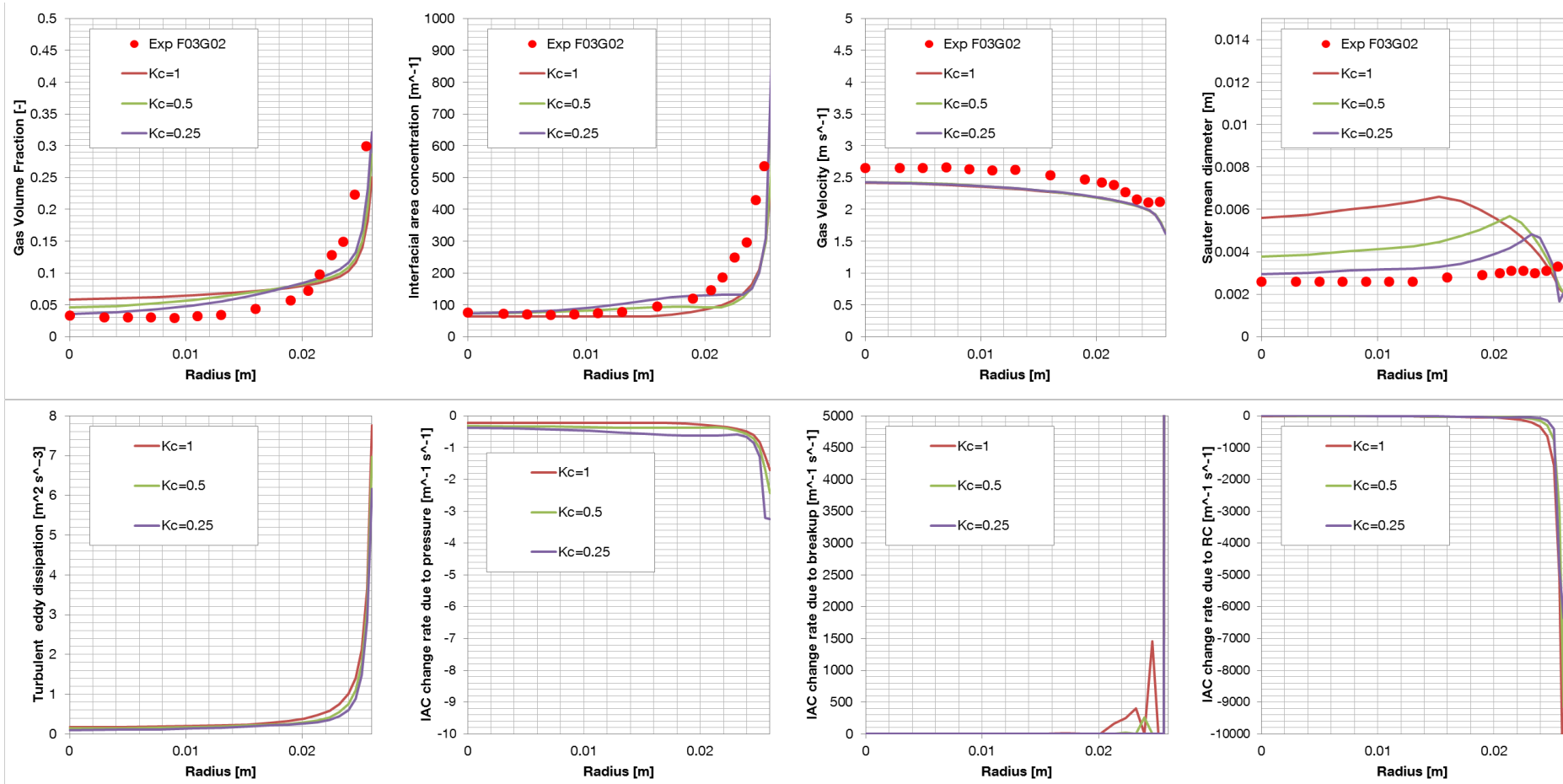


Figure 66: Effect of the coalescence coefficient on the radial profiles of:
 (up from left to right) gas volume fraction, interfacial area density, gas velocity, Sauter mean diameter
 (down from left to right) turbulence eddy dissipation, IAC change rate due to pressure, due to breakup and due to coalescence.

This page has been intentionally left blank.

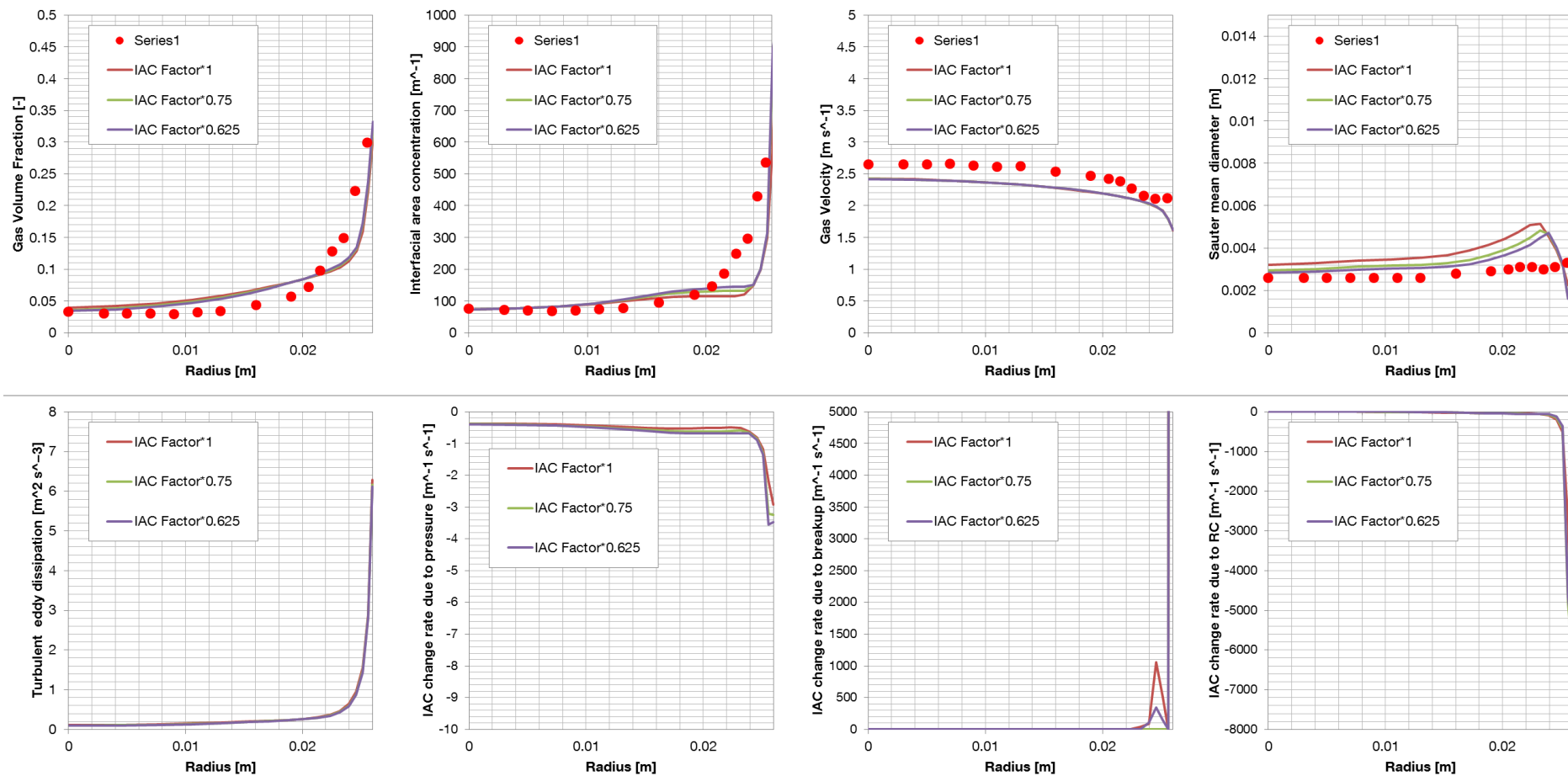


Figure 67: Effect of the IAC factor coefficient on the radial profiles of:
 (up from left to right) gas volume fraction, interfacial area density, gas velocity, Sauter mean diameter
 (down from left to right) turbulence eddy dissipation, IAC change rate due to pressure, due to breakup and due to coalescence.

This page has been intentionally left blank.

11.2 Results of the Simulations for Several Experimental Conditions

In this section results of several cases obtained using the newly implemented IATE constitutive models for bubble breakup and coalescence are shown. The cases under study are F02G02, F03G01, F03G02 and F03G03. They have been selected in order to give an overview of the effect of the modifications of the liquid superficial velocity (F02G02 to F03G02) and of the gas superficial velocity (F03G01 to F03G02 to F03G03) on the results.

Given the analysis of section 11.1, the coefficients summarized in Table 3 have been used for simulations.

Table 3: List of non-drag forces models and coefficients used for the simulations

Case	Wall lubrication coefficient	Lift coefficient	Turbulent dispersion
A	Antal (-0.0064, 0.016)	0.1	FAD 1
B	Antal (-0.0064, 0.016)	0.05	FAD 1
C	Antal (-0.01, 0.05)	0.25	Loped de Bert. 1
D	Antal (-0.01, 0.05)	0.288	Loped de Bert. 0.75

The set of models that have been selected based on our previous experience as basis to perform the simulations are:

- Drag force: Grace
- Turbulence model: SST
- Bubble induced turbulent model: Morel
- IATE breakup and coalescence models: present work (see chapter 0)

The ultimate goal for the choice of the parameters listed in Table 3 is to reach a balance of forces that allows the successful representation of the gas phase distribution along the pipe radius. In the conditions of the experiments considered in this work, the lift force and the turbulent dispersion force are acting in opposite

directions and it is possible to reach a correct balance with a specific combination of values. The actual interfacial forces models rely on tuning parameters that can assume a wide range of values depending on the authors and on the flow conditions.

At the actual stage of development, the forces are not studied separately in order to understand the effect of the forces on the gas phase. The goal of the different authors is more concentrated on the definition of sets of coefficients that would allow the successful representation of the phase distribution along the pipe radius. However, efforts should be directed more to a correct description of the forces and the mechanistic formulation of the models in order to avoid the use of coefficients.

For example, the turbulent dispersion force model should be directly dependent on the turbulence parameters. Now, this force is dependent on a derived parameter such as the void fraction. A bad prediction of the radial profile of the gas volume fraction can lead then to a wrong estimation of the turbulent dispersion force and to a wrong balance of forces.

Cases A, B and C,D are representative of two different combinations of the horizontal interfacial forces coefficients. Cases A and B combine a lower lift coefficient with a lower wall lubrication force coefficient and a moderate turbulent dispersion force. Cases C and D, on the contrary, combine higher lift coefficient with higher wall lubrication force coefficient and more turbulent dispersion.

The value of the wall lubrication force coefficient needs to be increased in combination with a higher lift coefficient since the turbulent dispersion force models are not able to counterbalance the stronger influence of the lift force. Otherwise in the near wall region the net interfacial non-drag force would be directed toward the wall. The result, in this case, is an over-estimation of gas volume fraction at the wall. Increasing the value of the wall lubrication force coefficient helps to reduce or to invert the sign of the net force in the near wall region and to reduce the value of the gas volume fraction in that area. It is then possible to reproduce the height and the position of the gas volume fraction “wall peak” adequately.

In the next pages the results are presented for the following variables in this order:

- Gas volume fraction (Figure 68)
- Interfacial area density (Figure 69)
- Gas velocity (Figure 70)
- Sauter mean diameter (Figure 71)

- Turbulence eddy dissipation (Figure 72)
- IAC change rate due to RC (Figure 73)
- IAC change rate due to breakup (Figure 74)

For the case **F02G02**, the 4 model set-ups under-predict both the volume fraction profile and the gas interfacial area density. The lift coefficient equal to 0.05 is too weak to reproduce adequately the wall peak of the gas volume fraction. The lift coefficient equal to 0.1 or even slightly higher adequately represents the phases distribution. In general, all the combinations of the 4 models under-predict the interfacial area density both in the pipe central region and near the wall, but they adequately represent the evolution along the radial direction. No appreciable differences can be seen in the diagram of the gas velocity and the different simulations reproduce the dispersed phase velocity in good agreement with the experimental data.

The Sauter mean diameter, however, is over-predicted. The diameter of the gas phase is the result of the ratio between the void fraction and the interfacial area density. In the special case of the simulation F02G02, the interfacial area density has been under-predicted while the level of the void fraction has been well calculated except that at the wall. The turbulence eddy dissipation results are very similar for the different combinations. For this reason very similar results for the breakup and coalescence interfacial area density change rate have been obtained.

If the liquid superficial velocity is increased (**F03G01**, **F03G2** and **F03G03**) a lift coefficient equal to 0.1 (case A) it is not appropriate to reproduce the correct profiles. The lower value equal to 0.05 (case B) is able to deliver results in much better agreement with the experimental data. This is valid for the interfacial area and for the gas volume fraction.

Also the cases C and D show a good agreement with the gas volume fraction experimental results for the cases F03G01, F03G02 and F03G03. As the gas superficial velocity becomes higher, the interfacial area density is increasingly over-predicted. Furthermore, for the simulation of case F03G03, for the volume fraction and in minor way for the interfacial area density radial profiles, numerical instabilities arises and the results present a particular chessboard pattern. The maximum level of the interfacial area density has been limit to 800 m^{-1} for numerical stability of the calculations.

If the Sauter mean diameter is concerned, combinations C and D show for the three cases strange numerical oscillations in the profiles. For the cases F03G01 and F03G02

combination B seems to deliver the best results. For the case F03G03 all the four combinations deliver results with a different behavior if compared to the experimental data and bubbles with higher diameter are concentrated in the liquid bulk.

In Figure 72 the turbulence eddy dissipation is shown. If attention is concentrated on the cases F03G0Xs, the case A reproduces a different form of the radial profile of turbulent dissipation: it has lower value and it is flatter in the central region and in the near wall region the steep of the curve is in general higher than for the other 3 cases. In fact, the lift coefficient 0.1 (case A) has been demonstrated not to adequately reproduce the volume fraction radial distribution. Since the BIT model of Morel is used, this has a direct impact of the source terms in the turbulence equations.

Regarding the interfacial area change rate due to coalescence and breakup, it is possible to note how the level of interactions is in general much higher for the cases at higher liquid superficial velocity (F03G0Xs compared against F02G02). Also increasing the gas superficial velocity delivers in general higher coalescence and breakup rates.

The lift coefficient should not be considered as a constant. It should be a variable (as already introduced in section 4.3.2.2) dependent on the bubble dimension and on the bubble Reynolds number. Using a single constant value of the lift coefficient for several flow conditions does not represent the adequate solution given its dependency from the flow parameters. This has been clearly shown in the cases presented here as the lift coefficient equal to 0.1 (case A) has been found adequate for the simulation of the cases F02s while out of range for the cases F03s.

Since uncertainties in the determination of the Sauter mean diameter have been experienced, in the framework of this analysis, constant values for the lift coefficient have been used similarly to Lopez de Bertodano and Prabhudharwadkar [Lopez de Bertodano and Prabhudharwadkar 2010] or Yao and Morel [Yao and Morel 2004]. This has been necessary to avoid oscillations due to the possible inversion of the lift coefficient.

In case of air-water upward turbulent bubbly flow simulations with the newly presented model, good results are obtained if the Morel BIT model is used in combination with following interfacial non-drag forces models:

- Lift force coefficient around 0.1 dependent on flow conditions
- Wall lubrication force: Antal (-0.0064,0.016)
- Turbulent dispersion force: FAD with coefficient 1

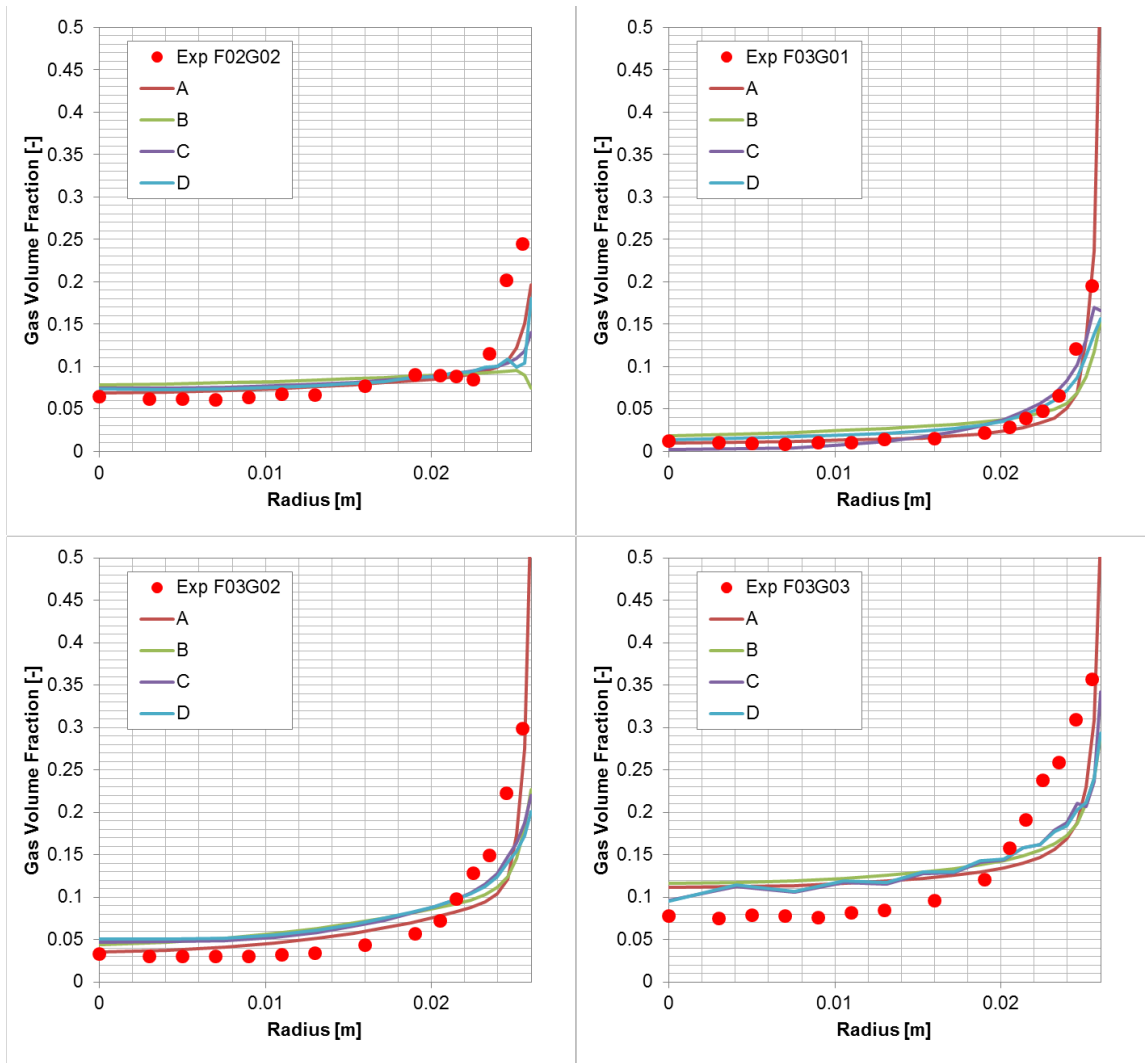


Figure 68: Radial profiles of the gas volume fraction for the cases F02G02 (up left), F03G01 (up right), F03G02 (down left), F03G03 (down right) and for several interfacial forces model configurations

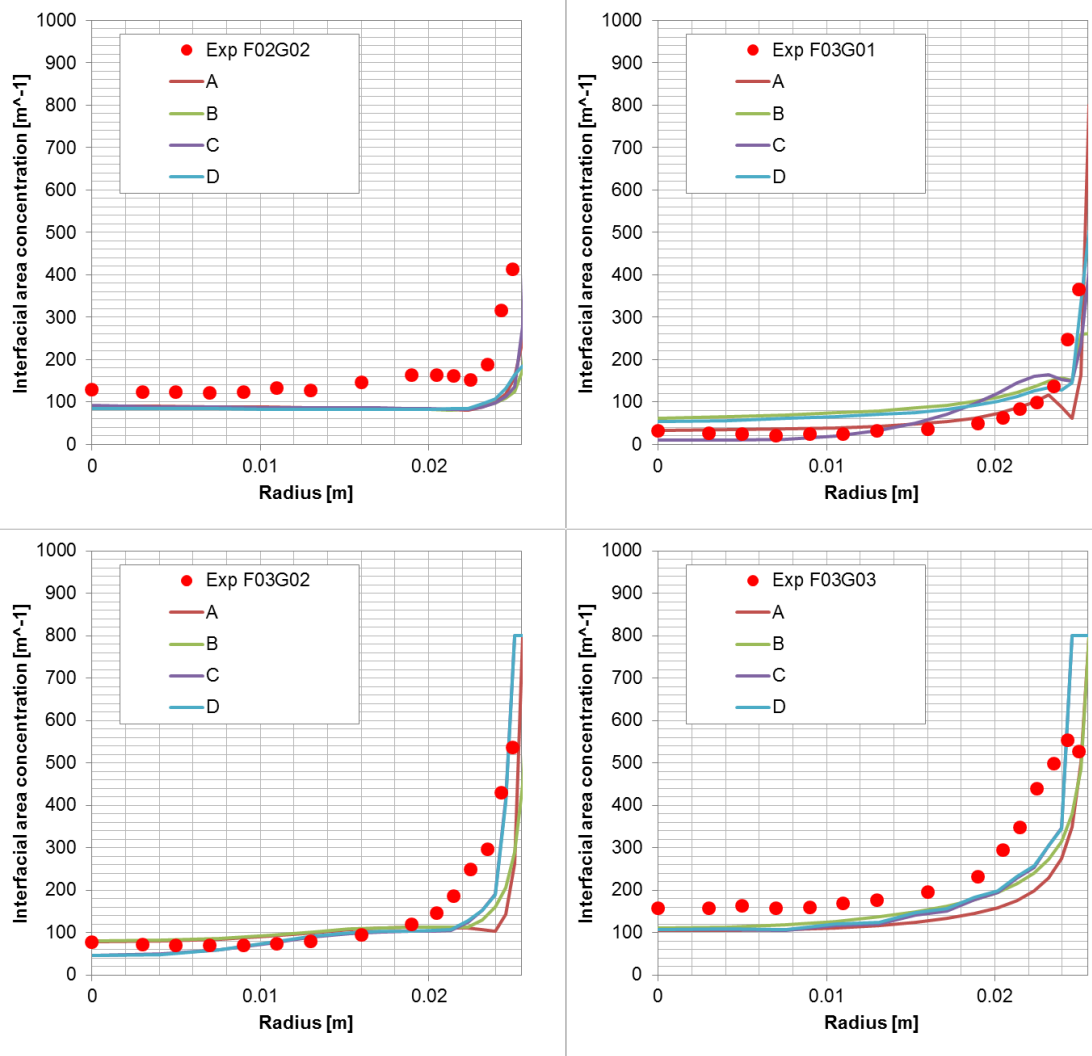


Figure 69: Radial profiles of the interfacial area concentration for the cases F02G02 (up left), F03G01 (up right), F03G02 (down left), F03G03 (down right) and for several interfacial forces model configurations

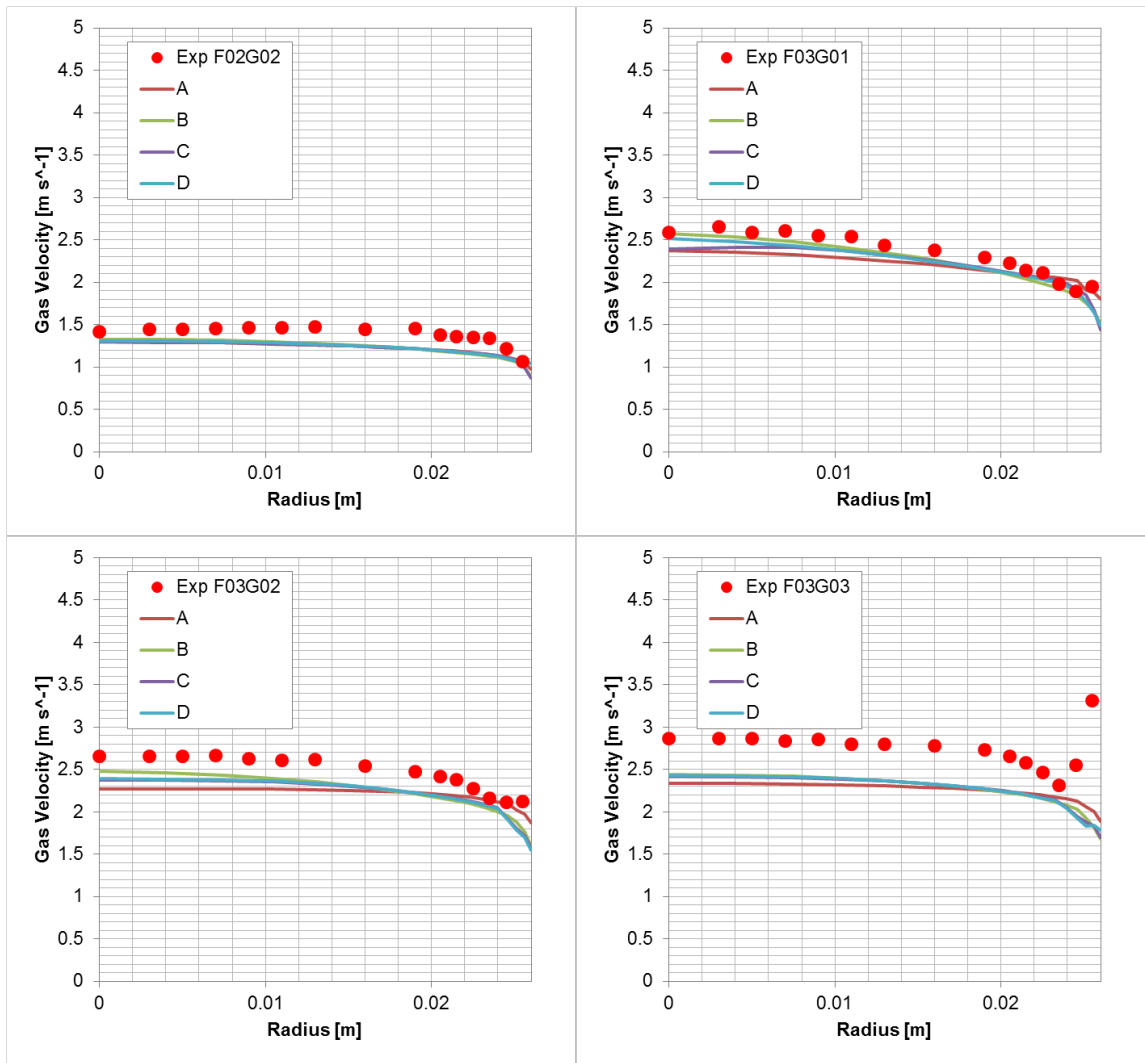


Figure 70: Radial profiles of the gas velocity for the cases F02G02 (up left), F03G01 (up right), F03G02 (down left), F03G03 (down right) and for several interfacial forces model configurations

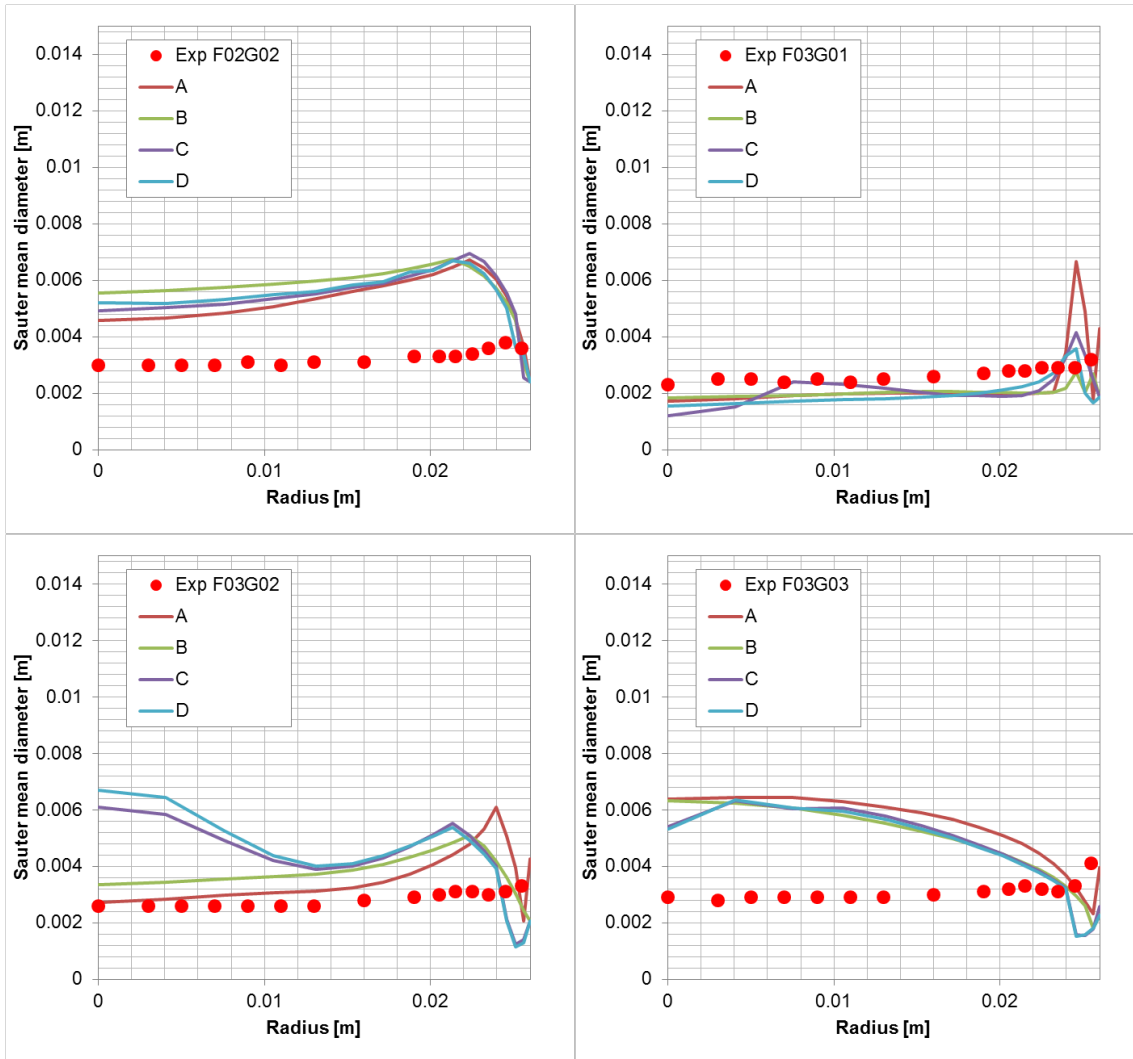


Figure 71: Radial profiles of the Sauter mean diameter for the cases F02G02 (up left), F03G01 (up right), F03G02 (down left), F03G03 (down right) and for several interfacial forces model configurations

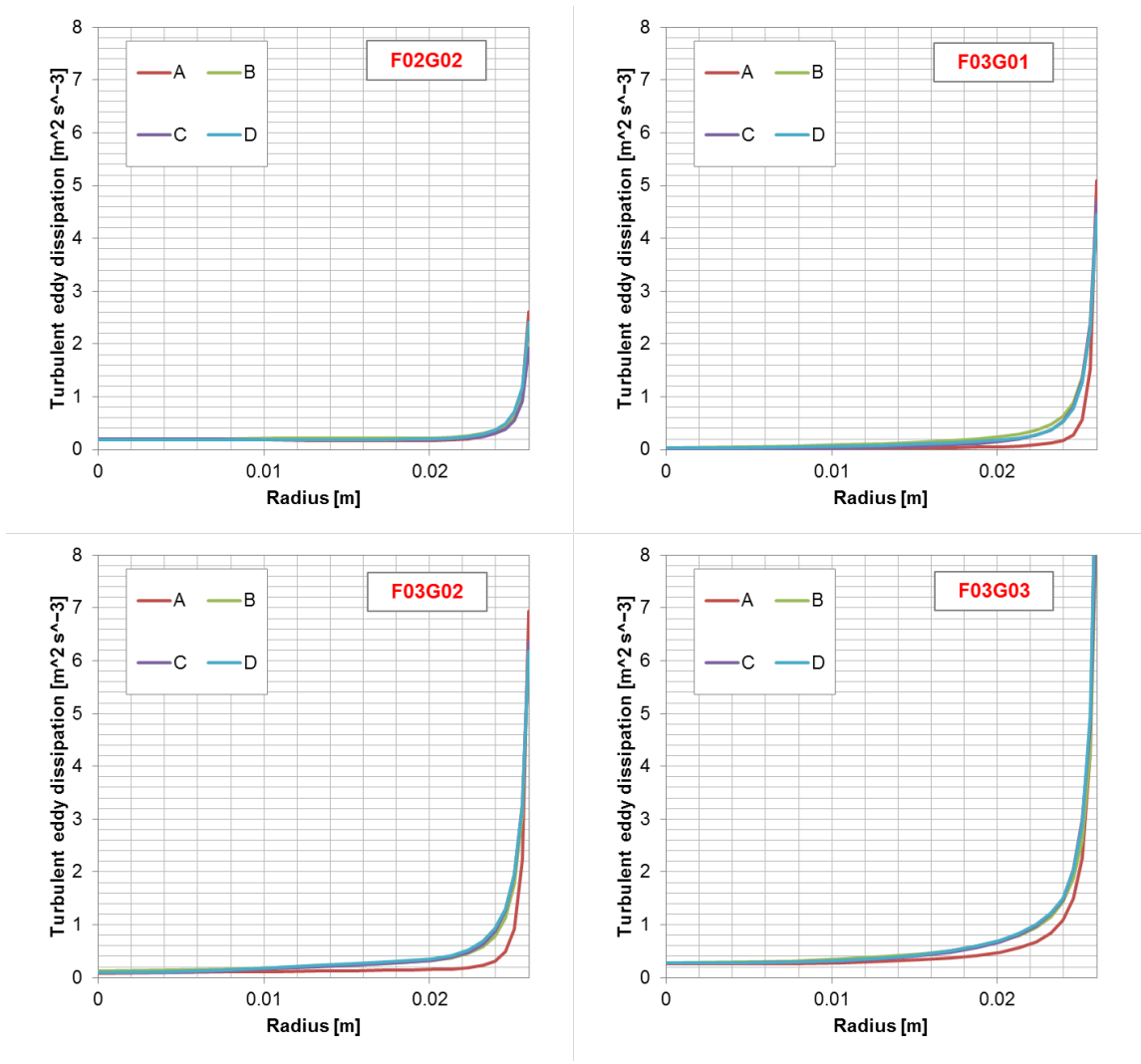


Figure 72: Radial profiles of the turbulence eddy dissipation for the cases F02G02 (up left), F03G01 (up right) F03G02 (down left), F03G03 (down right) and for several interfacial forces model configurations

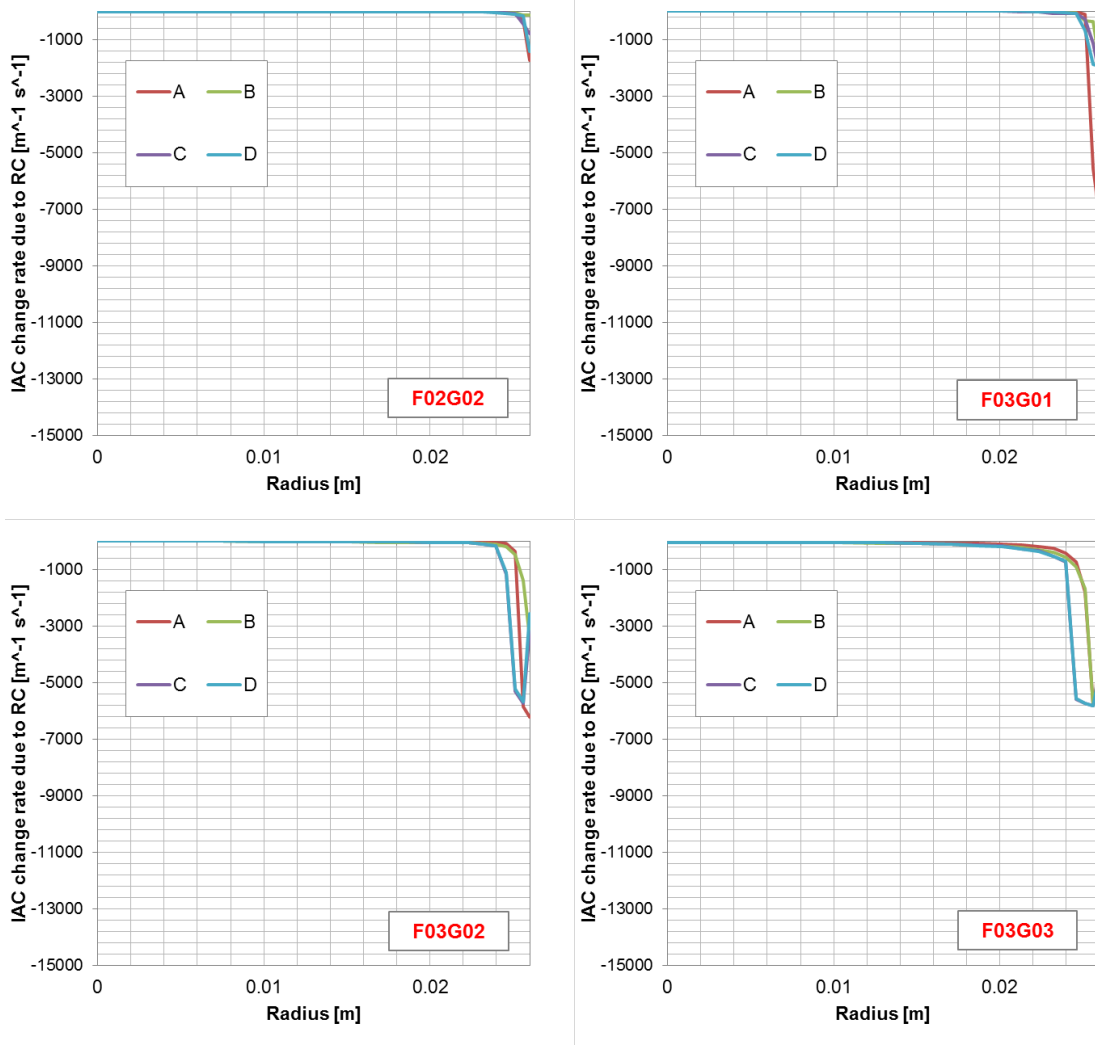


Figure 73: Radial profiles of the IAC change rate due to RC for the cases F02G02 (up left), F03G01 (up right) F03G02 (down left), F03G03 (down right) and for several interfacial forces model configurations

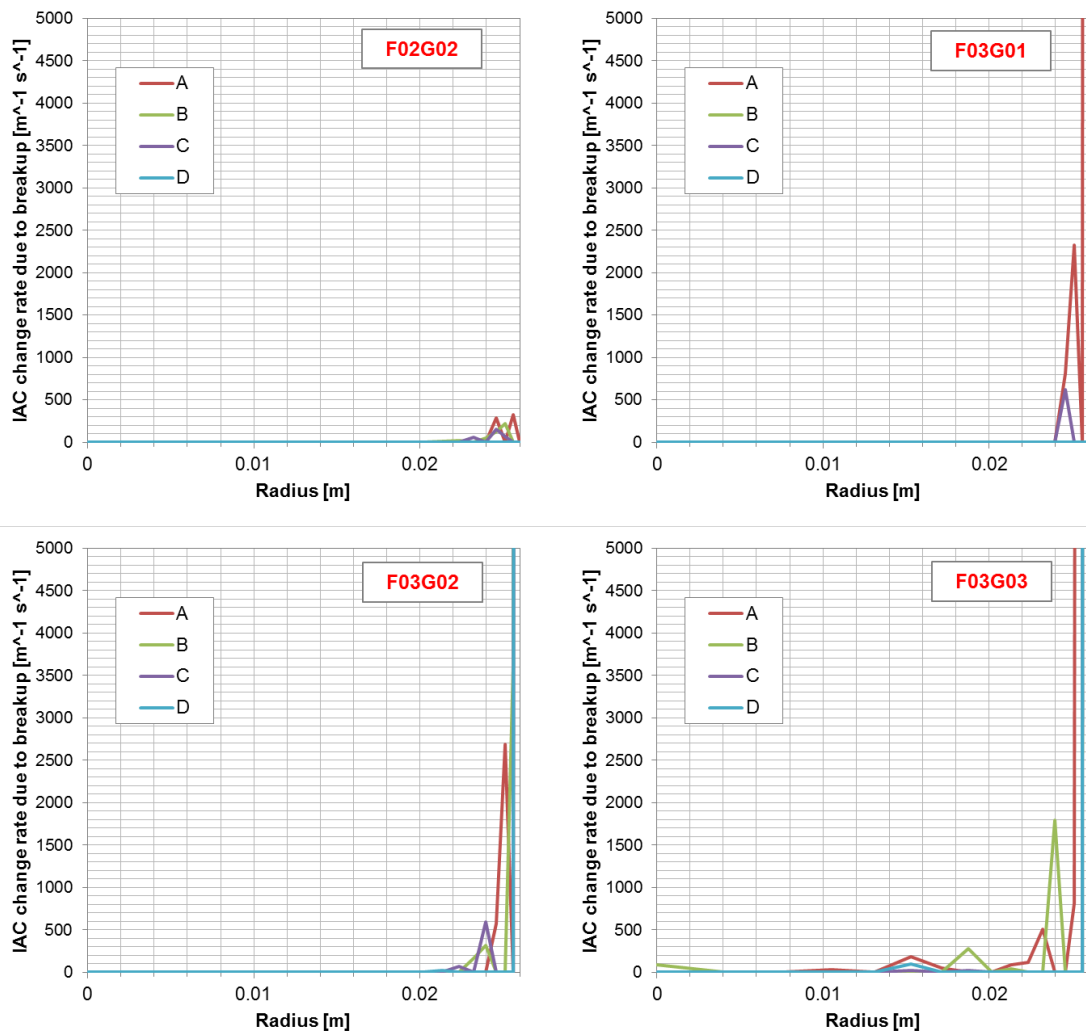


Figure 74: Radial profiles of the IAC change rate due to breakup for the cases F02G02 (up left), F03G01 (up right) F03G02 (down left), F03G03 (down right) and for several interfacial forces model configurations

11.3 Main Conclusions of this Chapter

In chapter 10, the inconsistencies in the use of the 1D definition of the bubble interaction terms for 3D simulations have been explained. Furthermore, a new local mechanistic formulation of bubble interaction models for coalescence and breakup has been developed and presented. In this chapter, the effect on the simulation results of various model parameters and coefficient is shown in detail. Furthermore, radial profiles of the main variables are presented in order to explain the behavior of the newly developed models. Several set of experimental data have been simulated in order to test the model for a wide range of conditions.

11.3.1 Main Conclusions of the Analysis of the Effects of Several Parameters on the Results

A sensitivity analysis of the influence on the results for several parameters has been performed. The relevant parameters taken into consideration to perform the analysis are those already considered in Chapter 9: namely the lift, wall lubrication and turbulent dispersion forces and the Bubble Induced Turbulence (BIT). Furthermore the influence of the breakup and coalescence coefficients, introduced in Chapter 10, has been investigated. For each of the parameters tested, diagrams showing the radial profiles of several flow variables have been presented. Results for the sensitivity at the variation of the **lift, wall lubrication and turbulent dispersion** forces have been presented: these three parameters have the greatest influence on the results.

The **lift force coefficient** influences mainly the value of the void fraction in the near wall region. As this coefficient is reduced the void fraction becomes smaller and approaches the experimental results. Also the Sauter mean diameter profile is influenced by the lift coefficient changes: the peak near the wall decreases as the lift coefficient decreases.

The **wall lubrication force** has its highest influence on the near wall region. Increasing the value of the coefficient has an effect similar to a reduction of the lift force. In fact, they are acting in opposite directions.

The **turbulent dispersion force** is the other parameter that has been shown to have an important effect on the results. If this force has not been taken into account an irregular form of the profiles is observed and there is not bubble redistribution operated by the dispersion force from regions of higher concentration and gradient. If the FAD

model is compared with the Lopez de Bertodano model, the second one shows a much stronger dispersive effect.

Parameters that also influence the results but in a less strong manner are the **Bubble Induced Turbulence (BIT)** model, the **level of the turbulence eddy dissipation**, the **breakup and coalescence coefficients** and of the **IAC factor**.

The **Bubble Induced Turbulence (BIT)** model has also an influence of the results. In the analysis the Sato's model is compared against the Morel's model. The results are similar in the two cases but they show a more regular numerical behavior if the Morel model is used.

The effect of the **level of the turbulence eddy dissipation** predicted by the Morel model has also been investigated by applying a constant modification coefficient to the breakup and coalescence rate terms in the interfacial area transport equation in front of the turbulence eddy dissipation. In this way, the influence of the turbulence prediction has been shown and seems to have a small influence on the results.

The effects of the **breakup coefficient** K_b , the **coalescence coefficient** K_c and of the **IAC factor** have also been investigated. The breakup coefficient K_b has shown no influence in case of steady state simulations. The coalescence coefficient K_c has a clear influence. It affects in a minor way the gas volume fraction and the interfacial area density profiles, but it has a much higher influence on the determination of the Sauter mean diameter. The diameter approaches the experimental data as the value of the coalescence coefficient decreases. The discrepancies could be explained by the fact that the cross collision sectional area determined thanks to the ideal gas kinetic theory **is not** suitable in case of deformed bubbles with a moving interface if a term considering bubble deformation is not taken into account.

A similar effect to that explained for the coalescence is observed if the **IAC factor** is taken into consideration. In general, this coefficient has a minor influence on the results than the coalescence coefficient K_c .

11.3.2 Main Conclusions of the Analysis for Several Experimental Conditions

The results of several cases obtained using the newly implemented IATE constitutive models for bubble breakup and coalescence have been presented for several gas and

liquid superficial velocity conditions in combination with the Morel's Bubble Induced Turbulence model.

Several sets of models for the definition of the interfacial forces coefficients have been tested in order to reach a balance of forces that allows the successful representation of the gas phase distribution along the pipe radius. In the conditions of the experiments considered in this work, the lift force and the turbulent dispersion force are acting in opposite directions and it is possible to reach a correct balance with different combination of values of the parameters present in the expressions of the forces coefficients. They can assume a wide range of values depending on the authors and on the flow conditions.

At the actual stage of development, the goal of the different authors has been more concentrated on the definition of sets of coefficients that would allow the successful representation of the phase distribution along the pipe radius. However, efforts should be directed more to a correct description of the forces and the mechanistic formulation of the models in order to avoid the use of coefficients since these have been shown to have a major impact on the simulation results.

The choice of the coefficients for the analysis presented in this chapter is representative of two different combinations of the radial interfacial forces coefficients that allow a successful representation of the gas phase distribution along the pipe radius. Cases A and B combine a lower lift coefficient with a lower wall lubrication force coefficient and a moderate turbulent dispersion force. Cases C and D, on the contrary, combine a higher lift coefficient with higher wall lubrication force coefficient and more turbulent dispersion. In general not one of the four combinations of models is able to reproduce correctly the phases distribution along the pipe radius for all the experimental conditions tested. Furthermore, the lift coefficient should not be considered as a constant. Using a single constant value of the lift coefficient for several flow conditions does not represent the adequate solution given its dependency from the flow parameters. It should be a variable dependent on the bubble dimension and on the bubble Reynolds number.

Finally, in case of air-water upward turbulent bubbly flow simulations with the newly implemented model, good results are obtained with the Morel's BIT in combination with the following interfacial force models:

- Lift force coefficient around 0.1 dependent on flow conditions

- Wall lubrication force: Antal (-0.0064,0.016)
- Turbulent dispersion force: FAD with coefficient 1

Chapter 12

Conclusions and Further Work

12.1 Conclusions

By means of an extensive theoretical and simulation based analysis, it has been shown that the definition of bubble interaction mechanisms is of primary importance to obtain an accurate and reliable reproduction of two-phase flow phenomena by means of CFD simulations. Among others, a better manner to model the interfacial area concentration than an algebraic approximation is to do it directly by means of a transport equation, especially for the three-dimensional formulation of two-phase flow. The accurate determination of the interfacial area is important to achieve good local and global prediction of two-phase flow characteristics. This approach is also able to reproduce dynamic and transient phenomena like phase change or flow regime transitions that cannot be simulated by the monodispersed approach alone.

An extensive literature review of bubble interaction mechanisms and a critical review of the most important available one-group interfacial area density constitutive models have been carried out as a basis for the work presented in this thesis.

The insights obtained from the reviews and from the validation of current bubble dynamics models used in ANSY-CFX have led to the development and implementation of a one-group interfacial area transport equation in this CFD code. Some problems occurring because of the different form of the theoretically derived interfacial area equation if compared with the form required by the software have been overcome and a solution to reduce numerical diffusion and to adequately implement the source and sink terms in the code has been developed.

The analysis of the state of the art methods and models for the simulation of dispersed two-phase flow as implemented in ANSYS CFX has been performed with the experimental data from the PUMA experimental facility [Santos Mendez 2008].

In this analysis the monodispersed approach together with the newly-implemented additional interfacial area transport equation and several constitutive models for bubble breakup and coalescence from the literature have been tested.

The main goals of the analysis were to validate the correct implementation of the additional transport equation and to analyze the influence of its state-of-the-art constitutive models on the results and to try to find their limits. Thus, formulations describing different aspects of bubble dynamics from Hibiki and Ishii 2001, Yao and Morel 2004, Wu et al. 1998, Ishii and Kim 2001 and Wang 2010 have been implemented in the code and tested. These models have been described and discussed in detail in sections 7.1 to 7.5.

In general, the five models listed above are able to reproduce with good agreement the gas volume fraction radial profile and their differences with the experimental measurements are small (Figure 50 and Figure 51). This happens except when, in combination with all the state-of-the-arts five Interfacial Area Transport Equation constitutive models, the Sato's Bubble Induced Turbulence model is used in combination with a lift force coefficient equal to 0.1 (similarly to Figure 42 in case of monodispersed simulations).

Problems arise if the interfacial area density or the Sauter mean bubble diameter radial distributions are considered though. For instance, the interfacial area concentration is in relative good agreement with the experimental data in the central region of the pipe whereas, in the near wall region the discrepancies are much larger and, in most cases, the models are not able to predict the interfacial area density or the Sauter mean diameter of the bubbles adequately.

The best agreement with the experimental data has been obtained with the Yao and Morel's constitutive model for the interfacial area transport equation.

Nevertheless, the interfacial area constitutive models tested in Chapter 9 contain a number of empirical coefficients. For Wu et al. 1998 and Ishii and Kim 2001 and Hibiki and Ishii 2001 the empirical coefficients have been tuned to fit the 1D vertical evolutions of the main flow parameters. In case of Wang 2010, the set of coefficients has been obtained through a very time and resource intensive calibration procedure for three-dimensional calculations. This means that they are not universal and that modifying the flow conditions or the geometry of the system under exam can lead to the need to calibrate the model coefficients again.

Furthermore, Yao and Morel [Yao and Morel 2004] do not explain a coefficient in their formula for the determination of the cross sectional area for bubble collisions (see (Eq.200)). Finally, both in Hibiki and Ishii 2001, as also in Yao and Morel 2004 the expressions for the determination of the energy content of the eddies that can break the bubble are difficult to be validated against experimental data [Liao and Lucas 2009] (Hibiki and Ishii 2001 and Yao and Morel 2004) or have been selected *ad hoc* to better fit upward vertical turbulent bubbly flow experiments [Yao and Morel 2004], thus they are not universally applicable.

As result of the analysis described above, the limit of the actual formulation have been understood and a new local mechanistic formulation of bubble interaction models for coalescence and breakup for the one-group interfacial area transport equation has been developed. This has been done in agreement and within the limits of the actual theory.

In Chapter 10 the inconsistencies in the use of the 1D definition of the bubble interaction terms for 3D simulations have been explained. In 1D calculation, the fluid dependent parameters needed for the evaluation are intended as averaged values along the radial direction. The distortion caused by this assumption has been adjusted by means of “*tuning*” parameters in the final expressions of the terms [Hibiki and Ishii 2000a]. This modeling strategy yields the best agreement with the axial evolution of the flow parameters. The axial profile variation of the turbulence eddy dissipation is much less pronounced than the radial one (see Figure 56). If the radial profiles are considered and the Yao and Morel’s BIT model is used, the values in the near wall region reach valued 10 to 40 times the average.

Based on the considerations above, in order to overcome the limits of the current formulation, we have performed several analytical studies that have provided us with the insights regarding the modeling of bubble breakup and coalescence and new local mechanistic formulations have been developed and presented in Chapter 10.

The **breakup model** developed in the current work is based on the considerations of Martinez Bazán [Martinez Bazan 1998]. No closure parameters that can alter significantly the model behavior needs to be set and no bubble breakup efficiency has to be defined. These two aspects linked together lead to a great simplification of the breakup problem. The bubble breakup model is based only on kinematic considerations and if compared with previous formulations is practically independent from tuning parameters. The bubble surface is deformed by the energy provided by the

turbulent stresses provided by the surrounding fluid. Once these turbulent stresses overcome the surface tension stresses breakup happens. Using this approach means that no bubble breakup frequency model is involved in the calculation. There is also no need to define “a priori” size and energy content of turbulent eddies in the fluid flow. Another advantage of this model is that all the energy spectrum of turbulence is considered while other authors selected a specific range to obtain better agreement with the experimental data. The current Thesis represents the first attempt to model bubble breakup for the interfacial area transport equation by using the approach proposed in 1998 by Martinez Bazán.

The **coalescence model** developed in the current work is based on the concepts of bubble collision, liquid drainage and film rupture. A collision frequency has been defined as also a coalescence efficiency. This manner of modeling the coalescence process is not new and other authors previously derived a general expression similar to the one presented here. In the current work attention has been concentrated, however, on consistent sub-models based on geometric consideration only and neglecting, as much as possible, considerations based on the order of magnitude of the phenomena. The only consideration based on the order of magnitude used, largely accepted in the literature, is that the eddies interacting with the bubbles have a characteristic dimension of the same order of magnitude of the bubbles present in the system.

The collision model, derived from the gas kinetic theory, is based on the widely used collision of spheres behaving as ideal particles (see section 6.2.1). Coefficients are applied to take into consideration that bubbles in reality do not interact like ideal particles (coefficient K_c), that the presence of the other bubbles influences their behavior (coefficient γ) and that the ratio mean distance between particles to their average relative turbulent path needs also to be taken into account to define the collision rate (coefficient Π).

In this Thesis the coefficients needed for the calculation both of the turbulent stresses that produce the surface deformation energy causing bubble breakup and of the relative bubble approaching velocity have been analytically calculated and they have been defined to be correlated. Their definition is based on the concept of difference of fluctuation velocities at two neighboring points in the flow under isotropic and homogeneous turbulent conditions introduced in section 3.8. In that section two different cases were considered. The first, used for the determination of the **longitudinal fluctuation velocity difference** [Rotta 1972] between two points in the

fluid, is valid for the determination of the **relative bubble approaching velocity** for bubbles collision in the coalescence model. The second, used the determination of the **absolute value of the fluctuation velocity difference** [Batchelor 1956] between two points in the fluid, is needed for the determination of the **turbulent stresses applied on the bubbles by the surrounding fluid** in the breakup model.

In this Thesis, the longitudinal fluctuation velocity difference [Rotta 1972] has been used, in case of coalescence modeling, for the determination of the coefficient C_c needed for the calculation of relative bubble approaching velocity. The absolute value of the fluctuation velocity difference [Batchelor 1956], has been used, in case of break-up modeling, for the determination of the coefficient β needed for the calculation of the turbulent stresses applied on the bubbles by the surrounding fluid. Finally It is important to notice that the coefficients C_c and β are correlated, linked with the dimensionless Kolmogorov constant α deduced experimentally and characteristic of the actual turbulence conditions (i.e. pipe flow). It means it is not possible to modify the value of one of them without consequently adjusting the value of the other. Furthermore, in this Thesis, for the definition of the coefficient C_c the aspect of the non-uniformity of the turbulence velocity component of particles has been taken into consideration [Kuboi et al. 1972a]. The bubble relative approaching velocity has been expressed by a Maxwell distribution to take into consideration the randomness of the bubble approaching phenomena (e.g. approaching angle etc.).

Following, Jo and Revankar [Jo and Revankar 2011b], the coefficient K_b , in the breakup model, has been defined to be equal to the diameter in millimeters for which the turbulent stresses are equal to the surface tension stresses.

The definition of the multiplication coefficient K_c in the coalescence model is not trivial as it is related to the modification of the cross sectional bubble collision areas due to the non-regular form of the bubbles. K_c is a reductive coefficient that should not be considered as a constant but a variable calculated depending on the actual flow conditions. If a significant bubble distortion is taking place, the bubble aspect ratio is much smaller than 1 and the coefficient K_c : (i.e. in case of bubble aspect ratio smaller than 0.5) should assume values smaller than 0.5. In case of less bubble distortion, such as the case of liquid drops in liquid as in reported by Kuboi et al. [Kuboi et al. 1972b], the coefficient takes values around 0.7.

In order to calculate the collision efficiency, the widely used film drainage model (see section 6.2.2.3) has been used. The expressions used for the definition of the

interaction and drainage time to calculate the coalescence efficiency are those proposed by Chesters and Hoffman in 1982. These models have not yet been used in the literature in the definition of constitutive terms for the interfacial area density transport equation. In the expression of the drainage time, the relative velocity of the centers of colliding particles has been defined consistently with the case of bubble collision explained above.

It is worth of notice that, both for the collision frequency and for the efficiency, Chesters 1991 did not define an equation to calculate the bubble relative approaching velocity and only furnished proportionality.

If compared to the polydispersed calculation methods, since only one group of bubbles is considered in the Interfacial Area Transport Equation there is no need to implement complicated and resources intensive integrals for the statistical determination of the size of the daughter bubbles produced after a breakup or coalescence event.

The new constitutive models explained above have been implemented in ANSYS CFX and have been tested against the data of the PUMA facility in chapter 11 where a sensitivity analysis of the influence on the results for several parameters have been performed. The actual bubble dynamics models are based on sphericity or nearly sphericity assumptions and have been shown to have a major influence on the results in chapter 9. In order to increase the accuracy of the results more experimental and theory work is needed to clarify the dependence of important flow parameters and to develop expressions for the determination of the bubble form or distortion based on local conditions.

The relevant parameters taken into consideration to perform the analysis are those already considered in Chapter 9: namely the lift, wall lubrication and turbulent dispersion forces and the Bubble Induced Turbulence (BIT). Furthermore the influence of the breakup and coalescence coefficients, introduced in Chapter 10, has been investigated. For each of the parameters tested, diagrams showing the radial profiles of several flow variables have been presented. Results for the sensitivity at the variation of the **lift, wall lubrication and turbulent dispersion** forces have been presented: these three parameters have the greatest influence on the results.

The **lift force coefficient** influences mainly the value of the void fraction in the near wall region. As this coefficient is reduced the void fraction becomes smaller and

approaches the experimental results. Also the Sauter mean diameter profile is influenced by the lift coefficient changes: the peak near the wall decreases as the lift coefficient decreases.

The **wall lubrication force** has its highest influence on the near wall region. Increasing the value of the coefficient has an effect similar to a reduction of the lift force. In fact, they are acting in opposite directions.

The **turbulent dispersion force** is the other parameter that has been shown to have an important effect on the results. If this force has not been taken into account an irregular form of the profiles is observed and there is not bubble redistribution operated by the dispersion force from regions of higher concentration and gradient. If the FAD model is compared with the Lopez de Bertodano model, the second one shows a much stronger dispersive effect.

Parameters that also influence the results but in a less strong manner are the **Bubble Induced Turbulence (BIT)** model, the **level of the turbulence eddy dissipation**, the **breakup and coalescence coefficients** and of the **IAC factor**.

The **Bubble Induced Turbulence (BIT)** model has also an influence of the results. In the analysis the Sato's model is compared against the Morel's model. The results are similar in the two cases but they show a more regular numerical behavior if the Morel model is used.

The effect of the **level of the turbulence eddy dissipation** predicted by the Morel model has also been investigated by applying a constant modification coefficient to the breakup and coalescence rate terms in the interfacial area transport equation in front of the turbulence eddy dissipation. In this way, the influence of the turbulence prediction has been shown and seems to have a small influence on the results.

The effects of the **breakup coefficient** K_b , the **coalescence coefficient** K_c and of the **IAC factor** have also been investigated. The breakup coefficient K_b has shown no influence in case of steady state simulations. The coalescence coefficient K_c has a clear influence. It affects in a minor way the gas volume fraction and the interfacial area density profiles, but it has a much higher influence on the determination of the Sauter mean diameter. The diameter approaches the experimental data as the value of the coalescence coefficient decreases. The discrepancies could be explained by the fact that the cross collision sectional area determined thanks to the ideal gas kinetic theory

is not suitable in case of deformed bubbles with a moving interface if a term considering bubble deformation is not taken into account.

A similar effect to that explained for the coalescence is observed if the **IAC factor** is taken into consideration. In general, this coefficient has a minor influence on the results than the coalescence coefficient K_c .

The results of several cases obtained using the newly implemented IATE constitutive models for bubble breakup and coalescence have been presented for several gas and liquid superficial velocity conditions in combination with the Morel's Bubble Induced Turbulence model.

Several sets of models for the definition of the interfacial forces coefficients have been tested in order to reach a balance of forces that allows the successful representation of the gas phase distribution along the pipe radius. In the conditions of the experiments considered in this work, the lift force and the turbulent dispersion force are acting in opposite directions and it is possible to reach a correct balance with different combination of values of the parameters present in the expressions of the forces coefficients. They can assume a wide range of values depending on the authors and on the flow conditions.

At the actual stage of development, the goal of the different authors has been more concentrated on the definition of sets of coefficients that would allow the successful representation of the phase distribution along the pipe radius. However, efforts should be directed more to a correct description of the forces and the mechanistic formulation of the models in order to avoid the use of coefficients since these have been shown to have a major impact on the simulation results.

The choice of the coefficients for the analysis presented in this chapter is representative of two different combinations of the radial interfacial forces coefficients that allow a successful representation of the gas phase distribution along the pipe radius. Cases A and B combine a lower lift coefficient with a lower wall lubrication force coefficient and a moderate turbulent dispersion force. Cases C and D, on the contrary, combine a higher lift coefficient with higher wall lubrication force coefficient and more turbulent dispersion. In general not one of the four combinations of models is able to reproduce correctly the phases distribution along the pipe radius for all the experimental conditions tested. Furthermore, the lift coefficient should not be considered as a constant. Using a single constant value of the lift coefficient for several

flow conditions does not represent the adequate solution given its dependency from the flow parameters. It should be a variable dependent on the bubble dimension and on the bubble Reynolds number.

Finally, in case of air-water upward turbulent bubbly flow simulations with the newly implemented model, good results are obtained with the Morel's BIT in combination with the following interfacial force models:

- Lift force coefficient around 0.1 dependent on flow conditions
- Wall lubrication force: Antal (-0.0064,0.016)
- Turbulent dispersion force: FAD with coefficient 1

More work is expected in the next years in the field of bubble dynamics because of the great influence of these parameters on the simulation results.

12.2 Further Work

Given the major influence on the results, the development of mechanistic models for the determination of the interfacial non-drag forces is of primary importance. The actual models rely on tuning parameters that can assume a wide range of values depending on the authors and the flow conditions. In the case of the turbulent dispersion force, its direct dependency on turbulence parameters, instead of depending on a derived parameter as the void fraction, is needed. It is important to study more, both experimentally and numerically, the separated effect of the lift force and of the turbulent dispersion force. It is very difficult to reproduce experimentally the conditions to study these two effects separately. Nevertheless, thanks to the DNS technique, it would be possible to reproduce the experiments imposing constant velocity profiles for the phases. In this way the curl vector of the velocity is zero and the lift force assumes a value equal to null. The only force responsible for the displacement of the gas phase from the pipe near wall region to the pipe centerline would be then the turbulent dispersion force. Combining the experimental results with the simulation results would be possible to study and understand the separate influence of these two forces and then derive mechanistic models for their correct reproduction.

Evolutions of the interfacial area transport equation could be addressed in two different directions.

It would be possible to complement the one-group interfacial area transport equation by means of the phase change and nucleation terms. This would allow the simulation

of phase change phenomena in the subcooled boiling and in the saturated boiling region without reaching the bubbly to slug transition region.

In the second case, the adiabatic approximation is maintained and attention is concentrated on the Two-group interfacial area transport equation. The others bubble interaction mechanisms terms not contemplated in the present work would need to be modeled. They are namely: wake entrainment, shearing off and surface instability. Inter- and Intra-group terms should be developed and the two-fluid models should be modified as proposed by Ishii and Hibiki [Ishii and Hibiki 2006]. This is needed to take into account the inter-group transfers of mass momentum and eventually energy between group one and two bubbles.

References

- [Al Issa and Lucas 2009] Two phase flow 1D turbulence model for poly-disperse upward flow in a vertical pipe, S. Al Issa, D. Lucas, Nuclear Engineering and Design, Volume 239, Issue 10, October 2009, Pages 1933-1943
- [Alopaeus et al 2002a] Simulation of the population balances for liquid-liquid systems in a non-ideal stirred tank. Part2 Parameter fitting and the use of the multiblock model for dense dispersions. Alopaeus V. et al., 2002, Chem. Eng. Sci. 57, 1815-1825
- [Alopaeus et al 2002b] Gas-liquid stirred tank reactor modeling with CFD and user subroutines, Alopaeus, V. et al., 2002, AIChE. Annual Meeting, Indianapolis, IN, USA
- [Ansys 2009] ANSYS CFX User Manual, Release 12.1, ANSYS Inc, 2009
- [Antal et al. 1991] Analysis of Phase Distribution in Fully Developed Laminar Bubbly Two-Phase Flow, Antal, S.P., Lahey, R.T., Flaherty, J.E., 1991, Int. Journal of Multiphase Flow, Vol 17, 635-652
- [Aybers and Tapucu 1969] Aybers N. M. and Tapucu A., 1969, Wärme-Stoffübertragung, 2, 171-177
- [Azbel and Athanasios 1983] A mechanism of liquid entrainment, D. Azbel, I.L. Athanasios, 1983, Handbook of Fluids in Motion, Ann Arbor Science Publishers, Ann Arbor, USA
- [Batchelor 1956] The theory of Homogeneous Turbulence, G. K. Batchelor, Cambridge at the University Press, Cambridge, 1956
- [Bratland 2009] The Flow Assurance Site, Ove Bratland, 2009, <http://drbratland.com/>
- [Burns et al. 2004] The Favre averaged drag model for turbulence dispersion in Eulerian multi-phase flows, A.D. Burns, T. Frank, I. Hamill, J.-M. Shi, 2004, Proceedings of the 5th International Conference on Multiphase Flow, ICMF'2004, Yokohama, Japan
- [Cai et al. 2010] Ziqi Cai, Yuyun Bao, Zhengming Gao, 2010, Hydrodynamic Behavior of a Single Bubble Rising in Viscous Liquids, Chinese Journal of Chemical Engineering, Volume 18, Issue 6, Pages 923-930
- [Chatzi 1983] Analysis of Interactions in Fluid-Fluid Dispersion Systems in Agitated Vessels. Chatzi E., 1983, Cleveland State University Press, Cleveland, OH

- [Chatzi et al. 1987] Analysis of interactions for liquid–liquid dispersions in agitated Vessels, Chatzi E. et al.,1987. Ind. Eng. Chem. Res. 26, 2263–2267
- [Chatzi et al. 1989] Generalized model for prediction of the steady-state drop size distributions in batch stirred vessels, Chatzi E. et al.,1989 Ind. Eng. Chem. Res. 28, 1704–1711
- [Chesters 1991] The modeling of coalescence processes in fluid-liquid dispersions: A review of current understanding, Chesters A.K., 1991, Chemical Engineering Research and Design: transactions of the Institution of Chemical Engineers: Part A 69, 259–270
- [Chesters and Hoffman 1982] Bubble coalescence in pure liquids, A.K. Chesters, G. Hoffman, Appl Sci Res, 38 1982, pp. 353–361
- [Clift et al. 1978] Bubbles, Drops and Particles, Grace J.R., Clift R., Weber M.E., 1978, Academic Press
- [Colin et al. 2004] Turbulence and shear-induced coalescence in gas–liquid pipe flows, Colin C. et al., 2004. Fifth International Conference on Multiphase Flow, ICMF'04, Yokohama, Japan, May 30–June 4
- [Collier and Thome 1994] Convective boiling and condensation, Third edition, Collier J.G. and Thome J.R., 1994, Oxford University Press, Oxford, UK.
- [Coulaloglou 1975] Dispersed phase interactions in an agitated flow vessel, Coulaloglou C.A., 1975, Ph.D. Thesis, Illinois Institute of Technology, Chicago, USA
- [Coulaloglou and Tavlarides 1977] Description of interaction processes in agitated liquid-liquid dispersions, Coulaloglou, C. A., Tavlarides, L. L., 1977 Chemical Engineering Science, 32, pp.1289-1297
- [DAtf 2011] Website of the Deutsche Atomforum e.V., Stand May 2012, <http://www.kernenergie.de/kernenergie/themen/kernkraftwerke/kernkraftwerke-in-deutschland.php>
- [Doublez 1991] The drainage and rupture of a non-foaming liquid film formed upon bubble impact with a free surface, Doublez L., 1991, International Journal of Multiphase Flow 17, 783–803
- [Drew and Lahey 1987] The virtual mass and lift force on a sphere in rotating and straining inviscid flow, Drew, D.A. and Lahey Jr, R.T., 1987, Int. Journal Multiphase Flow, v.13, n. 1, pp. 113-121

- [Duineveld 1994] Bouncing and coalescence of two bubbles in water, Duineveld P.C., 1994, Ph.D. Thesis, University of Twente, The Netherlands
- [Ervin and Tryggvason 1997] The rise of bubbles in a vertical shear flow, Ervin, E.A., Tryggvason, G., 1997, *Journal of Fluids Engineering*. 119 443–449
- [Frank et al. 2008] Validation of CFD models for mono- and polydisperse air–water two-phase flows in pipes, Frank, T., Zwart, P.J., Krepper, E., Prasser, H.-M., Lucas, D., 2008, *Nuclear Engineering and Design* 238, 647-659
- [Fu and Ishii 2002a] Two-group interfacial area transport in vertical air-water flow I. Mechanistic model, Fu X.Y., Ishii M., 2002 *Nuclear Engineering and Design*, 219, 143-168
- [Gauss 1876] Besprechung des Buchs von L. A. Seeber: Untersuchungen über die Eigenschaften der positiven ternären quadratischen Formen usw., Gauss, C. F., *Göttingische Gelehrte Anzeigen* (1831, July 9) 2, 188-196, 1876
- [Gibson 1962] Spectra of turbulence at high Reynolds number, M.M. Gibson, 1962, *Nature*, N. 4848, Pag. 1281
- [Grace et al 1976] Shapes and velocities of single drops and bubbles moving freely Through Immiscible Liquids, Grace, J. R., Wairegi, T., and Nguyen, T. H., 1976, *Trans. Inst. Chem. Eng.* 54, 167-173.
- [Hewitt 2012] Gas-Liquid Flow, Hewitt G.F., 2012, *Thermopedia*, <http://www.thermopedia.com/content/2/?tid=104&sn=1297>
- [Hibiki and Ishii 2000a] One-group interfacial area transport of bubbly flows in vertical round tubes, Takashi Hibiki and Mamoru Ishii, 2000 *International Journal of Heat and Mass Transfer*, 43, 2711-2726
- [Hibiki et al. 2001a] Hibiki T., Ishii M. and Xiao Z., Axial interfacial area transport of vertical bubble flows, 2001, *Int. J. Heat Mass Trans.*, 44, 1869-1888
- [Houston 2001] *Chemical Kinetics and Reaction Dynamics*, Houston P. L., McGraw-Hill: Boston, MA, 2001
- [Howarth 1967] Measurement of coalescence frequency in an agitated tank, Howarth, W.J., 1967, *AIChE Journal* 13, 1007–1013
- [IAEA 2011] *Power Reactor Information System – IAEA*, Stand May 2012, <http://pris.iaea.org/public/>

- [Ishii 1975] Thermo-fluid Dynamic Theory of Two-phase Flow, Ishii M., 1975, Collection de la Direction des Etudes et Recherches d'Electricite de France, EyroUes, Paris, France, 22.
- [Ishii and Chawla 1979] Local Drag Laws in dispersed Two-phase flow, Ishii M. and Chawla T.C., 1979, Technical Report, ANL-79-105
- [Ishii and Hibiki 2006] Thermo-Fluid Dynamics of Two-Phase Flow, Mamoru Ishii and Takashi Hibiki, 2006, Springer
- [Ishii and Kim 2001] Micro four-sensor probe measurement of interfacial area transport for bubbly flow in round pipes, M. Ishii, S. Kim, 2001, Nuclear Engineering and Design, Volume 205, Issues 1–2, Pages 123-131
- [Ishii and Mishima 1980] Study of two-fluid model and interfacial area, Argonne National Laboratory Report, ANL-80-111, 1980
- [Ishii and Mishima 1984] Two-fluid Model and Hydrodynamic Constitutive Relations, Ishii M. and Mishima K., 1984, Nucl. Eng Des. 82: 107-126
- [Ishii and Zuber 1979] Drag coefficient and relative velocity in bubbly, droplet or particulate flows. 1979, AIChE Journal, 25, 843
- [Ishii et al. 1998] Interfacial area transport equation for two-fluid model formulation, Ishii M., Wu Q., Assad A. and Uhle J., 1998, Proceedings of IMuST Meeting
- [Ishii et al. 2002] Interfacial area transport equation: model development and benchmark experiments, Ishii M., Kim S. and Uhle J., 2002 International Journal of Heat and Mass Transfer, 45, 3111-3123
- [Jo and Revankar 2011a] Jo D., T. Revankar S., 2011, Investigation of bubble breakup and coalescence in a packed-bed reactor – Part 1: A comparative study of bubble breakup and coalescence models, International Journal of Multiphase Flow 37, 995–1002
- [Jo and Revankar 2011b] Jo D., T. Revankar S., 2011, Investigation of bubble breakup and coalescence in a packed-bed reactor – Part 2: Development of a new bubble breakup and coalescence model, International Journal of Multiphase Flow 37, 1003–1012
- [Kennard 1938] Kinetic Theory of Gases, Kennard, E.H., 1938, McGraw-Hill, New York

- [Kim 1999] Interfacial area transport equation and measurement of local interfacial characteristics, Kim, 1999, Ph.D. Thesis of Purdue University, West Lafayette, IN, USA.
- [Kim and Lee 1987] Coalescence behavior of two bubbles in stagnant liquids, J. W. Kim and W. K. Lee, 1987, Journal of Chemical Engineering of Japan, vol. 20, no. 5, pp. 448–453
- [Kirkpatrick and Lockett 1974] The influence of approach velocity on bubble coalescence, Kirkpatrick, R.D., and Lockett, M.J, 1974, Chem. Eng. Sci. 29, 2363
- [Kocamustafaogullari and Ishii 1995] Foundation of the interfacial area transport equation and its closure relations, Kocamustafaogullari G. and Ishii M., 1995, International Journal of Heat and Mass Transfer, 38, 481
- [Kocamustafaogullari et al. 1994] Measurement of modelling of averaged void fraction, bubble size and interfacial area, Kocamustafaogullari G., Huang W.D. and Razi J., 1994, Journal of Nuclear Engineering and Design 148, 437
- [Konno et al 1980] Simulations model for break-up process in an agitated tank, Konno, M., Matsunaga, Y., Arai, K., Saito, S., 1980., J. Chem. Eng. Jpn. 13, 67–73
- [Krepper et al. 2005] On the Modelling of bubbly flow in vertical pipes, Krepper, E., Lucas, D., Prasser, H.-M., 2005, Nuclear Engineering and Design, 235, 597-611
- [Krepper et al. 2007] Application of a population balance approach for polydispersed bubbly flow, Krepper, E.; Beyer, M.; Frank, T.; Lucas, D.; Prasser, H.-M., 2007, 6th International Conference on Multiphase Flow, ICMF06, 09.-13.07.2007, Leipzig, Germany, Poster No PS6_6
- [Kuboi et al 1972a] Behavior of dispersed particles in turbulent liquid flow, Kuboi, R., et al., 1972, Journal of Chemical Engineering of Japan 5, 349-355
- [Kuboi et al 1972b] Collision and coalescence of dispersed drops in turbulent liquid flow, Kuboi, R., et al., 1972, Journal of Chemical Engineering of Japan 5, 423–424
- [Lasheras et al. 2002] A review of statistical models for the break-up of an immiscible fluid immersed into a fully developed turbulent flow, Lasheras J.C., Eastwood C. Martinez Bazan C. and Montañés J.L., 2002, International Journal of Multiphase Flow, 28, 247-278.
- [Lee et al. 1987a] Bubble breakup and coalescence in turbulent gas–liquid dispersions, Lee, C.H. et al., 1987, Chem. Eng. Commun. 59, 65–84

- [Lee et al. 1987b] Dynamics of bubble size distribution in turbulent gas–liquid dispersions, Lee, C.H. et al., 1987, Chem. Eng. Commun. 61, 181–195
- [Lehr and Mewes 1999] A transport equation for the interfacial area density in two-phase flow, Lehr, F., Mewes, D., 1999, Second European Congress of Chemical Engineering, October 5–7, Montpellier, France
- [Lehr et al. 2002] Bubble-size distributions and flow fields in bubble columns, Lehr, F., et al., 2002,, AIChE. J. 48, 2426–2443
- [Liao and Lucas 2009] A literature review of theoretical models for drop and bubble breakup in turbulent dispersions, Liao, Y., Lucas, D., 2009 Chemical Engineering Science, 64, pp.3389-3406
- [Liao and Lucas 2010] A literature review on mechanisms and models for the coalescence process of fluid particles, Liao, Y., Lucas, D., 2010 Chemical Engineering Science, 65, pp-2851-2864
- [Liao et al. 2011] Development of a generalized coalescence and breakup closure for the inhomogeneous MUSIG model, Liao Y., Lucas D., Krepper E., Schmidtke M., 2011 Nuclear Engineering and Design, 241, 1024–1033
- [Lopez de Bertodano and Prabhudharwadkar 20010] Lopez de Bertodano M. and Prabhudharwadkar D., CFD Two Fluid Model for Adiabatic and Boiling Bubbly Flows in Ducts, Computational Fluid Dynamics, pp. 420, January 2010, INTECH, Croatia
- [Lucas et al. 2004] Models for the forces acting on bubbles in comparison with experimental data for vertical pipe flow, D. Lucas, J.-M. Shi, E. Krepper, H.-M. Prasser, 2004, Third International Symposium on Two-Phase Flow Modelling and Experimentation, Pisa, Italy
- [Luo and Svendsen 1996] Theoretical model for drop and bubble breakup in turbulent dispersions, Luo, H., Svendsen, H.F., 1996, AIChE. J. 42, 1225–1233
- [Martinez Bazan 1998] Splitting and dispersion of bubbles by turbulence, Martinez Bazan C., 1998, Ph.D. Thesis, University of California San Diego.
- [Martinez Bazan 1999] On the breakup of an air bubble injected into fully developed turbulent flow. Part 1. Breakup frequency, Martinez-Bazan C. et al., 1999. J. Fluid Mech. 401, 157–182

- [Menter 1992] Influence of free stream values on k-w turbulence model predictions, Menter, F.R., 1992, AIAA Journal, 30(6), pp 1657-1659
- [Menter 1994] Two-equation eddy-viscosity turbulence models for engineering applications, Menter F.R., 1994, AIAA-Journal, 32(8), pp. 269-289
- [Moraga et al. 1999] Lateral forces on spheres in turbulent uniform shear flow. F. J. Moraga, F. J. Bonetto, R. T. Lahey, 1999, International Journal of Multiphase Flow, 25, Issues 6-7, 11, pp 1321-1372
- [Narsimhan and Gupta 1979] A model for transitional breakage probability of droplets in agitated lean liquid-liquid dispersions, Narsimhan, G., Gupta, J.P., 1979, Chem. Eng. Sci. 34, 257-265
- [NEA 2007] Best Practice Guidelines for the use of CFD in Nuclear Reactor Safety Applications, 2007, NEA/CSNI/R(2007)5, NUCLEAR ENERGY AGENCY, OECD
- [Panton 1996] Incompressible flows. 2nd edition, Panton, R. L., 1996, John Wiley and sons, Inc.
- [Park and Blair 1975] The effect of coalescence on drop size distribution in an agitated liquid-liquid dispersion, Park, J.Y., Blair, L.M., 1975, Chemical Engineering Science 30, 1057-1064
- [Patel et al. 1985] Turbulence models for near-wall and low Reynolds number flows - a review, Patel, V.C., Rodi, W. and Scheuerer, G., 1985, AIAA J. 23, 1308
- [Prince and Blanch 1990] Bubble coalescence and break-up in air-sparged bubble columns, Prince, M.J., Blanch, H.W., 1990, AIChE. J. 36, 1485-1499
- [Relap 2001] RELAP5/MOD3.3 Code Manual, Information Systems Laboratories, Inc., Rockville, Maryland, Idaho Falls, Idaho, December 2001
- [Rodi and Scheuerer 1986] Scrutinizing the k- ϵ turbulence model under adverse pressure gradient conditions, Rodi, W., and Scheuerer, G., 1986, J. Fluids Eng. 108
- [Ross 1971] Measurements and models of the dispersed phase mixing process, Ross S.L., 1971, Ph.D. Thesis, The University of Michigan, Ann Arbor, MI, USA
- [Rotta 1972] Turbulente Strömungen, J.C. Rotta, B.G. Teubner, Stuttgart, Germany, 1972.
- [Saleh 2002] Fluid Flow Handbook, Jamal Saleh, 2002, McGraw-Hill Professional

- [Santos Mendez 2008] Medida experimental de la concentración de Área interfacial en flujos bifásicos finamente dispersos y en transición, S. Mendez Diaz, Univeritat Politecnica de Valencia, PhD Thesis, 2008
- [Sari et al. 2009] S.Sari, S. Ergün, M. Barik, C. Kocar and C. N. Sokmen, 2009, Modeling of isothermal bubbly flow with interfacial area transport equation and bubble number density approach, *Annals of Nuclear Energy*, 36, 222–232
- [Serizawa et al. 1986] Serizawa, A. Kataoka, I. and Michiyoshi, I., 1986, Phase Distribution in Bubbly Flow – Data Set No. 24, *Proceedings of the Second International Workshop on Two-Phase Flow Fundamentals*, Troy, NY, USA
- [Simon 2004] Koaleszenz von Tropfen und Tropfenschwärmen, Simon M., 2004, Ph.D. Thesis, Technische Universität Kaiserslautern
- [Sovova 1981] Breakage and coalescence of drops in a batch stirred vessel-II Comparison of model and experiments, Sovova, H., 1981, *Chemical Engineering Science* 36, 1567–1573
- [Sun et al. 2002] Interfacial area of bubbly flow in a relatively large diameter pipe, Sun X., Todd R.S., Kim S., Ishii M., Uhle J., 2002, *Experimental Thermal and Fluid Science*, 27, 97-109
- [Taitel et al. 1976] A model for predicting flow regime transitions in horizontal and near horizontal gas-liquid flow, Taitel, Y. and Dukler, A. E., 1976, *AIChE J.*, 22, 47–55
- [Taitel et al. 1980] Modelling flow pattern transitions for steady upward gas-liquid flow in vertical tubes, Taitel, Y., Bornea, D. and Dukler, A. E., 1980, *AIChE J.*, 26, 345–354
- [Tennekes and Lumley 1972] A first course in turbulence, Tennekes H., and Lumley J.L., 1972, The MIT Press, Cambridge, Massachusetts, and London, England
- [Todreas and Kazimi 1990] NUCLEAR SYSTEMS I Thermal Hydraulic Fundamentals, Todreas N.E. and Kazimi M.S., 1990, Taylor and Francis, New York and London
- [Tomiyama 1998]. Struggle with Computational Bubble Dynamics, Tomiyama A., 1998, *Proceedings of the Third International Conference on Multiphase Flow, ICMF98*, Lyon, France
- [Tomiyama et al. 1995] Effects of Eötvös number and dimensionless liquid volumetric flux on lateral motion of a bubble in a laminar duct flow, Tomiyama, A., Sou, A., Zun, I., Kanami, N. & Sakaguchi, T., 1995, *Adv. Multiphase Flow*, 3–15

- [Tomiya et al. 2002] A. Tomiyama, G.P. Celata, S. Hosokawa, S. Yoshida, Terminal velocity of single bubbles in surface tension force dominant regime, *International Journal of Multiphase Flow*, Volume 28, Issue 9, September 2002, Pages 1497-1519
- [Tsouris and Tavlarides 1994] Breakage and coalescence models for drops in turbulent dispersions, Tsouris, C., Tavlarides, L.L., 1994, *AIChE. J.* 40, 395–406
- [Tsuchiya et al 1989] Visualization of bubble-wake interactions for a stream of bubble in a two-dimensional liquid solid fluidized bed, Tsuchiya K., Miyagata T. and Fan L.S., 1989, *International Journal of Multiphase Flow*, 15, 35
- [Turns 2000] *Introduction to Combustion*, Turns S., 2000, McGraw-Hill Publishing Co.
- [Uhle et al. 1998] Dynamic flow regime modelling, Uhle, J., Wu, Q., Ishii, M., 1998, *Proceedings of 6th International Conference on Nuclear Engineering, ICONE-6509.*
- [Vieser et al. 2008] Heat transfer predictions using advanced two-equation turbulence models, *Ansys CFX Validation Report*, 2008, W. Vieser, T. Esch, F. Menter, ANSYS Germany
- [Wang 2010] *Simulations of Two-phase Flows Using Interfacial Area Transport Equation*, Wang X., 2010, Ph.D. Thesis, The Ohio State University, USA
- [Wang et al. 2003] A novel theoretical breakup kernel function for bubbles/droplets in a turbulent flow. Wang, T., Wang, J., Jin, Y., 2003, *Chem. Eng. Sci.* 58, 4629–4637
- [Wang et al. 2005a] Theoretical prediction of flow regime transition in bubble columns by the population balance model, Wang, T., Wang, J., Jin, Y., 2005, *Chem. Eng. Sci.* 60, 6199–6209
- [Wellek et al. 1966] Wellek, R. M., Agrawal, A. K. and Skelland, A. H. P., 1966, Shape of liquid drops moving in liquid media, *AIChE J.*, 12: 854–862
- [Wilcox 1993] *Turbulence Modeling for CFD*, Wilcox D. C., 1993, *DWC Industries*, 1993
- [Wörner et al. 2004] Wörner, M., Ghidersa, B.E., Ilc, M., Cacuci, D.G., 2004. Volume-of-fluid method based numerical simulations of gas-liquid two-phase flow in confined geometries, *Advances in the modelling methodologies of two-phase flows*, Lyons, France, November 24–26, paper no. 04
- [Wu et al. 1998] Wu, Q., Kim, S., Ishii, M., Beus, S.G., 1998. One-group interfacial area transport in vertical bubbly flow. *Int. J. Heat Mass Trans.* 41, 1103–1112

[Yadigaroglu 2008] Course material of the 25th Course on Modelling and Computation of Multiphase Flows, Part I: Bases, Lesson 2: Basic Models for Two-phase Flows, Yadigaroglu G., 2008, Zurich, Switzerland

[Yao and Morel 2004] Volumetric interfacial area prediction in upwards bubbly two-phase flow, Yao, W., Morel, C., 2004, Int. J. Heat Mass Trans. 47, 307–328.

[Zhao and Ge 2007] A theoretical bubble breakup model for slurry beds or three-phase fluidized beds under high pressure, Zhao, H., Ge, W., 2007, Chem. Eng. Sci. 62, 109–115

Appendix A

iacexpdivergence.F

Subroutine `iacexpdivergence.F` for the calculation of the divergence in the source term

```
#include "cfx5ext.h"
dllexport(iacexpdivergence)
    SUBROUTINE iacexpdivergence(
        & NLOC,NRET,NARG,RET,ARGS,CRESLT,CZ,DZ,IZ,LZ,RZ)
C  ARGS(1:NLOC,1) holds parameter ?a? evaluated at all locations
C  RET(1:NLOC,1) will hold return result
#include "MMS.h"
#include "stack_point.h"
C -----
C      Argument list
C -----
        INTEGER ILOC,NLOC,NARG,NRET
        CHARACTER CRESLT*(*)
        REAL ARGS(NLOC,NARG), RET(NLOC,NRET)
        INTEGER IZ(*)
        CHARACTER CZ(*)*(1)
        DOUBLE PRECISION DZ(*)
        LOGICAL LZ(*)
        REAL RZ(*)
C -----
C      External routines
C -----
        INTEGER LENACT
        EXTERNAL LENACT
C -----
C      Local Variables
C -----
        CHARACTER*(MXDNAM) CGROUP,CEQN,CTERM,CPVAR,
        & CLVAR,CPATCH,CPHASE
        CHARACTER*120 User_Phase_Name, User_Variable_Name
C -----
```

```

C      Stack pointers
C -----
C      __stack_point__ pVFX, pVFY, pVFZ
C -----
C      Executable Statements
C -----

C      Initialise RET to zero.
C      CALL SET_A_0 ( RET, NLOC*NRET )
C
C
C---- Obtain divergence in the expansion term
C      in array shape GRAD_PHI2(1:3,1:NLOC) located at
C      RZ(pGRAD_PHI2)
C
C      CALL USER_GETVAR ('Gas.fvfx.Gradient', CRESLT, pVFX,
C      & CZ,DZ,IZ,LZ,RZ)
C      IF (CRESLT(1:LEN(CRESLT)) .NE. 'GOOD') GO TO 999
C
C      CALL USER_GETVAR ('Gas.fvfy.Gradient', CRESLT, pVFY,
C      & CZ,DZ,IZ,LZ,RZ)
C      IF (CRESLT(1:LEN(CRESLT)) .NE. 'GOOD') GO TO 999
C
C      CALL USER_GETVAR ('Gas.fvfz.Gradient', CRESLT, pVFZ,
C      & CZ,DZ,IZ,LZ,RZ)
C      IF (CRESLT(1:LEN(CRESLT)) .NE. 'GOOD') GO TO 999
C
C---- Calculate source expression in RET(1:NLOC,1)
C
C      CALL
C      USER_SOURCE_EXPDIV(RET(1,1),RZ(pVFX),RZ(pVFY),RZ(pVFZ),
C      & NLOC)

```

```

C
  999 CONTINUE

C
C Send any diagnostics or stop requests via master processor
  IF (CRESLT(1:LEN(CRESLT)) .NE. 'GOOD') THEN
    CALL MESSAGE( 'BUFF', 'iacexpdivergence returned
error:' )
    CALL MESSAGE( 'BUFF', CRESLT )
    CALL MESSAGE( 'BUFF-OUT', ' ' )
  END IF

C
C=====
=====
  END

  SUBROUTINE USER_SOURCE_EXPDIV (DivPhi, gradx, grady, gradz,
NLOC)
C
C Purpose: DivPhi = div(phi)
C
C Inputs
  INTEGER NLOC
  REAL gradx(3,NLOC), grady(3,NLOC), gradz(3,NLOC)
C Outputs
  REAL DivPhi(NLOC)
C Locals
  INTEGER ILOC
C
  DO ILOC = 1, NLOC

DivPhi(ILOC)=(gradx(1,ILOC)+grady(2,ILOC)+gradz(3,ILOC))
  END DO
C
  END

```

cfxgradientx.F

Subroutine `cfxgratientx.F` for the calculation of the gradient in the x direction in the source term

```
#include "cfx5ext.h"
dllexport (cfxgradx)
    SUBROUTINE cfxgradx(
        & NLOC,NRET,NARG,RET,ARGS,CRESLT,CZ,DZ,IZ,LZ,RZ)
C  ARGS(1:NLOC,1) holds parameter ?a? evaluated at all locations
C  RET(1:NLOC,1) will hold return result
#include "MMS.h"
#include "stack_point.h"
#include "common_sizes.h"
C -----
C     Argument list
C -----
    INTEGER ILOC,NLOC,NARG,NRET
    CHARACTER CRESLT*(*)
    REAL ARGS(NLOC,NARG), RET(NLOC,NRET)
    INTEGER IZ(*)
    CHARACTER CZ(*)*(1)
    DOUBLE PRECISION DZ(*)
    LOGICAL LZ(*)
    REAL RZ(*)
C -----
C     External routines
C -----
    INTEGER LENACT
    EXTERNAL LENACT
    CHARACTER          CFROMI*(4)
    CHARACTER*(MXDNAM) CCATI
    EXTERNAL          CCATI,CFROMI
C -----
C     Local Variables
C -----
    CHARACTER*(MXDNAM) CGROUP,CEQN,CTERM,CPVAR,
```



```

& CLVAR,CPATCH,CPHASE
CHARACTER*120 User_Phase_Name, User_Variable_Name
INTEGER phaseno,LPHASE,MAXDPHASES

CHARACTER*(MXLEN_XALIAS) CALIAS
CHARACTER*(80) WHERE,DATA_DIR
CHARACTER*(MXDNAM) WHO,LOCALE,ENTITY,WHEN,CZONE,CVARL
CHARACTER*(MXDNAM) CNAME,CNAMEUINT
CHARACTER*(4) CERACT,CRES,CDTYPE
INTEGER ILOCS,ILOCF,IENTS,IENTF
CHARACTER*(MXPNAM) USER_PRINTING, CFXVAR
C -----
C      Stack pointers
C -----
      __stack_point__ pGRADX
C -----
C      Executable Statements
C -----

C  Initialise RET to zero.
      CALL SET_A_0 ( RET, NLOC*NRET )

      USER_PRINTING = 'No'
      CALL PEEKCS ( '/USER/USER_PRINTING', USER_PRINTING, 'SKIP',
&                  CRES, CZ)

      CFXVAR = 'Unknown'
      CALL PEEKCS ( '/USER/CFXGRADVARIABLE', CFXVAR,
&                  'STOP', CRESLT, CZ )

      CFXVAR=trim(CFXVAR)
      CALL USER_GETVAR (CFXVAR, CRESLT, pGRADX,
& CZ,DZ,IZ,LZ,RZ)

      IF (CRESLT(1:LEN(CRESLT)) .NE. 'GOOD') GO TO 999

```

```

C
C---- Calculate source expression in RET(1:NLOC,1)
C
      CALL USER_SOURCE_GRADX (RET(1,1),RZ(pGRADX),NLOC)

C
      999 CONTINUE

C
C Send any diagnostics or stop requests via master processor
      IF (CRESLT(1:LEN(CRESLT)) .NE. 'GOOD') THEN
          CALL MESSAGE( 'BUFF', 'cfxgradx returned error:' )
          CALL MESSAGE( 'BUFF', CRESLT )
          CALL MESSAGE( 'BUFF-OUT', ' ' )
      END IF

C
C=====
=====
      END

      SUBROUTINE USER_SOURCE_GRADX (gradX, GX, NLOC)
C
C Purpose: CALCULATE THE X GRADIENT OF A GENERIC VARIABLE AND
C          RETURNING THE VALUE TO CFX
C
C Inputs
      INTEGER NLOC
C      REAL GX(3,NLOC,3)
      REAL GX(3,NLOC)
C Outputs
      REAL gradX(NLOC)
C Locals
      INTEGER ILOC
C
      DO ILOC = 1, NLOC
C          gradX(ILOC)=(GX(1,ILOC,3))

```

```
        gradX(ILOC) = (GX(1, ILOC))  
    END DO  
C  
    END
```

Similar to the subroutine reported above are those written for the calculation of gradients in the y and z direction. There is, for this reason, no need to report them explicitly.